UNIVERSITAT POLITÈCNICA DE VALÈNCIA

MARTA CARSÍ ROSIQUE / Valencia 2015

Molecular mobility. Structure-Property relationship of polymeric materials

MOLECULAR MOBILITY. STRUCTURE–PROPERTY RELATIONSHIP OF POLYMERIC MATERIALS

Marta Carsí Rosique

Thesis Advisors:
Prof. Dr. Ricardo Díaz Calleja
Prof. Dra.Maria Jesús Sanchis Sánchez

Valencia, December 2015

UNIVERSITAT POLITÈCNICA DE VALÈNCIA

UNIVERSITAT POLITÈCNICA DE VALÈNCIA

MOLECULAR MOBILITY.

STRUCTURE-PROPERTY RELATIONSHIP OF POLYMERIC MATERIALS

A Dissertation Presented by

MARTA CARSÍ ROSIQUE

to obtain the degree of Doctor of Philosophy at the
Universitat Politècnica de València

Valencia, December 2015

Programa de Doctorado TECNOLOGÍA ELÉCTRICA, MATERIALES, GENERACIÓN Y DISTRIBUCIÓN

Thesis Advisors: Prof. Dr. Ricardo Díaz Calleja

Prof. Dra.Maria Jesús Sanchis Sánchez

MOLECULAR MOBILITY.

STRUCTURE-PROPERTY RELATIONSHIP OF POLYMERIC MATERIALS

A Dissertation Presented

by

MARTA CARSÍ ROSIQUE

Approved as to style and content by:

_____

Silvina Cerveny Murcia,
(Chair of Committee)

_____

Galina Ivanova Zamfirova,
(Member)

_____

María Pilar Ortiz Serna,
(Secretary)

“Gutta cavat lapidem, non vi, sed saepe cadendo”

Ovidio

DEDICATION

This thesis is dedicated to the memory of my grandfather, Vicente Carsí Belenguer, who paved the way for me and upon whose shoulders I stand. He taught himself engineering while farming the very land that now houses the Polytechnic University of Valencia. Although his untimely death prevented me from knowing him, the first book of physics I discovered belonged to him. His memory inspired the scientific thinking in our lives.

I also dedicate this thesis to my beloved identical twin sons, Luis and Guille, who every day bring light, happiness and joy into my life. They will probably never read it, but I will do my best always to support and encourage them to learn and believe in themselves. This work is for you and because of you.

ACKNOWLEDGMENTS

I would like to thank the following institutions for their financial support for my thesis and research work:

- Universitat Politècnica de València through projects PAID-0608 and PAID05-08-4055.
- Ministerio de Ciencia y Tecnología through projects MAT2002-04042-C02-01, MAT2005-05648-C02-02, MAT2008-06725-C03-03 and FPI grant BES-2003-0390.
- Generalitat Valenciana through projects GRUPOS 03/030 and ACOMP/2010/204.
- Agencia Valenciana de Ciencia y Tecnología (AVCit) through projects ACOMP07/242, INFRA03/029 and MY07/ITE/S/101.

This work was carried out at the Universitat Politècnica de Valencia (Spain), in the Departamento de Termodinámica Aplicada (ETSII) under the supervision of Prof. Ricardo Díaz Calleja and Prof. María Jesús Sanchis Sánchez. First and foremost, I would like to express my deepest gratitude to my advisors for their unwavering support and mentorship, and without whom this thesis would not have been possible.

I am also very grateful for the help and support of all the other professors in the GCPTNM group: Prof. Enrique Sanchez, Prof. Vicente Compañ, Prof. José Vicente Lidón and Prof. Abel García.

My special thanks go to the late Dr. Evaristo Riande (1937-2012), who had the attitude, humility and substance of a genius. He continually conveyed to me a spirit of adventure with regard to research and I consider it an honor to have had the opportunity to work with him.

I would also like to thank Dr. Gustavo Ariel Schwartz, Dr. Rafael Muñoz Espí and Dr. Konstantinos Mpoukouvalas for taking time out from their busy schedules to serve as my

external supervisory committee, and especially for their careful and enriching review of this thesis.

I am very grateful to Dr. Michael Nugent for all his help and assistance during my internship at the Materials Research Institute at Athlone Institute of Technology.

I am greatly indebted to my dear colleagues and friends María, Pili, Gus, Carre and Belén and the special gems that came with them, Ali and Aurora. Thanks a lot for everything. We meet to part but, more importantly, we part to meet.

My dearest thanks to my family: my parents, Vicente and Carmen, and my brother and sister, Vicente and Mar. Thank you for all the unconditional love and support you have given in every way possible, and especially for all those times you scraped me off the ground and propped me back up again. I would never have been able to get to this stage without you!

I would also like to extend a special thank-you to Rafa, who became my husband during this time and always believed in me, sometimes more than I did myself. Thank you so much for your encouragement, your quiet patience and unwavering love. I knew I could always depend on you through thick and thin.

And finally I have to apologize…. to my sons, Luis and Guille, who patiently allowed me to spend time away from them. Now I can answer their constantly repeated question…"Are you done with your book yet, Mommy?" Yes, I am.

ABSTRACT

The present work examines the influence of the chemical structure of polymers on thermal, mechanical and dielectric behavior. The experimental techniques used for the purpose are differential scanning calorimetry, dynamo-mechanical analysis and dielectric spectroscopy. Additionally, in order to confirm the results obtained using the above methods, other techniques such as ray diffraction have also been employed.

Chapters 1 and 2 contain the introduction and the objectives, respectively. Chapter 3 briefly describes the experimental techniques used.

Chapter 4 contains the findings of the comparative analysis of the response to electrical noise fields for three poly(benzyl methacrylates) with different structures. The analysis was carried out under a wide range of frequencies and temperatures on three poly(benzyl methacrylates) containing two dimethoxy groups in positions 2,5-, 2,3- and 3,4-. The results show that the position of the dimethoxy groups on the aromatic ring has a significant effect on the molecular dynamics of poly(benzyl methacrylate). The spectra obtained were of high complexity and therefore, in order to perform a better analysis, numerical methods for time-frequency transformation including the use of parametric regularization techniques were used. We studied the effect of this structural change on the secondary relaxation processes and relaxation process α, relating to the glass transition. We also analyzed the effect of the dimethoxy group position on the formation of nanodomains, in which the side chains are predominant, and on the conduction processes of the materials tested.

In Chapter 5, the conductivity of rubbery liquids was studied by analyzing poly (2,3-dimethoxybenzyl methacrylate), which exhibits its own particular behavior. The chapter analyzes the principle of time-temperature superposition, employing different interrelated variables.

Chapter 6 focuses on how the presence of crosslinking affects the molecular mobility of polymethacrylates containing aliphatic alcohol ether residues. In this case, the effect of crosslinking on the secondary and primary relaxation processes was analyzed. The creation of nanodomains in the side chains as a result of the presence of crosslinking was also studied.

RESUMEN

En este trabajo se presenta un estudio de la influencia de la estructura química de los polímeros en su comportamiento térmico, mecánico y dieléctrico. Las técnicas experimentales empleadas para ello han sido la calorimetría diferencial de barrido, el análisis dinamo-mecánico y la espectroscopia dieléctrica. Adicionalmente, se han empleado otras técnicas como la difracción de rayos, con objeto de corroborar los resultados obtenidos por las primeras.

En los Capítulos 1 y 2 se recoge la introducción y los objetivos, respectivamente. El Capítulo 3 presenta una breve descripción de las técnicas experimentales empleadas.

En el Capítulo 4 se recogen los resultados obtenidos en el análisis comparativo de la respuesta a campos de perturbación eléctrica en un amplio rango de frecuencias y temperaturas para tres polimetacrilatos de bencilo con dos grupos dimetoxi en posiciones 2,5-, 2,3- y 3,4-. Los resultados obtenidos señalan el importante efecto de la posición de los grupos dimetoxi en el anillo aromático, sobre la dinámica molecular del polimetacrilato de bencilo. Los espectros obtenidos fueron muy complejos, por ello en orden a llevar a cabo un mejor análisis se emplearon métodos numéricos para la transformación tiempo-frecuencia que incluyeron el uso de técnicas de regularización paramétrica. Se ha estudiado el efecto que dicho cambio estructural ejerce tanto sobre los procesos de relajación secundaria como sobre el proceso de relajación α, relacionado con la transición vítrea. Así mismo, se ha analizado el efecto de la posición de los grupos dimetoxi en la formación de

nanodominios en los que predominan las cadenas laterales, y su efecto en los procesos de conducción de los materiales analizados.

En el Capítulo 5 se recoge el estudio de la conductividad de líquidos gomosos tomando como modelo el poli (metacrilato de 2,3-dimetoxibencilo), por su peculiar comportamiento. En este capítulo se ha realizado un análisis del principio de superposición tiempo-temperatura, empleando para ello diferentes variables relacionadas entre sí.

En el Capítulo 6 se recoge el efecto de la presencia de entrecruzante en la movilidad molecular de polimetacrilatos que contienen residuos de éteres de alcoholes alifáticos. En este caso, se ha analizado el efecto de la presencia de entrecruzante tanto en los procesos de relajación secundarios, como en el proceso de relajación principal. También se llevó a cabo un análisis del efecto que la presencia de entrecruzante tiene sobre la creación de nanodominios gobernados por las cadenas laterales.

RESUM

En aquest treball es presenta un estudi de la influència de l'estructura química dels polímers en el seu comportament tèrmic, mecànic i dielèctric. Les tècniques experimentals utilitzades han sigut la calorimetria diferencial de rastreig, l'anàlisi dinamo-mecànic i l'espectroscòpia dielèctrica. Addicionalment, s'han empleat altres tècniques com la difracció de rajos X a fi de corroborar els resultats obtinguts per les primeres.

En els Capítols 1 i 2 s'arreplega la introducció i els objectius, respectivament. Al Capítol 3 es presenta una breu descripció de les tècniques experimentals emprades.

En el Capítol 4 es recull els resultats obtinguts en l'anàlisi comparativa de la resposta a camps de pertorbació elèctrica en un ampli rang de freqüències i temperatures de tres polimetacrilats de benzil amb dos grups metoxi en posicions 2,5-, 2,3- i 3,4-. Els resultats obtinguts assenyalen l'important efecte de la posició dels grups metoxi en l'anell aromàtic, sobre la dinàmica molecular del polimetacrilat de benzil. Els espectres obtinguts van ser molt complexos, per aquesta raó per a dur a terme un millor anàlisi es van emprar mètodes numèrics per a la transformació temps-freqüència que van incloure l'ús de tècniques de regularització paramètrica. S'ha estudiat l'efecte que el dit canvi estructural exerceix tant sobre els processos de relaxació secundària com sobre el procés de relaxació α, relacionat amb la transició vítria. Així mateix, s'ha analitzat l'efecte de la posició dels grups metoxi en la formació de nanodominis en els que predominen les cadenes laterals, i el seu efecte en els processos de conducció dels materials analitzats.

En el Capítol 5 s’arreplega l'estudi de la conductivitat de líquids gomosos prenent com a model el poli-(metacrilat de 2,3-dimetoxibencilo), pel seu peculiar comportament. En aquest capítol s'ha realitzat un anàlisi del principi de superposició temps-temperatura, emprant per a això diferents variables relacionades entre sí.

En el Capítol 6 s'arreplega l'efecte de la presència d’entrecreuat en la mobilitat molecular de polimetacrilats que contenen residus d'èters d'alcohols alifàtics. En aquest cas, s'ha analitzat l'efecte de la presència d'entrecreuat tant en els processos de relaxació secundaris, com en el procés de relaxació principal. També es va dur a terme un anàlisi de l'efecte que la presència d'entrecreuat químic té sobre la creació de nanodominis governats per les cadenes laterals.

TABLE OF CONTENTS

Page

LIST OF TABLES

LIST OF FIGURES

Chapter 1:

Introduction

1. INTRODUCTION

1.1. The Glass Transition

1.1.1. General Aspects

According to classical physics, a solid can be compared with a liquid by some macroscopic properties. Thus, while a liquid is easily deformable, adapting to the shape of the vessel containing it, a solid presents dimensional stability with high resistance to deformation. Equally, a solid may differ from a liquid due to its infinite viscosity.

According to their spatial arrangement, solids can be classified into crystalline (such as salt, benzoic acid, etc.) and amorphous (glass used for windows, amber, etc.). In the first case, the solids have a regular structure repeating long distances from a reference point; it is called lattice. In the case of amorphous solids, also called glass, that order stops its repeating pattern at very short distances from the reference point considered. The diffraction of X-rays of an amorphous solid are very similar to those of a liquid so that, from a structural point of view and in a first approximation, an amorphous solid can be defined as a "frozen" liquid, exhibiting a grade of disorder characteristic of a liquid and a lack of mobility characteristic of a solid.

1.1.2. Phenomenology of the Glass Transition.

A polymer is formed by connecting many small monomeric structural units. The chemical structure of the monomeric segment is generally referred to as the microstructure of the polymer chain. Depending on its molecular mobility, a polymer chain can take up an enormous number of configurations as each chemical segment has the possibility to change among various pointing orientations. In a melt or solution the number of reachable configurations is worthy increased. In the solid state, the thermal effect is mainly determining the changes on polymer chain configurations.

The polymers in the solid state may also occur as amorphous or crystalline. Structurally and also in first approximation, a solid polymer in the amorphous state can be seen as a set of strings intermingled randomly without order, while a polymer in a crystalline state has chains oriented in preferential directions or parallel positioned so that they are sorted in some way.

In reference to amorphous polymers, the most important change in their properties occurs at a specific temperature called glass transition temperature (T_g). It can be considered that below this temperature the movements of chain segments are practically frozen while, upon reaching this temperature, long range molecular motions starts. This motions implies a large number of chain segments and for this reason has a great influence on the material properties and therefore, on its possible future applications.

In some polymers at temperatures below T_g, secondary transitions of lower intensity than glass transition were observed. These processes are associated with movements of

short lengths of chains or lateral movements of small groups. T_g may also be called temperature of the transition α. Secondary transitions in order of decreasing temperature are called β, γ, δ, etc. (McCrum, et al., 1991)

The analysis of the dependence with temperature of the properties of amorphous polymers shows that there is a temperature or rather, a relatively narrow temperature region, in which a sharp change of the physical and mechanical properties is manifested. Above this temperature region, the polymer is soft. It behaves as a more or less viscous liquid having elastic properties similar to rubbers, while below it, the polymer is hard, rigid and brittle with properties analogous to glasses. The temperature separating these two behaviors is the glass transition temperature, T_g. Other properties such as volume, heat capacity, viscosity, refractive index, etc. also change when the material passes through the region of the glass transition temperatures.

To study the glass transition, one of the most interesting properties is the volume. So, measuring the specific volume of a sample in function of temperature, it is observed that above and below the glass transition, there is a linear variation of the specific volume with temperature changes. However, in the vicinity of the glass transition there is a slope change. This change in slope occurs in an area of several degrees. The T_g is normally taken as the point at which the extrapolation of the two lines meet as show **Fig. 1.1**.

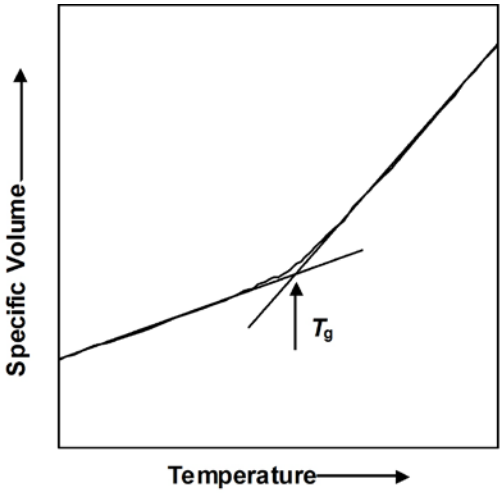

Figure 1.1. Variation of specific volume with temperature

The value of the glass transition temperature, determines the potential applications of an amorphous polymer. For example, styrene-butadiene copolymers (with approximate composition of 25/75 by mole) with a $T_{g.}$~-70ºC are used to manufacture tires due to its similar rubber elasticity at room temperature; however, they could not be used for structural applications, as they don't have good dimensional stability. For this purpose can be used other polymers as poly(methyl methacrylate) or poly(vinyl chloride), whose T_g values are about 105º and 80º C, respectively. (McCrum, et al., 1991)

While so-called amorphous polymers do not contain any crystalline region, the called crystalline or crystallizable polymers are polymers containing amorphous material with crystalline regions. There are difficult to obtain as fully crystalline materials and are

obtained only as semi-crystalline materials, containing, in most cases, appreciable amounts of amorphous material. (Christensen, 1982)

In reference to crystallizable polymers, such polymers may be crystallized or vitrified only depending on the thermal history received (see **Figure 1.2**). If such a polymer in the liquid state at high temperature is subjected to cooling with a relatively high viscosity, the material is compressed and its viscosity increases until it reaches a point such as A.

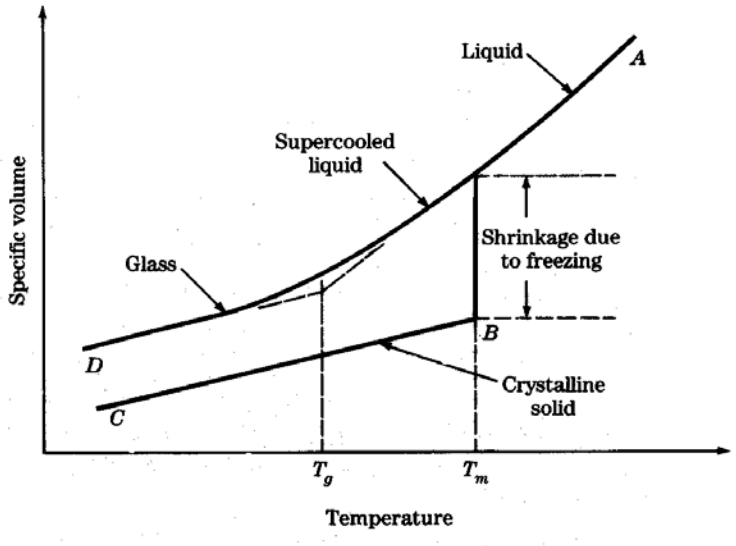

Figure 1.2. Specific volume changes at T_m and T_g.

After point A, the crystallizable polymers may follow any of the existing paths depending on the cooling conditions, unlike amorphous polymers, that always follow the upper path (A-D) whatever the cooling conditions are.

Crystallizable polymers follow the upper path if the cooling is quick, while if the cooling is slow follow the other path, reaching a temperature region indicated by the letter

B, in which the volume-temperature graph changes slope. Below this temperature region, the coefficient of thermal expansion, represented by the slope of the graph becomes smaller than it had when it was liquid.

The temperature when this change takes place is accompanied with a sudden change in mechanical and physical properties. If cooling is relatively slow, the material follows the lower path with an abrupt decrease in volume in a temperature range. In this temperature range, very narrow for low molecular weight substances, and wider in polymers, the material crystallizes. During crystallization, the material is ordered and, therefore, volume decreases sharply. If cooling is continued, the material follows a process similar to the upper path. The glass transition temperature is observed, although less sharply than in the previous case, as less amount of material undergoes transition, since much of it is crystallized. (Ferry, 1961)

1.1.3. Polymer Chain Dynamics

A typical solid, such as a metal bar, has an elastic behavior against an effort that is applied over it. The material deforms under the action of a force, more or less depending on the value of it, but when the effort ceases the material returns to its original state. A simple explanation at the molecular level involves considering the metal atoms occupy well defined places in a crystal lattice. The action of the effort moves them slightly from those

positions but when ceases the effort, the forces that hold atoms together make them quickly recover its equilibrium position, returning the energy that the effort had transmitted.

A conventional liquid such as water, under the action of an effort, for example, an internal turning rotor, undergoes an irreversible process in which water molecules move one over another by the action of the rotor. By stopping the effort, it is impossible for each molecule regain the position it had at the beginning. The energy supplied during deformation is dissipated as friction between the molecules, in a phenomenon called viscous, characterized by the liquid viscosity.

In the case of polymers, the presence of long chains in their macromolecular structure makes the solid and liquid polymer having a behavior somewhere between the two situations described before. There are polymers such as lightly crosslinked rubbers, which behave like elastic solids with great formability and almost full recovery after cessation of effort. However it is known that many plastics are deformed by the action of an effort but, upon cessation rarely recover the initial form. This is because, during exercise, the polymer chains constituting the moving over each other, a clear viscous phenomenon in which part of the energy supplied by the effort is consumed, preventing the total recovery of the elastic solid pathway.

This elastic and viscous behavior of the polymers has important implications for the processing and final properties of these materials and therefore for the possible applications.

Chains dynamics is a flourishing field of research in polymer science due in part to the practical applications of these studies in engineering (Graham, 1990). Furthermore, the prediction of the mechanical performance of polymeric structures requires an understanding of the chain dynamics of polymers. The glass-transition or α relaxation that arises from segmental motions of molecular chains freezes at T_g. This characteristic, in conjunction with the fact that the α relaxation is the dominant process in chain dynamics until molecular chains disentanglement occurs, leads to consider the glass-transition relaxation as the precursor of the glassy state and the viscous flow. Moreover, the α relaxation also occurs in oligomers of low molecular weight, well below the entanglement condition (Ezquerra, et al., 1999; Roland, et al., 2003). Besides the glass rubber relaxation, the relaxation spectra of polymers in the frequency domain present secondary relaxations produced by conformational transitions of the chains backbone or motions of flexible side-groups (McCrum, et al., 1991; Kremer, et al., 2003; Riande, et al., 2004). Unlike the glass-rubber relaxation and the normal mode process (Stockmayer, 1967) reflecting chains disentanglement, secondary relaxations remain operative below T_g.

Secondary relaxations can have a great impact on the mechanical properties of polymers in the glassy state (McCrum, et al., 1991; Kremer, et al., 2003; Riande, et al., 2004; Mpoukouvalas, et al., 2009; Ferry, 1961). For example, chair-inverse-chair conformational transitions of cyclohexyl in poly(cyclohexyl methacrylate) produce an ostensible secondary β relaxation that causes a significant decrease of the real relaxation modulus of the polymer in the glassy state (Heijboer, 1972; Ribes-Creus, et al., 1995; Domínguez-Espinosa, et al., 2005). Since to date, while no quantitative theory that describe

the glass-rubber relaxation and the secondary relaxations in terms of the chemical structure has been formulated, (i) the theory of the total dielectric relaxation strength for the α-process is well-established in terms of molecular dipole moments (McCrum, et al., 1991; Kremer, et al., 2003; Riande, et al., 2004; Volkenstein, 1963; Glarums, 1960; Cole, 1965; Cole, 1961; Cook, et al., 1970; Williams, 1979; Riande, et al., 1992) (Sanchis, et al., 2008; Sanchis, et al., 2010; Sanchis, et al., 2011; Roe, et al., 1992) and (ii) much success has been achieved in understanding the characteristic behavior of the dielectric α relaxation through computer "molecular dynamics" simulations (Takeuchi, et al., 1991; Boyd, et al., 2007; Boyd, 1985; Boyd, 1985; Buerger, et al., 1989; Buerger, et al., 1989; Heijboer, 1965). In this sense, actually the design of polymers with specific physical properties relies on empirical rules based on experimental studies of the relaxation properties of polymers with different chemical structures.

Poly(n-alkyl methacrylate)s and poly(n-alkyl acrylate)s have been widely used in the study of chain dynamics owing to the great dependence of the properties of the members of the series on the length of the alkyl residue (McCrum, et al., 1991; Kremer, et al., 2003; Riande, et al., 2004; Ferry, 1961; Mpoukouvalas, et al., 2009; Stockmayer, 1967; Giebel, et al., 1992; Garwe, et al., 1996; Schröter, et al., 1998; Floudas, et al., 1998) (Beiner, et al., 1999; Dudognon, et al., 2001; Dudognon, et al., 2002; Beiner, 2001; Beiner, et al., 2002; Hempel, et al., 2002; Beiner, et al., 2003; Pascui, et al., 2003; Hiller, et al., 2004; Menissez C, 2005) (Wind, et al., 2005; Beiner, 2006; Arbe, et al., 2008; Arbe, et al., 2010; Godard, et al., 1998; Godard, et al., 1998; Grenet, et al., 2002). The first member of the series, poly(methyl methacrylate) (PMMA), is widely used in household and

automotive applications (Mark, 2007). The fact that PMMA has a glass-transition temperature ca. 100K above that of poly (methyl acrylate) (PMA) puts in evidence how the rigidly of the methyl group attached to the polymer backbone hinders the conformational transitions. This results in the increase of the T_g of PMMA (McCrum, et al., 1991). Moreover, the tacticity of the PMMA has a significant influence in the dynamics of this polymer, thus the T_g value of the isotactic form is lower than the corresponding to the syndiotactic form and the β peak is located at slightly lower temperatures for the isotactic polymer than for the syndiotactic polymer. Moreover, the magnitude of the β relaxation is also very influenced by the tacticity. Thus, whereas the height of the β peak is about twice that of the α peak for the conventional polymer, the opposite situation exists in the case of the isotactic polymer (McCrum, et al., 1991). Moreover, the X-ray spectra of poly(n-alkyl methacrylate)s melts with n ≥ 2, show that these polymers are heterogeneous systems formed by nanodomains integrated by side-chain groups flanked by the chains backbone (Beiner, et al., 1999; Beiner, et al., 2003; Hiller, et al., 2004). Cooperative motions of the side chains in the domains produce an α_{EP} peak located at higher frequencies than the glass-rubber relaxation arising from segmental motion of the chains backbone.

Chapter 2:

Objectives

2. OBJECTIVES

2.1. General and specific objectives

In recent years many studies have been conducted in order to establish correlations between structure and properties of materials. These studies are very interesting both (i) from a conceptual point of view, as they can provide light on the microscopic origin of macroscopic properties and (ii) from the point of view of application, since knowledge of the connections between them can be a key point for the design and preparation of materials with properties to the letter.

A critical interpretation of their macroscopic properties can contribute to obtain a better understanding of the relationship between chemical structure and properties of the macromolecular chains of the studied polymers. It is for this reason that the main aim of the thesis has been to establish connections between the properties and structure of two families of different methacrylates. The first one consists of three structural methacrylic isomers. The second family is a methacrylate with / without chemical crosslinking.

Referring to the first family consisting on three structural methacrylic isomers, the specific objectives were as follows:

- To know how the position of two methoxy substituents in the side chain of the benzyl ring affects both the dipolar processes (principal and secondary relaxations) and conductive processes.

- To establish some correlation between the response of materials to electrical disturbance fields and their molecular structure.
- To analyze the time-temperature superposition principle from several interrelated variables, which are different ways of expressing the response of a material to an electric field disturbance.

Referring to the second family integrated by a methacrylate with and without chemical crosslinking, the specific objectives were as follows:

- To know how the presence of crosslinking affects the molecular mobility. For this purpose the sample with and without crosslinking agent were subjected to external perturbation fields of different nature (thermal, mechanical and electrical).
- To analyze, from dielectric relaxation measurements, both dipole relaxation processes and the conductive processes for samples with/without crosslinking agent.
- To establish some correlation between the response of materials to electrical perturbation fields and their molecular structure.
- To analyze, from dynamic mechanical analysis, the relaxation processes for samples with/without crosslinking agent.
- To establish some correlation (i) between the response of materials to mechanical perturbation field and their molecular structure, and (ii) between the response to both electrical and mechanical perturbation field.

We hope that these studies contribute to a better understanding of the structure-property relationship and therefore shed new light on the determinants for the design of new materials. That is, providing tools for predicting the macroscopic properties of materials from the knowledge of their microstructure.

Chapter 3:

Materials and Methods

*The experimental methods described in this Chapter were published in: M. J. Sanchis, M. Carsí, P. Ortiz-Serna, G. Domínguez-Espinosa, and R. Díaz-Calleja, E. Riande,L. Alegría, L. Gargallo, and D. Radiç, *Macromolecules* vol 43, pp. 5723–5733, **2010;** M. Carsí, M. J. Sanchis, P. Ortiz-Serna, B. Redondo-Foj, R. Díaz-Calleja, E. Riande, *Macromolecules* vol 46, pp. 3167−3175, **2013**; M. Carsí, M.J. Sanchis, R. Díaz-Calleja, E. Riande, M.J.D. Nugent, *Macromolecules* vol 45, pp. 3571−3580, **2012**; M. Carsí, M.J. Sanchis, R. Díaz-Calleja, E. Riande, M.J.D. Nugent, European Polymer Journal, vol. 49, pp. 1495–1502, **2013**.

3. Materials and Methods

The aim of this chapter is to describe the experimental methods and techniques commonly carried out in all the sections of this thesis. A more detailed description will be specified in each corresponding chapter for the sake of clarity.

3.1.Materials

In this thesis, two families of polymers have been analyzed in order to determine their properties as function of their chemical structure.

The first family of polymers studied was poly(*x*,*y*-dimethoxybenzyl methacrylate), specifically poly(2,3-dimethoxybenzyl methacrylate) (PDBM23), poly(2,5-dimethoxybenzyl methacrylate) (PDBM25), and poly(3,4-dimethoxybenzyl methacrylate) (PDBM34).

The second family of polymers characterized was the poly(2-ethoxyethyl methacrylate) with and without cross-linker agent (PEOEMA/CEOEMA).

3.1.1. Synthesis of poly(*x*,*y*-dimethoxybenzyl methacrylate)

Synthesis and characterization of the monomers

The monomers 2,3-dimethoxybenzyl, 2,5-dimethoxybenzyl and 3,4-dimethoxy benzyl methacrylates were obtained respectively by reaction of methacryloyl chloride with 2,3-dimethoxybenzyl alcohol, 2,5-dimethoxybenzyl alcohol and 3,4-dimethoxybenzyl

alcohol at reflux temperature using toluene as solvent following the procedure of Burtle et al. (Burtle, et al., 1954) improved by Gargallo et al. (Gargallo, et al., 1986) The monomers were isolated and purified at reduced pressure (80ºC to 95ºC, 1 mmHg). The purity of the monomers was checked by 1H NMR spectroscopy. Both monomers and polymers were characterized with a Bruker apparatus using tetramethylsilane (TMS) as internal reference. The main signals of monomers: 2,5-Dimethoxybenzylmethacrylate (DBM25) : 1H-NMR(ppm), 1.91(s, 3H, CH_3-C=C-) 3.70(s, 6H, -OCH_3), 5.4 (s, 2H, O-CH_2-C=0) 5.55(m,1H, H- C =C-), 6.15 (m, 1H, H-C=C-), 6.55 (s, 3H, Aromatic); 3,4-Dimethoxybenzylmethacrylate (DBM34): 1.90 (s, 3H, CH_3-C=C-) 3.72 (s, 6H, -O-CH_3), 5.40 (s, 2H, -O-CH_2-), 5.56 (m,1H, H- C =C-) 6.00 (m, 1H, H- C =C-) , 6.63 (s,1H, aromatic), 6.58 (s, 2H, aromatic) and 2,3-Dimethoxybenzylmethacrylate (DBM23) : 1.90 (s,3H CH_3-C=C) 3.73 (s,3H, CH_3-C=C-), 5.40 (s,6H, -O-CH_3), 5.4 (s,2H, -O-CH_2-C-) 6.64 (s,2H, aromatic), 6.60 (s, 1H, aromatic).

Synthesis and characterization of the polymers

Polymerization reactions of the respective monomers were carried out at 323K in toluene solutions, under nitrogen atmosphere, using α,α'- azo-bis-isobutyronitrile (AIBN) as initiator. Polymers were precipitated with methanol, dissolved in chloroform, precipitated again with methanol and dried in a vacuum oven at 333K.

The purity of the polymers was checked by 1H NMR spectroscopy. Poly(2,5-dimethoxybenzylmethacrylate) (PDBM25): 1.30-1.34 (s, 3H, CH_3-C=C-)) (broad), 1.90-1.95 (s,2H-C-CH_2-C-) (broad), 3.70 (s,6H, -O-CH_3) (broad) 5.33-5.35 (s, 2H, -O-CH_2-C-)

(broad), 6.57-6.60 (m, 3H, aromatic); Poly(3,4-dimethoxybenzylmethacrylate) (PDBM34): 1.28-1.34 (s, 3H, CH_3-C=C-) (broad), 1.90-1.93 (s, 6H,-C-CH_2-C-)) (broad), 3.72 (s, 6H, -O-CH_3) (broad) 5.30 (s,2H, -O-CH_2-C-) (broad), 6.60 (s, 3H, aromatic) (broad) and Poly(2,3-dimethoxybenzylmethacrylate (PDBM23): 1.29-1.34(t,1 HCH_3-C=C-) broad, 1.91 (m,2 H, -CH_2-)broad 3.73 (s, 6H, - O-CH_3) broad, 5.34 (s, -CH_2-) broad 6.59-6.64 (s, Aromatic) broad.

The weight-average molecular weights ($g \cdot mol^{-1}$) of the polymers determined by Gel Permeation Chromatography (GPC) were 1.4×10^5, 2.1×10^5 and 1.7×10^5 for PDBM23, PDBM25 and PDBM34, respectively, and the molecular weight heterodispersity index was about 1.8. The stereochemical structure of the samples as determined by NMR was atactic. The repeating units of the polymers are shown in **Figure 3.1.**

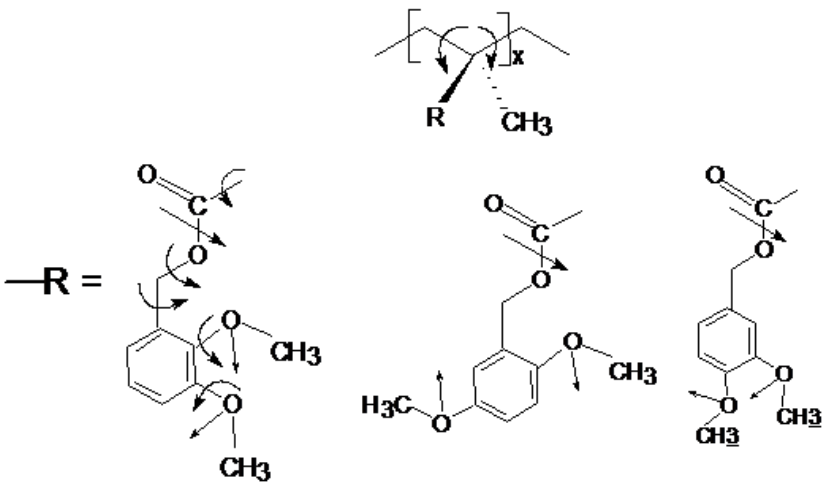

Figure 3.1. From left to right, schemes of the planar structures of the side chains of PDBM23, PDBM25 and PDBM34. As an example, rotations that may produce dielectric activity are indicated in the scheme of PDBM23 and the backbone (top). Notice that the C(O)-O bond is planar, i.e. it is restricted to the trans state. Arrows indicate dipole moments associated with polar moieties of the side chains.

These samples have been synthesized by the Group of Prof. Deodato Radic and Prof. Ligia Gargallo of Departamento de Química Física, Pontificia Universidad Católica de Chile.

3.1.2. Synthesis of poly(2-ethoxyethyl methacrylate)

Commercial monomer 2-ethoxyethyl methacrylate (Aldrich, 99%) (**Figure 3.2**) and the crosslinking agent ethyleneglycol dimethacrylate (EGDMA, Aldrich, 98%) (**Figure 3.3**) were purified by distillation under high vacuum. Dioxane (Aldrich; 99%) was distilled twice: the first time over sodium hydroxide and the second time over sodium. 2, 2'–Azobisisobutyronitrile (AIBN, Fluka; 98%) was recrystallized from methanol and dried

under high vacuum at room temperature. All other materials and solvents used for the synthesis were commercially available and they were used as received unless otherwise indicated.

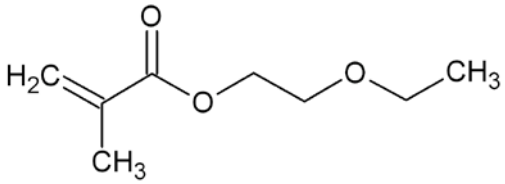

Figure 3.2. Structure of 2-ethoxyethyl methacrylate (EOEMA).

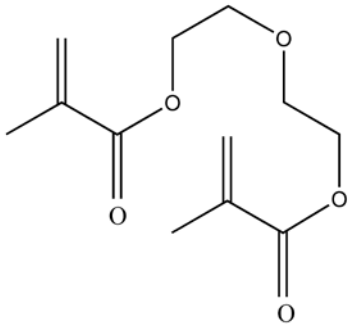

Figure 3.3. Structure of ethyleneglycol dimethacrylate (EGDMA).

Poly 2-ethoxyethyl methacrylate (PEOEMA) was obtained by radical polymerization of 2-ethoxyethyl methacrylate in dioxane solution using 1 *wt%* of 2,2'–azobisisobutyronitrile (AIBN) as initiator. The reaction was carried out in nitrogen atmosphere, at 343 K, for 5 h. The polymer was precipitated with methanol, washed several times with this organic compound and finally dried under high vacuum at 60ºC. The number- and weight-average molecular weights of PEOEMA were measured by size exclusion chromatography (SEC) in a Perkin-Elmer apparatus with an isocratic pump serial

200 connected to a differential refractometric detector (serial 200a). Two Resipore columns (Varian) were conditioned at 343K and used to elute the samples (1.0 $mg \cdot mL^{-1}$ concentration) at 0.3 $mL \cdot min^{-1}$ HPLC-grade N,N´-dimethyl formamide (DMF) (Scharlau) supplemented with 0.1 v/v % LiBr. Calibration of SEC was carried out with monodisperse standard poly(methyl methacrylate) samples in the range of 2.9 x 10^3 to 480 x10^3 obtained from Polymer Laboratories. The values of M_n and M_w were 82649 and 250774 $g \cdot mol^{-1}$, respectively. The chemical structure of the PEOEMA is shown in **Figure 3.4**.

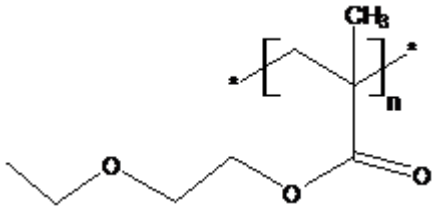

Figure 3.4. Scheme of the chemical structure of poly(2-ethoxyethyl methacrylate) (PEOEMA)

CEOEMA was prepared by radical copolymerization of 2-ethoxy ethyl methacrylate and ethylene glycol dimethacrylate, the mass fraction of the latter comonomer or crosslinking agent in the feed being 2.5*wt%*. The polymerization reaction took place at 343 K in a silanized-glass mold of about 100 μm thickness, in oxygen free atmosphere, using AIBN as initiator. The cross-linked film (CEOEMA) was maintained in hot toluene overnight to extract very small amounts of un-cross-linked polymer, washed several times with methanol and dried under vacuum at 60ºC.

3.2.Experimental Techniques

The main idea of this thesis is to evidence the existing relationship between properties and structure by means of the study of two representative families of polymers. The study has mainly carried out by using a combination of techniques such as Dielectric Relaxation Spectroscopy (DRS), Dynamic Mechanical Analysis (DMA) and Differential Scanning Calorimetry (DSC). The DSC technique is sensitive to the thermal properties whereas DRS technique is also selective to dipole moment fluctuations. Moreover, other complementary physical and chemical characterization techniques were also performed to support the interpretation of DSC and DRS results.

3.2.1. Fourier Transform Infrared Spectroscopy (FTIR)

In order to characterize the polymer, Fourier Transform Infrared Spectroscopy (FTIR) was used to study the structure and complexation of the polymers (Schlessinger, 1995). Infrared spectroscopy was performed on a Nicolet Avator 360 FTIR spectrometer (see **Figure 3.5**), with a 32 scan per sample cycle. For each sample, scans were recorded from 4000 to 400 cm^{-1} with a resolution of 4 cm^{-1}. The spectra obtained show a signal at 1700 cm^{-1} associated with the C=O stretching vibration of carboxylic group, one signal at 2900 cm^{-1} due to CH_2 stretching and the signal at 1125 cm^{-1} associated with C-O-C asymmetric stretching. (Lewis et al., 2001)

Figure 3.5. Picture of Nicolet Avator 360 FTIR spectrometer

The infrared spectrum of a molecule is the result of transitions between two different vibrational energy levels. The vibrational motion of a molecule can mimic the movements observed in the harmonic oscillator (ball system attached to a spring) in the case of chemical bond, it would be a system "two balls in a spring", however differs from this in molecules where are permissible only certain vibrational energy levels, that is, the vibrational energy is quantified and depends on the type of link.

At normal temperatures, the molecules are in their lowest vibrational levels being the harmonic oscillator model a good approximation to the chemical bond.

The absorption of light energy equal to the energy difference between two vibrational energy levels (ΔE_{vib}) causes the vibrational transition, resulting in spectral bands. Light with this energy is situated in the infrared region of the electromagnetic spectrum.

The number of spectral bands that appear in a molecule is related to its number of degrees of freedom and equal to the sum of all necessary coordinates to locate all the atoms of that molecule in space.

The conditions determining the presence in the spectrum of a infrared absorption band are:

-A change due in the dipole moment of the molecule during vibration.

-The band frequency must not conflict with any other fundamental vibration.

-The absorption should be within the infrared region (4000-400 cm^{-1}).

-The intensity of the absorption must be intense enough to be detected.

Table 3.1. Characteristic signals of IR spectrum

Spectral region		**link causing absorption**
Wavelength (μm)	Wavenumber (cm^{-1})	
2.7-3.3	3750-3000	O-H, N-H (elongation)
3.0-3.4	3300-2900	C≡C-H, >C=C<, aromatic-H
3.3-3.7	3000-2700	CH_3 -, $-CH_2$ -, O = C-H
4.2-4.9	2400-2100	C≡C, C≡N
5.3-6.1	1900-1650	C = O (aldehyde, ketone, ester, etc.)
5.9-6.2	1675-1500	>C=C< (Aliphatic and aromatic)
6.8-7.7	1475-1300	C-H (bending)
10.0-15.4	1000-650	C = C-H

Identifying characteristic absorption bands caused by the different functional groups is the basis for the interpretation of the infrared spectra. The eight most important and well defined areas in the preliminary examination of the infrared spectra are summarized in **Table 3.1**.

3.2.2. X-Ray Characterization

Wide angle X-ray Diffraction is a technique used to determine the crystalline structure of polymers. This technique allows us to carry out an analysis of Bragg peaks scattered to wide angles, which implies that they are caused by subnanometer-sized structures. From the diffraction pattern generated is possible to determine the chemical composition or phase composition of the sample, the texture of the sample (preferred alignment of crystallites), the crystallite size and presence of film stress.

Wide-angle X-ray diffraction (WAXS) patterns were recorded at room temperature using a Bruker D8 Advance diffractometer with Cu Kα radiation (λ = 0.1542 nm) operated at 40 kV and 4 mA (**Figure 3.6**). The diffraction scans were collected within the range of 2θ = 5–60° with a 2θ step of 0.024° and 0.5 s per step.

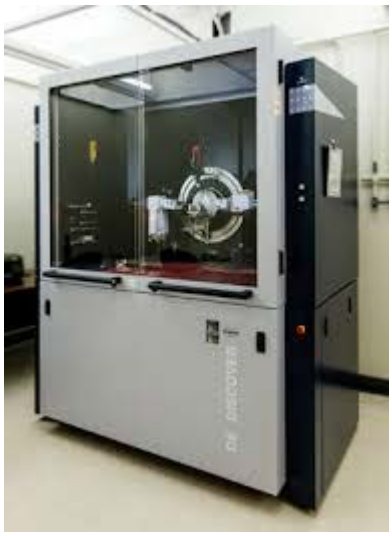

Figure 3.6. Picture of Bruker D8 Advance diffractometer

3.2.3. Differential Scanning Calorimetry (DSC)

DSC is one of the most widely used techniques to characterize the thermal properties of polymers. The DSC measures the difference in the heat flow between a sample and inert reference as a function of temperature and time while the substance and reference are subjected to a controlled temperature program (see **Figure 3.7**). DSC analyzer calculates the heat flow using the temperature difference generated between the sample and the reference. An exothermic heat flow indicates that the heat flows out of the sample, while an endothermic heat flow indicates that the heat flows into the sample. The samples are heated, cooled or held isothermally and the DSC analyzer measures the energy changes that occur at a specific temperature or over a temperature range. DSC can determine different parameters such as the glass transition temperature, the heat capacity jump at the glass transition, melting and crystallization temperatures, heat of fusion, heat of reactions, heat capacity measurements, kinetic evaluation of chemical reactions or of polymer crystallization, thermal degradation, etc. (Gabbott, 2008; Menczel & Bruce Prime, 2009)

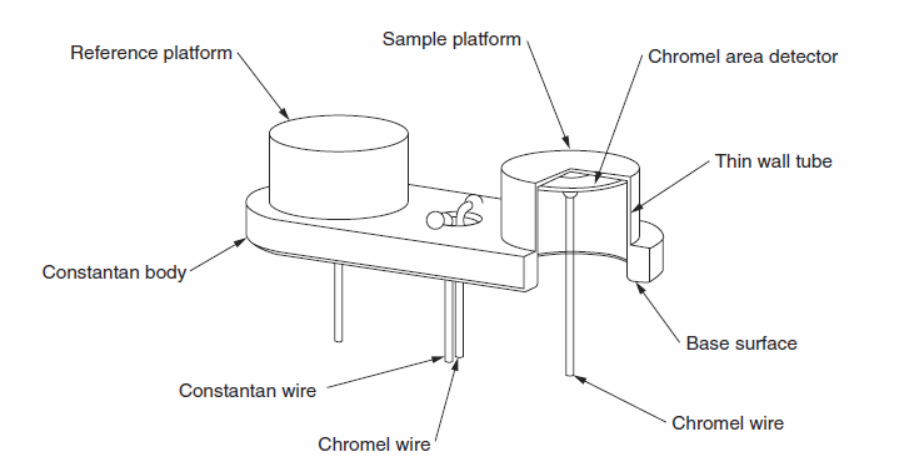

Figure 3.7. Schematic representation of the cell used in the DSC Q20. Picture taken from (Menczel & Bruce Prime, 2009).

A TA Instruments DSC Q-10 with a refrigerated cooling system was employed to analyze all the samples in this thesis (see **Figure 3.8**). The DSC tests were performed under a 50 $ml \cdot min^{-1}$ flow of nitrogen to prevent oxidation. High-purity indium was used to calibrate the cell. The measurements were conducted in crimpled non-hermetic aluminium pans, using an empty crimpled aluminium pan as the reference cell. For a defined peak and high resolution it recommends that the contact surface between the container and the sample is high, which is achieved if the sample is prepared in the form of thin discs, films or fine powder.

The samples were repeatedly stacked into a pan, with a weight of approx. 3.0 mg. Two heating cycles were carried out from 193 K to 423 K at a heating rate of 10 $K \cdot min^{-1}$ under nitrogen atmosphere. The first run was performed in order to remove the thermal history of the sample.

The T_g was evaluated as the intersection of the base line of the glassy region with the tangent to the endotherm in the middle point.

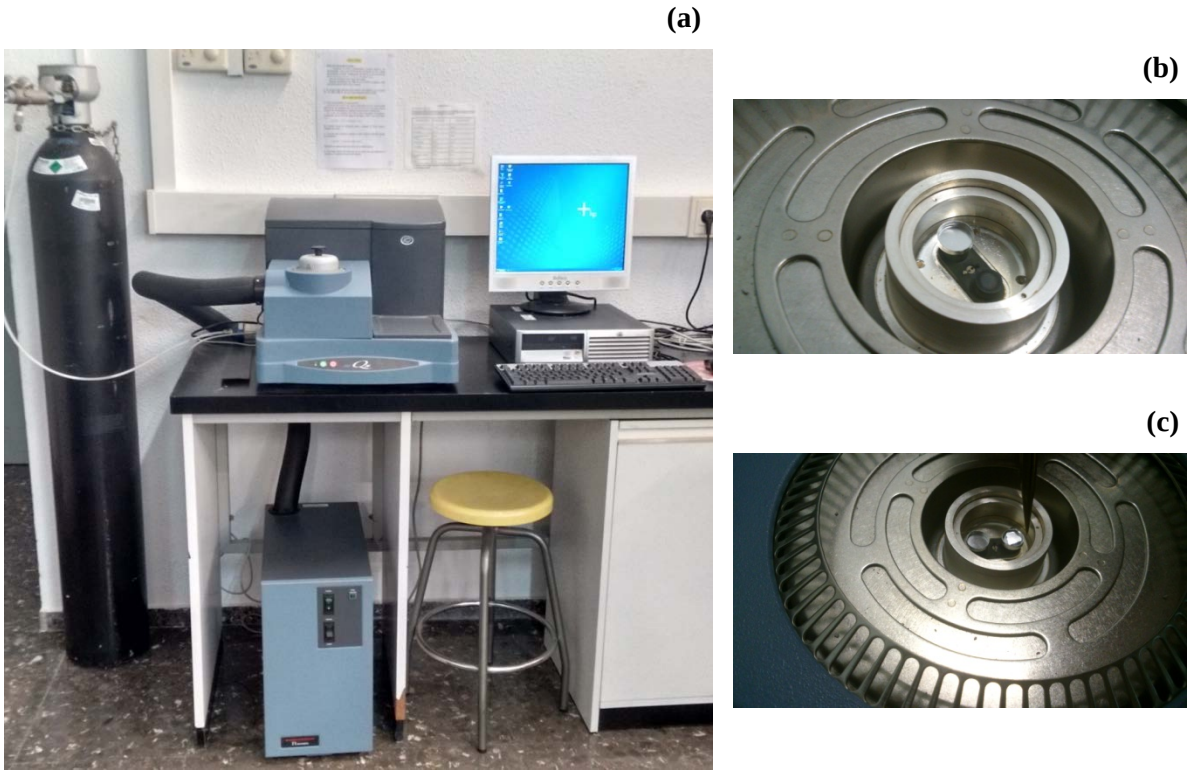

Figure 3.8. (a) Picture of the DSC TA Q-10 Instrument, the refrigerated cooling system and the dry nitrogen gas cylinder. Pictures of the measuring chamber (b) with only the reference pan and (c) with both the reference and the sample pan.

3.2.4. Broadband Dielectric Relaxation Spectroscopy (DRS)

The electrical properties have been related to the physical and chemical characteristics of materials. Dielectric relaxation processes taking place in a material can be

studied from the permittivity of the material in function of frequency and temperature. Such a study is the basis of dielectric relaxation spectroscopy (DRS).

Dielectric Relaxation Spectroscopy is a technique that analyzes the interaction of a sample with a time-dependent electric field. (Kremer & Schönhals, 2003). DRS is based in the application of external perturbation field (electric field) $\vec{E}$ to the sample, so the existing molecular dipole system is perturbed from the equilibrium until the field is removed.

Then, this dipole system returns to the equilibrium, so it is possible to obtain information about the spontaneous fluctuations in the system. The reorientation of dipoles and the translational diffusion of charged particles in this oscillating electric field provide the basis of the analysis based on alternating current (*ac*) dielectric technique. Thus, DRS technique measures changes in different physical properties of a polar material, such as polarization, permittivity and conductivity as a function of temperature and the frequency of the external electric field. The changes in the dielectric constant and polarizability of a polymer are detected during phase transitions (the glass transition, melting or crystallization) and secondary transitions (localized relaxation mechanisms). (Menczel & Bruce Prime, 2009)

The movements of certain parts of polymer are related to the presence of relaxation signals in the DRS spectrum. These signals offer information about the composition, the microstructure and morphology of the sample. The major advantage of DRS technique over other common techniques of thermal analysis is the possibility to obtain results in a broad frequency range (10 μHz-100GHz).

Debye published a study about the dielectric properties of polar liquids (Debye, 1945). In this work, for a non-equilibrium system, he proposed that the relaxation is produced at a rate that increases linearly with the distance to the equilibrium. The model proposed by Debye (see **Table 3.2**), takes into account different initial hypothesis: (i) there is no interaction between dipoles, (ii) only one process leads to the equilibrium, and (iii) all the dipoles can be considered equivalent, *i.e.* all the dipoles are relaxed in average in one single characteristic time. The Debye behavior is not usually observed for complex systems, such as polymers, except for a few exceptions. (Floudas, et al., 1995).

In general, the non-Debye behavior is interpreted as the existence of different relaxing units which relax at different relaxing times and follow an exponential decay. Thus, the material is interpreted as a set of heterogeneous regions and the global decay function is defined by the superposition of all the individual relaxation processes. (Ediger, et al., 1996)

K. S. Cole and R. H. Cole (Cole & Cole, 1941), D.W. Davidson and R.H. Cole (Davidson & Cole, 1950) and S. Havriliak and S. Negami (Havriliak & Negami, 1966) have proposed different modifications to the Debye model summarized in **Table 3.2**. The Havriliak-Negami model is the most used to characterize the relaxation processes.

Table 3.2. Empirical models of $\varepsilon^*(\omega)$ function

MODEL	$\varepsilon^*(\omega)$
DEBYE	$\varepsilon^* = \varepsilon_\infty + \frac{\varepsilon_s - \varepsilon_\infty}{1 + i\omega\tau}$
COLE/COLE	$\varepsilon^*(\omega) = \varepsilon_\infty + \frac{(\varepsilon_s - \varepsilon_\infty)}{1 + (i\omega\tau_{CC})^{a_{CC}}}$
COLE/DAVIDSON	$\varepsilon^*(\omega) = \varepsilon_\infty + \frac{(\varepsilon_s - \varepsilon_\infty)}{[1 + (i\omega\tau_{CD})]^{b_{CD}}}$
HAVRILIAK/NEGAMI	$\varepsilon^*(\omega) = \varepsilon_\infty + \frac{(\varepsilon_s - \varepsilon_\infty)}{\left[1 + (i\omega\tau_{HN})^{a_{HN}}\right]^{b_{HN}}}$

According to the previous models, the peak of $\varepsilon''(\omega)$ function is characterized by (i) the frequency of the maximum, f_{max}, with which the characteristic relaxation time can be calculated as $\tau = 1/2\pi f_{\max}$; (ii) its shape properties as breadth and symmetry, and (iii) the strength of the relaxation, which is given by:

$$\Delta\varepsilon = \varepsilon_s - \varepsilon_\infty = \int_{peak} \varepsilon''(\omega)\, d\ln\omega \tag{3.1}$$

The relaxation strength, $\Delta\varepsilon$, is related to the effective dipolar moment and can be evaluated with the Debye theory of the dielectric relaxation. (Fröhlich, 1958) This theory

was improved by Onsanger-Fröhlich and Kirkwood and they proposed the following relation:

$$\Delta\varepsilon = \varepsilon_s - \varepsilon_\infty = F_{Onsanger} \cdot g \cdot \frac{N \cdot \mu^2}{3 \cdot k_B \cdot T} \tag{3.2}$$

with $F_{Onsager} = \frac{1}{3}\frac{\varepsilon_s\left(\varepsilon_\infty + 2\right)^2}{2\varepsilon_s + \varepsilon_\infty}$; μ is the dipolar moment; N is the number of dipoles that participates in the relaxation; k_B is the Boltzmann constant; and g is the correlation factor, an empirical parameter introduced by Kirkwood as $g = 1 + \left\langle \cos\theta_{ij} \right\rangle$, where θ_{ij} is the angle formed by the dipolar moment i with his neighbor j. This factor g can be obtained using, for example, statistical mechanics.

Therefore, the relaxation strength, which is obtained by the fitting of the experimental data to one of the empirical models previously described, allows obtaining information about the correlation of the dipolar moments. As a consequence, $\Delta\varepsilon$ also allows obtaining information about the correlation between molecules.

In order to measure the dielectric permittivity of a material, the sample is introduced between two electrodes, forming a capacitor. When the sinusoidal electric field $E^*(\omega) = E_0 \cdot \exp(i\omega t)$ is applied to this capacitor, the capacitance C^* increases due to the polarization of the sample. A sinusoidal voltage U is applied at fixed frequency f and the corresponding current I oscillates with the same frequency than that of the voltage. There is a phase shift between the current and the voltage which is described by the phase angle φ (see **Figure 3.9**). The expressions that relate these magnitudes are:

$$U(t) = U_0 \cdot \cos(\omega t) = \mathrm{Re}\left(U^* \exp(i\omega t)\right) \tag{3.3}$$

$$I(t) = I_0 \cdot \cos(\omega t + \varphi) = \mathrm{Re}\left(I^* \exp(i\omega t)\right) \tag{3.4}$$

with $\left|U^*\right| = U_0$ and $I^*(\omega) = I' + iI''$; $I_0 = \sqrt{I'^2 + I''^2}$; $\tan(\varphi) = \frac{I''}{I'}$, where ω is the angular frequency with $\omega = 2\pi f$ and the symbol * refers to the complex character of the quantity.

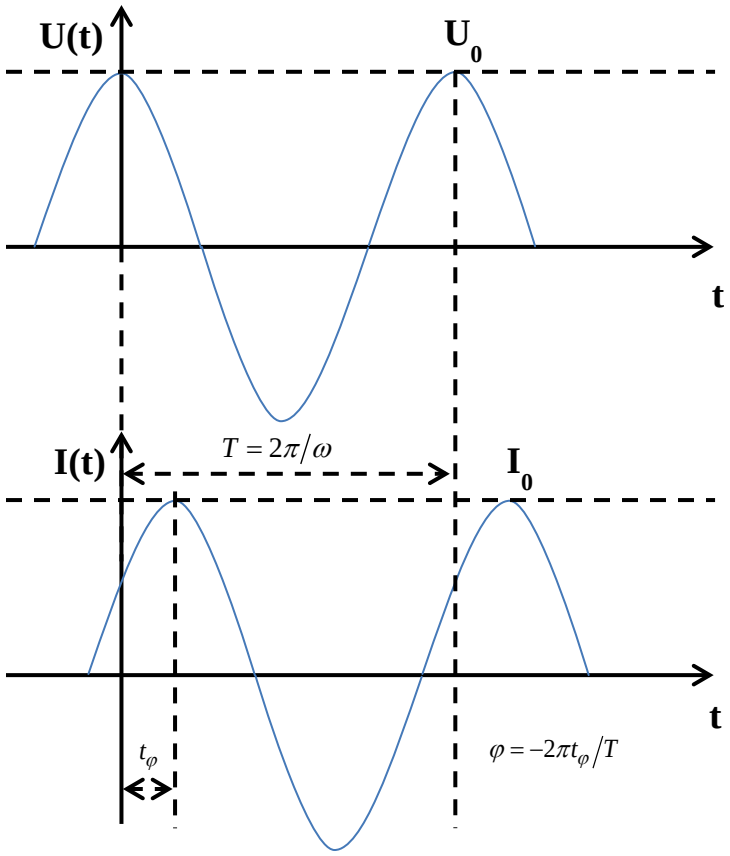

Figure 3.9. Time dependence of the voltage and current functions (T is the period and t_φ is the phase shift time).

The complex dielectric permittivity can be obtained by measuring the complex impedance $Z^*(\omega)$ of the sample:

$$Z^*(\omega) = Z' + iZ'' = \frac{U^*(\omega)}{I^*(\omega)} \tag{3.5}$$

The equation 3.5 is related to the complex dielectric permittivity $\varepsilon^*(\omega)$ and the complex capacitance by:

$$\varepsilon^*(\omega) = \varepsilon'(\omega) - i\varepsilon''(\omega) = \frac{C^*(\omega)}{C_0} = \frac{1}{i\omega Z^*(\omega) C_0} \tag{3.6}$$

where C_0 is the vacuum capacitance of the empty capacitor, ε_0 the permittivity of free space. $\varepsilon'(\omega)$ and $\varepsilon''(\omega)$ are the real and imaginary part of the complex dielectric function.

The experimental measurements depend on the sample geometry placed between the parallel plates of the capacitor with area *A*, being *d* the distance between plates ($A \cdot d$):

$$C_0 = A \cdot \varepsilon_0 / d \tag{3.7}$$

The basic measuring principle is shown in **Figure 3.10**.

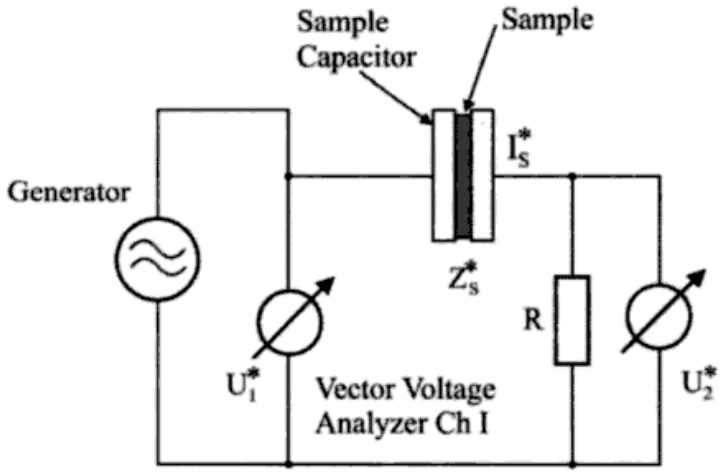

Figure 3.10. Scheme of a Fourier Correlation analyzer. Picture taken from (Kremer & Schönhals, 2003).

All this is implemented in the Broadband Dielectric Spectrometer (Novocontrol Concept 80), from Novocontrol Gmbh (Hundsagen, Germany). Novocontrol instrument is composed of a system (Quatro Cryosystem) to control the temperature over a range from 113 K to 673 K, an impedance analyzer (Alpha Analyzer) to measure impedances from 10^{-5} Hz to 10 MHz and a network impedance analyzer (Agilent 4191A) to measure impedances from 1MHz to 3GHz. The dielectric measurements for low frequency range are based on an impedance bridge, while the high frequency range the complex permittivity was determinated by measuring the reflection coefficient at a particular reference plane.

The temperature controller (Quatro Cryosystem) has four circuits controlling the sample temperature, the gas temperature, the temperature of the liquid nitrogen in the

Dewar and the pressure in the Dewar. The sample temperature is controlled by the heating of the N_2 (gas), achieving an accuracy of ±0.01 K.

The **Figure 3.11** and **Figure 3.12** show two pictures of the system and the **Figure 3.13** shows a scheme of the Novocontrol Temperature Controler used in this thesis.

The isothermal relaxation spectra of the samples were collected by using a Novocontrol Broadband Dielectric Spectrometer (Hundsagen, Germany) consisting of an Alpha analyzer to carry out measurements from $5 \cdot 10^{-2}$ to $3 \cdot 10^{6}$ Hz and an Agilent 4991A RF analyzer for measurements lying in the range 10^{6} to 10^{9} Hz. Both devices were coupled to a Quattro temperature controller, which allows measure with a temperature error of 0.1 K during every single sweep in frequency. The measurements were carried out in inert N_2 atmosphere.

Figure 3.11. Picture of the Novocontrol Concept 80 instrument and the liquid nitrogen Dewar

(a)

(b)

Figure 3.12. View of the Alpha active cell inside the cryostat and the RF extension line out of the cryostat (a). Zoom of the Alpha active (b).

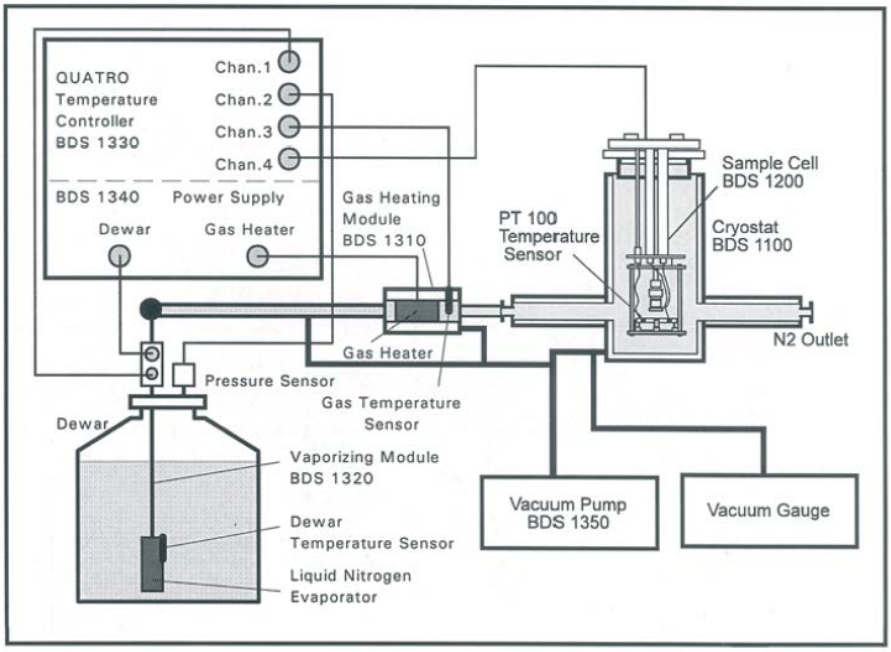

Figure 3.13. Scheme of the Novocontrol Concept 80 instrument.

Molded disc shaped samples of about 0.1 mm thickness and 20 mm and 10 mm diameter were used, respectively, for the low and high frequency analyzers. In order to keep constant the distance between the electrodes in the samples, especially at high temperatures, a silica spacer was utilized. The electrodes used were gold disks of 20 and 10 mm, respectively, for the measurements carried out in the range 10^{-1} - 10^{6} Hz and 10^{6} – 10^{9} Hz.

The measurements of the poly(2,3-dimethoxy benzyl methacrylate), poly(2,5-dimethoxy benzyl methacrylate) and poly(3,4-dimethoxy benzyl methacrylate) samples were performed in a temperature range from 150K to 433K.

The measurements of the CEOEMA and PEOEMA samples were performed in a temperature range from 123K to 423K and 123 K to 343K, respectively.

The experimental uncertainty was better than 5% in all cases.

3.2.5. Dynamic Mechanical Analysis (DMA)

Dynamic Mechanical Analysis (DMA) allows measuring the mechanical properties of a sample as a function of time and temperature. The dynamic mechanical analysis (DMA) measures mechanical stiffness (modulus) and energy absorption by subjecting a specimen to oscillating mechanical stress or strain within the linear viscoelastic region. Thus, DMA imposes a small cyclic strain on a sample and measures the resulting stress response, or equivalently, it imposes a cyclic stress on a sample and measures the resultant strain response. There is a difference between the oscillatory input applied (stress or strain) to the sample response (strain or stress) measured. This difference is represented by the phase angle δ or phase shift between the input and the response (see **Figure 3.14**). (Menczel, et al., 2009). Materials respond to the applied field (stress or strain) by dissipating the input energy in a viscous flow (non-reversible response), by storing the energy elastically (reversible response), or through a combination of both of these two extremes. Thus, since the modulus is stress/strain, the complex modulus (E^*) can be calculated. From E^* and the measurements of δ, the storage modulus (E') and loss modulus (E'') can be calculated:

$$
\begin{aligned}
E^{*} &= stress/strain \\
E' &= E^{*} \cdot \cos\delta \\
E'' &= E^{*} \cdot \sin\delta \\
\tan\delta &= E''/E'
\end{aligned}
\tag{3.8}
$$

E' is the storage modulus and is related to the samples stiffness. E'' is the loss modulus and is the viscous component, which is related to the samples ability to dissipate mechanical energy through molecular motion. The tangent of phase difference, or tan δ is another common parameter that provides information on the relationship between the elastic and inelastic component. These parameters can be calculated as a function of time, temperature, frequency, or amplitude (stress or strain) depending on the application.

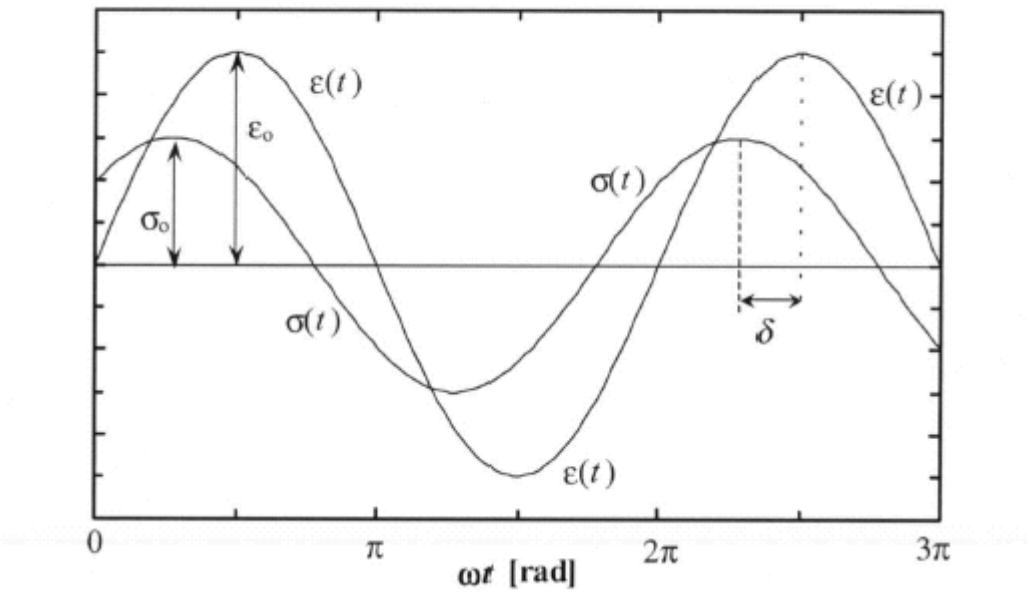

Figure 3.14. Basic principle of DMA technique. In this example, a sinusoidal strain is applied to a sample and the resulting sinusoidal stress is measured.

DMA is used both to study molecular relaxation processes in polymers and to determine inherent mechanical or flow properties as a function of time and temperature. The usual applications of DMA are to study: glass transition, secondary transitions, crystallinity, molecular mass/crosslinking, phase separation, composites, physical and chemical aging, curing of networks, orientation effect of additives. (Menczel, et al., 2009)

DMA is the most similar technique compared to DRS. DMA and DRS results obtained in the same frequency range, are usually compared. Since the DMA has a narrower width of the frequency window available (broadest range 1 mHz- 1 kHz), dielectric analysis can add information on certain physical properties at much higher frequencies.

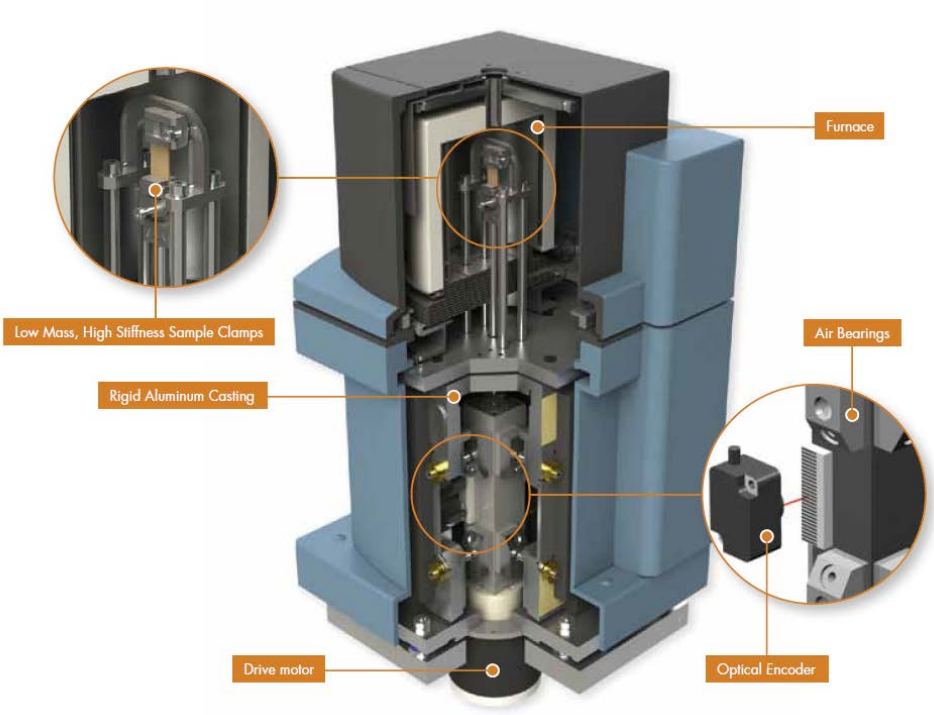

Figure 3.15. Picture of the different parts of a TA Instruments DMA Q800. Taken from TA Instruments.

The Dynamic Mechanical Analyzer used in this thesis was a TA Instruments DMA Q800 (see **Figure 3.15** and **Figure 3.16**). The DMA Q800 is composed of different parts: (i) a non-contact drive motor, used to provide the oscillatory or static force required; (ii) rectangular air bearing slides, which receive directly the force from the non-contact drive motor; (iii) a high resolution linear optical encoder, used to measure displacement on the DMA Q800; (iv) a rigid aluminium casting, within which the drive motor, the air bearing slide assembly with optical encoder and air bearing are all mounted at a controlled temperature; (v) low mass, high stiffness sample clamps, which provide multiple modes of deformation; (vi) a furnace with automated movement, which combined with the Gas Cooling Accessory, provides efficient and precise temperature control.

Among all the different modes of deformation provided by the DMA Q800, the tension mode was the configuration used in this thesis. In this mode, the sample is placed in tension between a fixed and moveable clamp. In oscillation experiments, the instrument uses different methods for applying a static load to prevent buckling and unnecessary creep.

Dynamic mechanical measurements of PEOEMA and CEOEMA were performed by means of a Dynamic Mechanical Analyzer (TA Instruments DMA Q800) calibrated with steel standards. The measurements were carried out in the tension mode on molded probes of $10 \times 7 \times 0.1$ mm over the temperature range from 133K-400K. Before the measurements, samples were dried in vacuum oven at 303K to remove moisture. Measurements were carried out at 1 $K \cdot min^{-1}$ heating rate, at frequencies of 0.3, 1, 3, 10 and 30 Hz. In the case of CEOEMA, the measurements of the Young's modulus in the frequency domain were extended up to 100 Hz.

Figure 3.16. Picture of the TA Instruments DMA Q800 (left) and the tension mode clamp used in the measurements (right).

Chapter 4:

Dipolar and Ionic Relaxations of Polymers Containing Polar Conformationally Versatile Side Chains

Results presented in this Chapter were published in: M. J. Sanchis, M. Carsí, P. Ortiz-Serna, G. Domínguez-Espinosa, and R. Díaz-Calleja, E. Riande,L. Alegría, L. Gargallo, and D. Radiç, *Macromolecules* vol 43, pp. 5723–5733, **2010**

Abstract

This work reports a comparative study of the response of poly(2,3-dimethoxy benzyl methacrylate), poly(2,5-dimethoxy benzyl methacrylate) and poly(3,4-dimethoxy benzyl methacrylate) to electrical perturbation fields over wide frequency and temperature windows with the aim of investigating the influence of the location of the dimethoxy substituents in the phenyl moieties on the relaxation behavior of the polymers. The dielectric loss isotherms above T_g exhibit a blurred relaxation resulting from the overlapping of secondary relaxations with the glass-rubber or α relaxation. At high temperatures and low frequencies, the α relaxation is hidden by the ionic conductive contribution to the dielectric loss. As usual, the real component of the complex dielectric permittivity in the frequency domain increases with decreasing frequency until a plateau is reached corresponding to the glass-rubber (α) relaxation. However, at high temperatures, the real permittivity starts to increase again with decreasing frequency until a second plateau is reached, a process that presumably reflects a distributed Maxwell-Wagner-Sillars relaxation or α′ absorption.

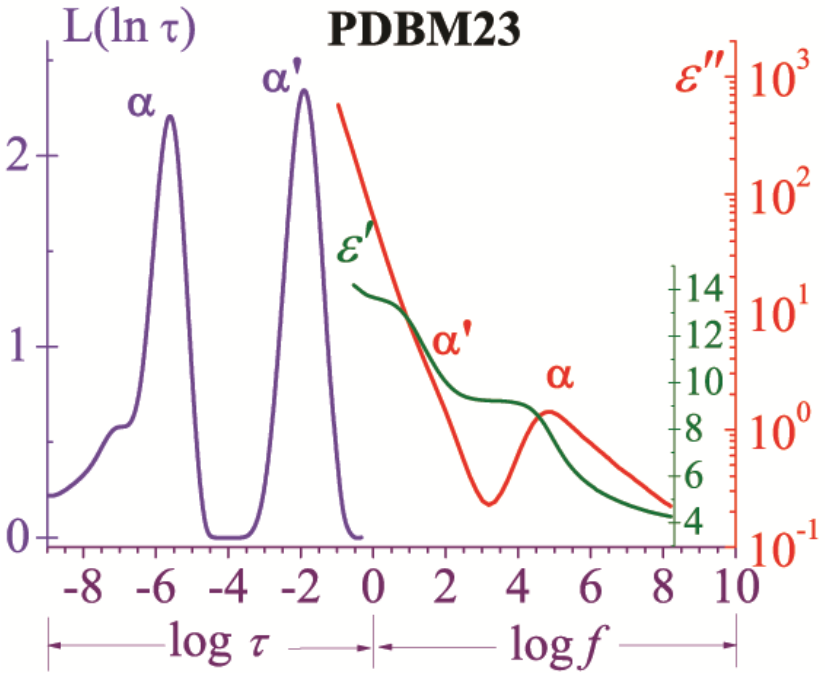

The α and α′ processes appear respectively as asymmetric and symmetric relaxations in the loss electrical modulus isotherms in the frequency domain. To facilitate the deconvolution of the overlapping absorptions, the time retardation spectra of the polymers were computed from the complex dielectric permittivity in the frequency domain using linear programming regularization parameter techniques. The spectra exhibit three secondary absorptions named, in increasing order of time γ′, γ and β followed by the α relaxation. At long times and well separated from the α absorption the α′ relaxation appears. The replacement of the hydrogen of the phenyl group in position 2 by the oxymetyl moiety enhances the dielectric activity of the poly(dimethoxy benzyl methacrylate)s. The temperature dependence of the relaxation times associated with the different relaxations is studied and the molecular origin of the secondary relaxations is qualitatively discussed.

4. Dipolar and ionic relaxations of polymers containing polar conformationally versatile side chains

4.1. Introduction

Owing to the rich dynamics of poly(n-alkyl methacrylate)s, the relaxation processes of a series of these polymers have been studied using different experimental techniques involving dielectric and NMR spectroscopies, dynamic mechanical analysis, dilatometry and modulated calorimetry (Ishida & Yamafuji, 1961; Williams, 1964; McCrum, et al., 1991; Sasabe & Saito, 1968; Ishida, 1969; Kuebler, et al., 1997; Floudas & Stepanek, 1998; Schröter, et al., 1998; Beiner, et al., 2001; Beiner & Huth, 2003) (Gomez, et al., 2001;

Beiner, 2001; Wind, et al., 2003; Wind, et al., 2005; Ngai, et al., 2006; Arbe, et al., 2008; Mpoukouvalas, et al., 2009). Many of these studies have been focused on both the evolution of the relaxation processes of the homologous series of polymethacrylates with side chains length and the crossover region where the α and β relaxations merge to form a single $\alpha\beta$ absorption. (Beiner, 2001; Wind, et al., 2003; Wind, et al., 2005; Ngai, et al., 2006; Williams, 1979; Kremer & Schönhals, 2003; Floudas, 2004) Based on the fact that the β absorption is a thermally activated process whereas the glass-rubber or α relaxation also depends on the free volume, as earlier as in the 1960s Williams (Williams, 1966) studied the influence of pressure on the relaxation behavior of polymers finding that merging of the α and β relaxations to form the $\alpha\beta$ process takes place as temperature is raised, at ambient pressure, and demerging is accomplished by application of a hydrostatic pressure. Recently, Mpoukouvalas et al. (Mpoukouvalas, et al., 2009) derived the canonical equations that describe the effects of the thermodynamic variables *p*, *v*, *T* on the average relaxation times in poly(ethyl metacrylate). These authors found that although both intra- and intermolecular interactions, controlled respectively by temperature and volume, contribute to the α relaxation, it is the temperature the variable that exerts the stronger influence; in fact, without thermal energy relaxations could not occur at all. Moreover, the study of the activated volume reveals that the $\alpha\beta$ relaxation presents the characteristics of a segmental process, and not the characteristics of the local β absorption whose apparent activation volume is much smaller.

Dielectric activity in poly(n-alkyl methacrylate)s arises from motions of the dipole moment associated with the side ester moiety of the repeating units (Gomez, et al., 2001; Williams, 1966; Mpoukouvalas, et al., 2009). The α relaxation is produced by motions of dipole components μ_b rigidly attached to the chain backbone which move when cooperative motions of the backbone occurs. Before the crossover region, the dipoles components μ_s in the flexible side groups move independently or in concert with local motions of the backbone giving rise to the β relaxation. Above coalescence the side groups move in concert with the overall motions of the backbone giving the αβ process. In spite of the non-polarity of the alkyl residues, the dynamics of the chains of poly(n-alkyl methacrylate)s in the liquid rubbery state is strongly dependent on the number of methylene groups of the alkyl residue. A great deal of work has been mainly focused on the crossover region of the dynamic glass transition where the α relaxation and the β mode approach each other. At high temperature, a process appears above the crossover different from the cooperative α relaxation operative below the crossover. In principle, an increase in chains length increases the free volume shifting this scenario to lower frequency and temperature. An important discovery in these studies is the nanophase separation of incompatible main- and side chain parts of the higher members of the poly(n-alkyl methacrylate)s series (Beiner, 2001; Beiner & Huth, 2003). The existence of two dynamic glass transitions for the higher members of the series, the conventional α process and an additional low temperature glass transition $\alpha_{PE.}$, is put in evidence in shear measurements carried out in combination with dielectric, calorimetric and WAXS data (Beiner, 2001). The α_{PE} absorption is related to cooperative

motions of the polyethylene-like side chain parts whereas the α relaxation arises from segmental motions of the chains backbone flanking the nanodomains. The presence of static monodomains in the range 0.5 to 1.5 nm is confirmed by X-Ray Scattering data (Beiner, 2001).

Despite the great amount of work reported in the literature on the dynamics of poly(n-alkyl methacrylate)s, relatively little work deals with the dynamics of poly(methacrylate)s with alcohol residues containing polar moieties in their structure. Recent experiments (Díaz-Calleja, et al., 2000; Domínguez-Espinosa, et al., 2005; Domínguez-Espinosa, et al., 2006; Domínguez-Espinosa, et al., 2006; Díaz-Calleja, et al., 2007; Sanchis, et al., 2008) carried out on the relaxations of poly(benzyl methacylate)s show that changes in the location of polar atoms replacing hydrogen atoms in the phenyl group greatly affects the relaxation behavior of the polymers. For example, the dynamics of poly(benzyl methacylate)s in which hydrogen atoms of the phenyl groups are replaced by halogen atoms is strongly dependent not only on the degree of substitution and nature of the halogen atoms but also on the location of the substitutions. Preliminary studies carried out in our laboratories focused on the response of poly(2,3-dimethoxy benzyl methacrylate) (PDBM23) to electrical perturbation fields showed that the isochrone at 1 Hz of the real component ε' of the complex dielectric permittivity ε^*, apparently exhibits two maxima centered respectively at 318K and 373K. The two maxima might be associated with the existence of polar and non-polar nanodomains formed, respectively, by polar side groups of the chains and the nonpolar backbone. Another possibility is that the lower temperature maximum corresponds to the glass-rubber relaxation whereas the second one could be

attributed to charge transport. It must be emphasized that as a consequence of the conductivity response, the high temperature maximum observed in the isochrone ε' is not detected in the dielectric loss isotherms. This at first sight anomalous dielectric behavior prompted us to study in detail the relaxation behavior of PDBM23 paying special attention to the processes of charge transport detected at low frequencies and high temperatures. Other objective of this work was to carry out a comparative study of the dielectric behavior of poly(2,3-dimethoxy benzyl methacrylate) with that of poly(2,5-dimethoxy benzyl methacrylate) (PDBM25) and poly(3,4-dimethoxy benzyl methacrylate) (PDBM34) with the aim of assessing how the locations of the oxymethylene moieties affect dipolar relaxations and ionic transport.

4.2. Results and discussion

4.2.1. Differential Scanning Calorimetry (DSC)

The glass transition temperature was measured with a TA DSC-Q10 apparatus at a heating rate of $10K \cdot min^{-1}$, under nitrogen atmosphere, and the pertinent thermograms obtained in the second run are shown in **Figure 4.1**. The glass transition temperatures of PDBM23, PDBM25 and PDBM34, estimated as the temperature at the midpoint of the endotherms, were 320, 310 and 330K, respectively.

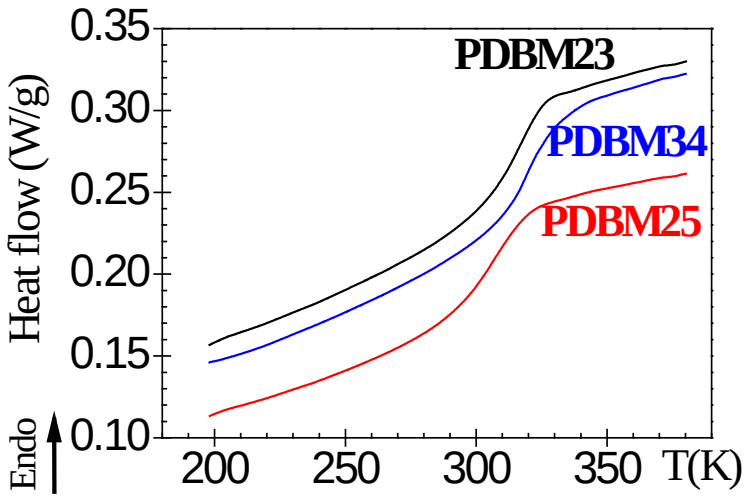

Figure 4.1. DSC thermograms corresponding to the PDBM23, PDBM25 and PDBMA34.

4.2.2. Dielectric Relaxation Spectroscopy Characterization

Isochrones showing the variation of the real component ε' of the dielectric complex permittivity ε^* of the polymers with temperature, at several frequencies, are shown in **Figure 4.2**. All the isochrones display the same pattern in the sense that they present two steps, a low temperature step associated with the glass rubber or α relaxation followed by a second step at higher temperature, named α′ absorption, whose nature will be discussed later. The isochrones corresponding to the dielectric loss ε'', for details see **Figure 4.3**, present an ostensible α relaxation followed by a rather sharp increase of the loss as temperature increases as a result of the strong contribution of the conductivity to ε''. It is worth noting that in the low temperature side of the α relaxation a shoulder appears corresponding to a secondary relaxation, presumably the β process associated with side chain motions.

Isotherms for ε' in the frequency domain corresponding to PDBM23, PDBM25 and PDBM34, at several temperatures, are shown in **Figure 4.4**. Let us focus on the isotherms corresponding to PDBM23. As usual, ε' increases as frequency decreases reaching a plateau corresponding to the relaxed dipoles. However, after the plateau and as frequency decreases further, ε' increases again reaching a second plateau. The two rather steeply changes in the values of ε' correspond in the order of decreasing frequency to the α and α' relaxations detected in the isochrones of ε' in **Figure 4.2**. The isotherms of PDBM25 and PDBM34 present the same pattern as those of PDBM23, though to reach the second plateau would require data obtained at lower frequencies than those used in this study. In order to better visualization of this process, Thermally Stimulated Depolarization Current Spectroscopy (TSDC) was used. The frequency equivalent of this technique is 10^{-3} Hz. In **Figure 4.5** is shown the spectra obtained for PDBM25.

The dielectric loss isotherms in the frequency domain, shown in **Figure 4.6**, do not present well-defined relaxations in the high frequencies region. However, they exhibit an ostensible relaxation associated with the glass rubber relaxation, which at higher temperatures and lower frequencies is apparently hidden by the conductive contribution. Better definitions of the loss peaks are obtained by plotting the dielectric results in terms of the dielectric loss modulus, M''. The isotherms of M'' in the frequency domain, shown in **Figure 4.7**, exhibit two ostensible peaks corresponding in decreasing order of frequency to the α and α' relaxations. The isotherms at different temperatures for M', the real component of the complex dielectric modulus M^* of the polymers, are shown in **Figure 4.8**. In all the

cases the modulus increases with frequency reaching a plateau corresponding to the α relaxation and then the modulus increases again until a second plateau corresponding to the α′relaxation process.

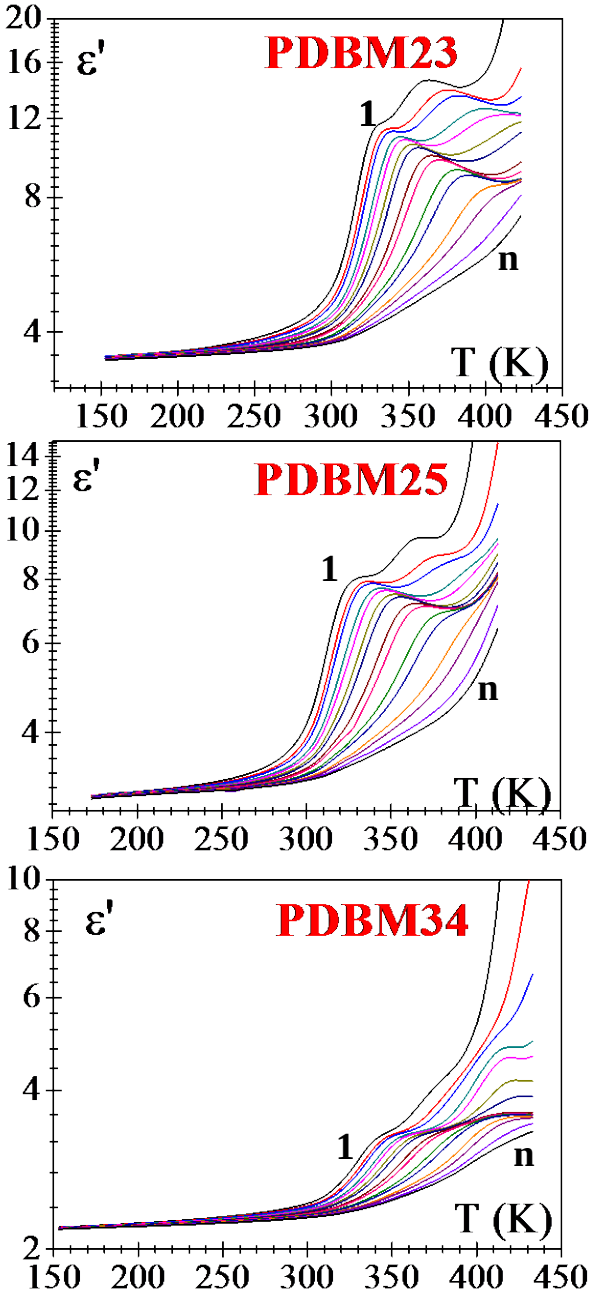

Figure 4.2. The dielectric permittivity as a function of temperature for PDBM23, PDBM25 and PDBM34 at several frequencies (1……n): 1.09 × 10^{-1}, 5.37× 10^{-1}, 1.19, 5.86, 1.3×10^{1}, 4.29×10^{1}, 9.52×10^{1}, 4.69×10^{2}, 1.04×10^{3}, 5.12×10^{3}, 1.13×10^{4}, 5.58×10^{4}, 1.24×10^{5}, 4.09×10^{5} Hz

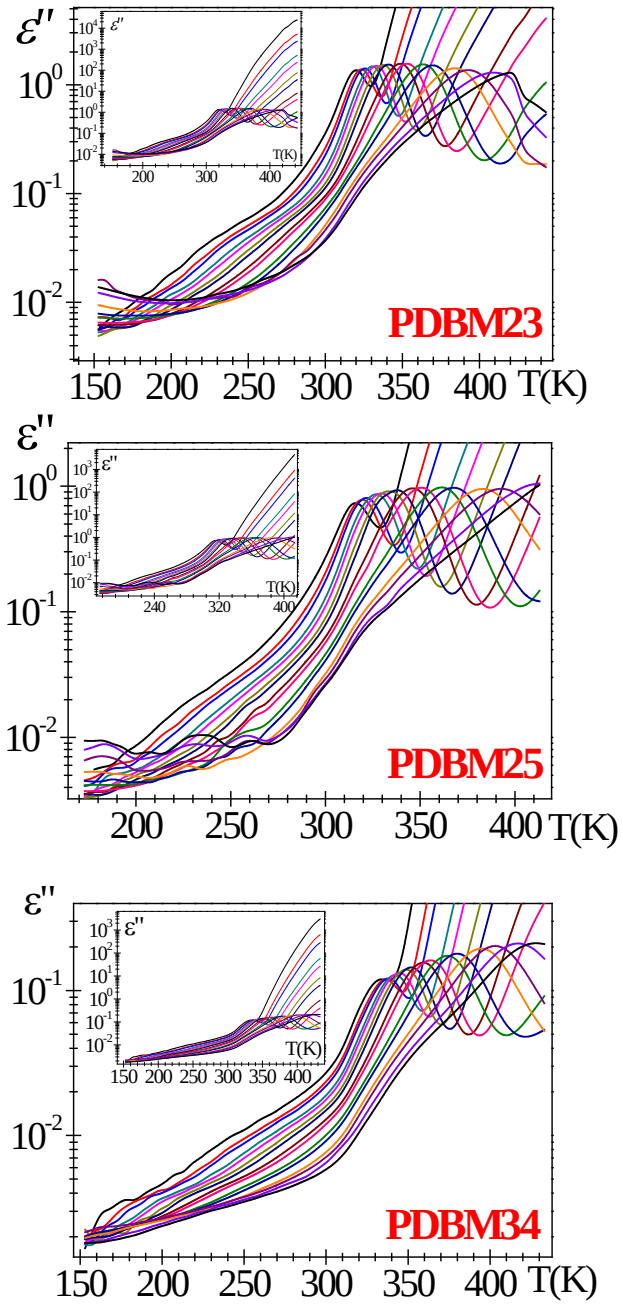

Figure 4.3. The dielectric loss as a function of temperature of PDBM23, PDBM25 and PDBM34 at several frequencies (1.09×10^{-1}, 5.37×10^{-1}, 1.19, 5.86, 1.3×10^{1}, 4.29×10^{1}, 9.52×10^{1}, 4.69×10^{2}, 1.04×10^{3}, 5.12×10^{3}, 1.13×10^{4}, 5.58×10^{4}, 1.24×10^{5}, 4.09×10^{5} Hz).

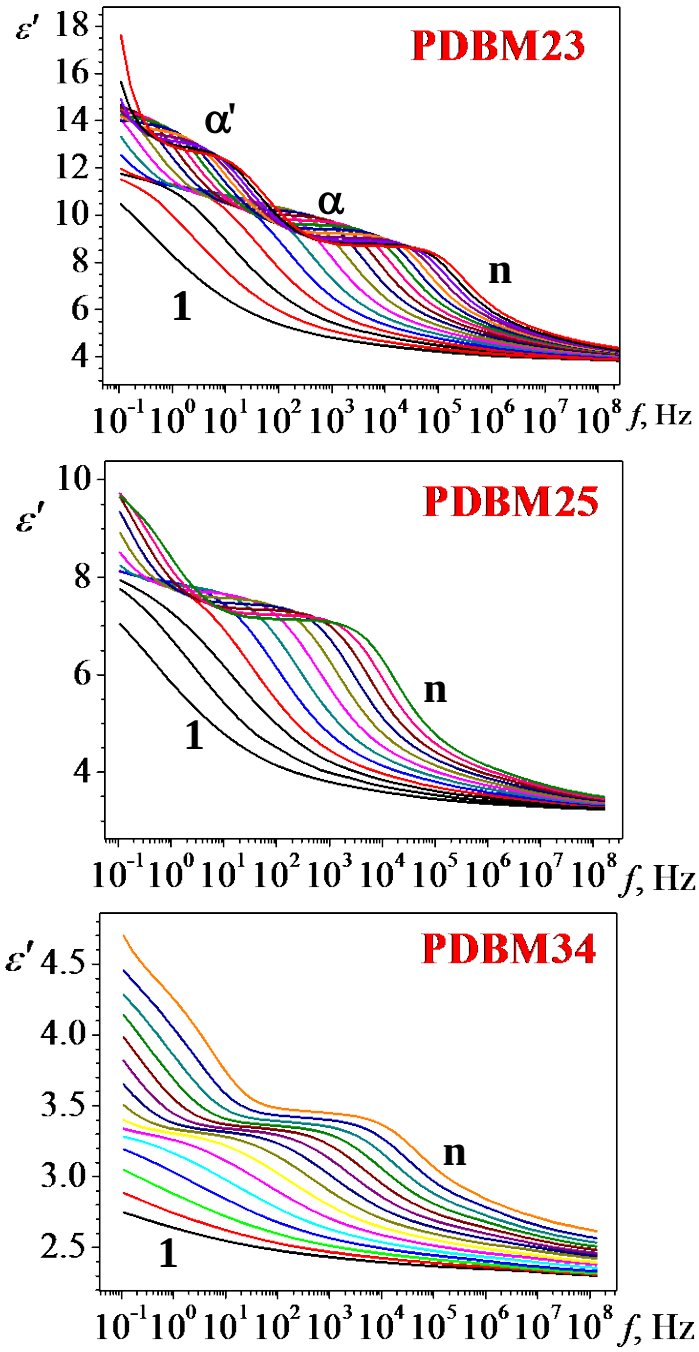

Figure 4.4. The dielectric permittivity in the frequency domain for PDBM23, PDBM25 and PDBM34 in the temperature ranges (1……n) 323 – 408 K, 318 - 373 K and 323 – 393 K, respectively, at 5 K steps

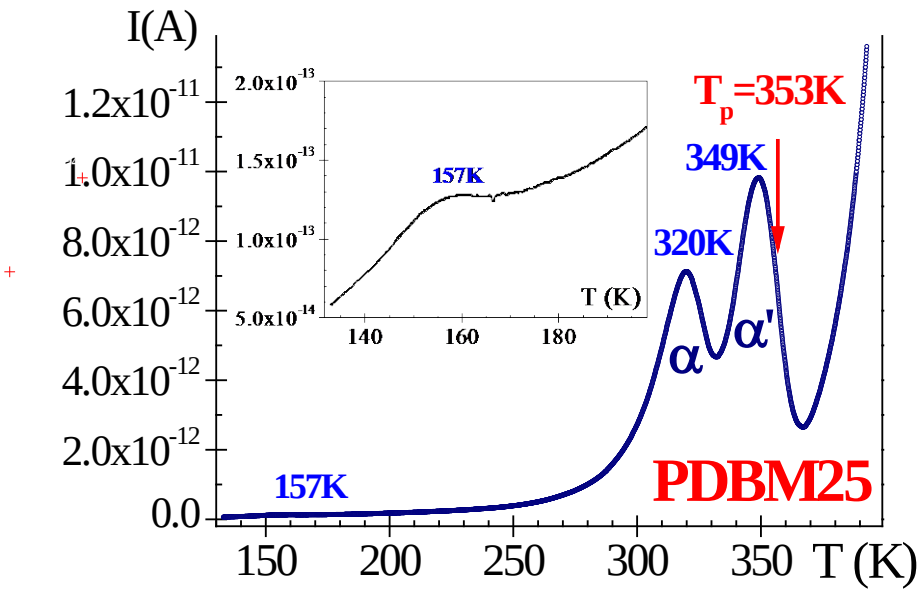

Figure 4.5. TSDC spectra of PDBM25.

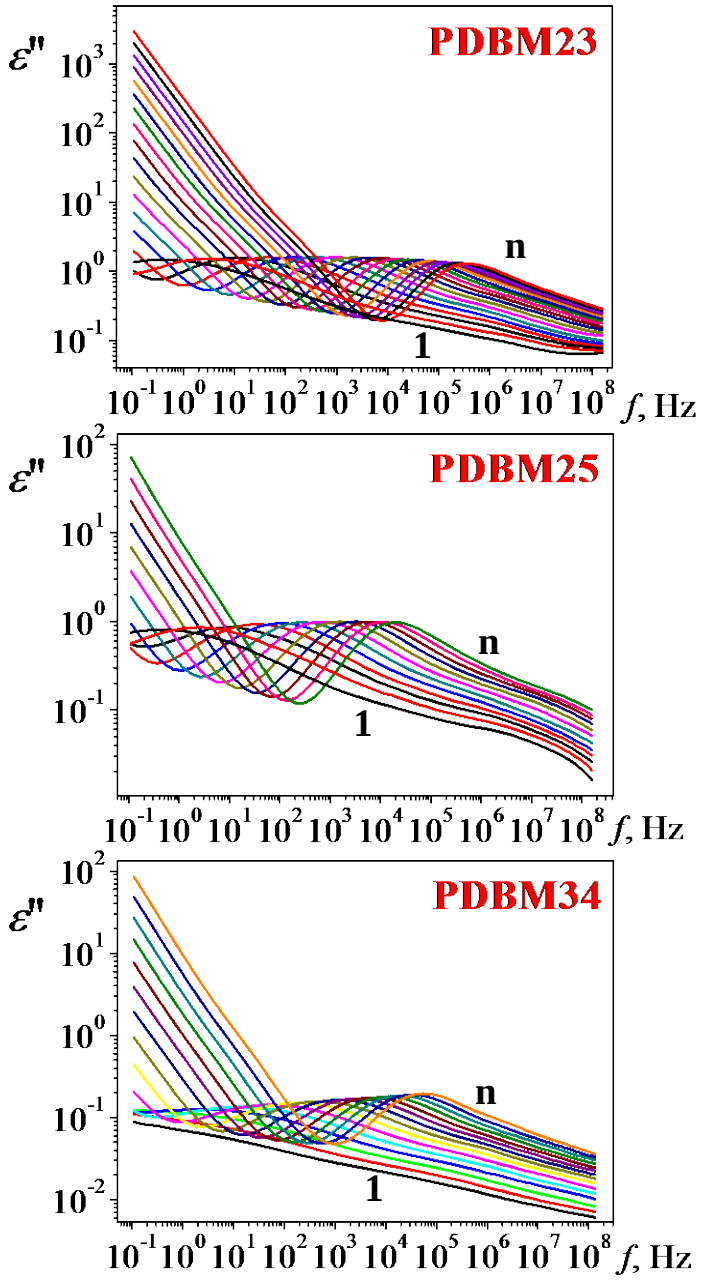

Figure 4.6. The dielectric loss in the frequency domain for PDBM23, PDBM25 and PDBM34 in the temperature ranges (1……n) 323 – 408 K, 318 - 373 K and 323 – 393 K, respectively, at 5 K steps.

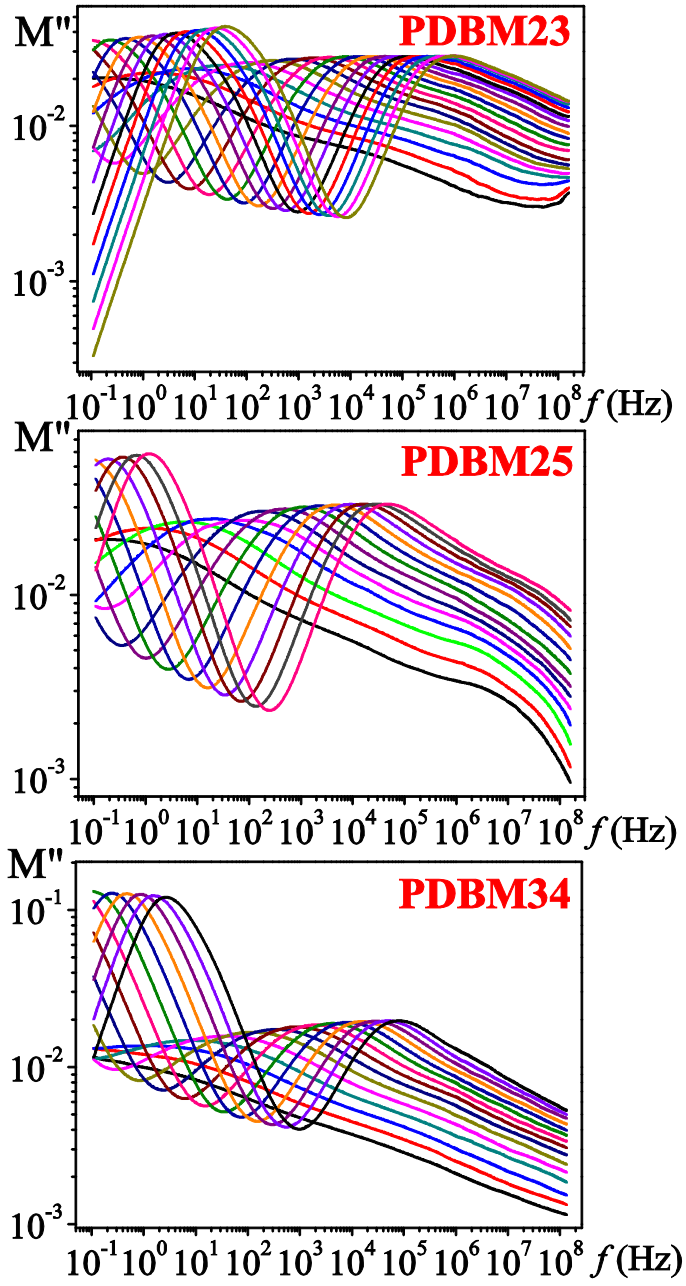

Figure 4.7. The dielectric loss modulus *M″* in the frequency domain for PDBM23, PDBM25 and PDBM34 in the temperature ranges (1……n) 323 – 408 K, 318 - 373 K and 323 – 393 K, respectively, at 5 K steps.

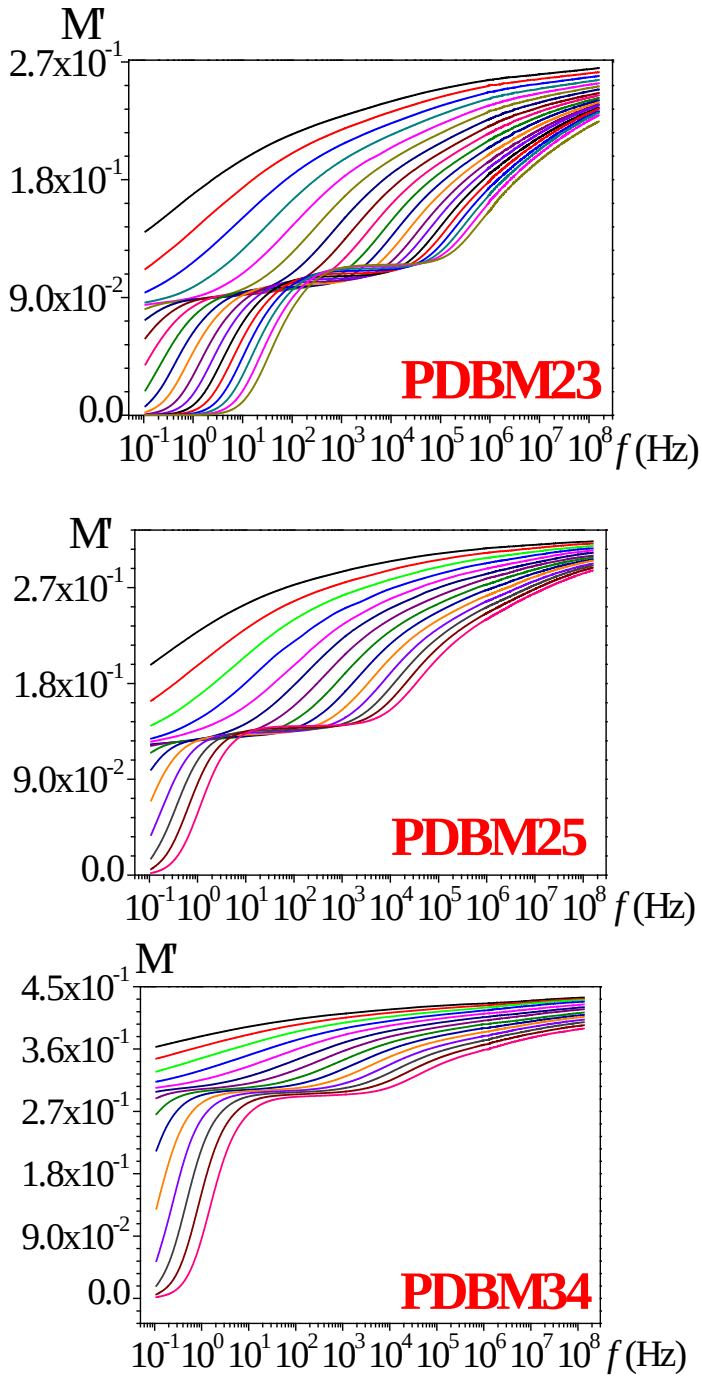

Figure 4.8. The real component of the complex modulus *M** in the frequency domain of PDBM23, PDBM25 and PDBM34 in the temperature ranges 323 – 408 K, 318 - 373 K and 323 – 393 K, respectively, at 5 K steps.

4.2.3. Retardation Spectra

The isotherms for ε' in frequency domain corresponding to PDBM23 clearly show the presence of two ostensible relaxations at $T > T_g$ so that $\varepsilon^*(\omega)$ can be written as

$$\varepsilon^*(\omega) = \varepsilon_\infty + \sum_{\substack{i,\mathrm{second.}\\ absorp.}} \frac{\varepsilon_{0i} - \varepsilon_{\infty i}}{1+(j\omega\tau_{si})^{a_{si}}} + \frac{\varepsilon_{0\alpha} - \varepsilon_{\infty\alpha}}{\left[1+(j\omega\tau_{\alpha})^{a_\alpha}\right]^{b_\alpha}} + \frac{\varepsilon_{0\alpha'} - \varepsilon_{\infty\alpha'}}{1+(j\omega\tau_{\alpha'})^{a_{\alpha'}}} - j\frac{\sigma}{\varepsilon_f \omega} \qquad (4.1)$$

where ε_f (= 8.854 pF·m^{-1}) is the free space dielectric permittivity and σ is the ionic conductivity arising from interfacial polymer-electrode phenomena. The subscript *i* in equation (4.1) refers to secondary absorptions (β, γ,..) not well defined in the dielectric loss spectra whereas the subscripts 0 and ∞ mean, respectively, relaxed and unrelaxed dielectric permittivities. The shape parameters *a* and *b* are related, respectively, to the departure of the complex ε'' *vs* ε' plot from a semi-circumference, at low frequencies, and to the skewness of the plot along a straight line, at high frequencies (Havriliak & Havriliak, 1997). Owing to the symmetry of the secondary absorptions and that of the α′ relaxation observed in the M'' curves in the frequency domain, the complex plots are arcs so that the shape parameter *b* is the unit. For a Debye type relaxation $a = b = 1$. Deconvolutions of overlapping relaxations are usually carried out utilizing equation (4.1). However, relaxations are better defined in the retardation spectra than in the dielectric loss spectra in the frequency domain The ability to resolve two processes with comparable retardation times is higher in the spectrum than in the imaginary part of the permittivity curves because the peaks associated with each process are narrower in the former. This extreme can easily be understood if we consider that the Debye relaxation in the time domain is a Dirac delta

function, whereas the half width of the relaxation in the frequency domain is slightly greater than one decade. As a result, time retardation spectra facilitate deconvolutions of overlapping relaxations. The complex dielectric permittivity can be expressed in terms of the retardation spectra by (McCrum, et al., 1991; Riande & Díaz-Calleja, 2004)

$$\varepsilon^*(\omega)-\varepsilon_\infty=\left(\varepsilon_0-\varepsilon_\infty\right)\int_{-\infty}^{\infty}L(\ln\tau)\frac{1}{1+j\omega\tau}d\ln\tau+\frac{\sigma}{j\omega\varepsilon_f} \tag{4.2}$$

where L is the normalized time retardation spectrum. For a frequency ω_i the retardation spectrum can be written in discrete form and equation (4.2) can approximately be written as

$$\varepsilon^*(\omega_i)-\varepsilon_\infty \cong \sum_{k=1}^{N}R^*_{ik}L_k+\frac{\sigma}{j\omega_i\varepsilon_f} \tag{4.3}$$

where

$$R^*_{ik}=\frac{\Delta\ln\tau_k}{1+j\omega_i\tau_k} \tag{4.4}$$

and $L_k=\left(\varepsilon_0-\varepsilon_\infty\right)L(ln\,\tau_k)$. The computation of the retardation spectra of the polymers can be accomplished by minimization of the error function (Dominguez-Espinosa, et al., 2008)

$$E=\sum_{i=1}^{N}\left\{\varepsilon(\omega_i)-\sum_{k=1}^{N'}R^*_{ik}\,L_k-\frac{\sigma}{j\omega\varepsilon_f}-\varepsilon_\infty\right\}^2 \tag{4.5}$$

Owing to the ill conditioned behavior of the error function, the Tikhonov (Press, et al., 1992; Morozov, 1984)[33] regularization technique was used to minimize *E*. The pertinent steps to carry out the minimization that leads to the calculation of the retardation spectrum were described in detail elsewhere (Dominguez-Espinosa, et al., 2008).

The retardation spectrum of PDBM23, shown in **Figure 4.9**, exhibits two ostensible peaks corresponding in increasing order of time to the α and α′ relaxations. In addition three secondary absorptions can be detected at short times called in order of decreasing time β, γ and γ′. The retardation spectra are strongly sensitive to the location of the dimethoxy moieties in the phenyl group of the alcohol residue as the retardation spectra of PDBM23, PDBM25 and PDBM34, presented at a single temperature in **Figure 4.10**, show. It can be seen that the intensities of the α and α′ relaxation peaks increase in the order PDBM23 > PDBM25 > PDBM34.

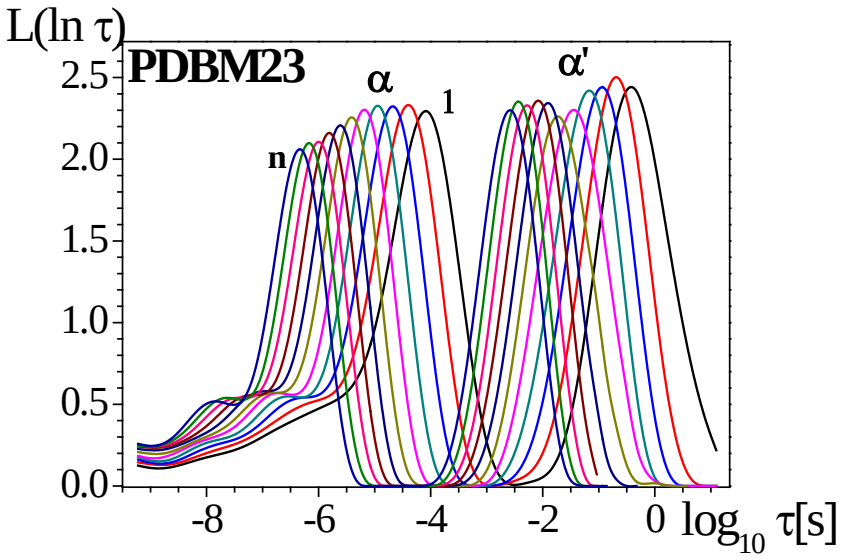

Figure 4.9. Retardation spectra for PDBM23 in the temperature range (1……n) 358 - 408 K, at 5 K steps.

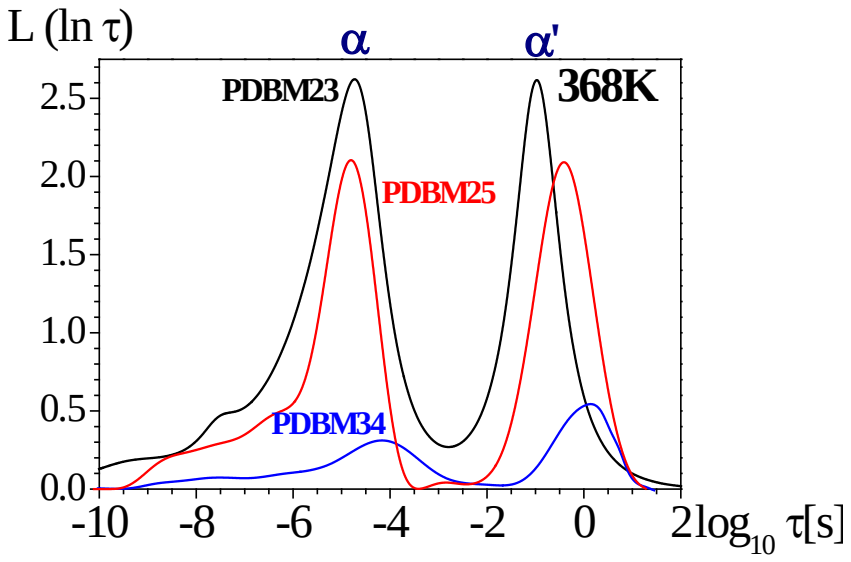

Figure 4.10. Retardation spectra for PDBM25, PDBM23, and PDBM34 at 368 K.

Deconvolutions of the retardation spectra can be carried out by using the analytical retardation spectra for HN type equations given by (Riande & Díaz-Calleja, 2004; Havriliak & Negami, 1966; Zorn, 1999)

$$L_i(\ln\tau)=\frac{1}{\pi}\frac{\Delta\varepsilon_i(\tau/\tau_{HN;i})^{a_i b_i}\sin b_i\theta_i}{\left[(\tau/\tau_{HN;i})^{2a_i}+2(\tau/\tau_{HN;i})^{a_i}\cos a_i\pi+1\right]^{b_i/2}} \qquad (4.6)$$

In this expression, $0 < a_i\, b_i \leq 1$ and θ_i is given by

$$\theta_i=\arctan\left[\frac{\sin\pi a_i}{(\tau/\tau_{HN;i})^{a_i}+\cos\pi a_i}\right]+c \qquad (4.7)$$

where c is zero or π if the argument of the arctan function is, respectively, positive or negative (Kremer & Schönhals, 2003) and i denotes de relaxation (γ′, γ, β, α, α′). The parameter $\Delta\varepsilon_i = \varepsilon_{0i} - \varepsilon_{\infty i}$ is the strength of the relaxation i. Owing to the fact that the degree of overlapping between α and α' relaxations is rather small at most temperatures, the α′ relaxation was deconvoluted from the spectrum first. In an initial step, the fitting procedure was carried out using partial parts of the retardation spectrum as briefly described below. The high time side of the α relaxation was used as reference for the deconvolution of this process; once separated the α relaxation, the high time side of the spectrum was used to deconvolute the β relaxation and so on. Once obtained the starting parameters, we proceeded to deconvolute the global spectrum delimiting, in the fitting procedure, the values of HN parameters for each relaxation in a range that includes the preliminary adjustment parameters, with the condition that $0 < a_i,\ b_i \leq 1$ and the sum of the dielectric strengths of the relaxations is equal to the global dielectric strength calculated by means of

the expression $\varepsilon_0 - \varepsilon_\infty = \int_{-\infty}^{\infty} L(\ln\tau)\, d\ln\tau$. Finally the deconvolutions were refined by slightly changing the parameters until the difference between the original spectrum and that obtained from the deconvolutions using the expression $L(\ln\tau) = \sum_{i=1}^{4} L_i(\ln\tau)$ is lower than 2% for any retardation time.

The retardation spectra for the relaxations γ′, γ, β, α and α′ of PDBM23, PDBM25 and PDBM34 at several temperatures, are presented in **Figure 4.11, Figure 4.12 and Figure 4.13**. As an example, the deconvoluted spectrum of these relaxations at 363K for PDBM25 is shown in **Figure 4.14**.

An inspection of **Figure 4.11** shows that the α and β relaxations coexist in the range of temperatures T_g < T < 365K; then the β process is apparently swallowed by the α relaxation forming a single relaxation. The strength of the relaxations can directly be obtained from the deconvoluted spectra by means of the following expression

$$\varepsilon_{0i} - \varepsilon_{\infty i} = \int_{-\infty}^{\infty} L_i(\ln\tau)\, d\ln\tau \qquad (4.8)$$

where i denotes the type of relaxation (γ′, γ, β, α and α′). Values of the strength for PDBM23, PDBM25 and PDBM34 are plotted as a function of the reciprocal of temperature in **Figure 4.15**. The strength of the α relaxation of PDBM23 decreases with increasing temperatures whereas that of the β increases until a temperature is reached at which both relaxations have the same strength. At this temperature both relaxations form a single absorption whose strength rises steeply and then decreases as temperature increases. The

evolution of the strengths of the α and β relaxations with temperature for PDBM34 is similar to that of PDBM23 in the sense that both processes form a single absorption at the same temperature, though the strength of the β relaxation at this temperature is lower than that of the α. For PDBM25, the strength of the α relaxation decreases with increasing temperature whereas that of the β increases becoming equal to that of the α at 373K. The strength of the α′ relaxation of PDBM23 decreases with increasing temperature varying from 4.27 at 358 K to 3.09 at 408 K. The α′ relaxations of PDBM25 and PDBM34 are only observable at a reduced number of temperatures. The data available indicate that the strength of the α′ relaxation of PDBM25 is somewhat smaller than that of PDBM23, whereas that of PDBM34 is significantly smaller than the strength of the α′ relaxation of PDBM23. The strengths of the γ and γ′ relaxations are significantly lower than those of the β process, independently of the polymer considered. The total dielectric strength of the dipolar processes calculated from the retardation spectra follows the trends $\Delta\varepsilon$(PDBM23) ≥ $\Delta\varepsilon$(PDBM25) > $\Delta\varepsilon$(PDBM34), in agreement with the results of **Figure 4.4**.

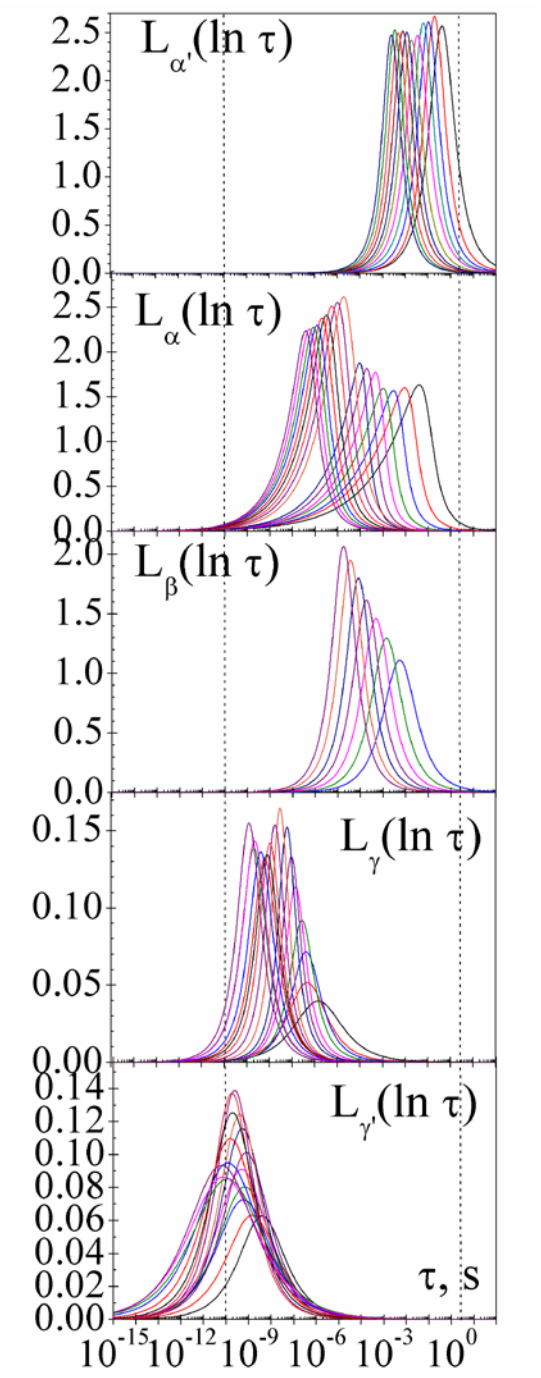

Figure 4.11. Retardation spectra for PDBM23 corresponding to α′, α, β, γ , and γ′ processes (318 - 408 K, at 5 K steps). The dashed lines indicate that out of the limits the values of $L_i(\ln \tau)$ should be regarded as approximate.

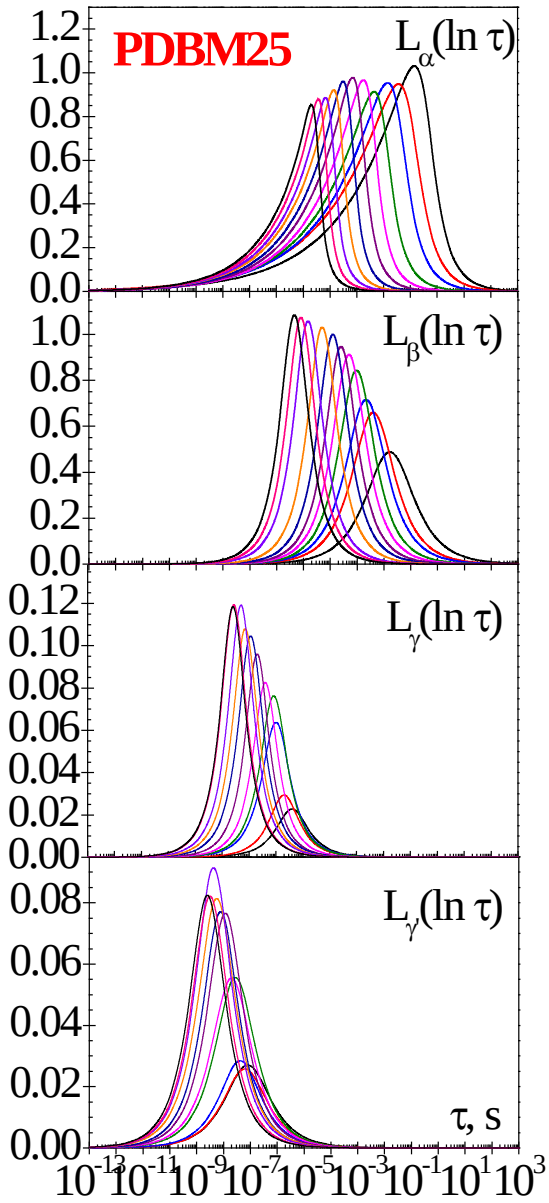

Figure 4.12. Retardation Spectra of PDBM25 corresponding to α, β, γ, and γ′ processes (318 - 373 K, at 5 K steps).

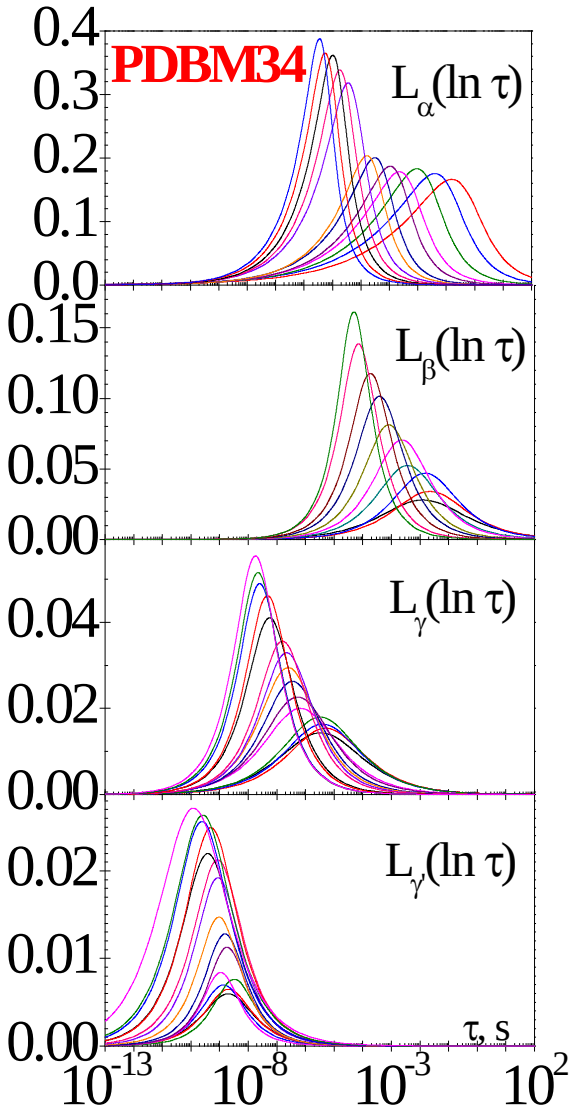

Figure 4.13. Retardation Spectra of PDBM34 corresponding to α, β, γ, and γ′ processes (323 - 393 K, at 5 K steps).

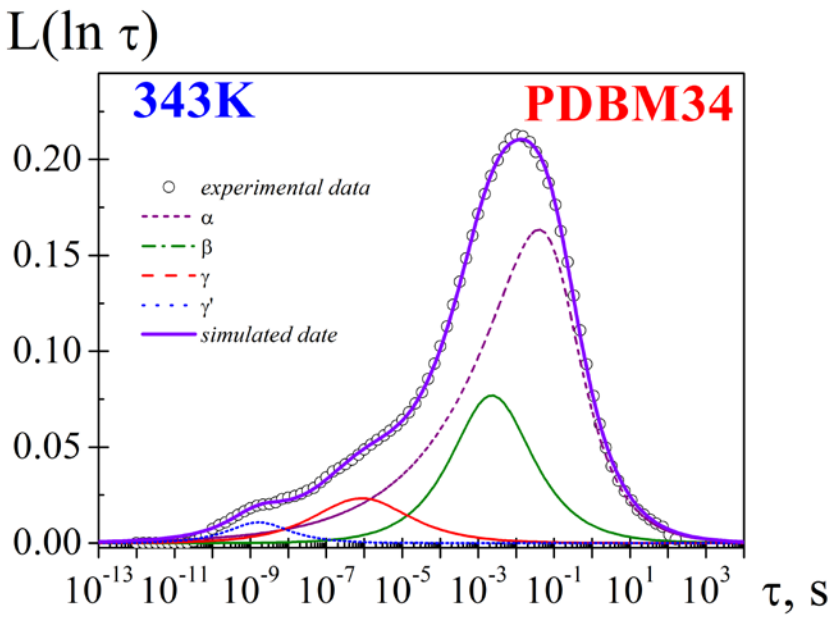

Figure 4.14. Deconvolution of the retardation Spectra of PDBM34 at 343K.

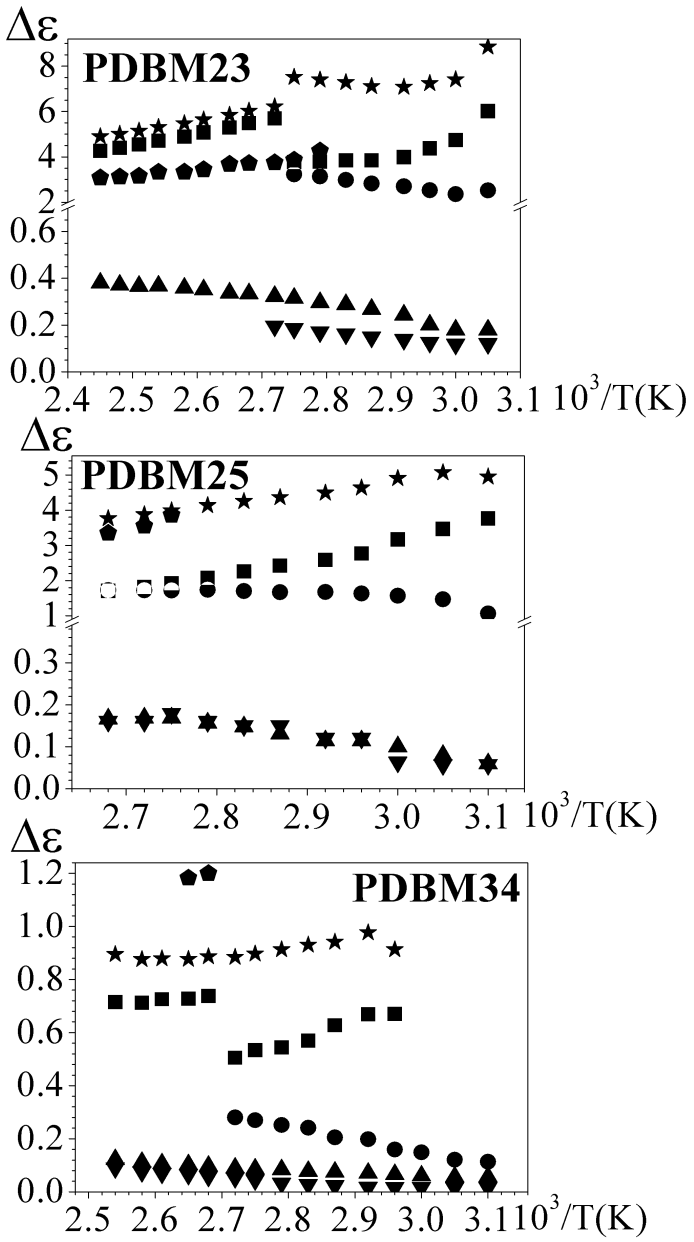

Figure 4.15. Temperature dependence of the strengths of the α′ (pentagons), α (squares), β(circles). γ (up triangles) and γ′ (down triangles) relaxations. Star symbols represent the total dipolar dielectric strength.

The shape parameters for the retardation spectra associated with the relaxations are shown as a function of temperature in **Figure 4.16**. The value of *a* for the α relaxation, higher than that for the β process, moderately increases with increasing temperature. However, the parameter *a* for PDBM23 steeply decreases in the vicinity of 368K and then slightly increases as temperature goes up. This parameter also increases with temperature for the β and γ relaxations, though for this latter process *a* undergoes a moderate decrease as temperature increases. The values of *a* do not follow a definite trend for the γ′ absorption. For PDBM23, the *b* parameter related with the skewness of the ε'' vs ε' plot in the α relaxation rises steeply in the vicinity of 368K; below and above this temperature, *b* slightly increases with temperature. For PDBM25, the value of *b* is rather low and nearly independent on temperature, whereas the variation of *b* with temperature for PDBM34 follows similar trends as for PDBM25, though the change in the vicinity of 368 K is somewhat smaller. Finally, the plots of **Figure 4.16** show that the shape parameter *b* for the α′ relaxation lies in the vicinity of the unit in the whole temperature range suggesting that the absorption in the retardation spectra is symmetric.

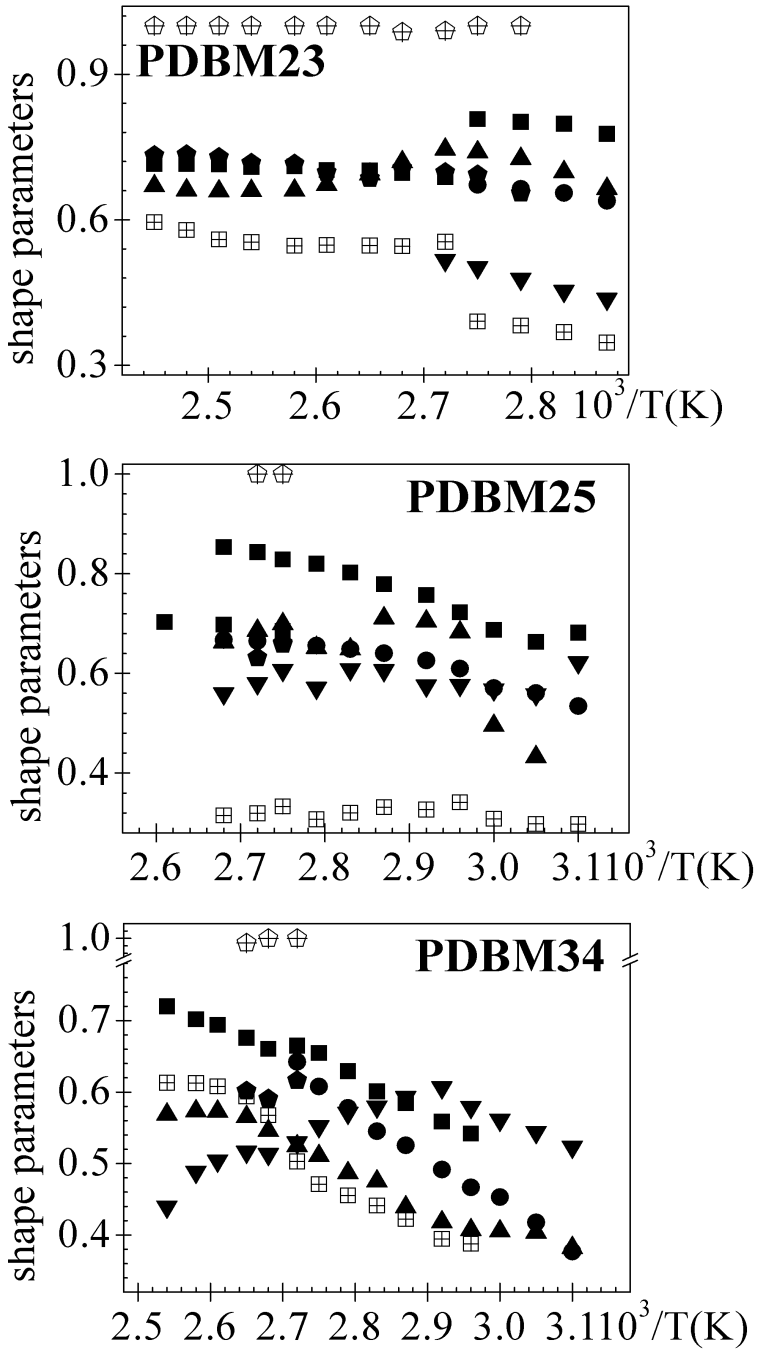

Figure 4.16. Temperature dependence of the shape parameters (a_k, b_k) for the α′ (⬟,⊕), α (■,⊞), β (●), γ (▲) and γ′ (▼)relaxations for PDBM23, PDBM25, and PDBM34.

4.2.4. Temperature Dependence of Retardation Times

Arrhenius plots for the secondary absorptions and the α relaxation are plotted in **Figure 4.17**. The activation energies E_a of the secondary absorptions are obtained from the slope of the plots, and the pertinent values are given in **Table 4.1**. In general the values of the activation energy of the relaxations follow the trends $E_a(\beta) > E_a(\gamma) > E_a(\gamma')$. Moreover, the activation energies of the γ and γ′ relaxations vary in the way E_a(PDBM25) > E_a(PDBM23) > E_a(PDBM34). In the case of the β relaxation, E_a(PDBM34) > E_a(PDBM25) > E_a(PDBM23). As usual, the average relaxation time associated with the α relaxation is described by the Vogel-Fulcher-Tammann-Hesse (VFTH) equation (Vogel, 1921; Fulcher, 1925; Tamman & Hesse, 1926) expressed in terms of the fragility parameter D_0 (Angell, 1996; Angell, 1995) by

$$\tau = \tau_0 \exp\left[\frac{D_0}{(T/T_V)-1}\right] \tag{4.9}$$

where τ_0 is a pre-factor of the order of picoseconds, T_V is the Vogel temperature currently associated with the temperature at which the entropies of the glassy system and the crystal are similar, *i.e.* the configurational entropy of the glassy system is nil. Values of the parameters that fit equation (4.9) to the experimental results are collected in **Table 4.1**. The results show that D_0 is lower than 10, the limit value which separates fragile materials (D_0 < 10) from strong ones (D_0 > 10) (Angell, 1996; Angell, 1995). It is worth noting that T_V is about 50 K below the T_g of the polymers. By comparing equation (4.9) with the Doolittle equation (Doolittle, 1951; Doolittle, 1952)

$$\tau_\alpha = \tau_0 \exp\left(\frac{B}{\Phi}\right) \tag{4.10}$$

where Φ is the relative free volume and B is a parameter close to the unit related with ratio between the critical volume necessary for a relaxation process to take place and the volume of the segments intervening in the relaxation, it is found that the relative free volume at T_g , Φ_g, and the thermal expansion coefficient $\alpha_f = (1/v)(dv/dT)_p$ are given by (Ferry, 1961)

$$\Phi_g / B \cong \frac{T_g - T_V}{D_0 T_V}; \;\; \alpha_f / B \cong 1/(D_0 T_V) \tag{4.11}$$

The fact that the ratio of constant volume to constant pressure activation energies for polymers is not zero (Mpoukouvalas, et al., 2009) as free volume theories require raises questions concerning the applicability of these theories to α relaxations. However, it is an experimental fact that the values of the parameters Φ_g/B and α_f/B for most flexible polymers lie in the vicinities of 0.025 ± 0.005 and (4 to 6) × 10^{-4} K^{-1}. For PDBM23, PDBM25 and PDBM34 the values of Φ_g/B , collected in **Table 4.1**, are slightly higher than the indicated average value of this quantity, but the results for α_f, also shown in **Table 4.1**, are in agreement with those reported for other flexible polymers (Ferry, 1961) which lie in the vicinity of 5 × 10^{-4} K^{-1}.

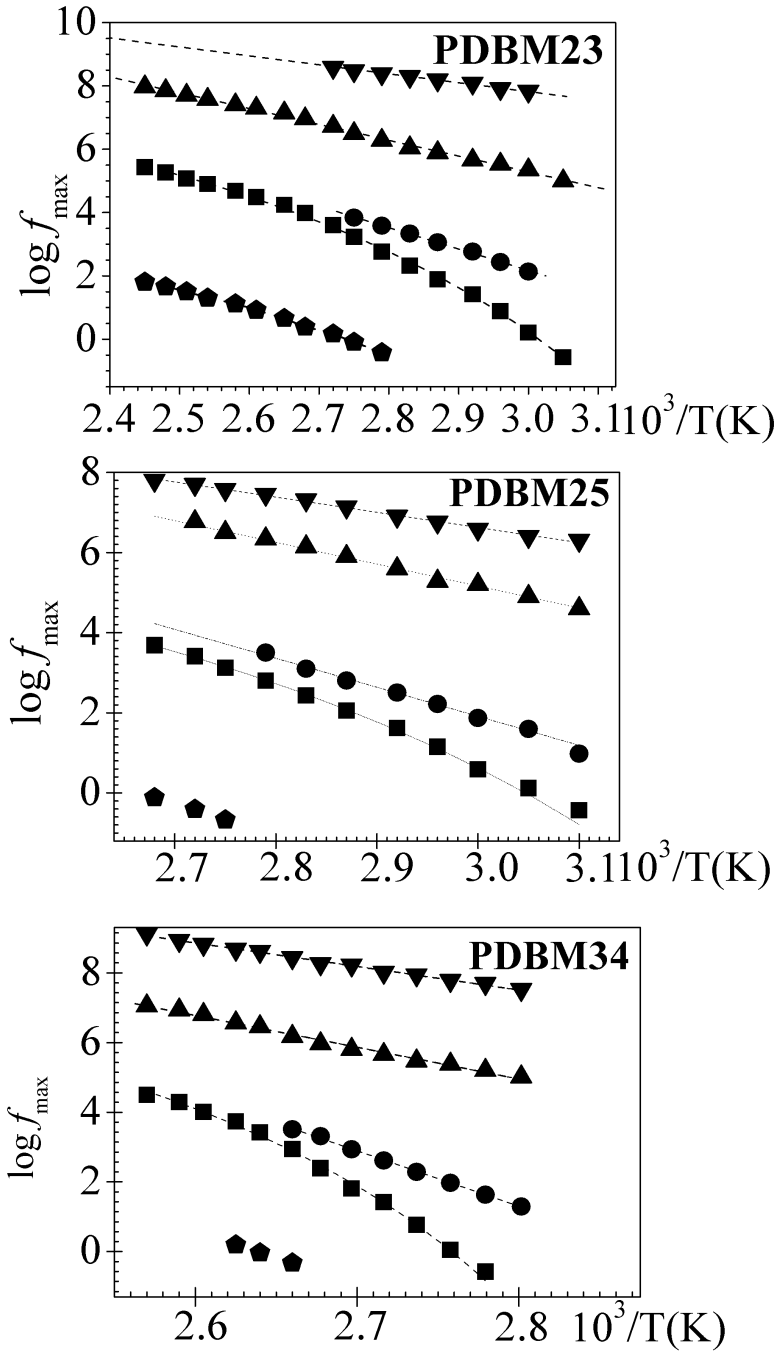

Figure 4.17. Arrhenius plot for the α′ (pentagons), α(squares), β(circles). γ (up triangles) and γ′ (down triangles) relaxations of PDBM25, PDBM23 and PDBM34.

Table 4.1. Activation energies of the secondary relaxation and parameters of Vogel-Fulcher-Tammann-Hesse equation for PDBM25, PDBM23, and PDBM34.

Sample		PDBM23	PDBM25	PDBM34
$E_{a,\gamma'}(kJ\ mol^{-1})$		54 ± 1	73 ± 2	39 ± 5
$E_{a,\gamma}(kJ\ mol^{-1})$		95 ± 2	104.± 3	80 ± 4
$E_{a,\beta}(kJ.mol^{-1})$		132 ± 2	138 ± 4	168 ± 3
$E_{a,\sigma}(kJ\ mol^{-1})$		126 ±2.0	136 ±4	167 ±3
	D_0	6.1± 1.8	6.5± 1.2	6.7 ± 1.1
	$T_v\ (K)$	265± 7	252± 11	271 ± 1
α	$10^2 \times \phi_g / B$	3.4±0.9	3.5±0.7	3.3±0.6
	$10^4 \times \alpha_f \left(K^{-1}\right)$	6.2±1.3	6.1±1.3	5.5±1.2

The Arrhenius plot for the retardation time of the α′ relaxation of PDBM23, shown in **Figure 4.17**, suggests that the absorption may not be a pure thermal activated process. However, the fact that the data available cover a relatively narrow span of temperature impedes to reach a definite conclusion concerning the temperature dependence of this relaxation.

The values of the ionic conductivity obtained by minimization of equation (4.5) are plotted as a function of the reciprocal of temperature in **Figure 4.18**. The plots show that the conductivity of the polymers obeys Arrhenius behavior following the trends σ(PDBM23) > σ(PDBM25) > σ(PDBM34). The values of the activation energy associated with the ionic transport of the polymers, shown in the fourth row of **Table 4.1**, are of the same order as those associated with the β relaxation process of the polymers.

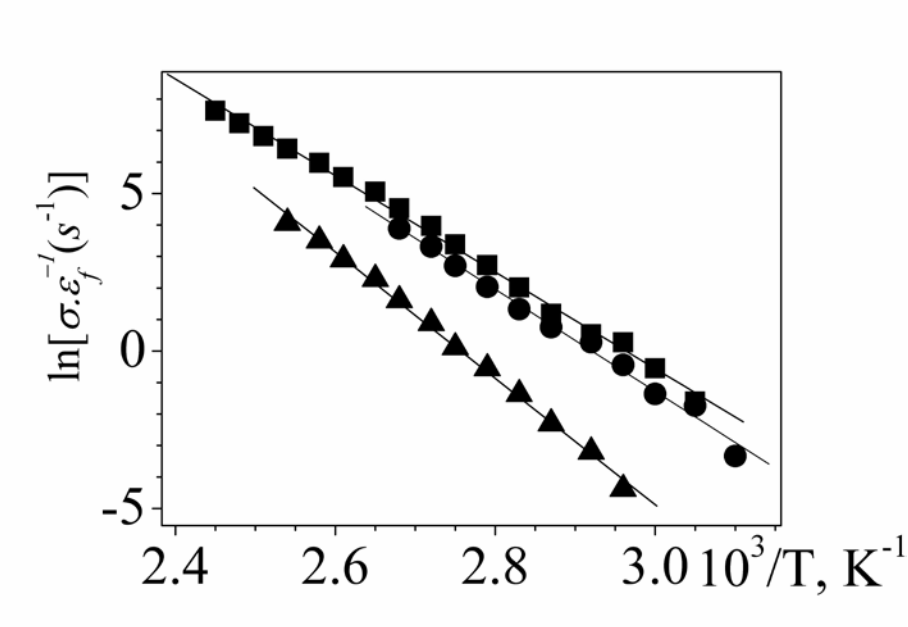

Figure 4.18. Dependence of the ionic conductivity with the temperature for PDBM23 (■), PDBM25 (●) and PDBM34 (▲).

4.2.5. X-Rays Characterization

X-Ray diffraction patterns of poly(n-alkyl methacrylate)s (PnMAs) show the aggregation of the side groups of different monomeric units forming self-assembled alkyl nanodomains (Beiner, et al., 2001; Beiner & Huth, 2003; Beiner, 2001) whose sizes depend on the side-chains length. The two glass transition temperatures detected in these polymers by dynamic heat capacity measurements are believed to be associated with the freezing of motions within the alkyl nanodomains (α_{PE}) and main chain dynamics. By using neutron-scattering with istopic labeling Arbe et al were able to study separately the dynamics of the alkyl nano-domains and the main chain (Arbe, et al., 2008). The results obtained strongly support the suggested nanosegregation of side groups and main chain (Beiner, et al., 2001;

Beiner & Huth, 2003). Structural studies carried out by WAXS on the polymers used in this work, presented in **Figure 4.19**, show the presence of a peak, centered in the vicinity of q = 5nm^{-1} (peak I), and a second peak (peak II) centered at q = 11.5, 12.1 and 13.8 nm^{-1} for PDBM23, PDBM34 and PDBM25, respectively. In principle, tacticity may affect the crystallinity of poly(methacrylate) derivatives and therefore their X-ray patterns. Actually, iso-poly(methyl methacrylate) develops crystalline order from the melt and the same occurs with syndio-poly(methylmethacryate) but in this latter case only from solution (Davis, 1997). However, development of crystallinity in iso-poly(methyl methacrylate) melts is slow, even for a nearly monodisperse sample with isotactic triad content of 100%. Crystallinity is not obtained in samples with isotactic content triad less than 53% (Lemieux & Prud'homme, 1989). In view of this and taking into account the atactic nature of PDBM23, PDBM25 and PDBM34, crystalline order arising from estereoregularity is absent in these polymers.

Peak II, also appears in PnMAs, centered in the vicinity of 12-13 nm^{-1}. The fact that this high q peak is nearly independent on the side chains length in PnMAs led to conclude that it is produced by correlations involving the side group atoms, thus reflecting the average distance between the nonbonded atoms of the side chains. According to this interpretation and taking into account the Bragg approximation, the average distance of the side chains in PDBM23, PDBM25 and PDBM34 are respectively 0.55, 0.52 and 0.49 nm. Peak I also appears in PnMAs for values of q lying in the range 6 nm^{-1}, 5 nm^{-1} and 4 nm^{-1} for poly(ethyl methacrylate), poly(butyl methacrylate) and poly(hexyl methacrylate). The shifting of peak I to lower values of q as the length of the alkyl chains increases suggests

that it reflects main chain correlations and therefore it is associated with average distances between the backbone. In consonance with this, it can be assumed that peak I in the diffraction patterns of the dimetoxy phenyl substituted poly(benzyl methacrylate)s also arises from main chain correlations. Then, it could be postulated the existence of side chain nanodomains flanked by the backbone in the polymer melts, the average distance between the backbone being *ca.* 1.26 nm. Accordingly interfaces in the nanodomains of PDBM23, PDBM25 and PDBM34 may condition charge transport in the polymers melts at low frequencies, as discussed below.

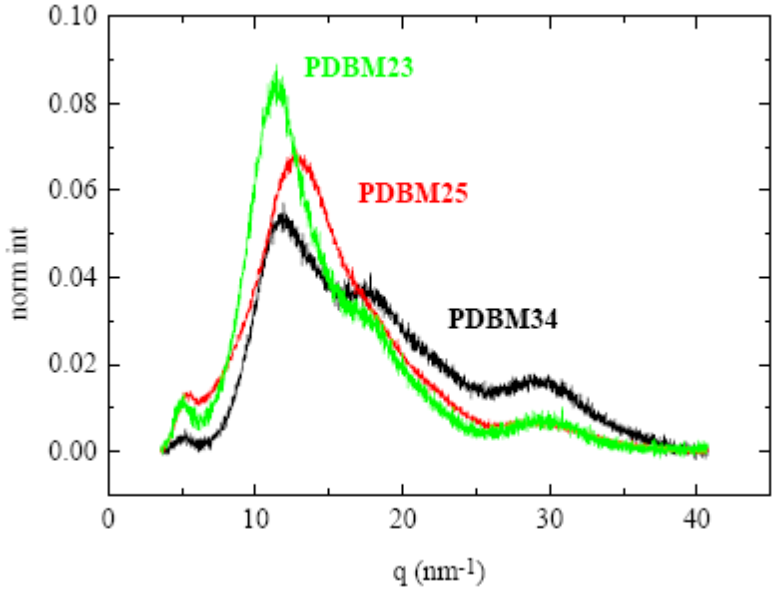

Figure 4.19. X-Ray diffraction pattern for PDBM23 (green), PDBM25 (red) and PDBM34 (black).

4.2.6. Electrode polarization and Maxwell-Wagner-Sillars relaxation

An inspection of the retardation spectra shows that in addition to the high frequency absorptions comprising the secondary and the glass-rubber relaxations, processes arising from either interfacial and/or electrode polarization must be considered. Electrode polarization proceeds from accumulation of charges at the electrodes-polymer interface whereas the interfacial polarization is due to the build-up of charges at the interfaces of components of heterogeneous systems (Satti & McLachlan, 2007). The contribution to the dielectric loss of the polarization produced at the electrodes-polymer interface scales with frequency as ω^{-s} where s is a parameter close to the unit. This contribution corresponds to the last term of the right hand side of equation (4.1). The interfacial polarization in the bulk is known as Maxwell-Wagner-Sillars (MWS) relaxation (Laredo & Herandez, 1997; Maxwell, 1893; Wagner, 1914; Sillars, 1937; Mijovic & Fitz, 1998; Perrier & Bergeret, 1997). For example MWS relaxations have been found in silicon-polyester resins (Arbe, et al., 2008), nylon/clay nanocomposites (Perrier & Bergeret, 1997; Lee, et al., 2005), PZTfibers/epoxy resins (Hammami, et al., 2007), polycarbonate/styrene-acrylonitrile copolymer multilayer composite (Daly, et al., 1992), amorphous-crystal interface in Nylon 1010 (Lu & Zhang, 2006), etc. The MWS relaxation is associated with polarization processes produced by charges separated over a considerable distance with respect to the atomic or segments size. In view of these antecedents, the MWS polarization of PDBM23 may be interpreted as caused by nano-heterogeneities arising from the two types of environments existent in this apparently homogeneous system. However, the sizes of the

nanodomains are not large-enough or the polar side groups are not sufficiently flexible to develop cooperative motions independently of the backbone. It is worth noting that cooperative motions of the side chains of the higher series of poly(n-alkyl methacrylate)s produce a low temperature glass-rubber (α_{PE}) relaxation, in addition to the glass rubber absorption arising from segmental motions of the backbone (Beiner, 2001). Although the symmetry of the α' relaxation in PDBM23fulfills one of the requirements of MWS relaxations, the process is not described by a single relaxation time. This means that the α' absorption is a distributed MWS relaxation produced by a wide variety of environments. The isotherms corresponding to the real component of the complex conductivity of these nanoheterogeneous systems are characterized by a plateau in the low frequency region and a critical frequency ω_c describing the onset of the dispersion of σ'. Empirically it has been found that $\omega_c \cong \omega_M$ for a series of systems where ω_M is the angular frequency at the peak maximum of the dielectric loss. Charge transport in these systems can be interpreted in terms of a random barrier model proposed by Dyre (Dyre, 1988; Dyre, 1986) which assumes that transport occurs by hopping of charge carriers in spatially varying random energy landscape. The time involved in overcoming the highest barrier that determines the conductivity is one of the parameters characteristic of the model, denoted by τ_e. The Dyre model approximates the complex dielectric permittivity by the following expression

$$\varepsilon^*(\omega) = \varepsilon_0 + \frac{\sigma_0 \tau_e}{\varepsilon_f \ln(1+\omega\tau_e)} \qquad (4.14)$$

where ε_0 is the relaxed value of the glass rubber relaxation and σ_0, the dc conductivity, is one of the characteristic parameters of the model. Taking into account that $(1+j\omega\tau_e)=(1+\omega^2\tau_e^2)^{1/2}e^{j\tan^{-1}(\omega\tau_e)}$, the real and imaginary components of ε^* are given by

$$\varepsilon'(\omega)=\varepsilon_{sd}+\frac{1}{2}\frac{\left(\frac{\sigma_0}{\varepsilon_f}\right)\omega\tau_e\ln(1+\omega^2\tau_e^2)}{(1/4)\ln(1+\omega^2\tau_e^2)+\left[\tan^{-1}(\omega\tau_e)\right]^2}$$
$$\varepsilon''(\omega)=\frac{1}{2}\frac{\left(\frac{\sigma_0}{\varepsilon_f}\right)\omega\tau_e\tan^{-1}(\omega\tau_e)}{(1/4)\ln(1+\omega^2\tau_e^2)+\left[\tan^{-1}(\omega\tau_e)\right]^2} \qquad (4.15)$$

Notice that the model is not applicable at very low frequencies where electrode polarization effects show up because these effects are not considered in the model. As can be seen in **Figure 4.20**, equation (4.15) fits rather well to the ε' isotherms of PDBM23 in the low frequency range provided that the values of σ_0 and ω_e plotted as a function of the reciprocal of temperature in **Figure 4.20** and **Figure 4.21**, respectively, are used. Although the values of σ_0 are roughly a decade higher than those of σ plotted in **Figure 4.21**, the temperature dependence of both quantities is similar. As can be seem in **Figure 4.21**, the values of ω_c, ω_M and ω_e apparently obey Arrhenius behavior and the results for ω_c and ω_M nearly fall in the same curve suggesting that they describe an identical underlying process, i.e. an electrical relaxation. As expected, the values of ω_e are rather close to those of ω_c and ω_M. Owing to the rather narrow span of temperature covered by the experiments where ω_M, ω_c and ω_e can be obtained no definitive conclusion can be reached regarding to whether these parameters are only thermally activated or they are also governed by the volume, *i.e.*

the temperature dependence of the parameters is described by the VFTH equation. It can be noted in this regard that the study of the temperature dependence of these parameters for low molecular weight ionic liquids carried out in a wide span of temperature show that they are governed by the temperature and volume (Krause, et al., 2010). The study of the ω_c, ω_M and ω_e dependence with temperature has only been made for the PDBM23, because in the case of PDBM25 and PDBM34 the experimental frequency does not reach low enough values to get a clear view of the process under study.

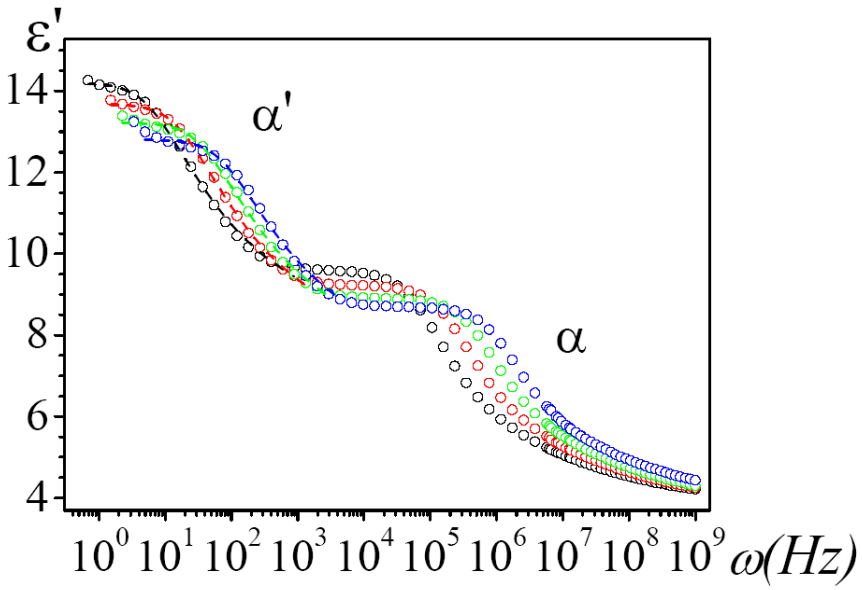

Figure 4.20. Fitting of the Dyre Model (continuous lines) to the experimental real component of the complex dielectric permittivity from 378 to 408K, at 10K steps.

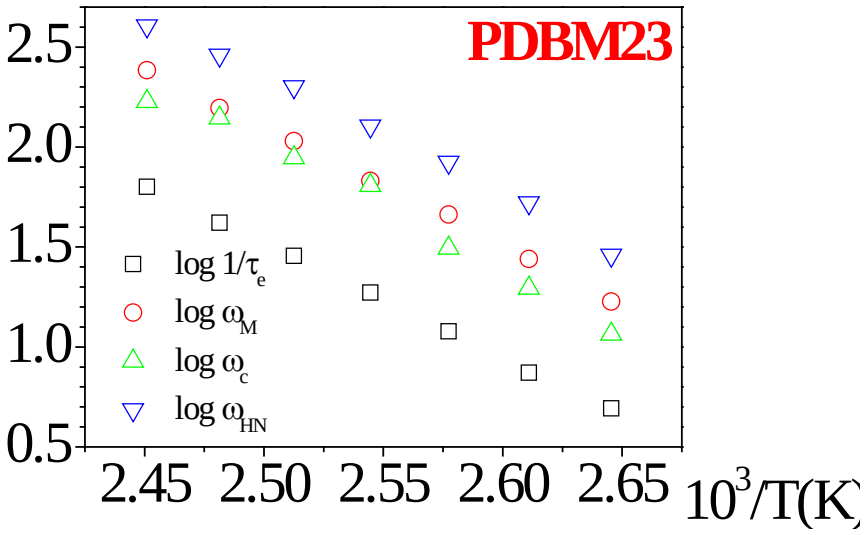

Figure 4.21. Arrhenius plots for the ω_c, ω_M , ω_{HN} and ω_e parameters.

To assess the influence of the fine structure on the stretch exponent of the decay function that describes the glass-rubber relaxation, the normalized α relaxation in the time domain was calculated from the spectra by means of the equation

$$\phi(t) = \frac{\int_{-\infty}^{\infty} L_{\alpha}(\ln\tau)\, e^{-t/\tau} d\ln\tau}{\int_{-\infty}^{\infty} L_{\alpha}(\ln\tau)\, d\ln\tau} \tag{4.16}$$

The normalized decay function that depicts the relaxation behavior of PDBM23 in the whole time range was calculated from the retardation spectra by means of equation (4.16). The decay functions obtained for PDBM23 at different temperatures are shown in **Figure 4.22**. As usual the decay function is inevitably described by the stretch exponential KWW equation (Williams, 1979)

$$\phi(t) = \exp\left[-\left(\frac{t}{\tau_0}\right)^{\beta_{KWW}}\right] \tag{4.17}$$

where $0 < \beta_{KWW} \leq 1$ and τ_0 is the characteristic relaxation time of the absorption. Values of the evolution of the stretch exponent and the characteristic relaxation time with temperature for PDBM23, PDBM25 and PDBM34 are depicted in **Figure 4.22**. As expected the temperature dependence of τ_0 obeys to the VFTH equation whereas the stretch exponent seems to increase as temperature increases. The three polymers exhibit rather low stretch exponents at low temperature that increase with increasing temperature, without observing differences in behavior that that can be attributed to the small variations of the fine structure of the polymers.

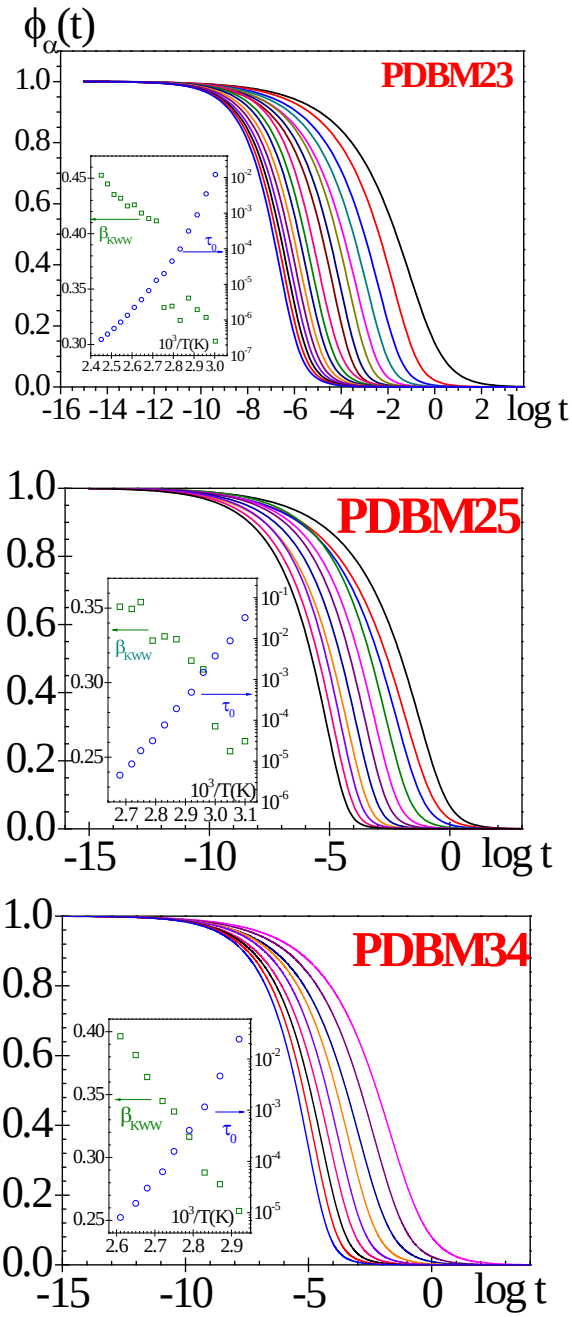

Figure 4.22. Normalized relaxations curves in the time domain for the α relaxation of PDBM23, PDBM25 and PDBM34 from 363 to 408K, at 5K steps. Inset: Temperature dependence of the stretch exponents β_{KWW} and the characteristic relaxation times τ_0 of KWW equation.

The rapidity with which the physical properties of a supercooled liquid vary as temperature approaches the glass transition temperature is characterized by the dynamic fragility *m* given by (Plazek & Ngai, 1991) (Qin & McKenna, 2006)

$$m = \lim_{T \to T_g} \left(\frac{d \log \xi}{d\left(T_g / T\right)} \right)_p \tag{4.18}$$

where ξ is a physical parameter depending of the dynamics of the system such as the viscosity η or the relaxation time τ. Obviously, as the fragility parameter increases, the temperature dependence of the relaxation time of the glass-rubber relaxation comes closer to Arrhenius behavior. Taking τ_g as reference and taking into account equation (4.9), the fragility parameter can be written as

$$m = \frac{D_0 T_V}{2.303 T_g (1 - T_V / T_g)^2} \tag{4.19}$$

The values of *m* for PDBM23, PDBM25 and PDBM34, collected in **Table 4.2**, slightly increase with the respective glass transition temperatures. However, the results are nearly 30% below those predicted by the straight line roughly fitting the values of *m vs* T_g for several polymers (Qin & McKenna, 2006). The apparent activation energy associated with the α relaxation at T_g can be obtained by equating the fragility index obtained from VFTH and Arrhenius behavior, *i.e.*

$$m=\left[\frac{d\log\tau_A}{d\log(T_g/T)}\right]_{T=T_g}=\left[\frac{d\log\tau_{VFTH}}{d\log(T_g/T)}\right]_{T=T_g} \tag{4.20}$$

Taking into account that $\tau_A=\exp(-E/RT)$, equation (4.20) leads to the following expression for the activation energy E_α at T_g,

$$E_\alpha(T_g)=\frac{RD_0T_V}{(1-T_V/T_g)^2} \tag{4.21}$$

From equations (4.21) and (4.18), the activation energy can be expressed by the alternative form

$$E_\alpha(T_g)=2.303RD_0T_VT_g \tag{4.22}$$

Accordingly the higher T_g, the higher the activation energy, assuming D_0 and T_V as constants. The results for the activation energy associated with the glass-rubber relaxation of PDBM23, PDBM25 and PDBM34 at T_g, collected in **Table 4.2**, increase with temperature but lie about 25% below those (Qin & McKenna, 2006) predicted by the straight line roughly fitting the plots of $E_{a,\alpha}$(Tg) vs T_g for a wide variety of polymers.

Table 4.2. Values of the glass transition temperature (T_g), the dynamic fragility index (m) and the activation energy associated with the α relaxation at T_g, $E_\alpha(T_g)$, for PDBM23, PDBM25 and PDBM34. The quantities with asterisk, m^* and $E_a^*(T_g)$, were calculated by empirical equations[61]
$m^* \approx 0.25(\pm 0.067)T_g\,(K) + 9(\pm 20); E_a^*(T_g) = \left[0.006\left(\pm 6.5\cdot 10^{-4}\right)T_g^2 - 35(\pm 66)\right] kJ/mol$

Sample	**PDBM23**	**PDBM25**	**PDBM34**
T_g, K	320	310	330
m	74	66	74
m^*	99	96	101
$E_\alpha(T_g)$, kJ·mol^{-1}	451	390	467
$E_\alpha^*(T_g)$, kJ·mol^{-1}	579	541	618

Aside from other procedures, a method to collect the behavior of a variety of systems with temperature in a single diagram is to consider the β relaxation, which obeys Arrhenius behavior, the elementary relaxation for the α relaxation of liquids (Fujimori & Oguni, 1995). Using this assumption, the α relaxation can be considered associated with an activation energy that depends on temperature. Then the ratio between the activation energy of the α relaxation at a temperature T and that of the β absorption, independent of temperature, may represent the size of correlate domains in the α relaxation. The ratio, represented by $R_\alpha(T)$ can be written as (Fujimori & Oguni, 1995)

$$R_\alpha(T) = \frac{RD_0T_VT^2}{E_\beta(T-T_V)^2} \tag{4.23}$$

It can be defined a temperature T_B at which $R_\alpha(T) = 1$ representing the upper bound below which the size of correlate domains starts to increase reaching a maximum at $T = T_g$.

The values of T_B for PDBM23, PDBM25 and PDBM34 are 388.3, 362.7 and 395.0 K, respectively. The variation of the size of correlate domains with temperature, shown in **Figure 4.23**, indicates that the correlated domains of PDBM23, PDBM25 and PDBM34, at the respective glass transition temperatures, are respectively, 3.4, 2.7 and 3.1 times the size of the elementary clusters at T_B.

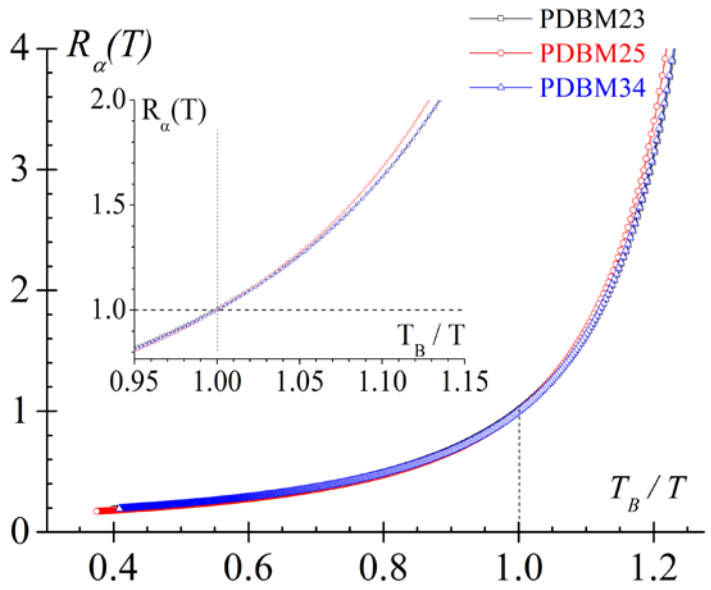

Figure 4.23. Temperature dependence of ratio of the activation energy of α-process to that of β-process, R_α(T), for PDBM23 (squares), PDBM25(circles) and PDBM34 (triangles).

A few comments should be done concerning the assignment of the secondary absorptions to specific molecular motions of the side groups. The CC(O)-OCH_2 residue of the side chain is associated with a dipole moment of 1.78 D forming an angle of 123º with the C-C(O)O bond (Riande & Saiz, 1992). On the other hand, the dipole associated with the C^{ar}-O-CH_3 moiety bisects the C^{ar}-O-C angle and has a value of 1.22 D (Riande & Saiz,

1992). With the exception of the bonds restricted to trans states, rotations about the remaining skeletal bonds of the side groups, including the C^{ar}-O-CH_3 bonds, give rise to dielectric activity. However, co-planarity between the phenyl group and the $C^{ar}OCH_3$ moiety is strongly disfavored due to strong repulsive interactions between the methyl group and nearby protons of the phenyl group. Then dipoles jumping between the two alternative gauche states about the C^{ar}-OCH bonds presumably produce the dielectric activity displayed in the fastest relaxation or γ' process. On the other hand, rotations about the C^{ar}-CH_2 bonds change the location in the space of the dipoles associated with the C^{ar}-OCH_3 moiety probably producing the dielectric activity reflected in the γ relaxation. In this case jumping between the two lower energy planar conformations about the C^{ar}-CH_2 bonds presumably produces that relaxation. Finally the β relaxation arises from motions involving the whole side group presumably coupled with local motions of the skeletal bonds of the main chain. In general the conformations of lower energy of the side groups of the chains with the C^{ar}-O-CH_3 bonds anchored to the position 2 of the phenyl group have the dipole associated with this moiety in a direction forming favorable angles with the dipole corresponding to the ester group. Hence, the high dielectric strength produced by the motions of the side chains of PDBM23 and PDBM25. The angles formed by the dipoles of the C^{ar}-O-CH_3 bonds in 3,4 positions with the dipole of the ester groups are not so favorable and as a result the dielectric strength of PDBM34 is significantly lower than that of the other polymers. (see **Figure 4.24**)

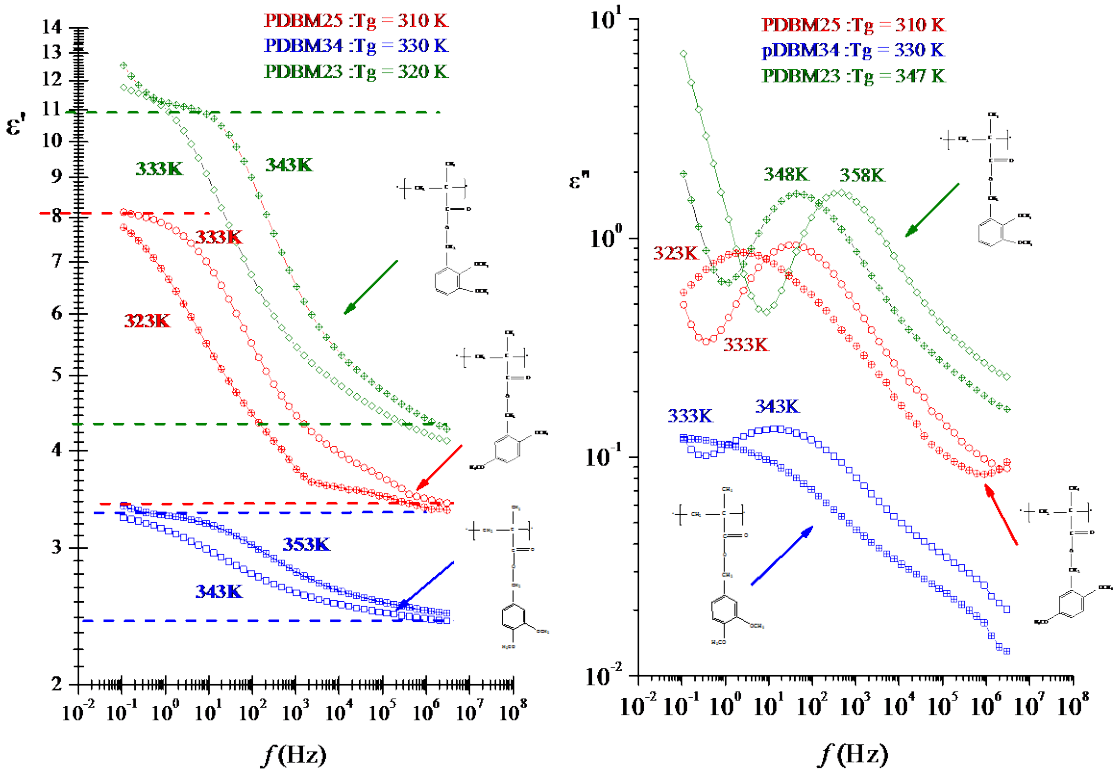

Figure 4.24. Frequency dependence of the permittivity and loss permittivity for PDBM23, PDBM25 and PDBM34.

4.3. Conclusions

The dielectric loss isotherms of the polymers in the frequency domain present a blurred relaxation resulting from the overlapping of the secondary absorptions with the glass-rubber (α) relaxation. The time retardation spectra computed from the complex dielectric permittivity allows a better deconvolution of overlapping relaxations than performing directly the deconvolutions in the dielectric loss.

A distributed MWS relaxation appears at long times in the retardation spectra at high temperatures hidden in the dielectric loss spectra by the interfacial polymer-electrode conductive contribution to the dielectric loss. The MWS relaxation presumably arises from the build-up of charges at the interfaces of nanoheterogenities formed in the bulk by segregation of the polar side groups from the non polar skeletal bonds. This relaxation is described by the Dyre model, which assumes that charge transport occurs by hopping of charge carriers in spatially varying ramdom energy landscape. The location of the polar oxymethylene substituents on the phenyl groups of the side chains greatly influences the relaxation behavior of the polymers. The location of the oxymethylene moiety in the position 2 of the phenyl group causes a significant enhancement of the dielectric strength of the relaxations. This study shows that small differences in the fine structure of polymers produce significant changes in the relaxation behavior.

Chapter 5:

Conductivity and time-temperature correspondence in polar rubbery liquids

[*] Results presented in this Chapter have been collected in: M. Carsí, M. J. Sanchis, P. Ortiz-Serna, B. Redondo-Foj, R. Díaz-Calleja, E. Riande, *Macromolecules* vol 46, pp. 3167−3175, **2013**

Abstract

This work is focused on the conductivity study of rubbery liquids taking as a model the poly(2,3-dimethoxybenzyl methacrylate). Each isotherm, displaying the conductivity in the frequency domain, shows a plateau in the low frequency region, representing the *dc* conductivity. The covered frequency range by the plateau increases with the temperature. The frequency corresponding to the end of the plateau, ω_c, marks the onset of the *ac* conductivity, which correspond in increasing order of frequency to Maxwell-Wagner-Sillars, glass-rubber transition and secondary relaxations. The contributions of the relaxation processes to the *ac* conductivity in the wholly frequencies range were analyzed. The time-temperature correspondence principle holds for the reduced *ac* conductivity. However, this principle does not hold for the components of the complex dielectric permittivity due, among other things, to the different temperature dependences of each dipolar relaxation processes. Analogies and differences between the conductivity behavior of rubbery liquids and disordered inorganic solids are discussed.

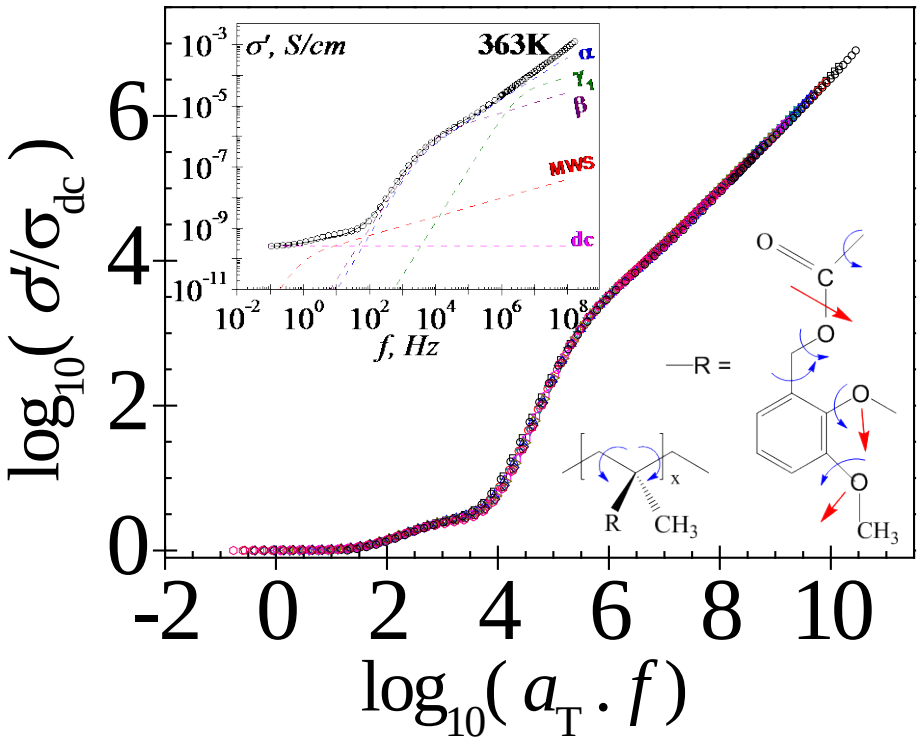

5. Conductivity and time-temperature correspondence in polar rubbery liquids

5.1. Introduction

In the frequency domain, the response of rubbery liquids to alternating mechanical force fields involves, in decreasing order of frequency, the following processes: a) secondary relaxations associated with local motions in the side chains, the backbone or both, b) the glass-rubber or α relaxation arising from segmental motions and c) the normal relaxation produced by chains disentanglement that give rise to flow (Ferry, 1961; Graessley, 1974; Graessley, 1982; Riande, et al., 2000). Since the α absorption freezes at T_g and the low frequency side of this relaxation overlaps with the high frequency side of the normal mode process, the glass-rubber relaxation is considered the precursor of the glassy state and liquid flow.

The experimental devices used in the mechanical measurements may present some limitations at frequencies above 50-100 Hz caused by their own-resonance. This fact precludes the experimental study of the fast secondary relaxations of rubbery liquids, consequently, the study of these processes by mechanical methods is mostly restricted to temperatures below T_g. On the other hand, responses associated with slower processes, such as the glass-rubber and the normal mode relaxations, can only be measured at a given temperature, in a time/frequency window of about four-five decades. As a result, the viscoelastic behavior of rubbery liquids over long time/frequency windows can only be obtained for thermoviscoelastic simple systems

(Ferry, 1961). Nevertheless, master curves covering twelve or more decades in the frequency/time domain, can be obtained for these systems by superposing the isotherms representing viscoelastic functions in the frequency/time domain with the isotherm corresponding to a reference temperature. However, the isotherms superposition requires that the time/frequency temperature correspondence holds, *i.e.* the relaxation times associated with the different relaxation mechanisms must have the same temperature dependence (Plazek, 1996). This might be so for the α and the normal mode relaxations, which are governed by the thermodynamic variables volume and temperature. On the other hand, creep experiments carried out on monodisperse polystyrene, using Plazek's (Plazek, 1965) frictionless creep apparatus, showed that the time-correspondence principle does not hold for the creep compliance function $J(t)$, though it does for the recovery creep compliance $J_r(t) = J(t) - t/\eta$ (where η is the zero-shear rate viscosity). This means that the relaxation times associated with segmental motions and with chains disentanglement do not have the same temperature dependence. On the other hand, since secondary relaxations are thermally activated processes (McCrum, et al., 1991), the time temperature correspondence may not hold in the region where the fast relaxations overlap with the slower α absorption (Ferry, 1961; Child, et al., 1957). Strictly speaking, the frequency temperature correspondence might hold in wide frequency/time range for the recovery compliance function only for (i) the systems were the changes in the viscoelastic functions caused by the secondary processes are negligible or (ii) severe overlapping between the α and the secondary relaxations is absent.

An alternative for the chains motions study in a wide time/frequency window is the dielectric spectroscopy technique, which may cover twelve or more decades at a

single temperature (McCrum, et al., 1991; Craig, 1995; Kremer, et al., 2003; Riande, et al., 2004; Floudas, et al., 2011). The *ac* electrical response of disordered systems to electric perturbation fields is the result of different contributions superposition. These contributions are related to: (i) the hopping process of localized charge carriers, (ii) the dispersive response of the bound charges (dipolar response) and (iii) the response produced by the molecular structure deformation, following the diffusion of charges through percolation paths (Dyre, et al., 2009). The dipolar response presents at high frequencies one or more secondary relaxations. These processes are followed in decreasing order of frequency by the glass-rubber relaxation (McCrum, et al., 1991; Williams G., 1995; Heijboer, 1972; Boyd, et al., 2007). The dipoles of most polar rubbery liquids bisect the skeletal bond angles or are separated from the backbone by flexible segments. In both cases, the dipole moment $\boldsymbol{\mu}$ and the end-to-end distance $\mathbf{r}$ of the chains are uncorrelated (Stockmayer, 1967). As a result, the normal mode relaxation is absent in the dielectric spectra of most rubbery systems. Only the dielectric spectra of the rubbery liquids with structural units having dipoles rigidly attached to the backbone, but not bisecting the skeletal bond angles, exhibit the normal mode, as for instance poly(propylene oxide). This is because $\langle(\Sigma_i \boldsymbol{\mu}_{\perp i}).\mathbf{r}\rangle = \mathbf{0}$ and $\langle(\Sigma_i \boldsymbol{\mu}_{\parallel i}).\mathbf{r}\rangle$ = constant $\cdot\langle r^2\rangle$, where $\boldsymbol{\mu}_{\perp i}$ and $\boldsymbol{\mu}_{\parallel i}$ represent, respectively, the components perpendicular and parallel to the chain contour of the dipole moment, $\boldsymbol{\mu}_i$, associated with the repeat unit *i*, $\mathbf{r}$ is the end-to-end distance of the chains, $\langle\ldots\rangle$ means average and $\langle r^2\rangle$ is the mean square end-to-end distance of the chains (Adachi, et al., 1984; Adachi, et al., 1988; Adachi, et al., 1993; Riande, et al., 1992).

This paper focuses on the effect of the dipolar relaxations on the time-temperature correspondence for the *ac* conductivity of polar rubbery liquids. Poly(2,3-

dimethoxybenzyl methacrylate) (PDMB23) was taken as model, whose repeat unit is shown in **Figure 5.1**. Earlier work carried out on this polymer (Sanchis, et al., 2010) showed that side group segregation from the backbone promotes relatively long distance charge jumps, reflected as a distributed Maxwell-Wagner-Sillars (MWS) relaxation (Maxwell, 1893; Wagner, 1914; Sillars, 1937; Mijovic, et al., 1998; Perrier, et al., 1997) in the low frequency side of the spectra. The aim of this work is to inquire the effects of the MWS process and the strong dispersive processes, arising from the complex motions of polar rubbery liquids, on the time-temperature correspondence of the *ac* conductivity. Attention is also paid to the time-temperature correspondence of the complex dielectric permittivity. It will be shown that the *ac* conductivity of polar rubbery liquids exhibits the main characteristic features displayed by the *ac* conductivity of disordered solids. However, in the latter case the local and segmental motions characteristic of these systems strongly affect the *ac* conductivity.

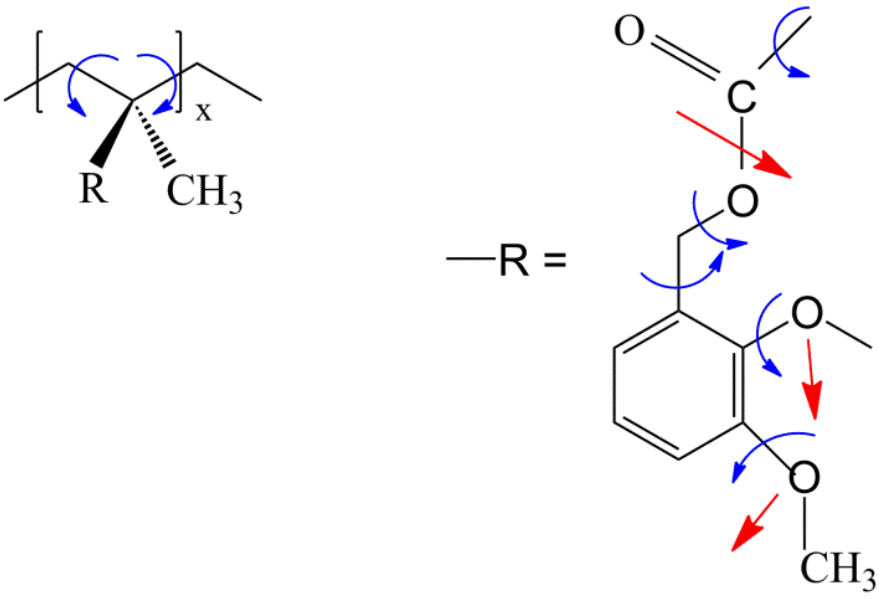

Figure 5.1. Structure scheme of the PDMB23.

Conductivity fundamentals

Under an alternating voltage $V(\omega) = V_0$ Im[$exp\ (j\omega t)$], where ω is the angular frequency of the electric field $(\omega = 2\pi f)$, the current crossing a sample sandwiched between two parallel plane electrodes is $i = dq/dt = V(\omega)/Z^*(\omega)$, where q is the charge of the capacitor and $Z^*(\omega)$ is the complex impedance. Taking into account that the charge in the capacitor can be defined as $q = C^*(\omega)/V(\omega)$ and $C^*(\omega) = \varepsilon^*(\omega) \cdot C_0$, where $C^*(\omega)$ is the capacity of the capacitor with the sample between the electrodes, C_0 is the vacuum capacity and $\varepsilon^*(\omega)$ is the complex dielectric permittivity, the current in the capacitor is $i = \varepsilon_0 A\ \varepsilon^*(\omega) j\omega V/l$. Notice that $C_0 = \varepsilon_0 A/l$, where ε_0 $(=8.854$ pF·m$^{-1})$ is the dielectric permittivity of the empty space and A and l are, respectively, the area and thickness of the sample between the electrodes. The admittance of the sample is $Y^*(\omega) = 1/Z^*(\omega)$ and taking into account that the conductivity is expressed in terms of the admittance by $\sigma^*(\omega) = Y^*(\omega)A/l$, the dielectric permittivity and the conductivity are found to be related by $\varepsilon^*(\omega) = \sigma^*(\omega)/j\varepsilon_0\omega$. On the other hand, the complex electrical modulus $M^*(\omega) = 1/\varepsilon^*(\omega)$ is an important parameter to separate charges transport from dipolar processes.

The beauty of the linear dielectric analysis is that impedance data allow the estimation of different dielectric functions related to: a) dipoles motions associated with local and cooperative micro-Brownian motions of the molecular chains and b) charges transport across the samples. In principle, the equivalent circuit modeling the complex impedance in the frequency domain is made up of a constant phase element of admittance $Y^*(\omega) = Y_0 (j\omega)^a$ $(0 < a \leq 1)$ in parallel with a polarization resistance R_p. In

these circumstances, the impedance of the equivalent circuit is given by (Barsoukov & JMacdonals, 2005)

$$Z^*(\omega) = \frac{R_p}{1+(j\omega\tau)^a} \tag{5.1}$$

where $Y_0 R_p = \tau^a$, being τ a mean-relaxation time. For some systems, the Cole plots are skewed arcs along a nearly straight line at high frequencies, and $Z^*(\omega)$ is better expressed in terms of the Havriliak-Negami equation (Havriliak, et al., 1966; Havriliak, et al., 1967; (Barsoukov & JMacdonals, 2005))

$$Z^*(\omega) = \frac{R_p}{\left[1+(j\omega\tau)^a\right]^b} \tag{5.2}$$

The shape parameters a,b lie in the range $0 < a,b \leq 1$.

5.2. Results and Discussion

5.2.1. Conductivity and Dipolar Relaxation Processes

Cole impedance plots, at several temperatures, are shown in **Figure 5.2**. The plots are deformed arcs, roughly described by equation (5.2), that intersect the abscissa axis at the extreme frequencies in such a way that $Z'(\infty) = 0$ and $Z'(0) = R_p$, being R_p the polarization resistance. **Figure 5.3** shows the Arrhenius plots of the R_p values, where it can be observed a strong decrease of this parameter with increasing temperature.

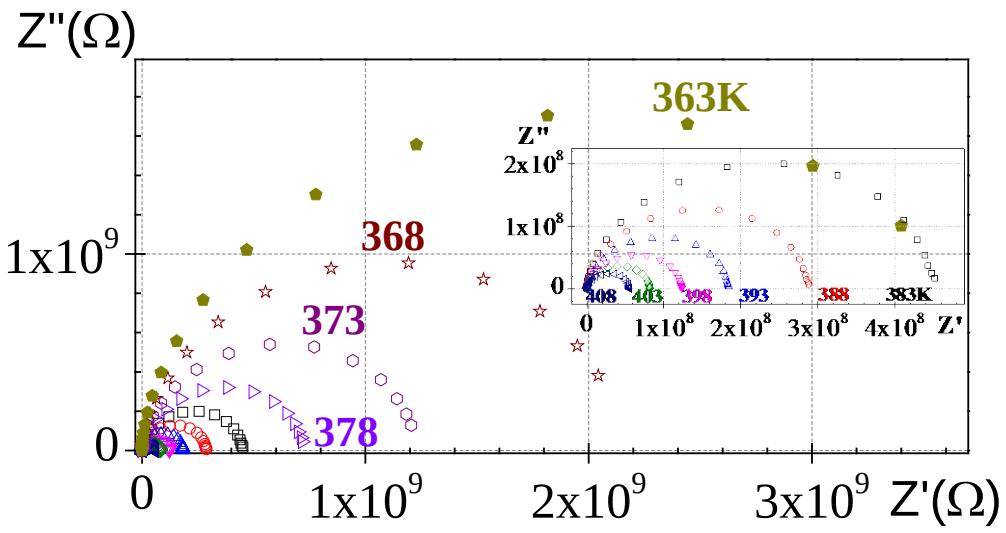

Figure 5.2. Cole impedance plots, at several temperatures for PDMB23.

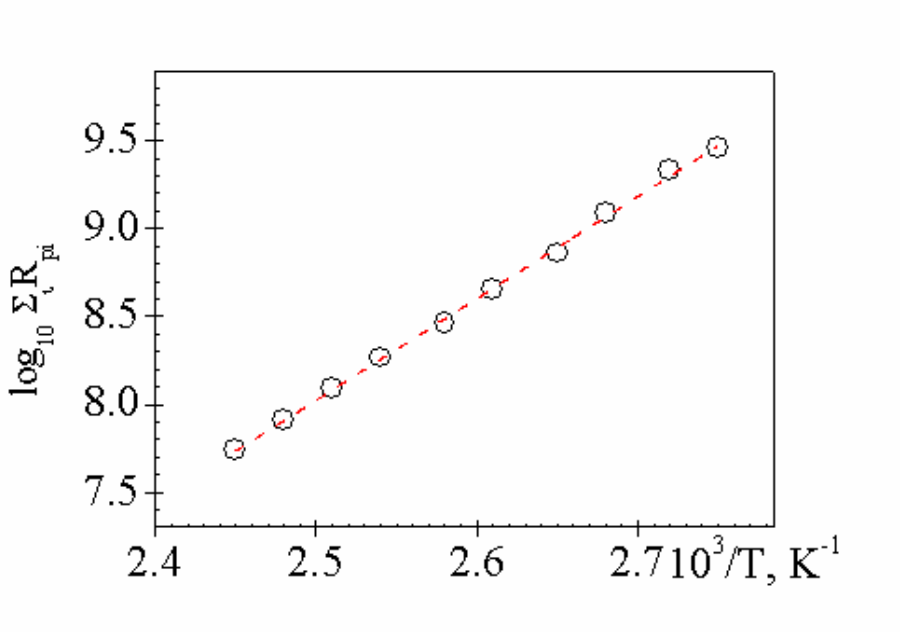

Figure 5.3. Temperature dependence of the polarization resistance values (R_p)

Figure 5.4 shows the double logarithmic plots of the real component σ' of the complex conductivity σ^* in the frequency domain at several temperatures. As usual, in

the frequency domain, the isotherms corresponding to high temperatures, exhibit a plateau in the low frequency region, reflecting a frequency independent conductivity, *i.e. dc* conductivity. The covered frequency range by the plateau increases with temperature. **Figure 5.5** shows the *dc* conductivity values as a function of the reciprocal of the absolute temperature. These values were estimated from: (i) the R_p values by means of the relationship $\sigma_{dc} = l / R_p A$ and (ii) the plateau at low frequencies of the σ' plots. In both cases, the obtained R_p values are in a reasonable good agreement.

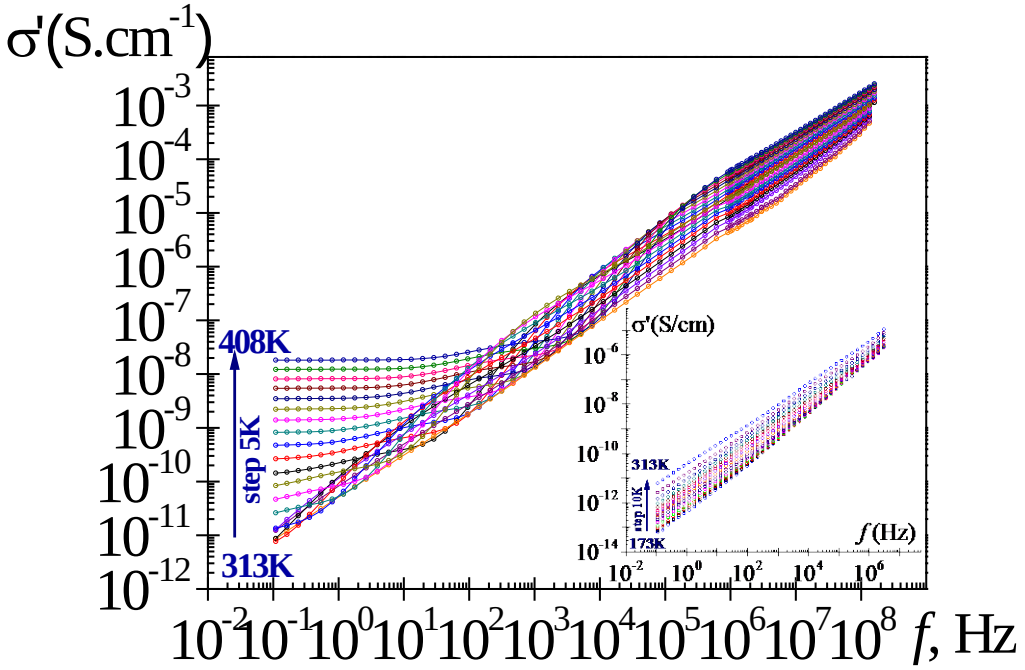

Figure 5.4. Frequency dependence of the real component σ' of the complex conductivity σ^* at several temperatures (from 313 to 408K, step 5K, and in the inset from 173 to 233K, step 10K).

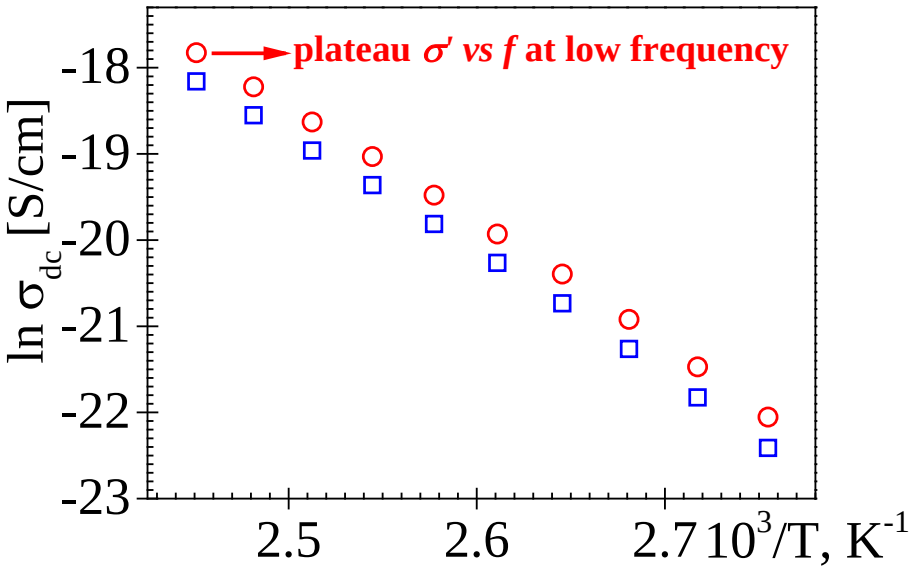

Figure 5.5. The *dc* conductivity at different temperatures of interest evaluated from the low frequency plateau and using the relationship $\sigma_{dc} = l \cdot A/R$.

Figure 5.6 shows the values of ω'_c for the isotherms as a function of the reciprocal of temperature. These values were estimated as the frequency at which the *dc* line intersects with the slope drawn at the inflexion point of the isotherm of interest. As we can see in this Figure, a sharp increase in σ' occurs at a frequency ω'_c, located at 150.5 rad·s^{-1}, at 363 K. At high frequencies, the double logarithmic plot of the conductivity *vs* frequency converges to a straight line, *i.e* the *ac* conductivity exhibits the power law $\sigma' \sim \omega^n$. It is worth noting that at $T < T_g$ the *ac* conductivity of PBDM23 nearly obeys the power law in almost the wholly frequencies range (see inset in **Figure 5.4**).

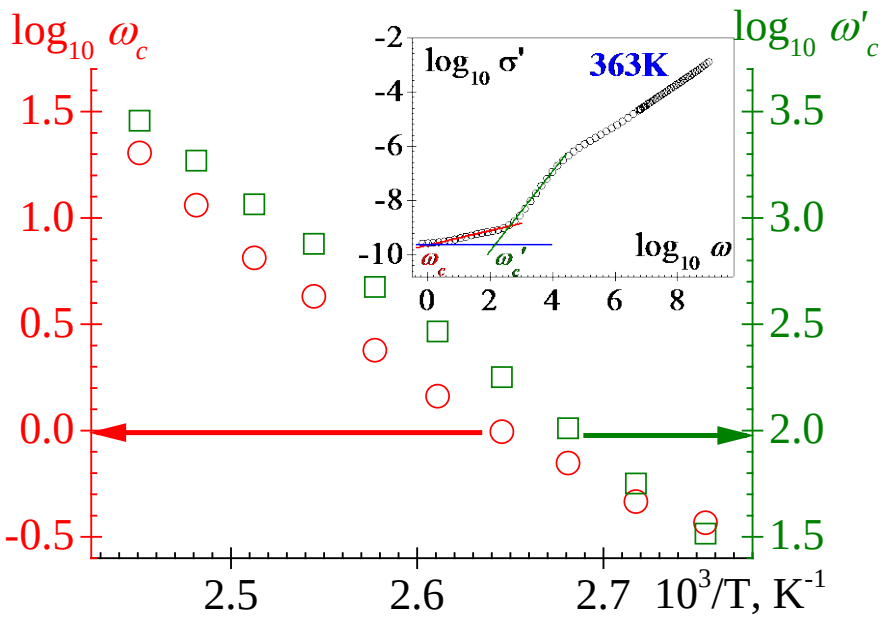

Figure 5.6. Temperature dependence of the critical frequency ω'_c for PDMB23. Inset shows the graphic determination of ω'_c.

A thorough inspection of the σ' isotherms in the frequency domain, corresponding to the rubbery liquid, shows that the departure of σ' from *dc* conductivity actually occurs at a frequency $\omega_c \cong \omega'_c/100$, caused by a process whose nature will be discussed latter. Then, the frequency ω_c can be considered the crossover frequency marking the onset of the *ac* conductivity. It is worth noting that ω_c like ω'_c shifts to higher values with increasing temperature. The Jonscher (Jonscher, 1977) type expression

$$\sigma'(\omega) = \sigma_{dc}\left[1+\left(\frac{\omega}{\omega_c}\right)^n\right] \tag{5.3}$$

has been proposed to describe the *ac* conductivity of disordered systems, such as inorganic glasses. However, this expression is not accurate because its fitting to the

experimental results requires increasing the exponent *n* with frequency. In spite of this shortcoming, equation (5.3) is usually utilized to analyze σ' data at low frequencies.

Dipolar dispersive processes, responsible for the abrupt increase of the *ac* conductivity at $\omega > \omega'_c$, are better reflected by expressing the impedance results in terms of the complex dielectric permittivity ε^*. Isotherms for the real permittivity ε', in the frequency domain, are shown in a relatively wide range of temperatures in **Figure 5.7**. As usual, ε' increases with decreasing frequency reaching a plateau that corresponds to the relaxed dielectric permittivity. However, after the plateau, ε' further increases with decreasing frequency until a second plateau is reached at a frequency that roughly coincides with the frequency ω_c, which marks the onset of the *ac* conductivity in the σ' isotherms. The interpretation of the X-Ray diffractograms of PDMB23 carried out elsewhere (Sanchis, et al., 2010) suggests the presence of nanodomains in the rubbery liquid, formed by polar side groups which are flanked by the backbone. Long distance charge transport across the interfaces of the nanodomains produces a distributed MWS relaxation, reflected in the increase of ε' from the first to the second plateau. The further increase of ε' with decreasing frequency observed in the isotherms at even lower frequencies and high temperatures is attributed to interfacial polymer-electrode phenomena.

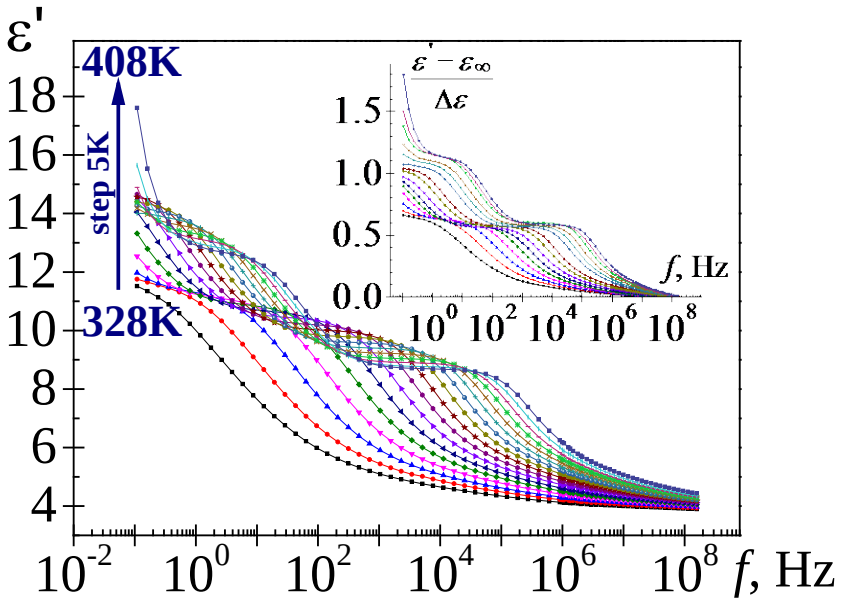

Figure 5.7. Frequency dependence of the real permittivity ε' in wide range of temperatures corresponding to PDMB23 (328K to 408K, step 5K).

The dielectric loss in the frequency domain is shown at several temperatures in **Figure 5.8**. At high frequencies, the loss isotherms present a relaxation, named γ process, whose low frequency side overlaps with the comparatively stronger secondary β absorption. The low frequency side of the β process overlaps with the high frequency side of the ostensible glass-rubber or α relaxation. In turn, the low frequency side of the α relaxation strongly overlaps with the MWS relaxation. This latter process undergoes a strong overlapping with the contributions to the dielectric loss of the *dc* conductivity and polymer-electrode interfacial phenomena. In all cases, the overlapping degree between neighboring relaxations increases with temperature.

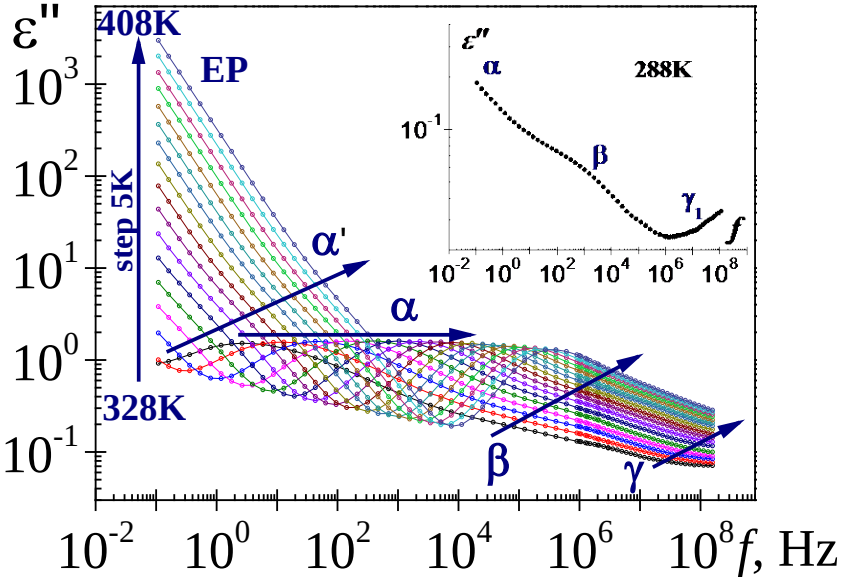

Figure 5.8. The dielectric loss in the frequency domain at several temperatures for PDMB23 (328 to 408K, step 5 K). Inset: zoom at 288K.

In order to study how the dipolar activity and the MWS process affects σ', the complex dielectric permittivity was expressed in terms of Havriliak-Negami type equations (Havriliak, et al., 1997; Havriliak, et al., 1966; Havriliak, et al., 1967), describing the relaxations processes involved in the response of the system to the perturbation field. The pertinent expression is given by

$$\varepsilon^*(\omega) = \sum_i \frac{(\varepsilon_{ri}-\varepsilon_\infty)_i}{[1+(j\omega\tau_i)^{a_i}]^{b_i}} + \frac{\sigma_{dc}}{j\varepsilon_o\omega} \qquad (5.4)$$

where σ_{dc} and ε_0 represent, respectively, the *dc* conductivity and the permittivity of the empty space. The subscript *i* refers to the relaxation processes involving the secondary absorptions, the glass-rubber and MWS relaxations, *i.e.* i = γ, β, α, MWS. The subscripts r and ∞ in equation (5.4) indicate, respectively, relaxed and unrelaxed dielectric permittivities, so that $\Delta\varepsilon_i = \varepsilon_{ri} - \varepsilon_{\infty i}$ represents the dielectric strength of the

relaxation *i*. The shape parameters *a* and *b* determine the departure of the relaxations from Debye behavior. For secondary relaxations and MWS process the value of *b* is the unit, but this parameter lies in the range $0 < b \leq 1$ for the α relaxation. Using minimization methods, the parameters that describe equation (5.4) were computed from the dielectric loss and the pertinent results for a_γ, a_β, a_α, a_{MWS}, b_α, $\Delta\varepsilon_\gamma$, $\Delta\varepsilon_\beta$, $\Delta\varepsilon_\alpha$, $\Delta\varepsilon_{MWS}$ and σ_d are collected in **Table 5.1**.

Let us consider now the changes in σ' caused by the dipolar relaxations and by the MWS process, taken as an example the isotherm at 363K in **Figure 5.6**. For this purpose, in **Figure 5.9** are plotted the contributions of the individual relaxations to the loss isotherm calculated from the parameters that describe the different dielectric relaxations collected in **Table 5.1**. The errors involved in the calculation, *i.e.* $\left(\varepsilon''_{calc} - \varepsilon''_{exptl}\right)/\varepsilon''_{exptl}$, are represented in the inset of the figure. Taking into account that $\sigma'(\omega) = \omega\varepsilon_0\varepsilon''(\omega)$, the changes in the *ac* conductivity by effect of the dipolar relaxations and the MWS process were calculated and the pertinent contributions are shown in **Figure 5.10**. The *ac* conductivity calculated from the sum of the contributions of the relaxations is indicated by a continuous line in the σ' isotherm, while the relative errors involved in the calculation of σ', *i.e* $\left(\sigma'_{calc} - \sigma'_{exptl}\right)/\sigma'_{exptl}$, are shown in the inset of **Figure 5.10**. Taking into account that in the high frequency range ($\omega \to \infty$), the dielectric loss of the secondary and MWS relaxations scales as $\varepsilon'' \sim \omega^{-a}$ whereas the glass-rubber or α relaxation scales as $\varepsilon'' \sim \omega^{-ab}$, the following scaling laws are obtained

$$\sigma_i'(\omega) \sim \omega^{1-a};\ i = \gamma, \beta, MWS \tag{5.5}$$

$$\sigma_\alpha'(\omega) \sim \omega^{1-ab} \tag{5.6}$$

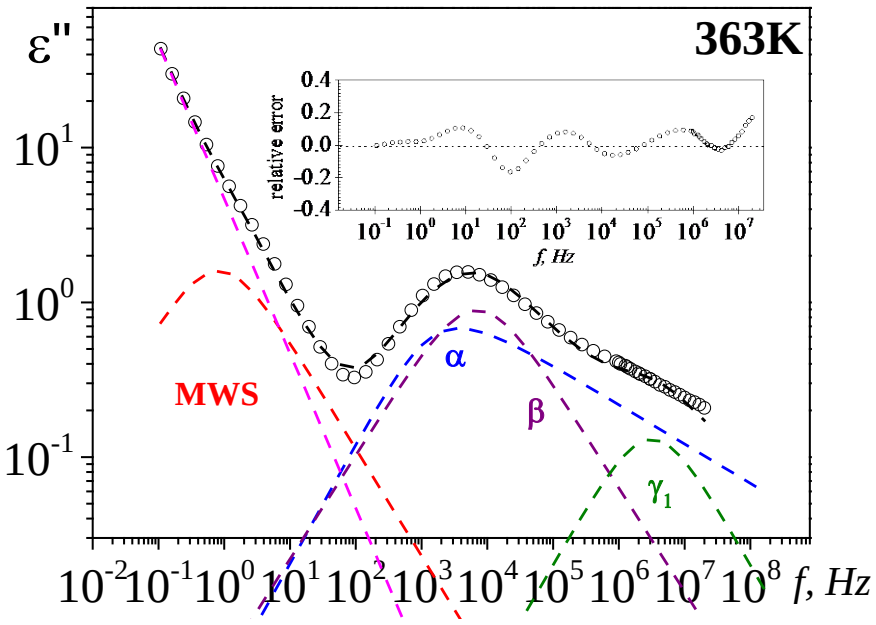

Figure 5.9. Dielectric loss permittivity for PDMB23 in the frequency domain at 363K. The pink line represent the *dc* conductivity, the red line the MWS process, the blue line the α relaxation, the purple β relaxation and the green line the γ relaxation. The black line represents the dielectric loss permittivity recalculated from the deconvoluted relaxations. Inset: relative error calculated as $(\varepsilon''_{calcd} - \varepsilon''_{exptl})/ \varepsilon''_{exptl}$.

The red line represents the α relaxation, the blue line the β process and the green line the γ relaxation. The black line represents the dielectric loss permittivity recalculated from the deconvoluted relaxations. Inset: relative error calculated as $(\varepsilon''_{calcd} - \varepsilon''_{exptl})/\varepsilon''_{exptl}$.

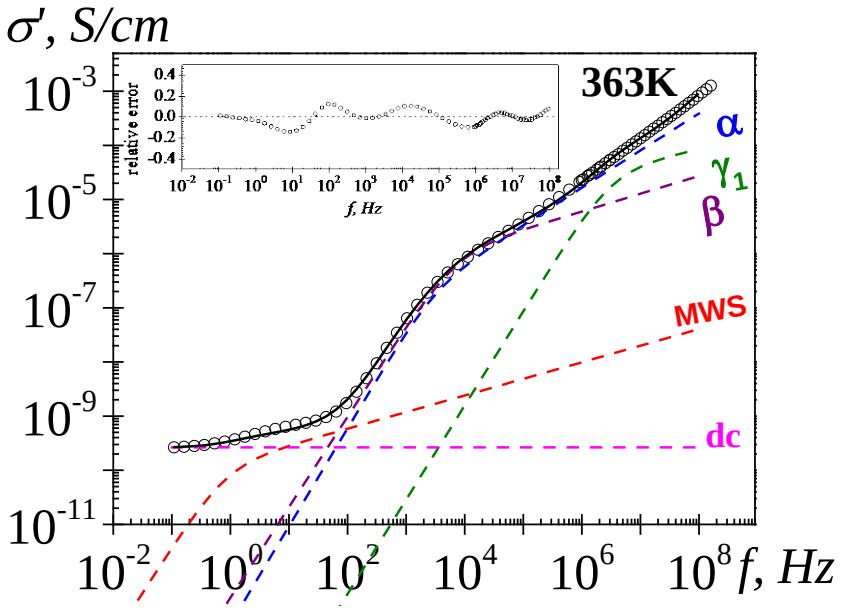

Figure 5.10. Dielectric conductivity for PDMB23 in the frequency domain at 363K. The pink line represent the *dc* conductivity, the red line the MWS process, the blue line the α relaxation, the purple β relaxation and the green line the γ relaxation. The black line represents the dielectric loss permittivity recalculated from the deconvoluted relaxations. Inset: relative error calculated as $(\sigma'_{calcd} - \sigma'_{exptl})/ \sigma'_{exptl}$.

The double-logarithmic plot of the contribution of each secondary relaxation, as well as the MWS process, to the *ac* conductivity is a straight line with slope *1-a*, in the high frequency limit. Accordingly, the lower the exponent *a* (or the higher the departure from a Debye process), the larger the slope of the straight line they is. For the α relaxation, the product of the shape factors, *ab*, governs the terminal *ac* conductivity in such a way that, the lower the product *ab*, the higher the slope of the contribution of the α relaxation in the limit $\omega \to \infty$ is. The upper bound limit of the slope is 1 that corresponds to $a = b = 0$. Notice that for a Debye relaxation $a = b = 1$, and $\lim_{\omega\to\infty}[d\log\sigma'(\omega)]/d\log\omega = 0$, *i.e.* the *ac* conductivity is independent on frequency.

Then, $0 < \lim_{\omega\to\infty}[d\log\sigma'(\omega)]/d\log\omega \leq 1$ for the contributions of the individual relaxations to σ' at $\omega \to \infty$.

5.2.2. Time Temperature Correspondence

The σ' isotherms were normalized with respect to the *dc* conductivity (see **Figure 5.11**) and shifted to the reference isotherm (408K). The isotherms superpose rather well over the isotherm of reference, obtaining the master curve shown in the inset of **Figure 5.11**. Notice that the master curve extends over roughly twelve decades. The frequency-temperature correspondence principle holds and the empirical shift factors a_T used are plotted as a function of temperature in **Figure 5.12**. An inspection of **Figure 5.6** inset clearly reveals the frequency ω_c at which the *ac* conductivity experiences a slow increase reaching a small plateau, followed by a sharp increase of σ' with increasing frequency at a frequency ω'_c. The double logarithmic plot of σ' *vs.* ω at high frequencies is a straight line of slope 0.75. It is worth noting that the extrapolation of the straight line to the low frequency region intercepts the σ' isotherm at ω_c. Being ω_c the frequency at which the low frequency side of the MWS relaxation intercepts with the abscissa axis.

Table 5.1. HN fit parameters for ε″(ω) at several temperatures for PDMB23

T(K)	$\Delta\varepsilon_\alpha$	$\Delta\varepsilon_{\alpha'}$	$\Delta\varepsilon_\beta$	$\Delta\varepsilon_\gamma$	a_α	$a_{\alpha'}$	a_β	a_γ	b_α	$b_{\alpha'}$	$\log_{10}\tau_\alpha$[s]	$\log_{10}\tau_{\alpha'}$[s]	$\log_{10}\tau_\beta$[s]	$\log_{10}\tau_\gamma$[s]
328	6.02			0.12	0.55			0.68	0.40		-0.38			-5.80
333	4.75		2.36	0.12	0.72		0.58	0.48	0.33		-1.15		-2.93	-6.15
338	4.38		2.53	0.13	0.74		0.61	0.54	0.34		-1.83		-3.23	-6.33
343	3.99		2.71	0.14	0.76		0.62	0.61	0.34		-2.36		-3.57	-6.46
348	3.86		2.84	0.15	0.78		0.64	0.66	0.35		-2.83		-3.86	-6.69
353	3.85		2.99	0.16	0.80		0.66	0.70	0.37		-3.27		-4.14	-6.85
358	3.78	4.27	3.14	0.17	0.80	0.65	0.66	0.73	0.38	1.00	-3.71	-0.38	-4.39	-7.08
363	3.77	3.87	3.24	0.18	0.81	0.69	0.67	0.74	0.39	1.00	-4.17	-0.71	-4.64	-7.30
368	5.69	3.75		0.20	0.69	0.70		0.75	0.55	0.99	-4.53	-0.97		-7.53
373	5.49	3.72		0.20	0.70	0.71		0.72	0.55	0.99	-4.91	-1.19		-7.76
378	5.30	3.69		0.21	0.70	0.69		0.69	0.55	1.00	-5.17	-1.46		-7.95
383	5.08	3.45		0.21	0.70	0.70		0.67	0.55	1.00	-5.41	-1.72		-8.10
388	4.90	3.34		0.21	0.71	0.72		0.66	0.55	1.00	-5.61	-1.92		-8.20
393	4.72	3.34		0.22	0.71	0.72		0.66	0.55	1.00	-5.83	-2.10		-8.38
398	4.55	3.16		0.23	0.71	0.73		0.66	0.56	1.00	-6.00	-2.30		-8.50
403	4.40	3.13		0.23	0.71	0.73		0.66	0.58	1.00	-6.19	-2.46		-8.65
408	4.27	3.09		0.24	0.71	0.73		0.67	0.60	1.00	-6.36	-2.61		-8.77
uncertainty	±0.01	±0.01	±0.01	±0.01	±0.01	±0.01	±0.02	±0.02	±0.02	±0.01	±0.02	±0.02	±0.02	±0.02

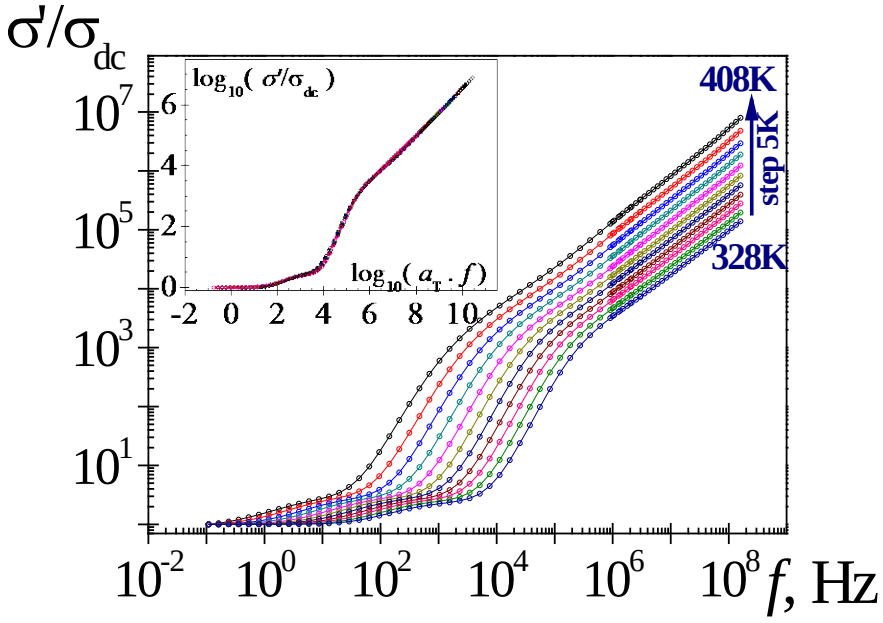

Figure 5.11. The σ' isotherms normalized with respect to the dc conductivity. The inset shows the master curve obtained using as the reference isotherm T_0=408K.

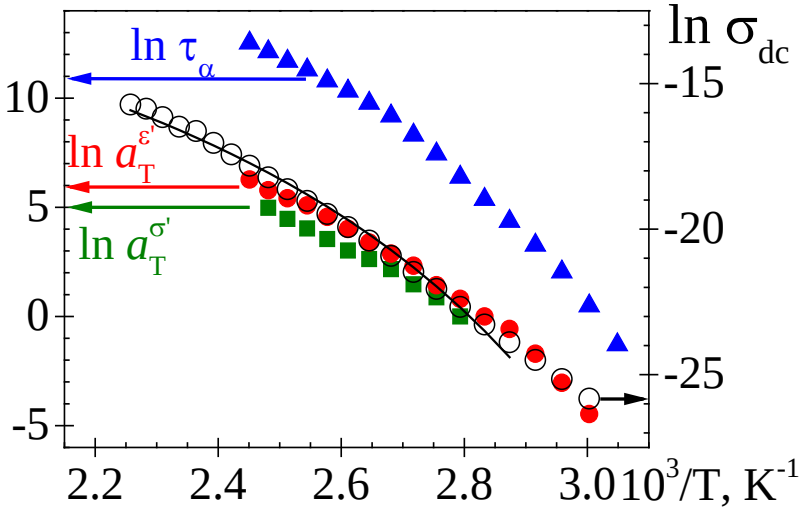

Figure 5.12. Temperature dependence of the empirical shift factors a_T (left-full square: σ' and left-full circle: ε'), the τ_α (left- full triangle) and of the σ_{dc} (right-open circle)

A general approach for the study of the time/frequency temperature correspondence for the *ac* conductivity is to use the scaling ansatz (Bowen, et al., 2006; Murugaraj, 2007; Papathanassiou, y otros, 2007)

$$\sigma'(\omega,T)=\sigma_{dc}\, f[\omega/\omega_c(T)] \qquad (5.7)$$

where $f(\omega/\omega_c)$ is the so-called scaling function and ω_c the previously defined angular frequency marking the onset of the *ac* conductivity. The results of **Figure 5.13** show that the scaling law not only holds for disordered ion conducting inorganic systems, but also for polar rubbery liquids. Long ago, several authors (Barton, 1966; Nakajima, 1972 ; Namikawa, 1975) formulated an empirical expression that permits to estimate ω_c in terms of the *dc* conductivity σ_{dc} and of the dielectric strength $\Delta\varepsilon$ in disordered inorganic ion conducting systems. This expression is known as the BNN equation and is given by

$$\omega_c=\frac{\sigma_{dc}}{p\varepsilon_0\Delta\varepsilon} \qquad (5.8)$$

where *p* is a parameter of the order of unity. Dyre et al have shown that through the low-frequency expansion of the conductivity (Dyre, et al., 2009), a connection between equations (5.7) and (5.8) can be made. Actually, according to equation (5.7), the complex conductivity at $\omega\rightarrow 0$ can be written as $\sigma^*(\omega)=\sigma_{dc}(1+jK\omega/\omega_c)$ where *K* is a real parameter. So dividing the two sides of this expression by $j\varepsilon_0\omega$, taking into account that $\varepsilon^*(\omega)-\varepsilon_\infty=\sigma_{ac}^*(\omega)/j\varepsilon_0\omega$, and equating the real components, in the limit $\omega\rightarrow 0$, it is obtained that $\varepsilon(0)-\varepsilon_\infty=\Delta\varepsilon=K\sigma_d/\omega_c$. Notice that $K = 1/p\varepsilon_0$. The values of ω_c calculated by means of equation (5.8), using $p = 1$, are compared in **Figure 5.14** with those estimated

from the isotherms. It can be seen that the calculated values lie roughly one decade below than those estimated from the BNN equation. However, the results corresponding to ω'_c, (the frequency that marks the onset of the glass-rubber relaxation, **Figure 5.6**), are in satisfactory agreement with those predicted by equation (5.8). This means, according to our results, that the BNN equation only holds for polar rubbery liquids where MWS process is absent.

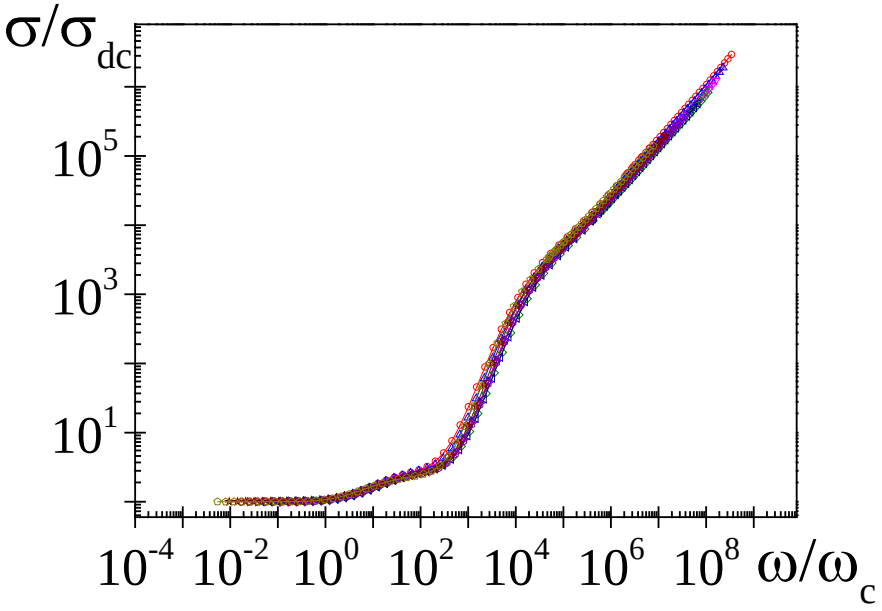

Figure 5.13. Temperature dependence scaling spectra for the *ac* conductivity using the scaling ansatz $\sigma'(\omega,T)=\sigma_{dc}\,f[\omega/\omega_c(T)]$

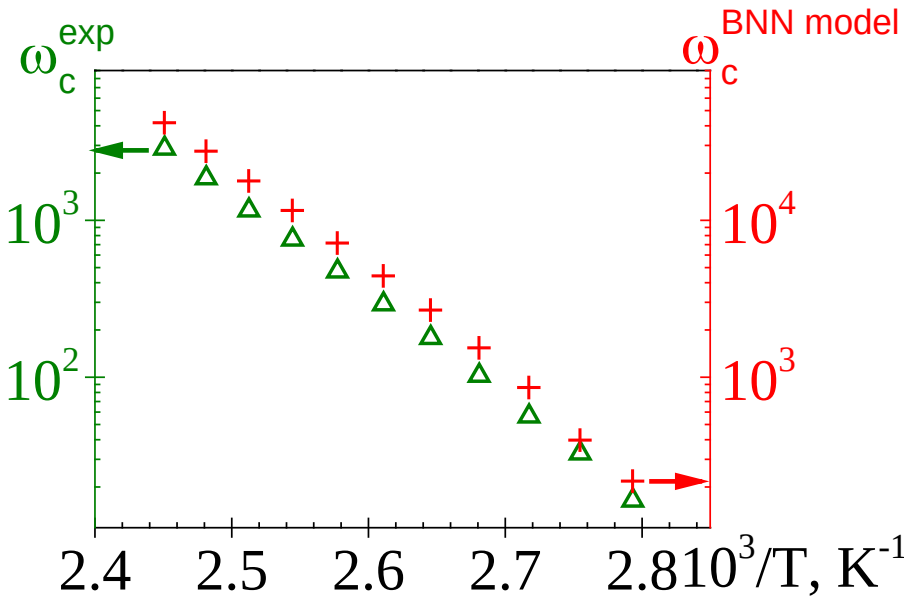

Figure 5.14. Temperature dependence of ω_c (Hz) obtained from the experimental isotherm (triangle-left) and from BNN model (plus-right).

5.2.3. Time-Temperature Correspondence for Dipolar Processes

Figure 5.15 shows the master curve obtained by shifting the isotherms representing values of $(\varepsilon' - \varepsilon_\infty)/\Delta\varepsilon$ over the 353K reference isotherm. It can be seen that the superposition is rather poor, in spite of the fact that a vertical shift to improve the superposition was employed. The failure is even more visible if the reduced isotherms for ε' are expressed in the logarithmic form (inset **Figure 5.15**). As can be seen in **Figure 5.15**, a good superposition is obtained at low frequencies but a great dispersion is observed at high frequencies, where dipole mechanisms that give rise to the glass-rubber and the secondary relaxations are active. The cause of the failure is multiple. For example, an increase in

temperature hinders the alignment of the dipoles with the electric field in the glass-rubber relaxation, thus reducing the relaxed dielectric permittivity and decreasing the height of the plateau. As a result, the width of the glass rubber relaxation tends to decrease with increasing temperature as show the PBDM23 data reported (Sanchis, et al., 2010) for the stretch exponent of the KWW equation. The vertical shifts necessary to superpose the plateaus, may not superpose the secondary relaxations. On the other hand, an augment of temperature tends to increase the dielectric strength of secondary relaxations. In order to the time-temperature correspondence holds, an important condition is that the relaxation times of all relaxations have similar temperature dependence. However, that dependence is much stronger in the glass-rubber relaxation than in the secondary processes. Therefore, the time-temperature correspondence for the components of the complex dielectric permittivity might only hold for weakly polar polymer systems. In this regard, Zorn et al. found a good time-temperature superposition for the dielectric loss of polybutadienes. The superposition only failed in the samples of polybutadiene with the lowest fraction of vinyl content (0.07) (Zorn, et al., 1997). In spite of the reasons indicated above for the failure of the time-temperature superposition of the dielectric permittivity in polar polymers, Zhao and McKenna (Zhao, et al., 1997) recently reported a good time-temperature superposition for poly(vinyl acetate) at $T > T_g$. However, a detailed analysis of the secondary relaxations, especially dielectric strengths and temperature dependence, hasn't been discussed.

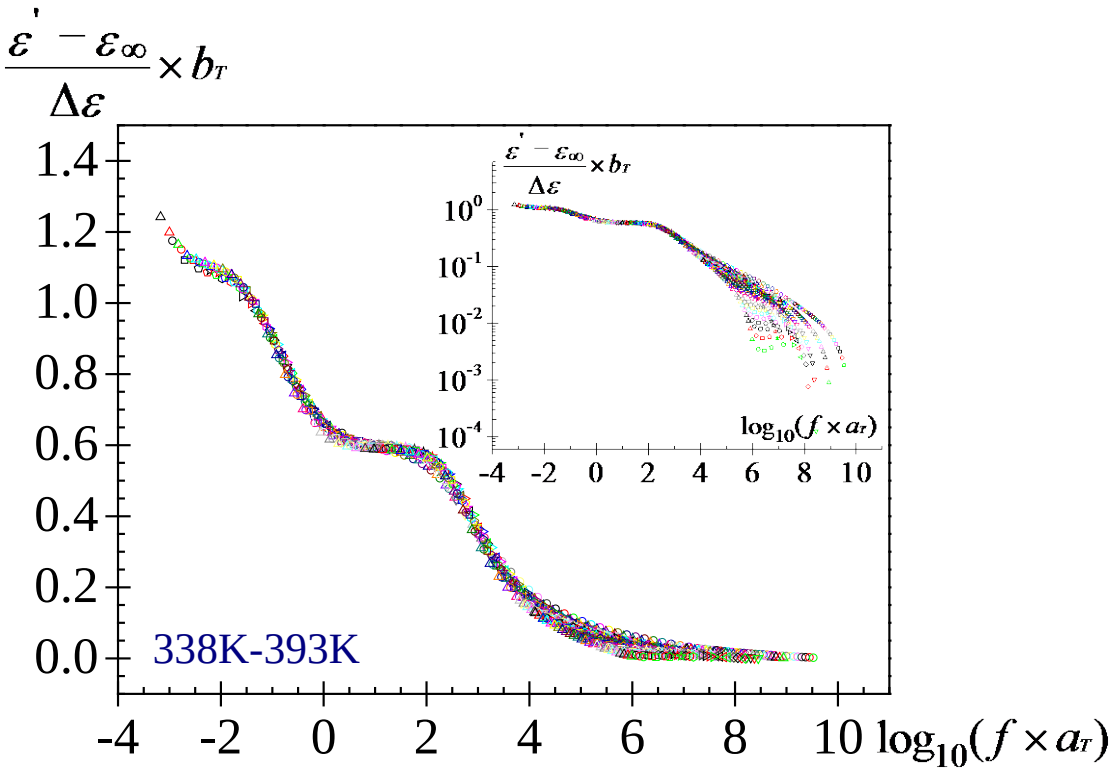

Figure 5.15. Master curve of the dielectric permittivity normalized for PDMB23 in the frequency domain (T_0=353K).

5.2.4. Temperature Dependence of the Conductivity and Relaxation Processes

As usual, the PBDM23 secondary relaxations, γ and β, obey Arrhenius behavior with activation energies in kJ·mol^{-1} of 95 and 132, respectively. The faster absorption, the γ process, is attributed to motions of the terminal dimethoxy phenyl group, whereas the β relaxation is associated with motions of the side groups, which are alone or coupled with local motions of the backbone. The relative closeness of the activation energies for the two

relaxations suggests that the β process is presumably only produced by motions restricted to the side groups.

Figure 5.12 shows the Arrhenius plots for σ_{dc} and a_T (used in the generation of the dielectric permittivity and conductivity master curves), which remind the temperature dependence of the relaxation time associated with the dipolar glass-rubber relaxation, also shown in the figure. This means that the *ac* charge transport is governed by both, the free volume and the temperature. By assuming that the Doolittle equation (Doolittle, 1951; Doolittle, 1952) holds, *i.e.* $\sigma(\omega,T)\sim[B/\Phi(T)]$, where Φ is the relative free volume and B is a parameter close to the unit, the Vogel-Fulcher-Tamman-Hesse (VFTH) equation (Vogel, 1921; Fulcher, 1925; Tamman, et al., 1926) is obtained. Actually, since the specific volume υ is related to temperature by $\upsilon=\upsilon_0+\alpha_f(T-T_V)$, where T_V is the Vogel temperature (or the temperature at which the configurational entropy of the system is nil) and α_f is the expansion coefficient ($\alpha_f=(1/v)(\partial v/\partial T)_p$), σ is given by

$$\sigma(\omega,T)=A\exp\left(\frac{m}{T-T_V}\right) \qquad (5.9)$$

where $m = Bv_0/\alpha_f$, being υ_0 the occupied volume in the specific volume υ. The **Figure 5.6** shows that σ' is described by equation (5.2). By combining the Doolittle equation (Doolittle, 1951; Doolittle, 1952) with equation (5.9) yields $\Phi_g/B=(T_g-T_v)/m$, where Φ_g is the relative free volume at T_g. Taking into account that T_V = 265K, and assuming that B = 1, it is obtained $\Phi_g = 4.0\cdot10^{-2}$ and $\alpha_f = 7.3\cdot10^{-4}K^{-1}$. These last parameters, obtained from

the Arrhenius fit (ln τ_α *vs* T^{-1}), are $3.4 \cdot 10^{-2}$ and $6.2 \cdot 10^{-4}$ K^{-1}, respectively (Sanchis, et al., 2010).

5.2.5. Conductivity Mechanisms and Concentration of Ionic Species

The conductivity mechanism in solid disordered systems is explained by the random barrier model (RBM) (Dyre, et al., 2000). The model considers the hopping of a simple particle on a lattice, with barrier energies between neighboring sites randomly drawn from a smooth probability distribution. The obtained results, for the evolution of the *ac* conductivity of rubbery liquids, can also be interpreted in terms of this model. Thus, the rather sharp decrease of the *ac* conductivity, in the frequency region where dispersive processes occur, is a consequence of the fact that local relaxations together with the glass-rubber relaxation contribute to the topological disorder of the material. As a result, the energy barriers of the charge transport undergo an anomalous increase, hindering the back and forth motion of the charges that contribute to the dispersive *ac* conductivity. The departure of the *ac* conductivity from the power law is comparatively small for rubbery liquids in the glassy state, where only secondary relaxations are displayed (Obrzut, et al., 2009). Long range motions that produce *dc* conductivity need to overcome a percolation barrier energy E_c, in such a way that the time necessary to accomplish it is $t_c \sim exp(-E_c/k_BT)$ (Bunde, et al., 1996). The reciprocal of t_c marks the onset of the *dc* conduction, *i.e.* $\omega_c \cong t_c^{-1}$ (Dyre, et al., 2000). Acting E_c as bottle neck explains the Arrhenius behavior of the *dc* conductivity. However, it is worth noting that the plot of ω_c *vs* the reciprocal of temperature is not a straight line.

Schröder and Dyre have recently shown (Schröder, et al., 2008) that if $\bar{\sigma}=\sigma^*(\omega)/\sigma_d$ and $\bar{\omega}$ is a suitable scaled frequency, *i.e.* ω/ω_c, the RBM theory predicts at $\omega > \omega_c$ that

$$\ln\bar{\sigma}=\left(\frac{j\bar{\omega}}{\bar{\sigma}}\right)^{2/3} \tag{5.10}$$

A better expression in the whole frequency range is

$$\ln\bar{\sigma}=\frac{j\bar{\omega}}{\bar{\sigma}}\left(1+\frac{8}{3}\frac{j\bar{\omega}}{\bar{\sigma}}\right)^{-1/3} \tag{5.11}$$

As shown in **Figure 5.16** and **Figure 5.17**, neither equation (5.10) nor equation (5.11) fit to the *ac* conductivity in the frequency domain. However, the fitting should be significantly better for PBDM23 in the glassy state, where segmental motions are frozen. Unfortunately, the fact that the *dc* conductivity of polar polymers in the glassy state cannot be estimated impedes the testing of these expressions in glassy PBDM23.

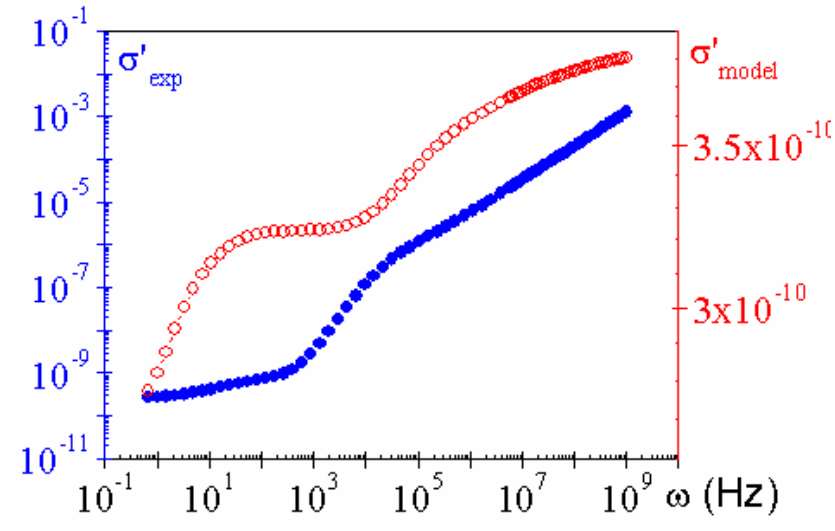

Figure 5.16. Blue points represent the experimental data and red points represent the testing with the equation (5.10).

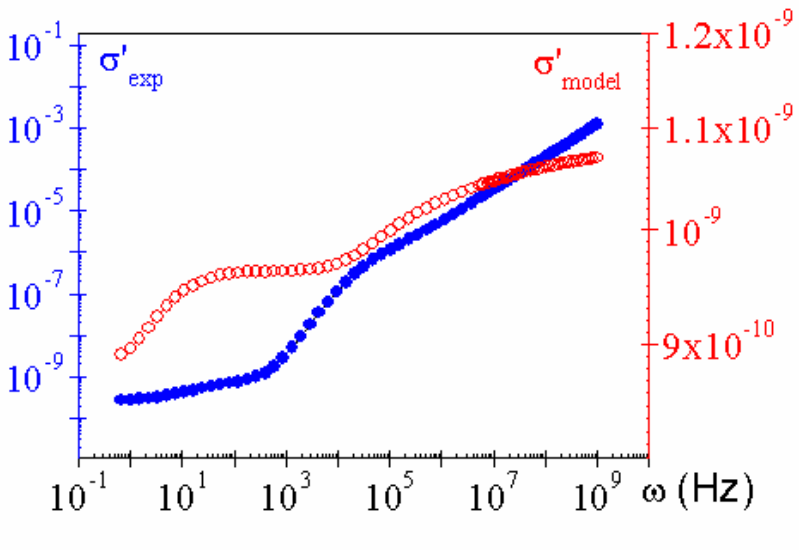

Figure 5.17. Blue points represent the experimental data and red points represent the testing with the equation (5.11).

5.2.6. Concentration of residual ionic species

In principle, the concentration of residual ionic species in rubbery liquids that produce *dc* conductivity can be estimated using phenomenological Nernst type equations to describe ion motion in these systems. Let us assume a system with N particles in a volume V, each with charge q, under an electric field $d\psi/dx$. Each particle is accelerated by action of the force $qd\psi/dx$. However, a velocity u_i is reached at which the friction interaction of each particle with the surroundings χu, (χ representing the interaction particle-surroundings), compensates the accelerating force in such a way that the particle reaches steady motion (u = constant). In these conditions, $u = -(q/\chi)d\psi/dx$. The flux of the particle is $J = Nu/V = -[q(N/V) / \chi]d\psi/dx$. Then, the current density is $i = qJ = -[q^2(N/V) / \chi]d\psi/dx$, and the *dc* conductivity is $\sigma_{dc} = -i/(d\psi/dx) = [q^2D(N/V) / k_BT]$, where D is the diffusion coefficient of the particles. Notice that the Einstein's relationship $D = k_BT/\chi$, where k_B is the Boltzmann's constant, was used. If N_+ cations and N_- anions of charges q_+ and q_- are present in the volume V of the system, and taking into account the electroneutrality principle $N_+q_+ + N_-q_- = 0$, the conductivity of the material is $\sigma_{dc} = (q_+^2/ k_BTV) [D_+N_+ - (N_+/N_-)^2 D_-N_-]$. However, unlike disordered ion conducting materials, which contain specific ions responsible for the *dc* conductivity in the glassy state and in the melt, the chemical nature of the transport charges in rubbery liquids is unknown. The *dc* conductivity observed in polymers, except in electronic and ionic conducting polymers, proceeds from humidity traces, impurities present in the reactants, solvents, etc. used in the synthesis of the material. In order to estimate the concentration of ion impurities in rubbery liquids, it

would be necessary to know beforehand the diffusion coefficients of the ions by other methods, as pulsed field gradient RMN, and to assume the value of 1 for the Haven ratio. However, since the nature of the ions is unknown, their concentration cannot be obtained from RMN results and dielectric conductivities. Models have been described based on the motion at low frequencies of the macrodipole, produced by the charges accumulation at the polymer-electrode interface at very low frequencies, which allows the determination of charge impurities (Coelho, 1991; Satti, et al., 2007; Klein, et al., 2006; Compañ, et al., 1996; Sanchis, y otros, 2011). However, the concentration of ions estimated by the models has not been experimentally tested and the reliability of the results predicted is unknown. The polarization phenomena can be quantitatively reproduced by an approach and the observed scaling laws at the interface between the electrode and the ion conductor has recently been formulated. However, the approach does not address the estimation of the concentration of ionic species (Serghei, et al., 2009).

5.2.7. *ac* Conductivity at High Frequencies

For a variety of solids including glassy, crystalline and molten ion conductors, independently of the physical and chemical structures, the *ac* conductivity in the high frequency region follows the power law $\sigma'(\omega) = A\omega^n$, with $n \cong 1$ (Burns, et al., 1989; Ngai, 1999). This zone is called the nearly constant loss (NLC) regime, because it corresponds to the frequency region in which the dielectric permittivity is nearly independent on frequency. The isotherms representing the PBDM23 *ac* conductivity, shown in **Figure 5.4**, also follow the power law at high frequencies. However, the exponent *n* depends on

temperature in such a way that its value lies in the vicinity of 0.75 at $T < 357$ K, but at $T >$ 357K it is observed an increase as T decreases reaching a value of about 0.82 at 318 K (see **Figure 5.18**). This behavior suggests that the less relaxed are the dipoles in the rubbery liquid, the higher the exponent is. In the glassy state, the exponent n lies in the vicinity of the unit reaching the value of 1.05 at 223 K, 370 K below T_g. On the other hand, whereas the temperature dependence of *dc* conductivity is of Arrhenius type, so that it is a thermally activated process, the parameter A for PBDM23 only follows Arrhenius behavior at temperatures below T_g (see **Figure 5.18**). However, for temperatures above T_g, the dependence of A on the reciprocal of temperature presents a curvature that resembles the behavior of $\sigma'(\omega)$, ω_c and ω'_c, *i.e.* the variation of A with T is governed by the free volume and temperature. Therefore, the variation of A with temperature is described by the VFTH equation. Thus, the plot ln A *vs* $1/(T - T_V)$ is a straight line whose slope is lower than one third of that corresponding to $\sigma'(\omega)$, ω_c and ω'_c. The possible origin of the NCL regime is discussed in detail elsewhere, Dyre et al (Dyre, et al., 2009). The most recent interpretation suggests that the NCL is the simple extension of the dispersive conductivity to higher frequencies.

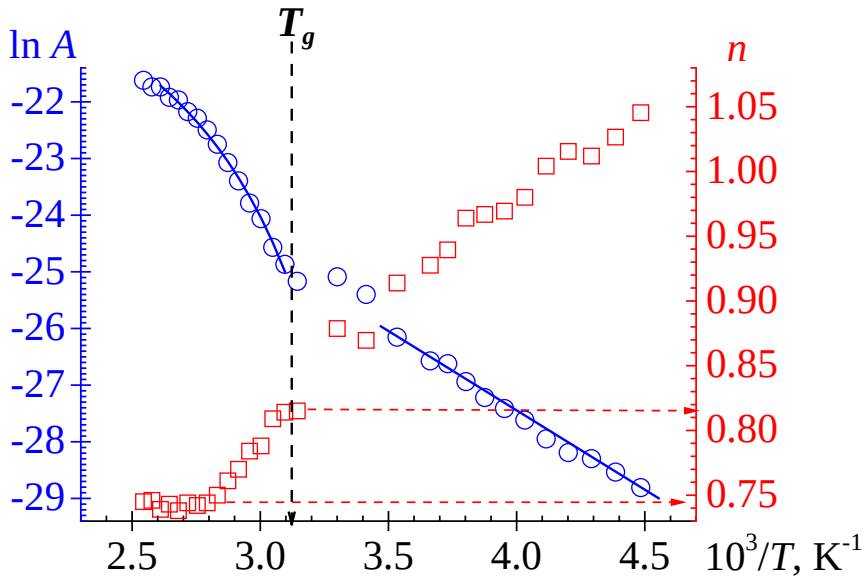

Figure 5.18. Temperature dependence of the *A* (circle) and *n* (square) parameters of the *ac* conductivity in the high frequency region ($\sigma'(\omega) = A\omega^n$)

5.3. Conclusions

The isotherms representing the *ac* conductivity of rubbery liquids in the frequency domain exhibit the same pattern as those corresponding to ion-conducting disordered solids. That is, they present a plateau in the low frequency region corresponding to the *dc* conductivity until a frequency ω_c is reached, which marks the onset of the *ac* conductivity. However, owing to strong dipolar relaxation processes taking place in rubbery liquids, the increase of the *ac* conductivity with frequency (at $\omega > \omega_c$) is not so smoothly as in the case of ion-conducting disordered solids.

The time-temperature correspondence principle for the *ac* conductivity of rubbery liquids obeys to the scaling ansatz, which governs the time-temperature superposition of ion conducting disordered solids. However, the time-correspondence principle does not hold for the components of the dielectric permittivity of rubbery liquids. The frequency at the onset of the *ac* conductivity, predicted by the BNN equation for the rubbery liquid used in this work, is nearly ten times higher than that estimated from the experimental results. However, it coincides with the maximum frequency, ω'_c, at which the dipoles are completely relaxed. The exponent of the power law in the NLC regime approaches to the unit as the temperature of the rubbery liquid comes close to T_g. On the other hand, the temperature dependence of proportional constant of the power law A (of the power law constant, A) obeys to the VFTH equation at $T > T_g$ and to the Arrhenius equation at $T < T_g$.

Chapter 6:

Effect of crosslinking on the molecular motions and nanodomains segregation in polymethacrylates containing aliphatic alcohol ether residues

The results collected in this Chapter were partially published in: M. Carsí, M.J. Sanchis, R. Díaz-Calleja, E. Riande, M.J.D. Nugent, *Macromolecules* vol 45, pp. 3571−3580, **2012**; M. Carsí, M.J. Sanchis, R. Díaz-Calleja, E. Riande, M.J.D. Nugent, European Polymer Journal, vol. 49, pp. 1495–1502, **2013**.

Abstract

The synthesis, thermal, dielectric and mechanical characterizations of uncrosslinked and lightly crosslinked poly(2-ethoxyethyl methacrylate) are reported. The relaxation spectra of the uncrosslinked poly(2-ethoxyethyl methacrylate) exhibits above T_g and at high frequencies a well-developed secondary γ relaxation. This process is followed in decreasing order of frequency for a relatively weak β relaxation and an ostensible glass-rubber relaxation which at high temperatures and low frequencies is dominated by electrode-polymer interfacial processes in the dielectric spectrum. By slightly crosslinking the polymer using 2.5% (mol) of ethylene glycol dimethacrylate as crosslinking agent, the β relaxation disappears, the γ relaxation remaining. The activation energy of the γ relaxation for the crosslinked and uncrosslinked polymers is ca. 30 kJ·mol^{-1}, about 10 kJ·mol^{-1} below the value of β relaxation. Crosslinking shifts the location of the glass-rubber relaxation nearly 283K to higher temperatures, without widening the distribution of relaxation times. The X-rays pattern of the crosslinked polymer presents two peaks at q =5.6 nm^{-1} and 12.76 nm^{-1} resembling the X-ray patterns of poly(n-alkyl methacrylate)s. The peaks in poly(n-alkyl methacrylate)s were attributed to the formation of nanodomains integrated by side chains flanked by the backbone. However, whereas this heterogeneity produces an α_{PE} peak in poly(n-alkyl methacrylate)s with $n \geq 2$, this microheterogeneity gives rise to a Maxwell-Wagner-Sillars (MWS) relaxation in the cross- linked polymer located at lower frequencies than the glass rubber relaxation. Nanodomains formed by side-groups flanked by the backbone give rise to a Maxwell-Wagner-Sillars relaxation in the dielectric spectra that have no incidence in the mechanical relaxation spectra. Finally the interfacial-electrode conductive processes of the crosslinked and uncrosslinked polymeric systems are studied in the light of current theories.

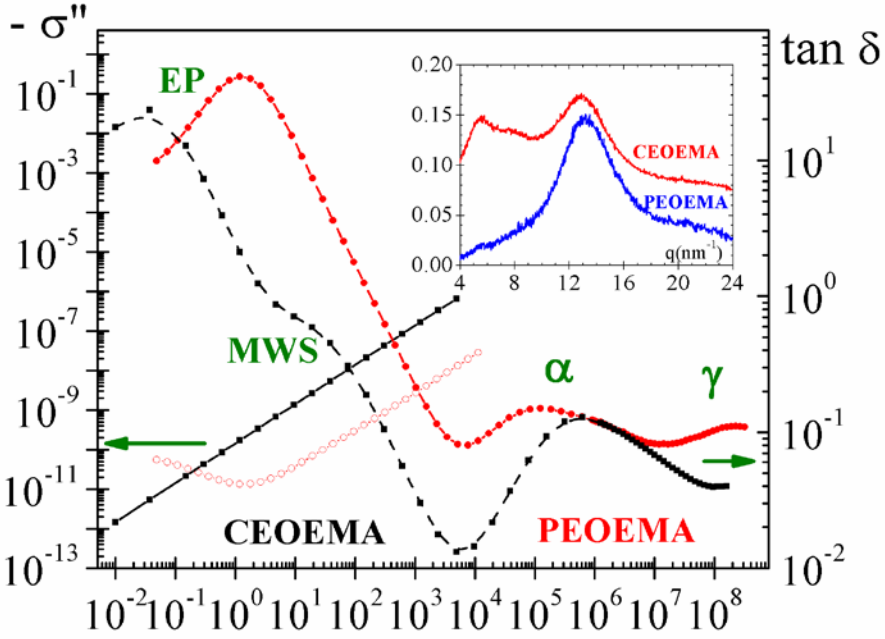
- σ"
tan δ
EP
MWS
α
γ
CEOEMA
PEOEMA
CEOEMA
PEOEMA
q(nm⁻¹)

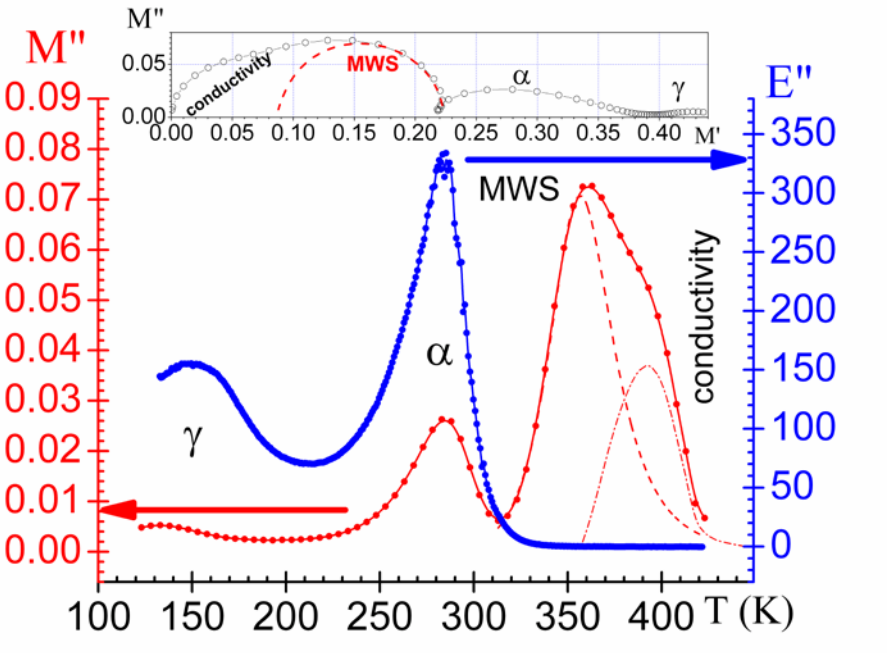
M"
E"
MWS
α
γ
conductivity
T (K)
M'

6. Effect of crosslinking on the molecular motions and nanodomains segregation in polymethacrylates containing aliphatic alcohol ether residues

6.1. Introduction

The time domain response of linear polymer chains without flexible side groups to a mechanic perturbation field Γ is given by $\Gamma(t) = \Gamma_0 \Delta(t)$, where $\Delta(t)$ is the Heaviside step function. This involves at very short times, the local motions of the skeletal bonds. Over time, an increasing amount of the skeletal bonds intervene in the response until the whole chains move and flow takes place. In the frequency domain the chain motions appear as relaxations in the mechanical loss spectra. At very low frequencies the normal mode, which reflects the disentanglement of the chains, appears. The normal mode is followed at higher frequencies by the glass-rubber or α relaxation produced by segmental motions of the chains. At even higher frequencies the so-called secondary relaxations are detected in the spectra. In order of increasing frequency the secondary relaxations are named β, γ, δ, etc. The secondary relaxations are present in the liquid and glassy states while the glass-rubber and normal mode relaxations freeze at T_g.

Unfortunately, the response of polymers to perturbation fields can only be obtained in a few decades of time/frequency in the case of mechanical force fields so that obtaining

information over a long frequency/time range requires the application of the temperature-frequency/time superposition principle, which only holds for thermorheological simple systems. This disadvantage can be overcome using broadband dielectric spectroscopy (BDS), a technique that enables analysis of the chains response over more than 10 decades in the frequency domain. However, a disadvantage of the BDS technique is that the total dipole moments associated with most polymer chains do not scale with chains length and therefore the BDS technique is insensitive to chains disentanglement reflected in the normal mode process. Only the normal mode of chains with dipole moments parallel to the chain contour can be studied with the BDS technique.

The term methacrylates cover a wide variety of polymers differing in the nature of the alcohol residue. The first member of the series, poly(methyl methacrylate), is the most commonly used of the methacrylate family, mostly in automotive/home applications (Mark, 2007). The polymer exhibits an ostensible β relaxation arising from rotation of the $C(CH_3)$-$C(O)OCH_3$ side group, located in the vicinity of the α relaxation. The position and relative intensity of the α/β relaxations depends on the nature, i.e. size and polarity, of the ester residue. If the residue results from n-alkyl alcohols (i.e. ethyl, propyl, butyl, etc.), it can be stated that longer alkyl groups will have a greater impact on the mechanical and dielectric properties of the polymers (Ishida, et al., 1961; Heijboer, 1972; Sasabe, et al., 1968; Cowie, 1980; Williams, et al., 1971; Gómez Ribelles, y otros, 1985; Diaz Calleja, et al., 1989; Diaz Calleja, et al., 1989; McCrum, et al., 1991; Floudas, et al., 1995) (Dudognon, et al., 2001; Dudognon, et al., 2002). A great deal of work has been reported related with the influence

of the size of the alkyl groups on the relaxations of these polymers (Garwe, et al., 1994; Garwe, et al., 1996; Schröter, et al., 1998; Arbe, et al., 2008; Beiner, et al., 1999; Beiner, 2001; Beiner, et al., 2002; Hempel, et al., 2002; Beiner, et al., 2003; Hiller, et al., 2004). Nanophase segregation of non polar alkyl side groups from the polar $–COO^-$ groups rigidly attached to the skeletal bonds of the chain, has been reported for these material types (Wind, et al., 2005). The carboxyl groups presumably are concentrated at the surface of alkyl nanodomains formed by side groups of different structural units and different chains. Small domain sizes of the order of one nanometer have been detected by X-rays diffractograms of poly(alkyl acrylate)s (PnAAs) and poly(alkyl mehtacrylate)s (PnAMAs) (Beiner, 2001; Beiner, et al., 2003; Hiller, et al., 2004).

The presence of nanophase separation has been confirmed by the study of the dynamics of amorphous side-chain polymers. Dielectric studies carried out for higher PnAMAs with the number of carbon atoms in the alkyl residue lying in the range $4 \leq C \leq 12$ have shown the existence of two coexisting relaxation processes with typical features of glass transitions: one detected at low temperatures associated with cooperative motions of the alkyl groups in the nanodomains and therefore it is a polyethylene (PE) like glass transition (α_{PE}). Another glass transition is detected at higher temperature resulting from cooperative motions of the skeletal bonds (Beiner, 2001; Beiner, et al., 2003). The spectra of poly(2,3-dimethoxybenzyl methacrylate) shows the glass-rubber relaxation followed at lower frequencies by another well-developed relaxation attributed to a MWS process

arising from the transport of electric charges in segregated nanodomains formed by the side chains surrounded by the skeletal bonds (Sanchis, et al., 2010).

In view of these antecedents, one of the aims of this work was to investigate whether the replacement of a methyl group for an ether group in poly(n-penthyl methacrylate) affects the segregation of hydrophilic and hydrophobic domains observed in poly(n-alkyl methacrylate)s. For that purpose the response of poly (2-ethoxyethyl methacrylate) (PEOEMA) to electric perturbation fields was studied at several temperatures over the wide frequency window 10^{-2}-10^{9} Hz. This polymer has been used as drug-eluting extent coating for percutaneous coronary interventions, providing durable, robust coatings with precise control over rapamycin elution rates (Cheng, et al., 2006). The chemical structure of the repeating unit of PEOEMA is shown in **Figure 3.4**.

6.2. Results and discussion

6.2.1. Fourier Transform Infrared Spectroscopy (FTIR)

In order to characterize the polymer, Fourier Transform Infrared Spectroscopy (FTIR) was used to study the structure and complexation of the polymers. Infrared spectroscopy was performed on a Nicolet Avator 360 FTIR spectrometer, with a 32 scan per sample cycle. For each sample, scans were recorded from 4000 to 400 cm^{-1} with a resolution of 4 cm^{-1}. The spectra obtained show a signal at 1700 cm^{-1} associated with the C=O stretching vibration of carboxylic group, one signal at 2900 cm^{-1} due to CH_2

stretching and the signal at 1125 cm^{-1} associated with C-O-C asymmetric stretching (**Figure 6.1**).

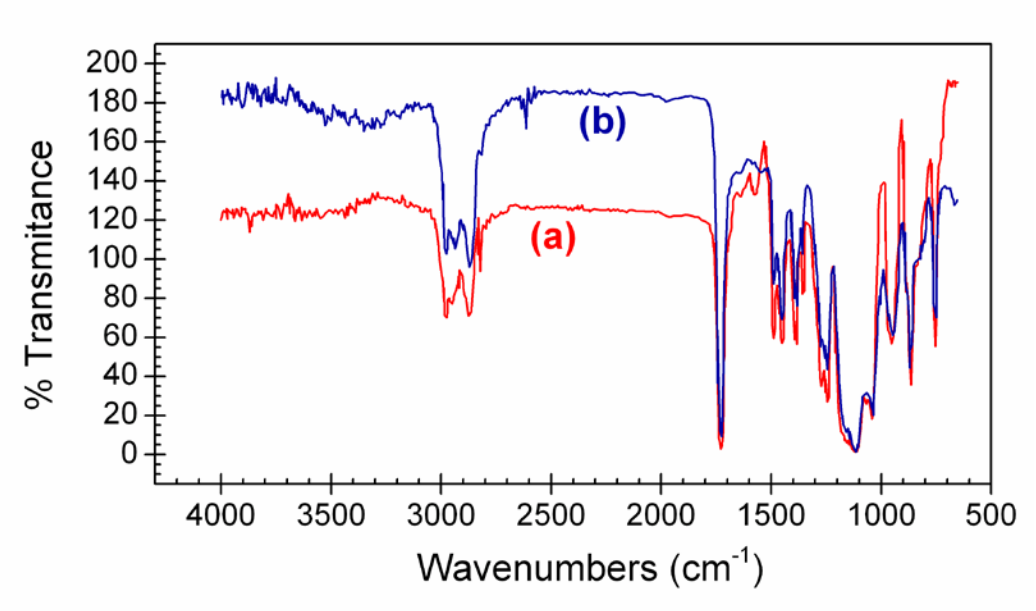

Figure 6.1. FTIR spectrum of (a) PEOEMA and (b) CEOEMA.

6.2.2. Differential Scanning Calorimetry (DSC)

Differential scanning calorimetry (DSC) of PEOEMA and CEOEMA was carried out with a TA Instruments DSC Q-10 differential scanning calorimeter in the range of 193K to 423K at a heating rate of $10K \cdot min^{-1}$ under nitrogen atmosphere.

The DSC thermograms for PEOEMA and CEOEMA exhibit well-developed endotherms associated with the glass transition temperature (**Figure 6.2**). The values of T_g of the samples, estimated as the temperature at the midpoint of the endotherms, and the heat capacity increments (Δc_p) at T_g were 278K, 0.27 $J \cdot g^{-1} \cdot K^{-1}$ and 268K, 0.28 $J \cdot g^{-1} \cdot K^{-1}$ for

CEOEMA and PEOEMA respectively. Thus, the crosslinking agent reduces the number of chains thermally activated and the chain mobility and thus raises the T_g *ca* 10K, and diminished the change in specific heat capacity (Δc_p). This effect can be understood in terms of decreasing free volume.

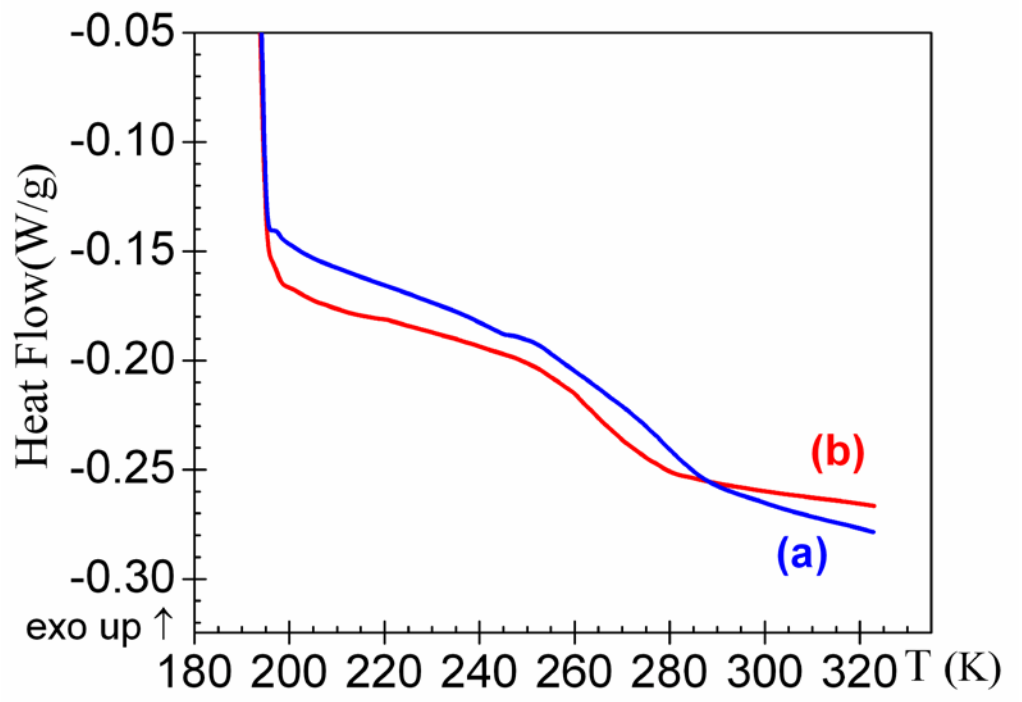

Figure 6.2. DSC curves taken at 10K·min^{-1} of (a) CEOEMA and (b) PEOEMA.

6.2.3. X-Rays Characterization

Poly(n-alkyl methacrylates) with $n \geq 2$ are characterized for forming self-assembled alkyl domains, whose sizes depends on the side chains lengths, arising from aggregations of the side groups of different monomeric units. Heat capacity measurements carried out in these polymers present a two glass transition temperatures associated respectively with

freezing of motions in within the alkyl domains (α_{PE}) and main chain dynamics (Beiner, 2001; Hempel, et al., 2002; Hempel, et al., 2003). The diffractogram patterns of WAXS and neutron-scattering spectra show two peaks respectively centered at $q \approx 5$ nm^{-1} (peak I) and 13.1 nm^{-1} (peak II). The value of q for peak I depends on the length of the n-alkyl group being 6, 5 and 4 nm^{-1} for poly(ethyl methacrylate), poly(buthyl methacrylate) and poly(hexyl methacrylate), respectively. The shifting of the peak to lower values of q with increasing alkyl length reflects main-chain correlations and therefore it is associated with average distance between the backbones. The value of q for Peak II poly(n-alkyl methacrylate)s lies in the vicinity of 12-13 nm^{-1} and therefore the peak is thought to be correlated with average distances between side-groups. With the aim to investigate whether main-chain and side-chain correlations still persist when a methyl group of the n-alkyl side chains are replaced by a methyl group, the WAXS diagrams of PEOEMA and CEOEMA were obtained. The diffractogram pattern of PEOEMA, presented in **Figure 6.3**, does not exhibit peak I, suggesting that main-chain correlations are not important enough to be detectable. Only peak II, centered at $q \cong 12.8$ remains, what means that segregation of side groups domains occurring in poly(n-butyl methacrylate) is absent in PEOEMA. However, the diffractogram of CEOEMA presents, in addition to the peak II that appears in PEOEMA ($q \cong 12.8$ nm^{-1}), a well-developed peak I centered at $q \cong 5.6$ nm^{-1}.

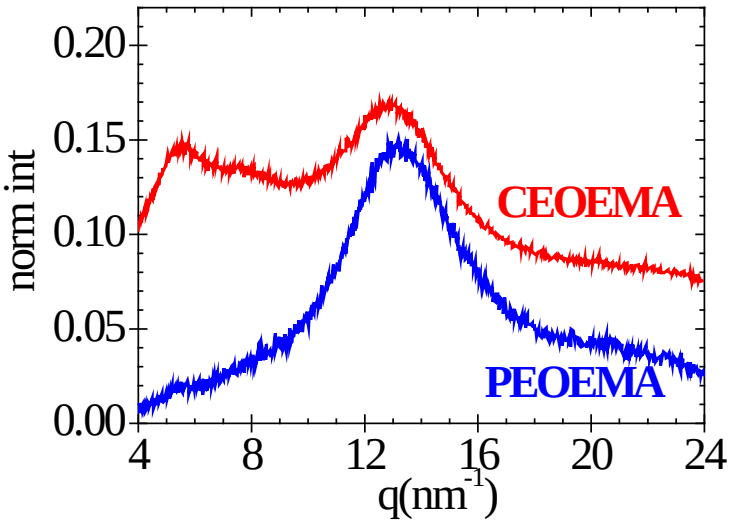

Figure 6.3. X-ray diffraction pattern for PEOEMA (blue) and CEOEMA (red).

The similarity of the difractograms of CEOEMA and poly(n-alkyl methacrylates) suggests the existence of side-chains nanodomains in the crosslinked polymer flanked by the backbone, the average distance between the backbone being about 1.13 nm. It seems that crosslinking stabilizes the formation of the nanodomains. To explain this behavior it is necessary to remind that PEOEMA exhibits a great conformational versatility. The restriction that the formation of nanodoamins impose to the polymer segments to visit the whole conformational space, to which otherwise they would have access, involves a decrease of entropy ($\Delta S < 0$), which must be compensated by intermolecular interactions. Then the absence of nanodomains in PEOEMA is the result of the fact that $|\Delta H| < T|\Delta S|$, where ΔH is the change in enthalpy. Notice that ΔH is assumed to be negative. Owing to the fact that crosslinking decreases the conformational versatility of the chains, $T|\Delta S|$ for CEOEMA is smaller than in the case of PEOEMA in such a way that $|\Delta H|_{\text{crosslinked}} >$

$T|\Delta S_{crosslinked}|$ and as a result the nanodomains in CEOEMA are stable. Finally, it should be pointed out that both the presence of a single endotherm in the DSC thermogram of CEOEMA and the symmetric nature of the α' relaxation rules out the possibility that the α' process is a glass-rubber relaxation.

6.2.4. Dynamic Mechanical Analysis (DMA)

Storage and loss moduli isochrones for PEOEMA and CEOEMA, over the temperature window 133–400K, are shown in **Figure 6.4** and **Figure 6.5**, respectively. The loss isochrones corresponding to PEOEMA show three differentiated relaxations zones. In order to a better comparation, in **Figure 6.6** are plotted the storage and loss Young's modulus as a function of the temperature for (a) PEOEMA and (b) CEOEMA at 1 Hz. Around 270K (1Hz), the dynamic mechanical response is dominated by the glass-rubber relaxation, but at lower temperatures, in the glassy state, a broad absorption centered around 210 K is evident. This absorption is labeled β relaxation. Finally, the loss isochrones show the presence of a γ-relaxation process below 145 K. The three relaxations observed in the isochrones of PEOEMA are reduced to two relaxations in the isochrones corresponding to CEOEMA. Thus the loss isochrones for the latter system exhibit at 1Hz a sub-glass absorption centered at 155 K (γ relaxation) followed in increasing order of temperature by the glass-rubber relaxation (α process) centered at 280 K at the same frequency. As would be expected, the location of the γ peak is shifted to higher temperatures as frequency increases, and the intensity of the peak increases as the

frequency of the isochrones increases. The location of the α relaxation is also displaced to higher temperatures, as frequency increases, but the intensity of the relaxation seems to be independent on the frequency of the isochrone.

The more significant differences between the mechanical behavior of PEOEMA and CEOEMA are the following: (i) the γ relaxation of former system is located at slightly lower temperature than that of the latter; (ii) the β relaxation detected in the isochrones of PEOEMA disappears in CEOEMA, and (iii) as a consequence of the reduction in chains mobility caused by crosslinking the location of the α relaxation is shifted to higher temperature, in consonance with the DSC results.

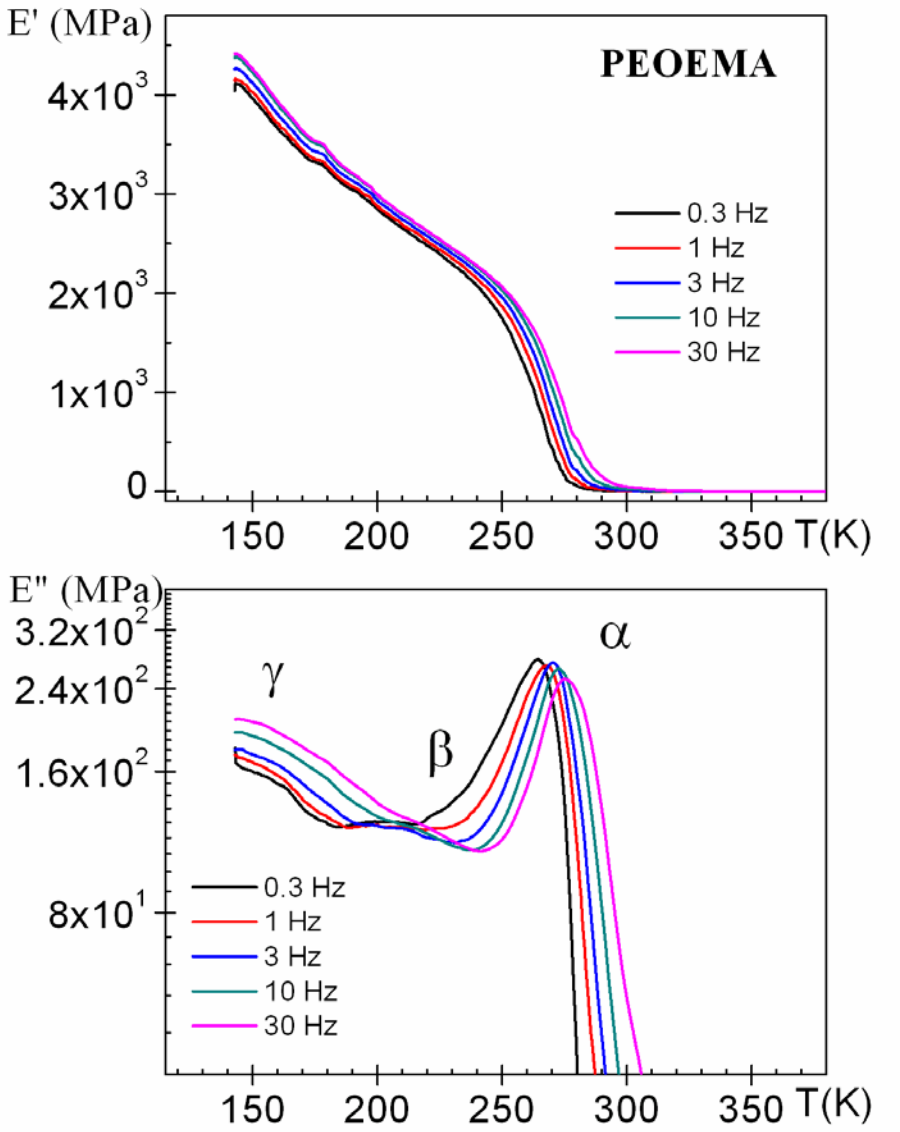

Figure 6.4. Storage and loss Young's modulus as a function of the temperature for PEOEMA at several frequencies (0.3, 1, 3, 10 and 30 Hz).

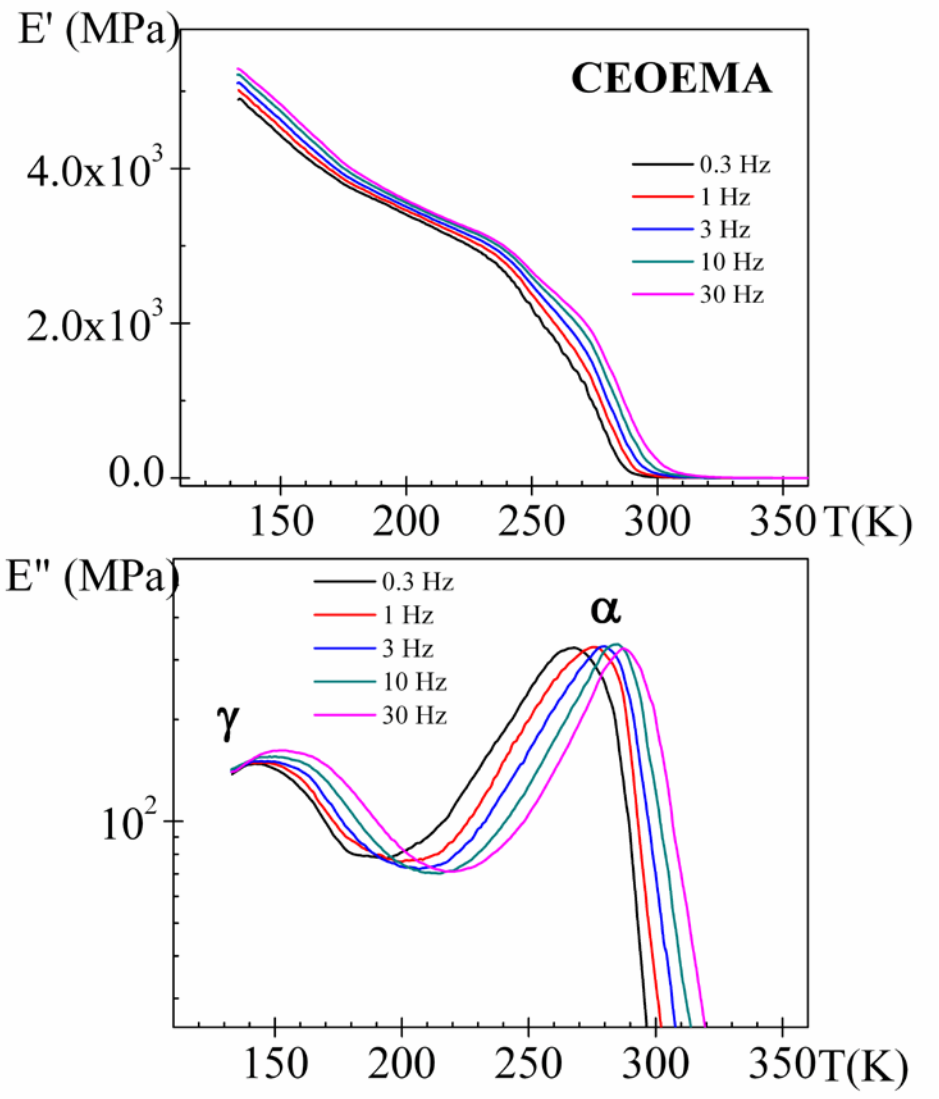

Figure 6.5. Storage and loss Young's modulus as a function of the temperature for CEOEMA at several frequencies (0.3, 1, 3, 10 and 30 Hz).

Since the γ-relaxation in the spectra falls just on the low temperature limit reached by the apparatus, it is difficult to estimate the parameters describing the relaxation. Using the Heijboer assumption that states that the Arrhenius equation describing the temperature

dependence of the relaxation times associated with the secondary relaxations of most flexible polymers has the same pre-exponential factor $\tau_0=10^{-14.5}$s (McCrum, et al., 1991), the activation energies of the γ relaxations of PEOEMA and CEOEMA are, respectively, 44.4 kJ·mol^{-1} and 47.4 kJ·mol$^{-1.}$.

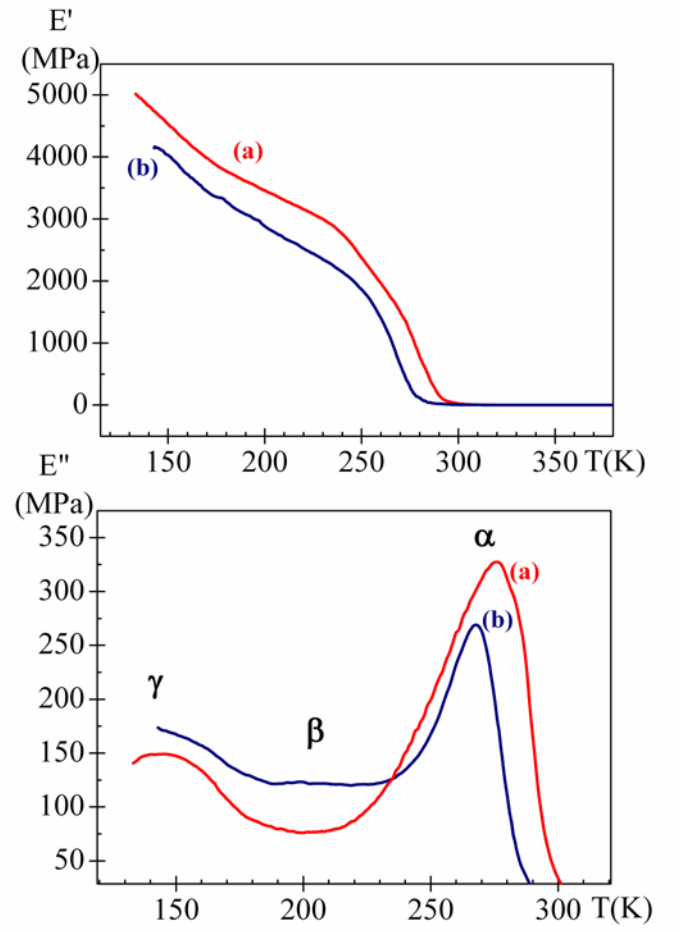

Figure 6.6. Storage and loss Young's modulus as a function of the temperature for (a) PEOEMA and (b) CEOEMA at 1 Hz.

An alternative method of obtaining directly the activation energies is to express the loss relaxation results in terms of compliance data, taking into account the following inequalities: $T(E''_{\max}) < T(\tan\delta_{\max}) < T(D''_{\max})$. This means that the loss compliance relaxations are shifted to higher temperatures than the loss modulus relaxation processes. The derivative of the logarithm of loss tan δ with respect to the temperature at peak maximun is given by $\frac{d\log\tan\delta_{\max}}{dT} = \frac{d\log E''}{dT} - \frac{d\log E'}{dT} = \frac{d\log D''}{dT} - \frac{d\log D'}{dT} = 0$ where D' and D'', are respectively the real and loss component of the complex compliance funcion D^* (= $1/E^*$). Taking into account that for any relaxation process E' and D' are respectively decreasing ($dE'/dT < 0$) and increasing ($dD'/dT > 0$) functions of temperature, at the peak maximum of the loss tan δ, the following inequalities hold. As can be seen in **Figure 6.7**, the compliance γ relaxation covers a temperature range that allows the estimation of the activation energy, strength and shape parameter of the process.

Sub-glass relaxations are usually nearly symmetric peaks, and therefore both isochrones and isotherms can be characterized by means of the Fuoss-Kirkwood equation (Fuoss, et al., 1941)

$$D'' = D''_{\max} \cdot \operatorname{sech}\, m\left[\frac{E_a}{R}\left(\frac{1}{T} - \frac{1}{T_{\max}}\right)\right] \qquad (6.1)$$

where T_{max} is the temperature where D'' have a maximum value ($D''_{\max}$), E_a is the apparent activation energy, R is the gas constant, and m is an empirical parameter ($0 < m < 1$) related to the broadness of the relaxation in the sense that the smaller m, the wider the distribution

is. The value of $m = 1$ corresponds to a single relaxation time (Debye peak). The strength of the mechanical relaxation peak can be calculated from the relationship $\Delta D = 2D''_{max}/m$ (Sasabe, et al., 1968).

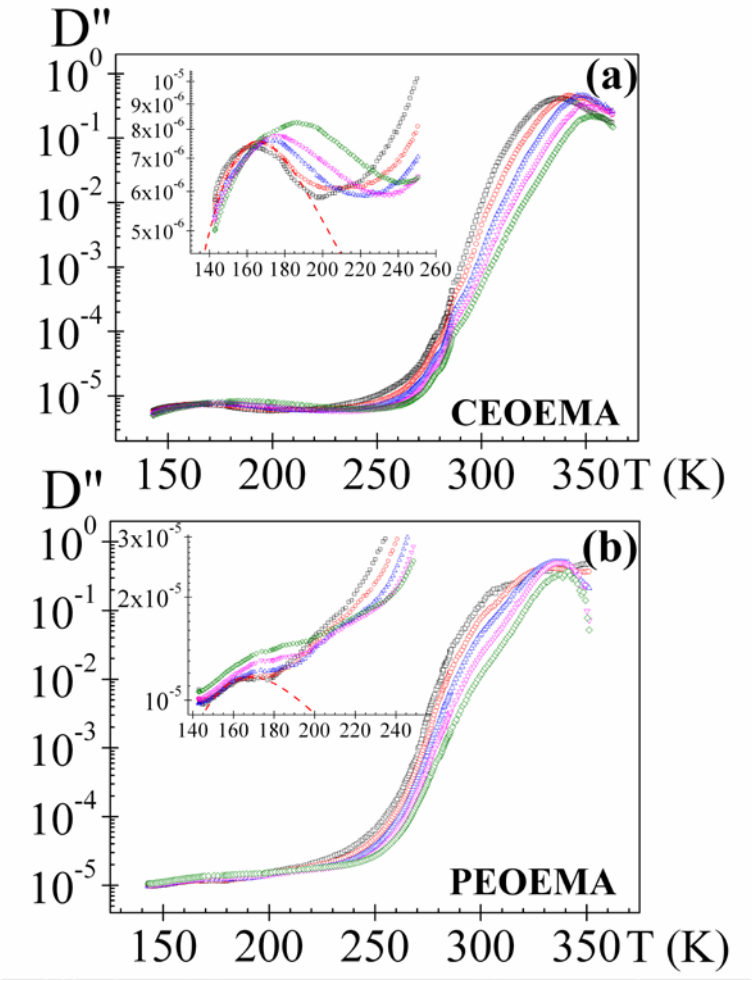

Figure 6.7. Temperature dependence of the loss compliance function at several frequencies (0.3 [square], 1 [circle], 3 [up triangle], 10 [triangle bellow], 30 [diamond] Hz) for (a) CEOEMA and (b) PEOEMA. Inset shows the quality of the fit at one temperature for each polymer at 1 Hz.

The parameters of equation (6.1) fitting the compliance γ processes of PEOEMA and CEOEMA were determined from a multiple nonlinear regression analysis of the experimental results, varying the three characterizing peak parameters (i.e., D''_{max}, mE_a/R, T_{max}). In the inset of **Figure 6.7** an example of the quality of the fit is shown. In the case of the PEOEMA the γ absorption is followed by the β process. However, the latter process is not well defined because the right side of the relaxation overlaps with the low temperature side of the α absorption. As a consequence, only the parameters that describe the γ relaxation were estimated and their values are collected in **Table 6.1**. The errors associated with the parameters show the quality of the fit at the frequencies investigated. The parameter m_γ does not show a noticeable dependence on frequency. Alternatively, the low values of m_γ are an indication of the distributed character of the γ process and, as expected, the temperature dependence of the relaxation exhibits Arrhenius behaviour (ARRH) (see **Figure 6.8**). The activation energy calculated from the Arrhenius plot was 54 kJ·mol^{-1} and 55 kJ·mol^{-1} for PEOEMA and CEOEMA, respectively.

Table 6.1. Values of fit Fuoss-Kirkwood parameters, and *m* and ΔD_γ of the γ relaxation process at different frequencies.

CEOEMA

f (Hz)	$D''_{max,\gamma}$ *(MPa)*	m_γ·*Ea/R, K*	m_γ	ΔD_γ *(MPa)*
0.3	$7.3\cdot10^{-6}\pm1.3\cdot10^{-8}$	805±13	0.122±0.000	$1.2\cdot10^{-4}\pm3.4\cdot10^{-7}$
1	$7.6\cdot10^{-6}\pm1.1\cdot10^{-8}$	884±14	0.134±0.000	$1.1\cdot10^{-4}\pm3.0\cdot10^{-7}$
3	$7.5\cdot10^{-6}\pm1.3\cdot10^{-8}$	934±13	0.141±0.000	$1.1\cdot10^{-4}\pm7.3\cdot10^{-8}$
10	$7.8\cdot10^{-6}\pm8.2\cdot10^{-9}$	916±9	0.139±0.001	$1.1\cdot10^{-4}\pm-5.0\cdot10^{-7}$
30	$8.2\cdot10^{-6}\pm1.3\cdot10^{-8}$	869±12	0.132±0.000	$1.2\cdot10^{-4}\pm1.5\cdot10^{-8}$

PEOEMA

f (Hz)	$D''_{max,\gamma}$ *(MPa)*	m_γ·*Ea/R, K*	m_γ	ΔD_γ *(MPa)*
1	$1.2\cdot10^{-5}\pm2.6\cdot10^{-8}$	780±19	0.117±0.003	$2.0\cdot10^{-4}\pm4.09\cdot10^{-6}$
3	$1.2\cdot10^{-5}\pm1.6\cdot10^{-8}$	696±7	0.104±0.004	$2.3\cdot10^{-4}\pm8.1\cdot10^{-6}$
10	$1.3\cdot10^{-5}\pm1.4\cdot10^{-8}$	661±5	0.099±0.004	$2.6\cdot10^{-4}\pm-9.8\cdot10^{-6}$
30	$1.4\cdot10^{-5}\pm2.0\cdot10^{-8}$	609±5	0.091±0.003	$3.1\cdot10^{-4}\pm1.1\cdot10^{-5}$

The temperature dependence of the mean relaxation time associated with the mechanical glass-rubber relaxation was analyzed in the context of the free volume theory by means of the Vogel-Fulcher-Tamman-Hesse (VFTH) equation (Vogel, 1921; Fulcher, 1925; Tamman, et al., 1926)

$$\ln f_{\max} = A - \left[\frac{M}{T - T_v}\right] \tag{6.2}$$

where A and M are constants, T_v is an empirical parameter related to the Kauzmann temperature or the temperature at which the conformational entropy is zero and f_{max} is the frequency at which E'' passes through the maximum value. The parameters of equation

(6.2) that fit the Arrhenius plots are A = (31.5.0±4.2), M = (1514±140)K, T_v = (233.1±7.2)K for CEOEMA and A = (23.3±0.2), M = (1114± 10)K, T_v = (218.3±2.2)K, for PEOEMA.

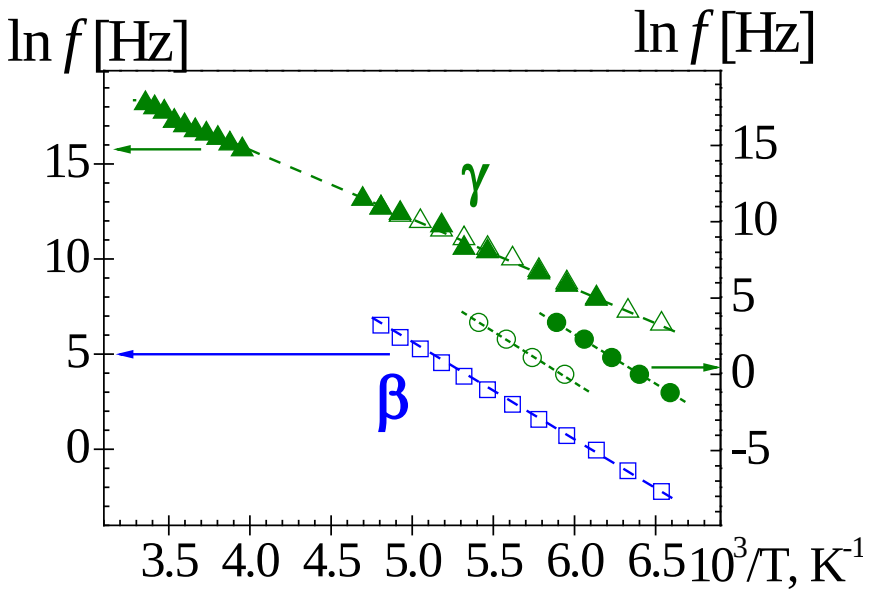

Figure 6.8. Arrhenius plots for the β (blue square) and γ (green triangle) dielectric relaxations. The temperature dependence of the mechanical γ relaxations for PEOEMA and CEOEMA are represented for open and filled circles, respectively.

By comparing equation (6.2) with the Doolittle expression (Doolittle, 1951; Doolittle, 1952), the fraction of free volume at the glass transition temperature, ϕ_g/B, and the free volume expansion coefficient $\alpha_f = (1/V)(\partial V/\partial T)_p$ are estimated from the following expressions

$$\frac{\phi_g}{B} = \frac{T_g - T_v}{M}$$
$$\frac{\alpha_f}{B} = \frac{1}{M} \qquad (6.3)$$

According to the Cohen-Turbull theory, B is a parameter close to the unit related to the ratio between the critical volume for a relaxation process to take place and the volume of the segments intervening in the process. Assuming $B = 1$, the values of the relative free volume at T_g for PEOEMA and CEOEMA were, respectively, 0.045±0.001 and 0.030±0.009 , whereas the values of α_f amount to $(0.90\pm0.01)\times10^{-3}\ K^{-1}$ and $(0.66\pm 0.19)\times10^{-3}\ K^{-1}$. It is worth noting that the values of ϕ_g and α_f are nearly twice the values reported for this quantities for most flexible polymers, presumably as consequence of the fact that the relaxation curves only extend over a rather limited span of frequency and temperature windows (Ferry, 1961).

A detailed inspection of the isochrones corresponding to the storage relaxation modulus of CEOEMA shows two inflexion points centered in the vicinities of 250K and 280K, which apparently reflects the presence of two relaxations. This is confirmed by the curve representing the derivative of the real component of E' with respect to the temperature. The curve *dE′/dT* for CEOEMA, shown in **Figure 6.9**, exhibits two peaks in the vicinity of the calorimetric glass transition temperature, absent in the curve *dE′/dT* corresponding to PEOEMA. The low temperature peak, centered at 250 K cannot be attributed to the β peak detected around 200 K in the relaxation loss spectra of PEOEMA. Although the glass transition temperature depends on the free volume and temperature,

thermodynamical considerations have shown recently that the contribution of thermally activated conformational transitions to the glass-rubber relaxation is more important than the volume (Mpoukouvalas, et al., 2009). According to Fujimori and Oguni (Fujimori, et al., 1995), the non-Arrhenius behavior of the α relaxation could be interpreted as caused by changes in the activation energy with temperature. The value of this parameter can be calculated as a function of temperature using the thermodynamic relationship

$$\left[\frac{\partial \ln f}{\partial(1/T)}\right]_{E'}\left[\frac{\partial(1/T))}{\partial E'}\right]_{\ln f}\left(\frac{\partial E'}{\partial \ln f}\right)_{T^{-1}} = -1 \tag{6.4}$$

Since the activation energy is given by the following equation

$$E_a = -R\left(\frac{\partial \ln f}{\partial(1/T)}\right)_{E'} \tag{6.5}$$

and taking into account the Schwarzl and Struik (Schwarzl, et al., 1967) approximation

$$E'' \cong \frac{\pi}{2}\frac{d\,E'}{d\ln f} \tag{6.6}$$

the following equations that relates the activation energy to the components of the complex modulus is obtained (Diaz-Calleja, et al., 1992; Diaz-Calleja, et al., 1994; Laredo, et al., 1997)

$$E_a = \frac{\pi R T^2}{2E''}\frac{d\,E'}{dT} \tag{6.7}$$

Curves depicting the variation of the activation energy for PEOEMA and CEOEMA in the whole temperature window, evaluated by using equation (6.7), at 30 Hz, are shown in

Figure 6.9. In this Figure also are represented the temperature dependence, of the *E′*, *E″* and *dE′/dT* at the same frequency. Two well-developed peaks are observed for CEOEMA centered at the same temperatures as the less defined *dE′/dT* peaks whereas a single peak associated with T_g appears in the distribution of activation energies of PEOEMA. Moreover, the temperature dependence of the apparent activation energy corresponding to the α relaxation was evaluated in terms of the VFTH parameters ($E_a^{\alpha}(T)=\left[R\cdot M\Big/\left(1-\left(T_v/T\right)\right)^2\right]$) (Schwarzl, et al., 1967). As we can observe, according to the VFTH prediction, the E_a decreases with the temperature increasing, and the values obtained near T_g are similar to those one obtained by using equation (6.7). In view of these results, the first peak, centered at 240 K, corresponding to the distribution of activation energies in CEOEMA seems to be associated with a low temperature glass rubber relaxation, neither detected in the calorimetric thermograms nor in the dielectric relaxations, presumably arising from segmental motions of dangling chains in the chemically crosslinked network. The location of the network, nearly 15 K below the peak associated with the T_g of PEOEMA, suggests that the dangling chains have relatively low molecular weight.

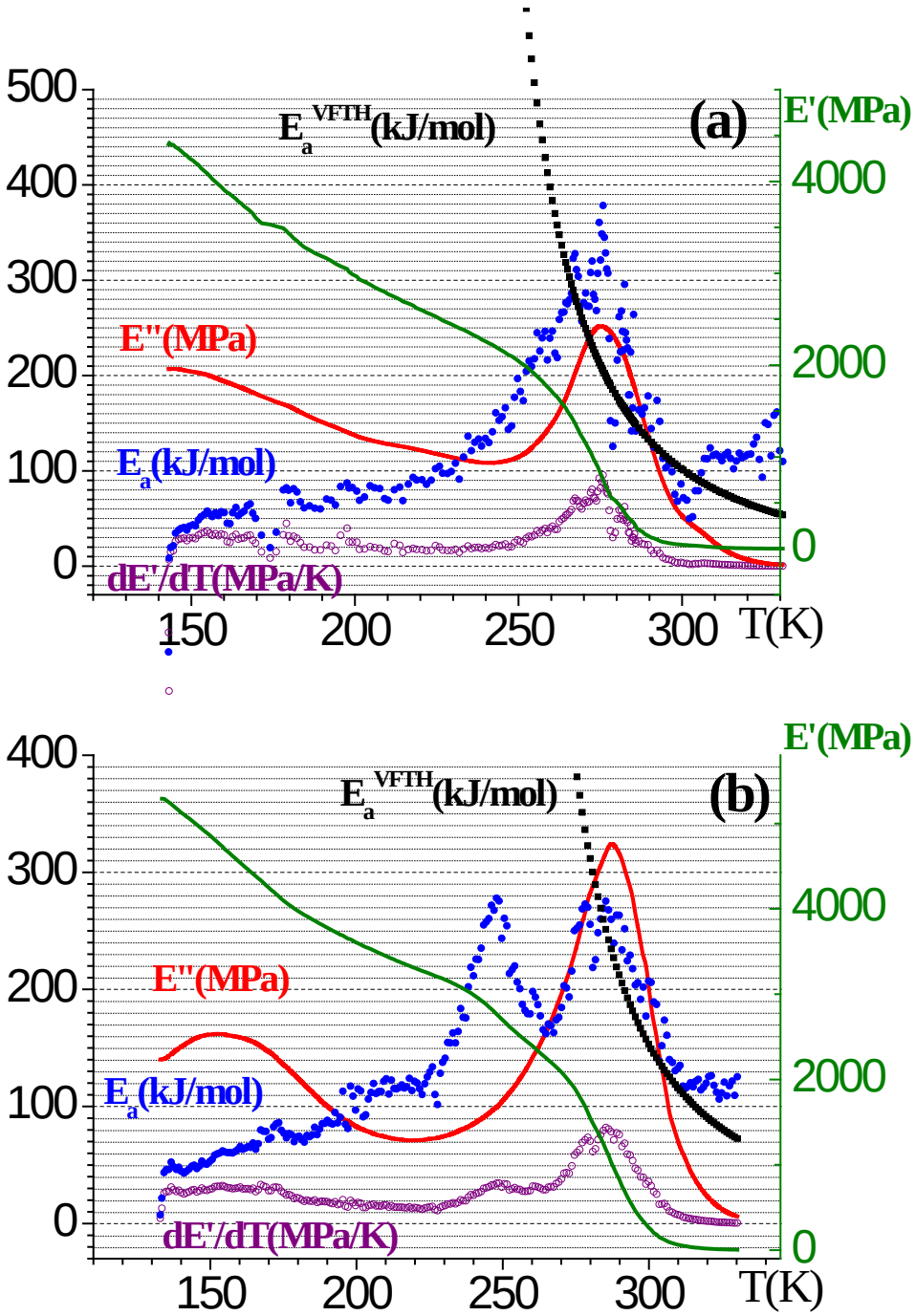

Figure 6.9. Plots showing the temperature dependence of *E′* (green curve), *E″* (red curve), d*E′*/*dT* (purple curve) and E_a (blue curve) for (a) PEOEMA and (b) CEOEMA at 30 Hz.

6.2.5. Dielectric Relaxation Spectroscopy (DRS)

The isochrones corresponding to the real component of the complex dielectric permittivity of PEOEMA exhibit a plateau associated with the glass-rubber or α relaxation followed at higher temperature for a steep increase of this parameter in the former polymer as temperature goes up. However, the isochrones for the real permittivity of CEOEMA present in addition to the plateau corresponding to the α relaxation another plateau at higher temperature associated with a relaxation, named α′, the nature of which will be discussed latter (see **Figure 6.10**). In increasing order of temperature the loss isochrones corresponding to PEOEMA present two absorptions named γ and β followed by the well-developed α relaxation. As usual, at high temperatures and low frequencies the α relaxation is obscured by conductive contributions arising from interfacial electrode-polymer (EP) processes. The loss isochrones corresponding to CEOEMA only present the γ relaxation followed by the α and α′ relaxations, the latter process strongly overlapping with the EP process (see **Figure 6.10**). A more detail of temperature dependence of the loss permittivity at several frequencies is plotted in **Figure 6.11**.

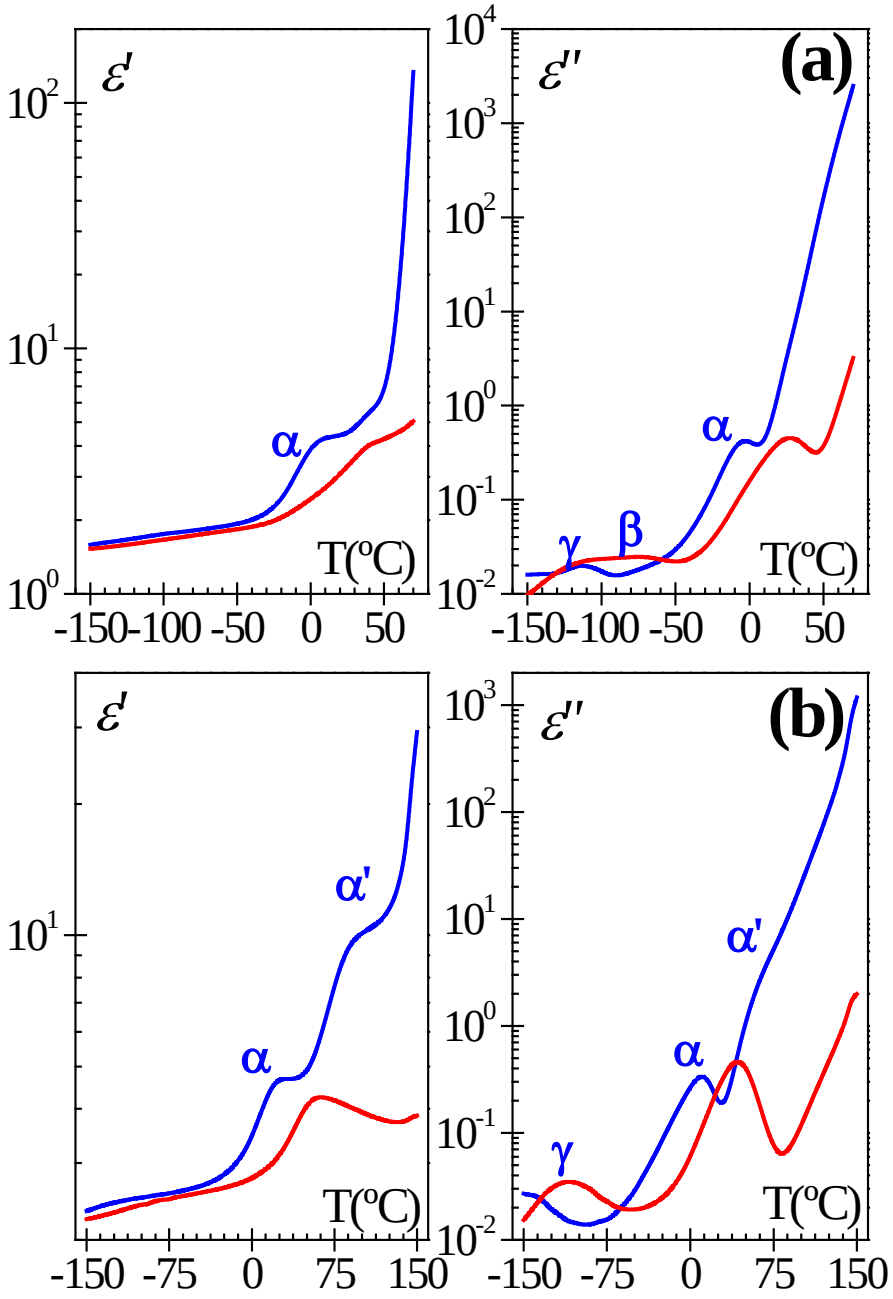

Figure 6.10. Temperature dependence of permittivity and loss permittivity at 100 (blue curve) and 10^3 (red curve) Hz for (a) PEOEMA and (b) CEOEMA.

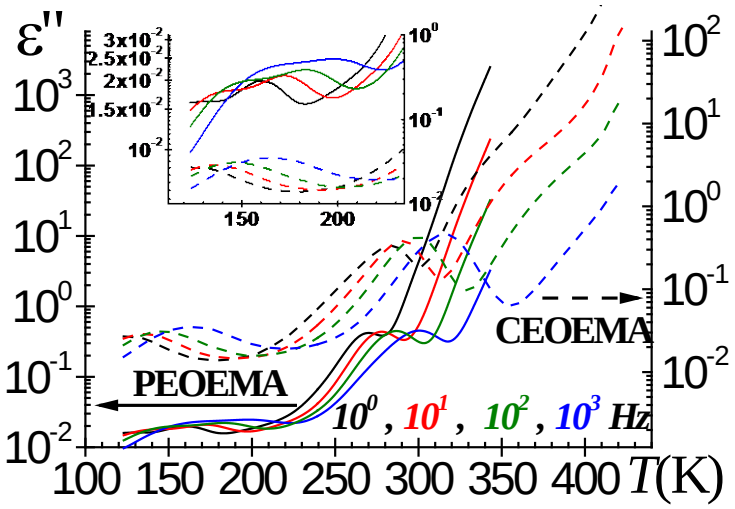

Figure 6.11. Temperature dependence of the loss dielectric permittivity for PEOEMA and CEOEMA at several frequencies.

The differences in microstructure of CEOEMA and PEOEMA are reflected in the dielectric spectra of the respective systems at high temperatures, shown in **Figure 6.12.** The isochrones corresponding to the dielectric modulus of PEOEMA present two well-defined peaks: the low temperature peak associated with the α relaxation is followed by a rather sharp peak centered at 313 K arising from conductive phenomena. However, the high temperature peak of CEOEMA presents in addition to the peak corresponding to the α relaxation an ostensible and wide peak that it is the result of two overlapping peaks (centered at 353 and 393 K). The low temperature peak reflects the MWS relaxation arising from transport of charges in the bulk over a considerable distance with respect to the atomic or segments caused by the heterogeneity of the system (Qin, et al., 2006; Maxwell, 1893;

Wagner, 1914; Sillars, 1937; Mijovic, et al., 1998). It can be concluded that the nanodomains to which we alluded before are responsible for this relaxation. As in the case of PEOEMA, the deconvoluted high temperature peak is produced by conductive phenomena. Owing to the crosslink nature of CEOEMA the loss modulus isochrones for these systems were extended to temperatures well-above T_g. The corresponding isochrones plotted in parallel with the loss dielectric modulus in **Figure 6.12** do not show an additional absorption above that of the α relaxation. However the nanodomains present in CEOEMA do not seem to have any incidence in the response of the system to mechanical perturbation forces.

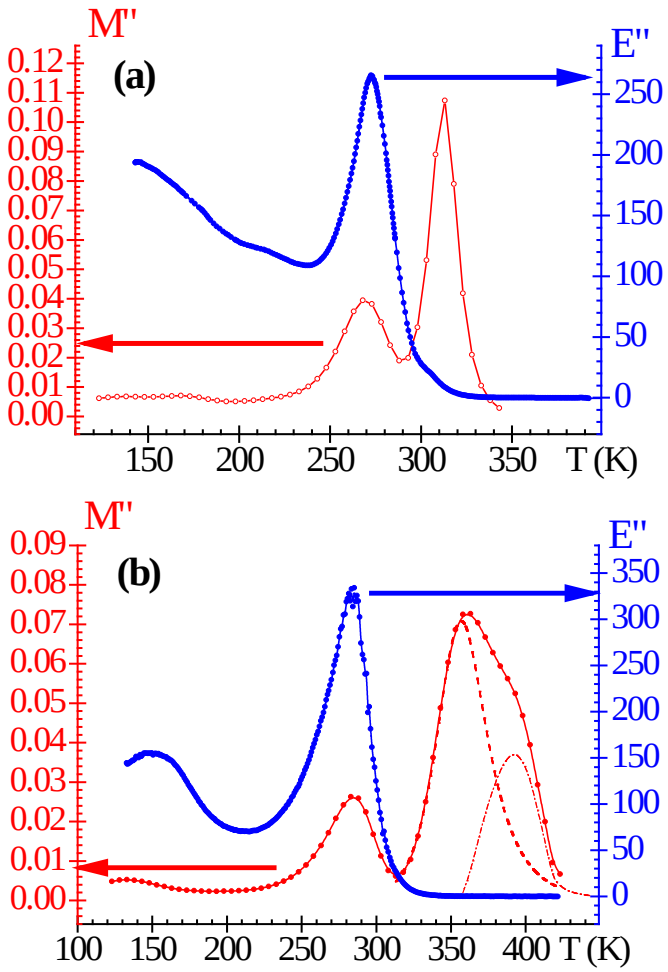

Figure 6.12. Mechanical loss Young's modulus E″ and dielectric loss modulus M″ as a function of temperature for (a) PEOEMA and (b) CEOEMA, at 10Hz.

A complete description of the relaxation behavior of the polymers is shown in **Figure 6.13** where the components of the complex dielectric permittivity in the frequency domain are presented at several temperatures for PEOEMA and CEOEMA, respectively.

The dielectric loss isotherms corresponding to the uncrosslinked polymer present at high frequencies a γ process followed in decreasing order of frequency by a weak β

absorption and an ostensible glass-rubber relaxation dominated at low frequencies by strong interfacial electrode-polymer (EP) processes. However, the dielectric loss isotherms for CEOEMA only exhibits at high frequencies a secondary single relaxation, named γ absorption, followed in decreasing order of frequency by the α relaxation which in the low frequency side overlaps with an apparently ostensible relaxation, named α′ process. This latter absorption appears as a shoulder of the EP process. It is worth noting that the α′ relaxation is well separated from the α and conductive processes in the isotherms corresponding to the real dielectric permittivity.

The β, α and conductive processes are well defined in the dielectric loss modulus of PEOEMA in the frequency domain, shown in **Figure 6.14a**. The rather narrow conductive peak of PEOEMA widens in the case of CEOEMA as a result of the overlapping of the α′ relaxation with the EP process (see **Figure 6.14b**).

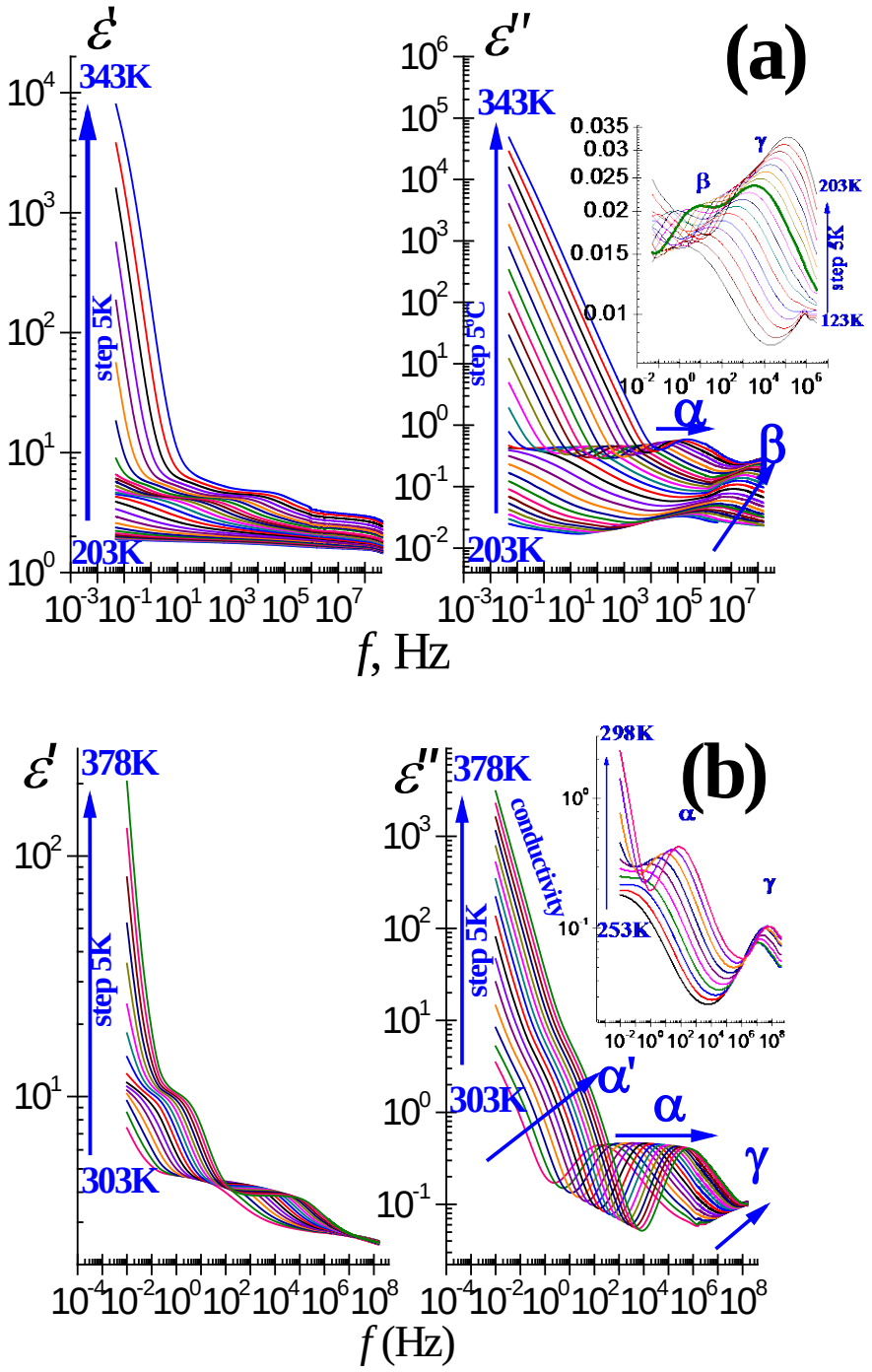

Figure 6.13. Dielectric permittivity and loss as a function of the frequency for PEOEMA (a) at temperatures between 203K and 343K, 5K steps (inset between 123 to 203K, step of 5K) and for CEOEMA (b) between 303K and 378K, 5K steps (inset between 253K to 298K, step of 5K).

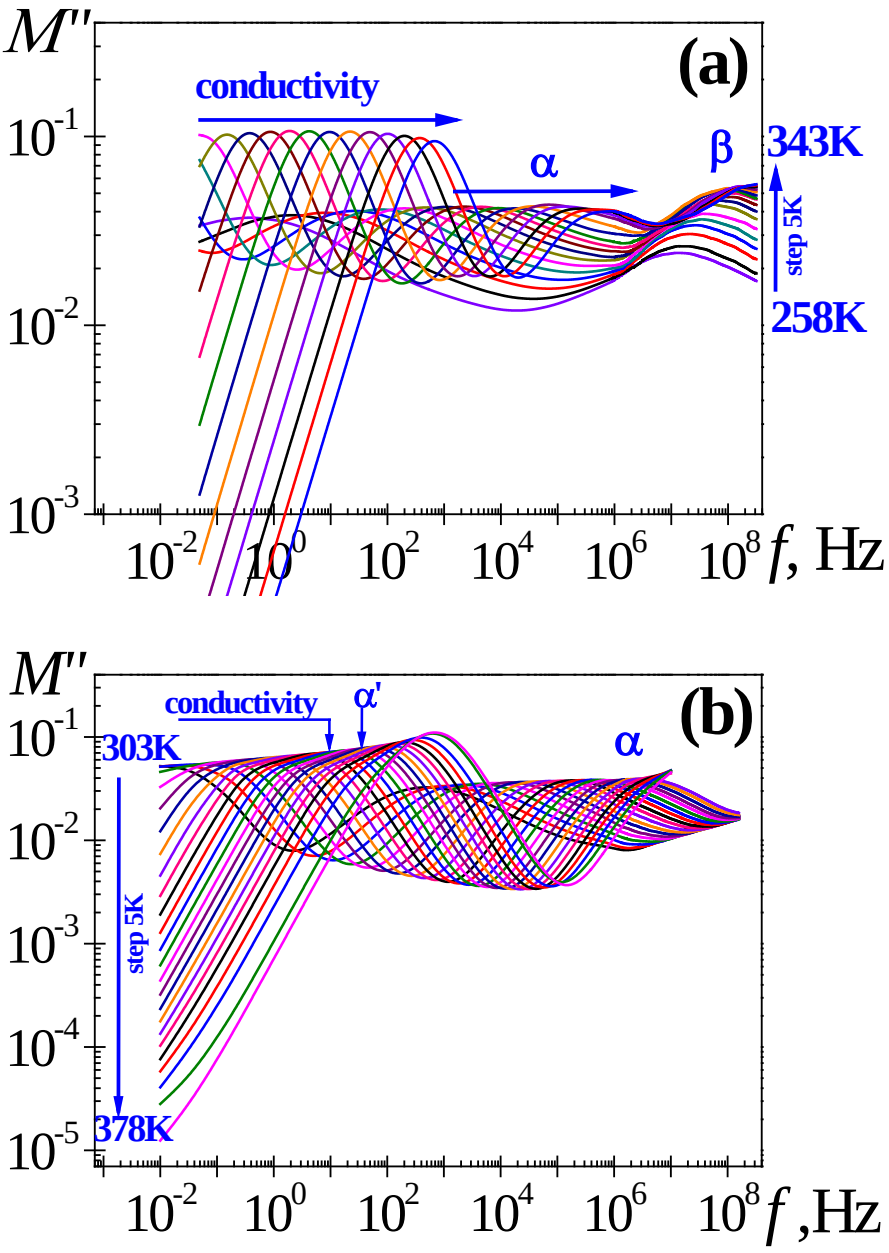

Figure 6.14. Dielectric loss modulus in the frequency domain, at several temperatures, for (a) PEOEMA and (b) CEOEMA.

Splitting of the overlapping relaxations in the isotherms were carried out by means of Cole-Cole and Havriliak-Negami type equations (Havriliak, et al., 1997)

$$\varepsilon^*(\omega) = \varepsilon_\infty + \sum_i \frac{\varepsilon_{0i} - \varepsilon_{\infty i}}{\left[1 + (j\omega\tau_i)^{a_i}\right]^{b_i}} - j\left(\frac{\sigma}{e_0\omega}\right)^s \qquad (6.8)$$

where e_0 (= 8.854 pF·m^{-1}) is the free space dielectric permittivity, σ is the ionic conductivity arising from interfacial polymer-electrode phenomena, τ denotes a specific relaxation time associated with the process and *s* is a parameter very close to the unit. The subscript *i* in equation (6.8) refers to the absorptions γ, β, α and α′ while the subscripts 0 and ∞ mean, respectively, relaxed and unrelaxed dielectric permittivity. The shape parameters *a* and *b* are related, respectively, to the departure of the complex $\varepsilon'' vs \varepsilon'$ plot from a semi-circumference, at low frequencies, and to the skewness of the plot along a straight line, at high frequencies. Owing to the symmetry of the secondary absorptions, the complex plots are arcs so that the shape parameter *b* is the unit. For a Debye type relaxation *a* = *b* = 1.

For $T < T_g$, the contributions to $\varepsilon^*(\omega)$ of the α and α′ relaxations as well as the ionic conductivity are nil. As usual, the HN and conductive parameters associated with each dipolar relaxation in equation (6.8) can be obtained by writing the real and loss component of the complex permittivity in the following way.

$$\varepsilon'(\omega) = \varepsilon_\infty + r^{-b/2}\cdot\left(\varepsilon_0 - \varepsilon_\infty\right)\cdot\cos b\theta \qquad (6.9a)$$

$$\varepsilon''(\omega) = r^{-b/2} \cdot (\varepsilon_0 - \varepsilon_\infty) \cdot \sin b\theta + \left(\frac{\sigma}{e_0 \omega} \right)^s \qquad (6.9b)$$

where

$$r = \left[1 + (\omega \cdot \tau_0)^a \cdot \cos(a \cdot \pi/2) \right]^2 + \left[(\omega \cdot \tau_0)^a \cdot \sin(a \cdot \pi/2) \right]^2$$
$$\theta = \text{arctg} \left[\frac{(\omega \cdot \tau_0)^a \cdot \sin(a \cdot \pi/2)}{1 + (\omega \cdot \tau_0)^a \cdot \cos(a \cdot \pi/2)} \right] \qquad (6.10)$$

The HN and conductive fitting parameters were determined at several temperatures from a multiple nonlinear regression analysis of the experimental data.

Examples of the deconvolutions of the loss dielectric curves for PEOEMA and CEOEMA at $T > T_g$ are shown in **Figure 6.15**. In the inset of the figure the relative error associated with the values of the dielectric loss recalculated from the strengths and shape factors associated with the split relaxations are also shown. It can be seen that in most cases the relative error is about 7% or lower. In the most unfavorable cases (extreme frequencies), the error comes close to 10%.

The shape parameters associated with the relaxation processes of the samples are shown in **Figure 6.16**.

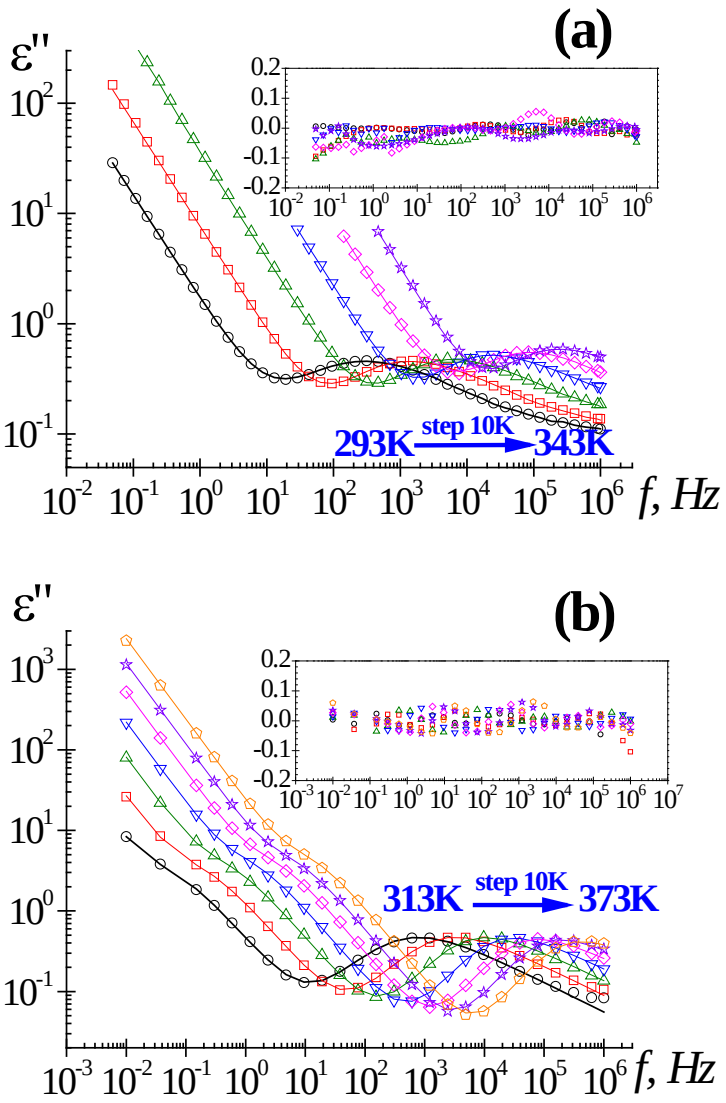

Figure 6.15. Reconstruction of the dielectric loss from the distribution of retardation times for PEOEMA (a) and CEOEMA (b) at several temperatures. Open circles represent the experimental data, and the continuous line represents the dielectric loss calculated as the sum of the individual processes. Inset: relative error calculated as $\left(\varepsilon_{CALC} - \varepsilon_{EXP}\right)/\varepsilon_{EXP}$.

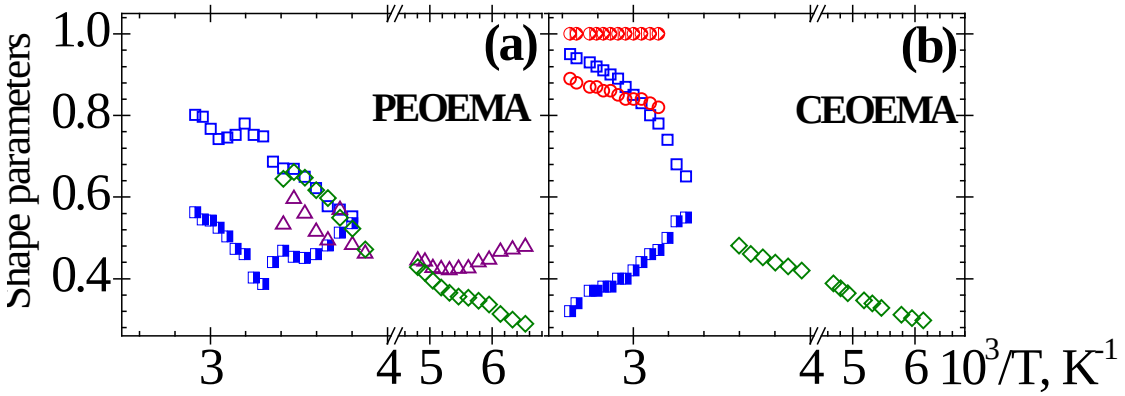

Figure 6.16. Temperature dependence of the shape parameter for (a) PEOEMA and (b) CEOEMA. α′ process: *a* parameter (open circle) and *b* parameter (half right circle), α process: *a* parameter (open square) and *b* parameter (half right square), β process: *a* parameter (up triangle) and γ process: *a* parameter (diamond).

An inspection of the parameters corresponding to the α′ process of CEOEMA indicates that the values of *a* slightly increase with increase temperature lying in the range 0.8 – 0.9 in the temperature interval 303-378K. The closeness of the *a* parameter to the unit suggests that the α′ relaxation exhibits a rather narrow distribution of relaxation times. As shown in **Figure 6.16**, the values of *a* for the α relaxation of CEOEMA are higher than those for the α′ process at temperatures above 333 K, smaller at temperatures below 333 K, and in both cases they moderately increase with increasing temperature, though the increase is somewhat higher for the uncrosslinked polymer. The *b* parameter corresponding to the α′ relaxation is very close to the unit and independent of temperature. This fact indicates the absence of skewness in the high frequency side of the ε'' *vs.* ε' plot, *i.e.* the α′ relaxation is a symmetric process. However, the parameter *b* for the α relaxation decreases with

increasing temperature, *i.e.* the skewness of the ε'' *vs.* ε' plot increases with temperature. In both cases the Cole-Cole plots at high temperature come close to a semicircle in the low frequency region. The values of the parameter *a* corresponding to the γ relaxations of PEOEMA and CEOEMA are rather close and in both cases they increase with increasing temperature. However, the temperature dependence of this parameter for the β relaxation of PEOEMA does not follow a definite trend.

The dielectric strength of the α′ relaxation corresponding to CEOEMA, presented in **Figure 6.17**, increases with temperature. This behavior differs from that displayed by the α relaxation of CEOEMA and PEOEMA whose strength, as usual, decreases with increasing temperature. The dielectric strengths of the secondary relaxations, also shown in **Figure 6.17**, increase with increasing temperature. Moreover the strength of the γ relaxation of CEOEMA is nearly the sum of the γ and β dielectric strengths of PEOEMA.

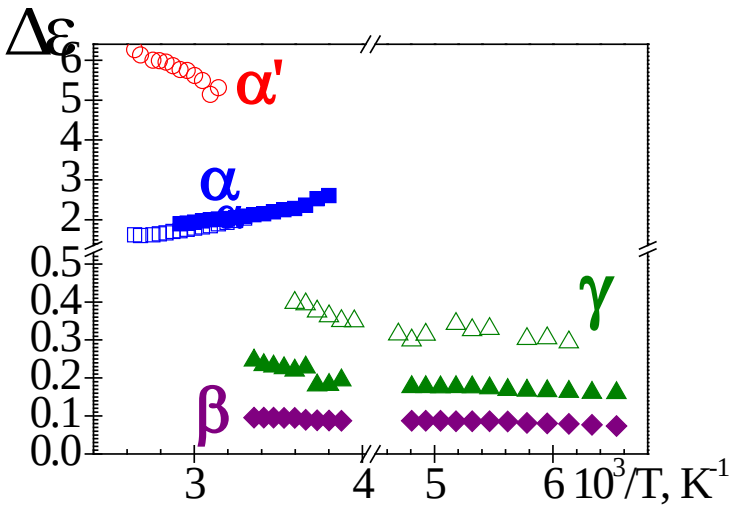

Figure 6.17. Temperature dependence of the strengths for the α (square), α′ (circle), β (diamond) and γ (triangle) relaxations for PEOEMA (full symbols) and CEOEMA (open symbols).

6.2.5.1. Temperature Dependences of the Deconvoluted Relaxations

Arrhenius plots of the relaxation times associated with the different absorptions presented in the spectra of PEOEMA and CEOEMA are shown in **Figure 6.18**.

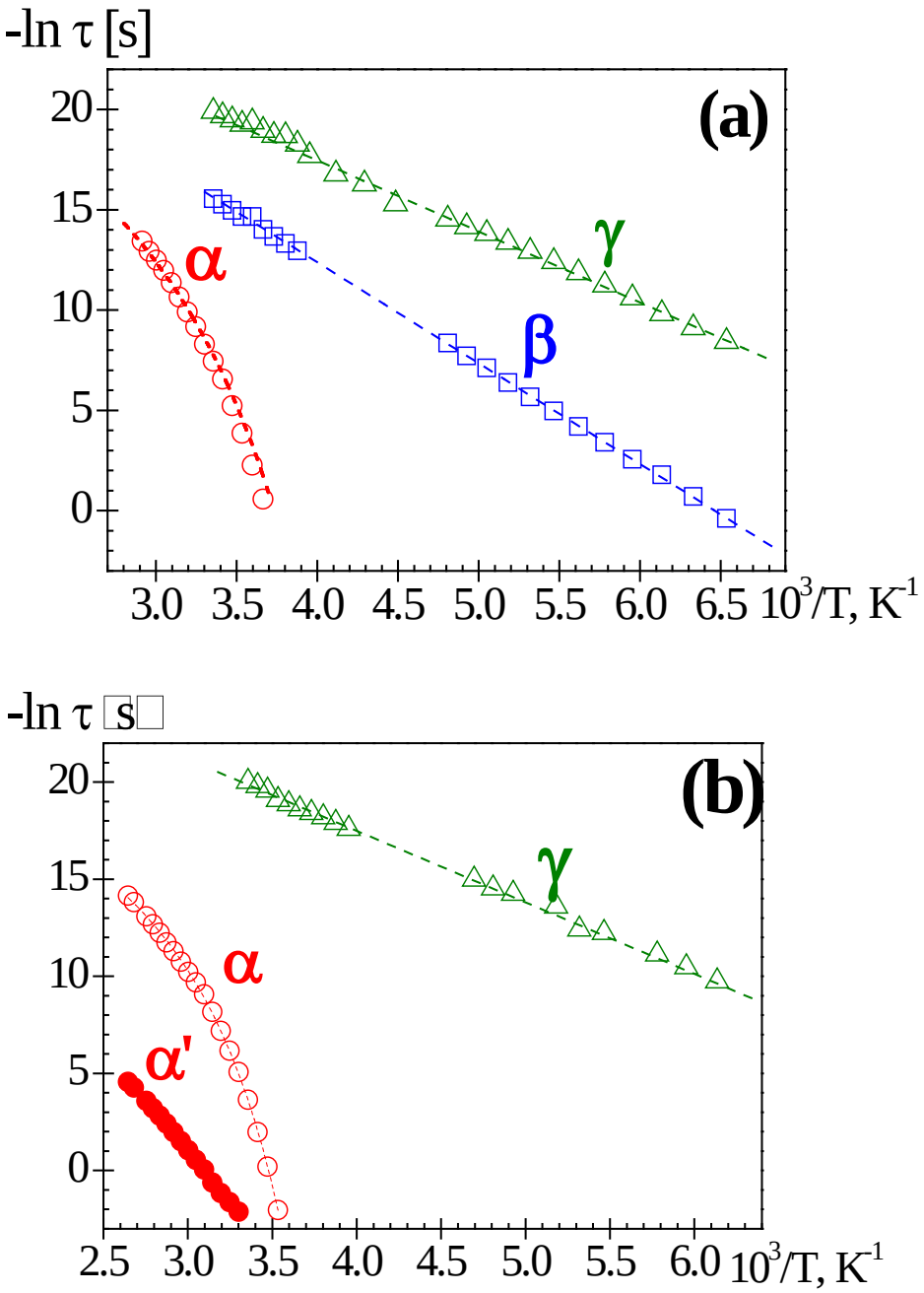

Figure 6.18. Arrhenius plots for the α′ (full circles), α (open circles), β (square), and γ (triangles) relaxations for (a) PEOEMA and (b) CEOEMA

The secondary relaxations are thermally activated processes and they obey Arrhenius behavior. The activation energies of the relaxations obtained from the slopes of Arrhenius plots are 41.6 ± 0.3 $kJ \cdot mol^{-1}$ and 29.9 ± 0.4 $kJ \cdot mol^{-1}$ for the β and γ relaxations of PEOEMA. The activation energy of the unique secondary relaxation of CEOEMA is 30.1 ± 0.4 $kJ \cdot mol^{-1}$. The fact that the activation energy of this relaxation is similar to that of the γ relaxation of PEOEMA suggests that the relaxation is also a γ process and so was labeled from the beginning. It is of interest to compare the activation energies of the secondary processes with these obtained from mechanical results. Thus in **Figure 6.18** is depicted in the plot to the secondary relaxations Arrhenius from DRS and DMA.

The molecular origin of the secondary dielectric relaxation can be qualitatively explained as follows. The ester group of the side chains of PEOEMA and CEOEMA has a dipole moment of 1.78 D that forms an angle of 153º with the $C(CH_3)$-C(O) bond while the dipole moment of the ether group bisects the skeletal CH_2-O-CH_2 bond and has value of 1.23 D (Riande, et al., 1992). In all *trans* conformation both dipoles have nearly the same direction and therefore the polarity of the all *trans* conformation of the side groups reaches the maximum value. On the other hand the C(O)-O bonds are restricted to the *trans* states and the O-CH_2 bonds strongly prefer the *trans* conformation. However, since the CH_2-CH_2 bonds prefer the *gauche* conformation, conformational transitions about these bonds produce dielectric activity, which can be responsible for the γ relaxation observable in the dielectric and mechanical spectra. It is more difficult to elucidate the origin of the β relaxation appearing in the mechanical and dielectric spectra of PEOEMA. However, the

fact that this relaxation is absent in the spectra of CEOEMA suggests that it proceeds mainly from motions in the polymer backbone, which are impeded by crosslinking. The fact that the mechanical γ relaxation exhibits an activation energy nearly 80% higher than the dielectric γ process, suggests that the molecular motions involved in the mechanical process are more complex than in the dielectric one. Combined molecular motions about $C(CH_3)$-C(O) and CH_2-CH_2 bonds of the side groups may be an origin of the mechanical γ process. As for the mechanical β relaxation, the absence of this process in the spectra of CEOEMA suggests that the crosslinking suppresses that process and, as occurs in the dielectric spectra, the mechanical γ relaxation of PEOEMA must be attributed to local cooperative motions of the backbone.

The glass-rubber relaxation arises from segmental motions involving thermally activated conformational transitions depending on barrier potentials. As the system comes close to T_g, the free volume available to accommodate the conformations resulting from segmental motions is severely reduced in such a way that the time to complete relaxation undergoes a considerable increase, the α relaxation freezing at T_g. The temperature dependence of the relaxation times associated with the glass-rubber relaxation, presented in **Figure 6.18** for PEOEMA and CEOEMA, is governed by the VFTH equation (Vogel, 1921; Fulcher, 1925; Tamman, et al., 1926) which expressed in terms of the dimensionless fragility factor D_0 (Angell, 1996; Angell, 1995; Rubi, et al., 1997) can be written as

$$\tau = \tau_0 \exp[D_0 T_V /(T - T_V)] \qquad (6.11)$$

where the prefactor τ_0 is of the order of picoseconds, T_V is the Vogel temperature, *i.e.* the temperature at which hypothetically the excess entropy of the glassy system is nil and D_0 is respectively below and above 10 for fragile a strong glass forming liquids.

Comparison of equation (6.11) with the Doolittle equation, $\tau = \tau_0 \exp(\Phi / B)$, where Φ is the relative free volume and B is a parameter close to the unit, the ratio Φ/B at T_g (Doolittle, 1951; Doolittle, 1952) can be written as

$$\Phi_g / B = (T_g - T_V) / D_0 T_V \qquad (6.12)$$

Moreover, the expansion coefficient at T_g is given by (Ferry, 1961)

$$\alpha_f / B = (1/V)\left(\partial V / \partial T\right)_p / B = 1 / D_0 T_V \qquad (6.13)$$

The Vogel temperature, and the values at T_g of the fragility factor, relative free volume and the expansion coefficients for PEOEMA and CEOEMA are shown in **Table 6.2**. It can be seen that decreasing of the mobility of the chains by crosslinking hardly affects the values of these parameters.

The temperature dependence of the relaxation time associated with the α' process of CEOEMA is shown in **Figure 6.18**. Notice that the values of τ extend only over nearly half of the decades covered by the α relaxation. The relaxation times corresponding to the α' relaxation are larger than those associated with the α, though the divergence between them decreases as temperature increases. In spite of the fact that the data available for the relaxation times of the α' relaxation only cover a narrow span of temperature, an attempt

inspection of their temperature dependence suggests that both temperature and volume may intervenes in the development of the α′ process.

Table 6.6.2. Activation energies and prefactors of the secondary relaxation and parameters of Vogel-Fulcher-Tammann-Hesse equation $\tau = \tau_0 \exp\left[\frac{D_0}{(T/T_V)-1}\right]$ for PEOEMA and CEOEMA

sample	PEOEMA	CEOEMA
$E_{a,\gamma}(k\ mol^{-1})$	29.9 ± 0.4	30.1 ± 0.4
$-ln\ \tau_{0,\gamma}$	32.0 ± 0.3	32.0 ± 0.2
$E_{a,\beta}\ (kJ.mol^{-1})$	41.6 ± 0.3	—
$-ln\ \tau_{0,\beta}$	32.3 ± 0.2	—
$-ln\ \tau_0$	25.3 ± 1.3	22.4 ± 0.2
D_0	5.5±0.4	5.2±0.1
$T_v\ (K)$	220.1±3.4	233.6±1.0
$\phi_g / B\ (\%)$	4.0 ± 0.3	3.7 ± 0.1
$\alpha_f \cdot 10^4 \left(K^{-1}\right)$	8.3 ± 0.8	8.3 ± 0.2

The conductive contribution to the dielectric loss in equation (6.8) follows Arrhenius behavior as the plots of **Figure 6.19** extending in the range of temperatures 273-378 K, show. In general, the conductivity of CEOEMA is nearly three decades lower than that of PEOEMA, and the activation energies are 93.9±1.2 kJ·mol^{-1} and 122.9±0.8 kJ·mol^{-1} for the former and latter systems, respectively.

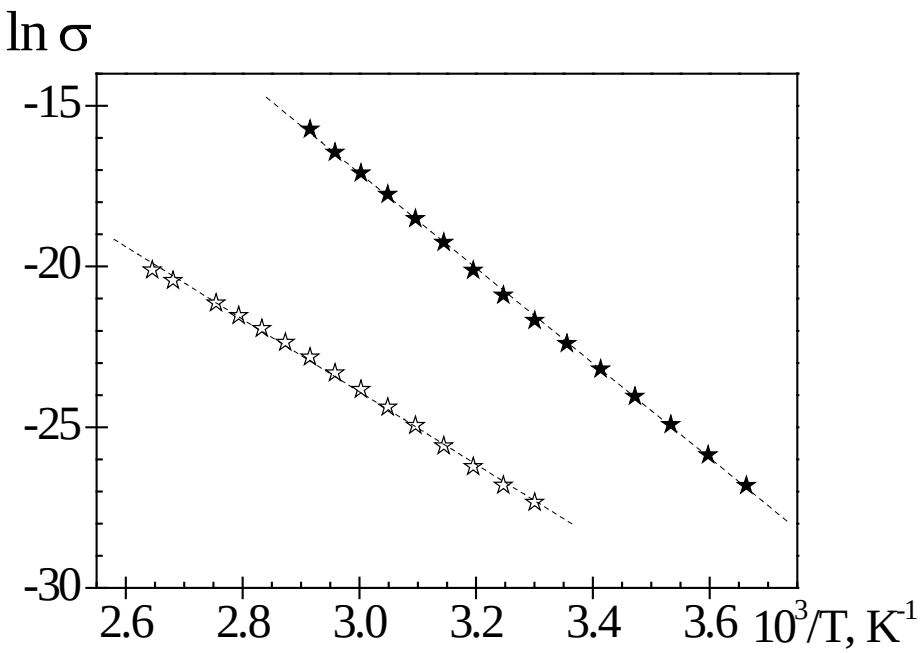

Figure 6.19. Arrhenius plot for the ionic conductivity, in S·m-1 of PEOEMA (full star) and CEOEMA (open star).

6.2.5.2. Dipolar Relaxation Processes

Owing to the similarities of the reactivities of 2-ethoxyetyl methacrylate and ethyl dimethacrylate, CEOEMA can schematically be viewed as a network with statistically distributed molecules of crosslinking agent. Some portions of the chains may be flanked by crosslink points whereas others may appear as dangling chains. The fact that a single α relaxation appears suggests a rather effective crosslinking reaction. Crosslinking reduces the mobility of the chains and as a result the glass transition temperature of CEOEMA is nearly 10 K above that of PEOEMA.

The normalized α relaxation in the time domain for PEOEMA and CEOEMA was calculated from the retardation loss spectra (Riande, et al., 2004; Kremer, et al., 2003) evaluated from the HN fit parameters by means of the following expression

$$\phi(t) = \frac{\int_{-\infty}^{\infty} L_{\alpha}(\ln\tau)\, e^{-t/\tau} d\ln\tau}{\int_{-\infty}^{\infty} L_{\alpha}(\ln\tau)\, d\ln\tau} \tag{6.14}$$

As usual, the function ϕ(t) is described by the KWW equation (Williams, 1979)

$$\phi(t) = \exp[-(t/\tau^*)^{\beta_{KWW}}] \tag{6.15}$$

where τ^* is a characteristic relaxation time and the stretch exponent (β_{KWW}) lies in the range 0–1. The KWW decay functions at different temperatures as well as the parameters that describe the functions are shown in **Figure 6.20**.

An inspection of the decay curves shows that contrary to one would expect, the heterogeneity imposed in the system by crosslinking does not widen the distribution of relaxation times of the glass-rubber relaxation. In this regard, notice that at high temperature the values of β_{KWW} for CEOEMA are slightly larger than for PEOEMA.

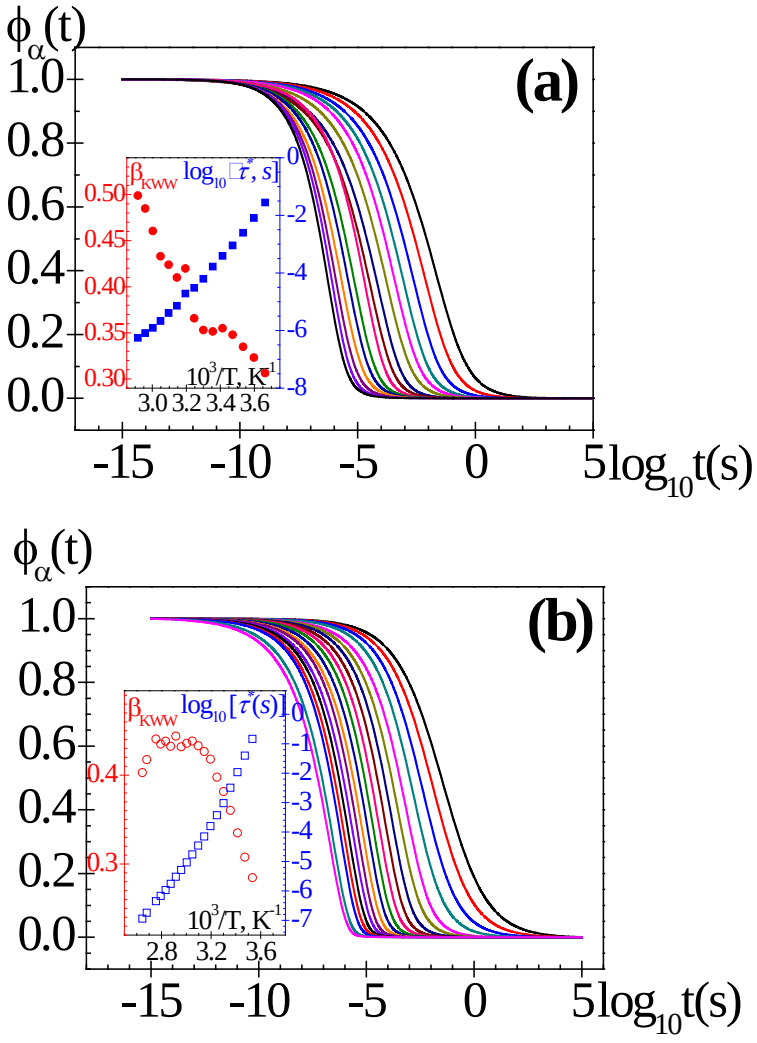

Figure 6.20. Normalized relaxation curves in the time domain for the α relaxation of (a) PEOEMA (273-343K) and (b) CEOEMA (283-378K). The decay curves are fitted by the KWW equation using the stretch exponents β_{KWW} and the characteristic relaxation times τ^* shown in the inset of the figure.

The dynamic fragility factor describes the increase of the relaxation times as temperature comes closer to T_g. It is defined as (Qin, et al., 2006; Plazek, et al., 1991)

$$m = \lim_{t\to\infty}\left(\frac{d\log\tau}{d(T_g/T)}\right) \tag{6.16}$$

A large dynamic parameter means that the temperature dependence of the glass-rubber relaxation comes closer to Arrhenius behavior. Taking T_g as reference and taking into account the VFTH equation

$$m = \frac{D_0 T_V}{2.303 T_g (1 - T_V/T_g)^2} \tag{6.17}$$

The values of *m* obtained for PEOEMA and CEOEMA are 61 and 74, respectively, indicating that a slight decrease in the chains mobility by effect of crosslinking produces a moderate increase in the dynamic fragility factor.

Local motions are reflected in the secondary relaxations. PEOEMA presents at high frequencies a γ relaxation presumably arising from motions of the side chains that change the orientation of the ether dipoles thus producing dielectric activity. At lower frequencies, a β relaxation appears that can be caused by combined motions of the ether and ester dipoles. It is worth noting that CEOEMA only exhibits the secondary γ relaxation. This fact suggests that the reduction in mobility caused by a slight crosslinking totally suppresses the β relaxation. This means that the β relaxation in PEOEMA may be produced by local motions of the backbone combined with motions of the side groups.

6.2.5.3. Interfacial and Electrodes Polarization Processes

Interfacial polarization arising from the buildup of charges at the nanodomains interfaces may be responsible for the α′ relaxation. Actually, transport of charges in the bulk over a considerable distance with respect to the atomic or segments produces the so-called Maxwell-Wagner-Sillars (MWS) relaxation (Maxwell, 1893; Wagner, 1914; Sillars, 1937). This process has been reported for heterogeneous systems, i.e. silicone-polyester resins (Arbe, et al., 2008), nylon/clay nanocomposites (Perrier, et al., 1997; Lee, et al., 2005; Ortiz-Serna, et al., 2011), PZT fibers/epoxy resins (Hammami, et al., 2007), polycarbonate/styrene-acrylonitrile multilayer composite (Daly, et al., 1992), amorphous-crystal interface in Nylon 1010 (Lu, et al., 2006), etc. MWS relaxations were also reported for poly(dimethoxy benzyl methacrylate)s as a result of the heterogeneities produced in the melts by side chains segregations (Sanchis, et al., 2010). Although the symmetry of the α′ relaxation, reflected in the fact that $b = 1$ in the Cole-Cole plot, fulfills one of the requirements of a MWS relaxation, the process is not described by a single relaxation time because a is close, but not equal, to 1. This suggests that the α′ process is a distributed MWS relaxation produced by a variety of environments. The real component of the complex dielectric permittivity associated with the α′ relaxation is well separated from both the dipolar relaxation in the high frequency region and EP processes at low frequencies. The separation is not so clear in the case of the dielectric loss. The relaxation can be interpreted by the Dyre model which assumes that charge transport in the bulk occurs by

hopping of charge carriers in spatially varying random energy landscape (Dyre, 1986; Dyre, 1988). According to the model,

$$\varepsilon^*(\omega) = \varepsilon_0 + \frac{\sigma_0 \tau_e}{e_0 \ln(1+\omega\tau_e)} \tag{6.18}$$

where ε_0 is the relaxed dielectric permittivity corresponding to the α relaxation, σ_0 the *dc* conductivity, e_0 the free space permittivity and τ_e. the time involved in overcoming the jump barrier in charge transport. Taking into account that $(1+j\omega\tau_e) = (1+\omega^2\tau_e^2)^{1/2} e^{j\tan^{-1}(\omega\tau_e)}$, the components of ε^* are given by

$$\begin{aligned} \varepsilon'(\omega) &= \varepsilon_0 + \frac{1}{2}\frac{(\sigma_0/\varepsilon_f)\omega\tau_e \ln(1+\omega^2\tau_e^2)}{(1/4)\left[\ln(1+\omega^2\tau_e^2)\right]^2 + [\tan^{-1}(\omega\tau_e)]^2} \\ \varepsilon''(\omega) &= \frac{1}{2}\frac{(\sigma_0/\varepsilon_f)\omega\tau_e \tan^{-1}(\omega\tau_e)}{(1/4)\left[\ln(1+\omega^2\tau_e^2)\right]^2 + [\tan^{-1}(\omega\tau_e)]^2} \end{aligned} \tag{6.19}$$

The parameters of the Dyre model were obtained at different temperatures by multiple nonlinear regression analysis of the values of ε' associated with the MWS relaxation. **Figure 6.21** shows the Arrhenius plot for the values of $\omega_e = 1/\tau_e$ as well as the same plot for the critical frequency, ω_c, that describes the onset of the dispersion of the real component of the complex conductivity.

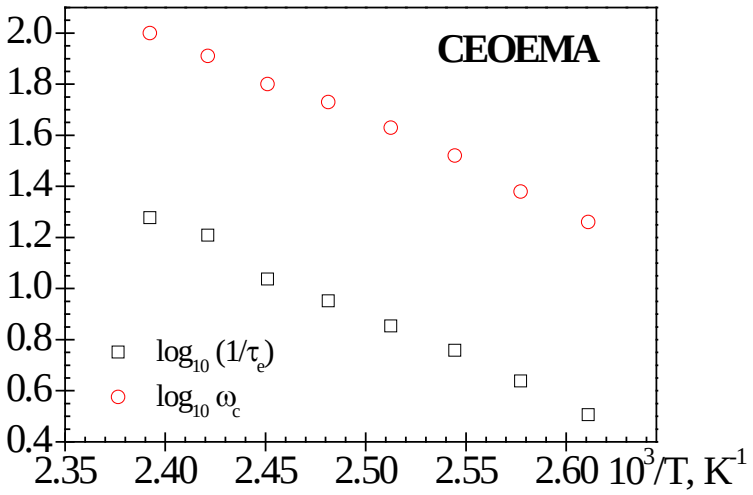

Figure 6.21. Arrhenius plots for the ω_c and $1/\tau_e$ parameters for CEOEMA.

The values of ω_e and ω_c are rather close suggesting that they describe an identical underlying process, *i.e.* an electrical relaxation. However, owing to the rather narrow span of temperature covered by the experiments where ω_c and ω_e can be obtained, no definite conclusion can be reached regarding to whether these parameters are only thermally activated processes or they also depend on the volume. It should be noted that the temperature dependence of these parameters for ionic liquids over a wide span of temperature also depends on the volume.

The increase observed in ε' at frequencies below those of the second plateau is caused by interfacial electrode-polymer polarization (EP) processes. These processes can be viewed as the result of relaxations of macrodipoles produced by charges located in the interface polymer-electrodes (Satti, et al., 2007). The charges proceed from impurities

contained in solvents and chemical compounds used in the synthesis of the probes. The orientation of the macrodipole goes from the positive to the negative electrode. As shown in **Figure 6.22**, the EP process manifests itself as a peak in tan δ isotherms in the frequency domain at very low frequencies. The peak is the result of the relaxation produced by the macrodipole following the electric field at very low frequencies (Macdonald, 1953; Coelho, 1991).

The macrodipole follows the electric field at low frequencies giving rise to a polarization process that can be represented by a Debye relaxation (Coelho, 1991; Klein, et al., 2006)

$$\varepsilon^*_{EP} = \varepsilon_r + \frac{\Delta\varepsilon_P}{1 + j\omega\tau_{EP}} \qquad (6.20)$$

where ε_r is the value of ε' at the plateau of PEOEMA and the second plateau of CEOEMA, $\Delta\varepsilon_P = \varepsilon_{rEP} - \varepsilon_r$ where ε_{rEP} is the relaxed dielectric permittivity of the Debye process which according to the theory is related to the Debye length L_D by

$$\varepsilon_{rEP} = \varepsilon_r L / 2L_D \qquad (6.21)$$

where L is the thickness of the material sandwiched between the electrodes. By simplification of the expression obtained for tan δ_{EP} from equations (6.20) and (6.21) (for details see supporting information of ref. [(Sanchis, et al., 2011)]), $tan\ \delta_{EP}$ can be written as

$$\tan\delta_{EP} = \frac{\omega\tau_{EP}}{1+\omega^2\tau_{EP}^2(2L_D/L)} \tag{6.22}$$

where

$$\tau_{EP} = \frac{LF}{2\sigma}\left(\frac{e_0\varepsilon_r\sum_i z_i^2 c_i}{k_B T}\right)^{1/2} \tag{6.23}$$

In this expression F is the Faraday's constant, and z_i and c_i are respectively the valence and concentration of the ionic species i. The frequency at the peak maximum of tan δ_{EP} is given by

$$\omega_{\max} = \frac{(L/2L_D)^{1/2}}{\tau_{EP}} \tag{6.24}$$

Then the value of tan δ_{EP} at the peak maximum is given by

$$\tan\delta_{EP} = \frac{1}{2}\left(\frac{L}{2D}\right)^{1/2} \tag{6.25}$$

Equations (6.23) and (6.24) in conjunction with the results for tan δ_{EP} in **Figure 6.22** allow the estimation of the characteristic relaxation time τ_{EP} and Debye's length.

The variation of τ_{EP} with temperature for CEOEMA and PEOEMA are shown in **Figure 6.23.** It can be seen that the characteristic time follows Arrhenius behavior with activation energy of 77.03 and 144.95 kJ·mol^{-1} for CEOEMA and PEOEMA. The results suggest that restrictions in chains mobility produced by crosslinking hinder the mechanism of charges transport in the polymer-electrodes interfaces.

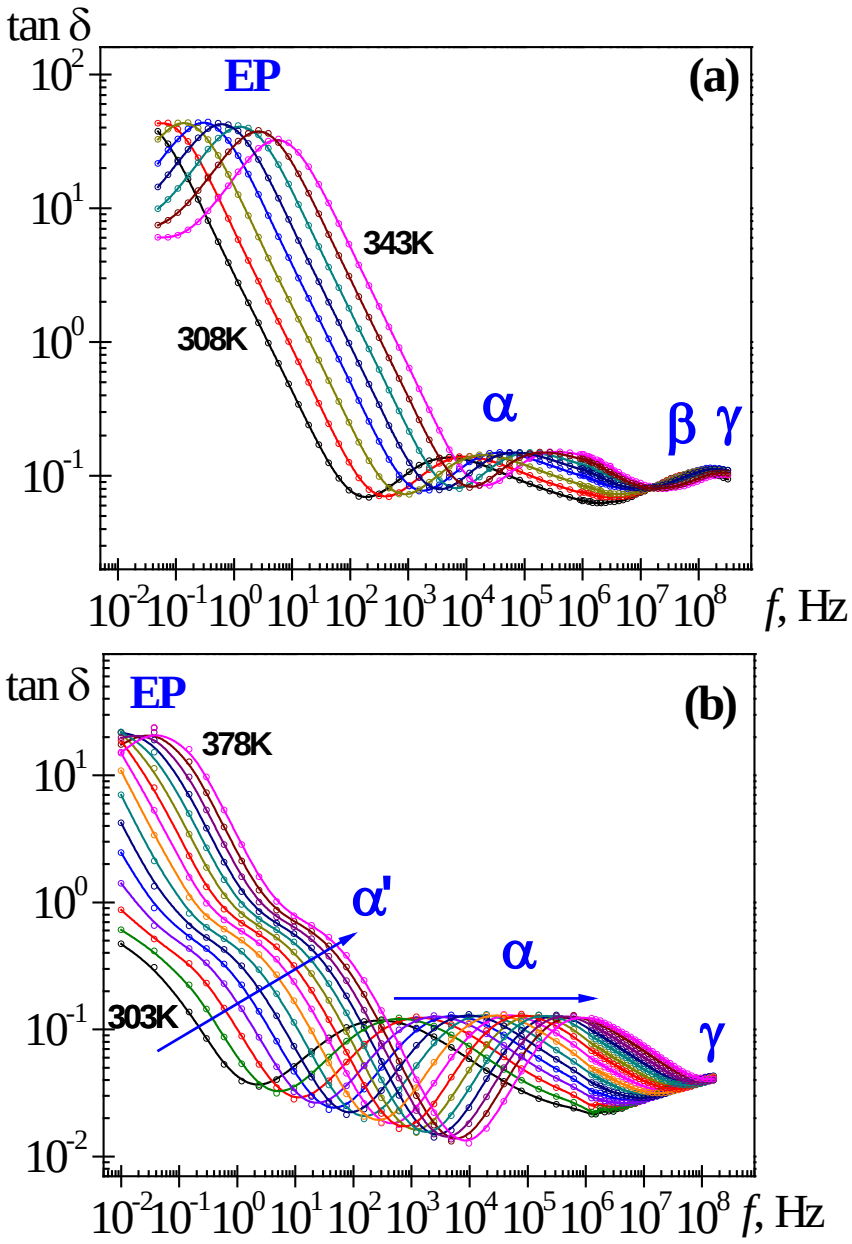

Figure 6.22. Loss tan δ in the frequency domain for (a) PEOEMA at 313-343 K and (b) CEOEMA at 303-373 K (at 5 K steps).

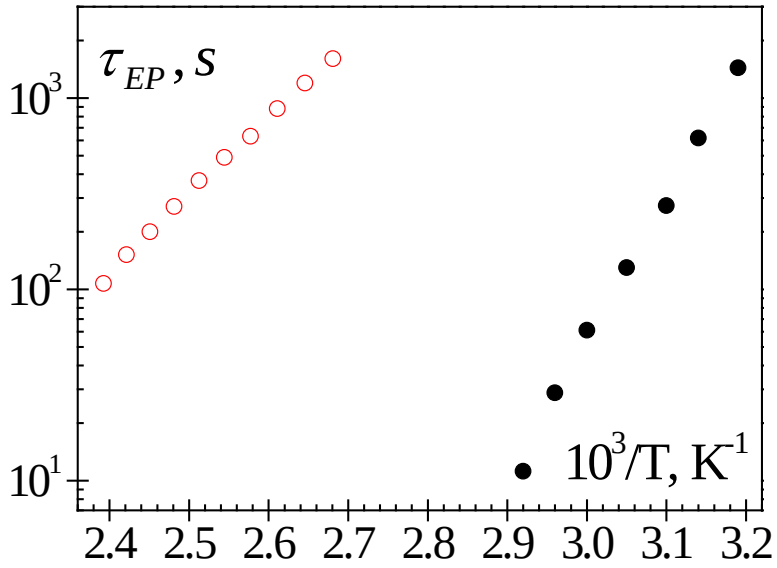

Figure 6.23. Temperature dependence of τEP(s) for PEOEMA (full symbols) and CEOEMA (open symbols).

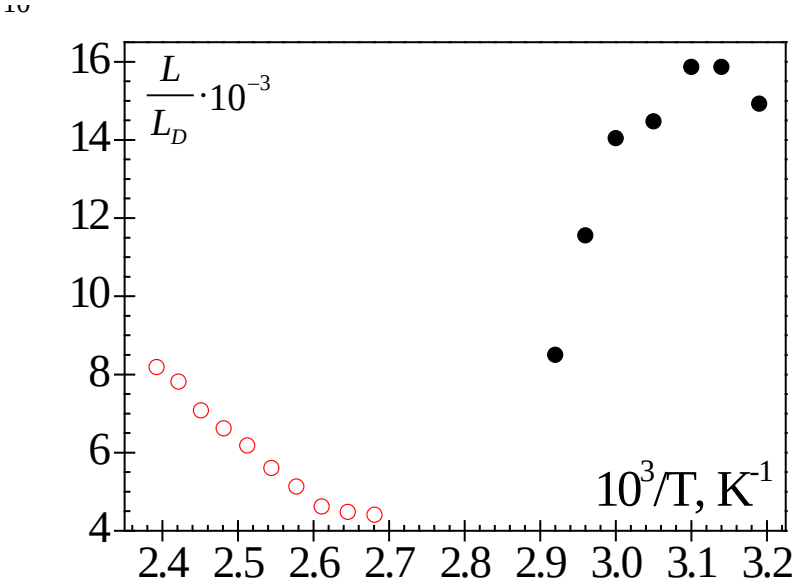

Figure 6.24. Temperature dependence of Debye length, $10^{-3}\cdot L/L_D$ for PEOEMA (full symbols) and CEOEMA (open symbols).

The temperature dependence of Debye length, plotted in **Figure 6.24**, shows that L_D decreases as temperature increases for PEOEMA, while increases with temperature for CEOEMA. For example, L_D decreases from 600 Å to 300 Å for PEOEMA when the temperature increases from 312 K to 342 K. The value of L_D is higher for CEOEMA, but in this case this quantity decreases as temperature goes down, the change being from 2500 Å to 1250 Å when the temperature passes from 420 K to 370 K. It is worth noting that temperature disrupts electronic clouds surrounding ions and as a result L_D increases as temperature increases in very dilute electrolyte solutions. However, decrease of the Debye`s length with increasing temperature has been reported for some polymers (Compañ, et al., 1996; Compañ, et al., 1999).

The diffusion of ionic species in CEOEMA and PEOEMA can be roughly estimated by assuming that the diffusive species are monovalent. By taking into account that the concentrations of anions and cations are the same in this case, and expressing the conductivity in terms of the ionic mobility, μ_i, *i.e.* $\sigma = F\sum_i c_i\mu_i$, i = +,-, the geometric average of the diffusion coefficients of the ionic species can be written as

$$D_{\pm} = \frac{RT\sigma}{FC} \qquad (6.26)$$

Notice that in the development of equation (6.26), use of the expression $\mu_i = FD_i / RT$ was made.

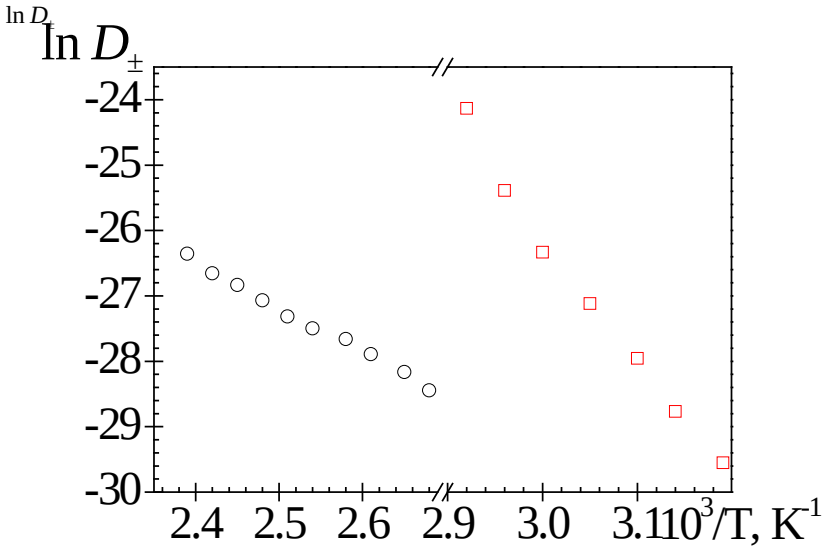

Figure 6.25. Temperature dependence of the geometric average diffusion coefficient of ionic species for PEOEMA (squares) and CEOEMA (circles).

Arrhenius plots for $D_{\pm}$ of CEOEMA and PEOEMA, presented in **Figure 6.25**, show that the values of the ionic diffusive coefficients corresponding to the latter polymer are higher than those corresponding to the crosslinked one. This means that reduction of the chains mobility by effect of crosslinking reduces ionic transport.

6.3. Conclusions

Uncrosslinked PEOEMA chains exhibit two secondary relaxation processes in the glassy state which in increasing order of frequency are called γ and β relaxations. The β relaxation is suppressed by slightly crosslinking the PEOEMA chains with only the γ relaxation remaining. The γ relaxation may be produced by conformational transitions

about the OCH_2-CH_2O bonds of the alcoholic residue whereas the β relaxation may arise from local motions of the polymer backbone. In this context the β relaxation would be a Johari-Goldstein relaxation (Johari, et al., 1970; Johari, 1976).

Although crosslinking decreases the mobility of the chains, thus increasing the glass transition temperature, the temperature dependence of the stretching exponent of the glass-rubber relaxation suggests that crosslinking of the poly(2-ethoxy methacrylate) chains does not widen the distribution of relaxation times associated with this process.

Results have been reported in the literature showing the formation of side-chain nanodomains flanked by the backbone in poly(n-alkyl methacrylate)s. Cooperative motions in the nanodomains are reflected in an α_{PE} peak, in addition to the glass-rubber relaxation arising from cooperative motions of the backbone. The schematic replacement of one of the methylene groups of the side group of the repeat unit of poly(n-pentyl methacryate) for an ether group to yield poly(2-ethoxy methacrylate) chains eliminates the α_{PE} peak in this polymer. However, the fact that the X-rays pattern of slightly crosslinked poly(2-ethoxy methacrylate) is similar to that of poly(n-pentyl methacrylate), suggests the formation of nanodomains in these systems which give rise to a symmetric relaxation. We attribute this peak not to a cooperative process, but to a MWS relaxation arising from a long distance charge transport-taking place in the bulk in heterogeneous systems. Crosslinking seems to slowdown interfacial electrode-polymer processes.

On the other hand, the storage relaxation modulus isochrones of CEOEMA present two inflexion points in the glass-rubber transition, centered at the peak maxima of the

variation of activation energy with temperature in the transition. These phenomena neither detected in the calorimetric thermograms nor in the loss dielectric spectra, presumably are associated with segmental motions of the dangling chains of the networks (low temperature inflexion point) and the segmental motions of the chains between crosslinked points (high temperature inflexion).

The mesoscopic structure of the crosslinked polymer that gives rise to a Maxwell-Wagner-Sillars relaxation in the dielectric spectra at high temperature does not seem to have any incidence in the relaxation mechanical spectra.

Conclusions

Conclusions presented in this Chapter were obtained by the analysis reported in : M. J. Sanchis, M. Carsí, P. Ortiz-Serna, G. Domínguez-Espinosa, and R. Díaz-Calleja, E. Riande,L. Alegría, L. Gargallo, and D. Radiç, *Macromolecules* vol 43, pp. 5723–5733, **2010;** M. Carsí, M. J. Sanchis, P. Ortiz-Serna, B. Redondo-Foj, R. Díaz-Calleja, E. Riande, *Macromolecules* vol 46, pp. 3167−3175, **2013;** M. Carsí, M.J. Sanchis, R. Díaz-Calleja, E. Riande, M.J.D. Nugent, *Macromolecules* vol 45, pp. 3571−3580, **2012**; M. Carsí, M.J. Sanchis, R. Díaz-Calleja, E. Riande, M.J.D. Nugent, European Polymer Journal, vol. 49, pp. 1495–1502, **2013**

The analysis makes it clear that there is a strong dependence between the chemical structure and the thermal, mechanical and dielectric properties. Due to the universality that exists among flexible polymers, the ideas and theories presented in this thesis, which have been systematically and quantitatively tested by the experimental results, should apply to other kinds of polymers.

Chapter 4 focused on the properties of three structurally related polymers, specifically the effect on thermal and dielectric properties of the relative position of the two oxymethylene groups in the phenyl group of side chains. The comparative study has provided a better understanding of how slight differences in chemical structure affect molecular responses to the perturbation field. According to our results:

- The slight structural difference has an important effect on the frequency/temperature dependence of the dielectric permittivity. For PDBM23 two steps were clearly observed, one relating to the glass transition temperature and the other to the MWS process. However, in the frequency/temperature experimental range, for PDBM25 and PDBM34 only one defined step was observed. In the latter case, data obtained at lower frequencies would be required in order to obtain a good definition of the MWS process. The loss of dielectric permittivity spectra for the three polymers shows the presence of several overlapping dipolar processes that are hidden at lower frequencies by the conductive contributions.

- The evaluation of the retardation time spectrum obtained from complex dielectric permittivity made it possible to characterize closely overlapping processes. This is due to the fact that, whereas the loss of spectrum from a Debye type relaxation covers more than two decades in the frequency domain, it becomes a Dirac delta function in the retardation time spectrum. Therefore the dielectric response to electrical perturbation fields will be better defined in the retardation time spectrum than in the loss of permittivity in the frequency domain.

- The DSC and DRS analyses show that the position of the two oxymethylene groups shifts the glass transition temperature from 310K for PDBM25 to 320K and 330K for PDBM23 and PDBM34, respectively. The global dielectric strength of the dipolar processes is also significantly affected by the position of the two oxymethylene groups. Thus the dielectric strength for PDBM34 is significantly lower than for the PDBM23 and PDBM25 polymers. The location of the oxymethylene moiety in position 2 of the phenyl group causes significant enhancement of the dielectric strength of the relaxations. This result is related to the fact that the angles formed by the dipoles of the C^{ar}-O-CH_3 bonds in 3,4 positions with the dipole of the ester groups are not as favorable and, as a result, dielectric strength for PDBM34 is significantly lower.

- The DRS analysis showed that the conductive contribution to the dielectric response is also affected by the slight differences in chemical structure. Thus the MWS process related to the build-up of charges at the interfaces of the side-chain nanodomains

flanked by the backbone is better defined for PDBM23 than for PDBM34 and PDBM25.

- Very rich dynamic information can be obtained from the dielectric spectra and used for comparative studies involving other spectroscopies and experimental techniques, such as infrared spectroscopy, X-ray spectroscopy, dynamic mechanical analysis, thermally stimulated depolarization current spectroscopy, etc. Such interplay among different probing techniques should greatly enhance the studies and applications of chain dynamics.

Chapter 5 focused on the conductivity analysis of viscoelastic liquids, taking PDBM23 as a model due to its peculiar behavior. This polymer showed that the side group's segregation from the backbone brings about relatively long distance charge jumps, reflected as a distributed MWS relaxation. The time−temperature correspondence principle for the AC conductivity and the complex dielectric permittivity was analyzed. This principle holds for reduced AC conductivity. However, it does not hold for the components of complex dielectric permittivity, due among other things to the different temperature dependences of each dipolar relaxation process.

Chapter 6 focused on the analysis of the effect of the crosslinking agent on molecular mobility. For this purpose a polymer with (CEOEMA) and without (PEOEMA) crosslinking was analyzed:

- The effect of the crosslinking agent was different for the two secondary relaxations. Whereas no significant effect was observed in the γ process, the crosslinking caused the blocking of the molecular motions related to the β process.
- As expected, through DSC, DRS and DMA analysis a reduction of chain mobility resulting in an increase in T_g was observed. The storage relaxation modulus isochrones of CEOEMA indicate two inflexion points, presumably related to the segmental motions of the dangling chains of the cross-linked networks and the cooperative motions of the chains between crosslinking points.
- Crosslinking gives rise to the formation of side-chain nanodomains flanked by the backbone, which in turn give rise to an MWS symmetric relaxation. Finally, crosslinking seems to slow down the interfacial processes.

Bibliography

Adachi, A. et al., 2003. *Contact Dermatitits,* Volume 48, pp. 133-136.

Adachi, K. & Kotaka, T., 1984. *Macromolecules ,* Volume 17, p. 120.

Adachi, K. & Kotaka, T., 1988. *Macromolecules ,* Volume 21, p. 157.

Adachi, K. & Kotaka, T., 1993. *Prog. Polym. Sci.,* Volume 18(13), p. 585.

Ahn, S. et al., 2008. *Soft Matter,* Volume 4, p. 1151–1157.

Alegría, A. et al., 1995. *Macromolecules,* Volume 28(5), pp. 1516-1527.

Alvarez, C., Lorenzo, V. & Riande, E., 2005. *J. Chem. Phys.,* Volume 122, p. 194905.

Alves, N., Gomez-Ribelles, J. & Mano, J., 2005. *Polymer,* 46(491–504).

Angell, C., 1988. *Relaxation in Complex Systems.* Springfield: US Dept. Commerce.

Angell, C., 1991. *J. Non-Cryst. Solids,* Volume 131-133, pp. 13-31.

Angell, C. A., 1985. *J. Non-Cryst. Solids,* Volume 73, pp. 1-3.

Angell, C. A., 1995. *Science,* Volume 267, pp. 1924-1935.

Angell, C. A., 1996. *Complex Behavior of Glassy Systems.* Sitges, Barcelona: Proceedings of the XIV Sitges Conference.

Anshyang, A., Lin, T., Kwei, K. & Reiser, A., 1989. *Macromolecules,* Volume 22, pp. 4112-4119.

Arbe, A. et al., 2010. *Macromolecules ,* Volume 43, pp. 3107-3119.

Arbe, A. et al., 2008. *Soft Matter ,* Volume 4, p. 1792.

Atkins, P., 1990. *Physical Chemistry.* Oxford: Oxford University Press.

Barsoukov, E. & JMacdonals, .., 2005. *Impedance Spectroscopy. Theory, Experiment, and Applications.* s.l.:Wiley Interscience.

Barton, J., 1966. *Verres Refr. ,* Volume 20, p. 328.

Beiner, M., 2001. *Macromol. Rapid Comm.,* Volume 22, p. 869.

Beiner, M., 2006. Melville, NY , Tokuyama, M., Maruyama, S., Eds. American Institute of Physics, p. 134.

Beiner, M. & Huth, H., 2003. *Nat. Matter,* Volume 2, p. 595.

Beiner, M., Kabisch, O., Reichl, S. & Huth, H., 2002. *J. Non- Crystalline Solids* , Volume 307, p. 658.

Beiner, M. et al., 2001. *Macromolecules,* Volume 34, p. 5927.

Beiner, M. et al., 1999. *Macromolecules* , Volume 32, p. 6278.

Bekin, S. et al., 2014. *Sensors and Actuators B: Chemical,* Volume 202, pp. 878-892.

Bergman, R., Alvarez, F., Alegría, A. & Colmenero, J., 1998. *J. Chem. Phys.,* Volume 109, p. 7546.

Bermejo, F. et al., 1997. *Complex Behaviour of Glassy Systems.* Berlin-Heidelberg: Springer Lecture Notes in Physics (Springer).

Bershtein, V. et al., 2002. *J Polymer Sci Part B:Polymer Phys* , Volume 40, p. 1056–1069.

Blythe, A. & Bloor, D., 2005. *Electrical properties of polymers.* New York: Cambridge University Press.

Bohmer, R. & Angell, C. A., 1992. *Phys. Rev. B,* Volume 45, pp. 10091-10094.

Bohmer, R. & Angell, C. A., 1993. *Phys. Rev. B,* Volume 48, pp. 5857-5863.

Bohmer, R., Ngai, K. L., Angell, C. A. & Plazek, D. J., 1993. *J. Chem. Phys.,* Volume 99, pp. 4201-4209.

Borns, M. et al., 2007. *Polymer,* Volume 48, pp. 7316-7328.

Böttger, H. & Bryskin, U., 1985. *Hopping conduction in solid.* Berlin: Akademie Verlag.

Bowen, C. R. & D.P., A., 2006. *Mater. Sci. Technol,* Volume 22, p. 719.

Bower, D., 2002. *An Introduction to Polymer Physics.* s.l.:Cambridge University Press.

Boyd, R., 1985. *Polymer* , Volume 26, p. 1123.

Boyd, R. H., 1985. *Polymer,* Volume 26, pp. 323-347.

Boyd, R. & Smith, G., 2007. *Polymer Dynamics and relaxations.* Cambridge: Cambridge University Press.

Brar, A. & Kumar, R., 2002. *J Mol Struct,* Volume 616, pp. 37-47.

Brar, A. & Kumar, R., 2002. J. Mol. Struct.. Volume 616, pp. 37-47.

Brar, A. S. & Kumar, R., 2002. *J. Appl. Polym. Sci.,* Volume 85, pp. 1328-1336.

Bueche, F., 1959. *J. Chem. Phys.,* Volume 30, pp. 748-752.

Buerger, D. & Boyd, R., 1989. *Macromolecules* , Volume 22, p. 2694.

Buerger, D. & Boyd, R., 1989. *Macromolecules* , Volume 22, p. 2699.

Bühler, V., 2005. *Polyvinylpyrrolidone Excipients for Pharmaceuticals: Povidone, Crospovidone and Copovidone.* Berlin: Springer.

Bunde, A. & Havlin, S., 1996. *Fractals and Disordered Systems.* Berlin: Springer.

Burns, A. et al., 1989. *Phys. Chem. Glasses,* Volume 30, p. 264.

Burtle, G. & Turek, W. N., 1954. *J. Org. Chem.* , Volume 19, p. 1567.

Cangialosi, D., Alegría, A. & Colmenero, J., 2006. *J. Chem. Phys.,* Volume 124, pp. 024906-024909.

Carsí, M., Sanchis, M. J., Díaz-Calleja, R. & Nugent, M. J. D., 2013. *Eur. Polym. J.*, Volume 49, p. 1495–1502.

Carsí, M. et al., 2012. *Macromolecules,* Volume 45, p. 3571−3580.

Casalini, R., Ngai, K. & Roland, C., 2003. *Physical Review B,* Volume 68, p. 014201.

Casalini, R. & Roland, C., 2003. *Phys Rev Lett,* Volume 91, p. 015702.

Casalini, R. & Roland, C., 2010. *Journal of Polymer Science: Part B: Polymer Physics*, Volume 48, pp. 582-587.

Cerrada, M., de la Fuente, J., Fernández-García, M. & Madruga, E., 2001. *Polymer*, Volume 42, pp. 4647-4655.

Cerveny, S., Alegría, A. & Colmenero, J., 2008. *J. Chem. Phys.,* Volume 128, pp. 044901-044907.

Chee, K., 1987. *Polymer*, Volume 28, pp. 977-979.

Chee, K., 1991. *J. Appl Polym. Sci*, Volume 43, pp. 1205-1208.

Chee, K., 1995. *Polymer*, Volume 36, pp. 809-813.

Cheng, P., Driessen, A., Tijsma, E. & Udipi, K., 2006. *Journal of Controlled Release* , 116(2), pp. e92-e94.

Child, J. W. & Ferry, J., 1957. *J.Colloid Sci.,* Volume 12, p. 327.

Christensen, R., 1982. *Theory of Viscoelasticity.* s.l.:Dover Civil and Mechanical Engineering.

Coelho, R., 1991. *J. Non-Cryst. Solids* , Volume 131-133, p. 1136.

Cohen, M. & Turnbull, D., 1959 . *J. Chem. Phys.,* Volume 31, pp. 1164-1169.

Cole, K. S. & Cole, R., 1941. *J. Chem. Phys.*, Volume 9, pp. 341-351.

Cole, R., 1961. *Theories of dielectric polarization and relaxation.*. s.l.: Progress in Dielectrics.

Cole, R., 1965. *Journal of Chemical Physics* , Volume 42, p. 637–43.

Colmenero, J. et al., 1991. *Phys. Rev. B,* Volume 44(14), p. 7306.

Compañ, V., Guzmán, J., Díaz-Calleja, R. & Riande, E., 1999. *J. Polym. Sci.: Part B: Polym. Phys.* , Volume 37, p. 3027.

Compañ, V., Sorensen, T., Díaz-Calleja, R. & Riande, E., 1996. *J. Appl. Phys.* , Volume 79, p. 403.

Compañ, V., Sorensen, T. S., Díaz-Calleja, R. & Riande, E., 1996. *J. Appl. Phys.* , Volume 79, p. 403.

Cook, M., Watts, D. & Williams, G., 1970. *Trans. Faraday Soc.,* Volume 66, pp. 2503-2511.

Cook, W., Scott, T., Quay-Thevenon, S. & Forsythe, J., 2004. *J Appl Polym Sci,* Volume 93, pp. 1348-1359.

Costa, V. et al., 2012. *J. Elastomers Plastics*, Volume 45, pp. 217-238.

Cowie, J. M. G., 1980. *Journal of Macromolecular Science, Part B* , Volume 18(4), pp. 569-623.

Craig, D., 1995. *Dielectric Analysis of Pharmaceutical Systems.* London: Taylor&Francis.

Cugini, A. & Lesser, A., 2014. *Polymer Engineering and Science.*

Daly, J. H., Guest, M. J., Hayward, D. & Pethrick, R. A., 1992. *J. Mat. Sci. Lett.* , Volume 11, p. 1271.

Daly, J. H., Guest, M. J., Hayward, D. & Pethrick, R. A., 1992. *J. Mat. Sci. Lett.* , Volume 11, p. 1271.

Davidson, D. & Cole, R., 1950. *J. Chem. Phys.*, Volume 18, pp. 1417-1418.

Davis, T., 1997. *Polyacrylates In Polymer Handbook.* New York: Olabisi, ed., Marcel Dekker.

Debye, P., 1929. *Polar Molecules.* New York: Chem. Catalog..

Debye, P., 1945. *Polar Molecules.* New York: Dover Publications.

Delpouve, N. et al., 2014. *Macromolecules,* Volume 47, pp. 5186-5197.

Deutsch, K., Hoff, E. A. & Reddish, W., 1954. *J. Polym. Sci.*, Volume 13, pp. 565-582.

Devine, D. & Higginbotham, C., 2003. *Polymer,* Volume 44, pp. 7851-7860.

Dhakate, S. et al., 2008. *Int. J. Hydrogen Energy,* Volume 33, pp. 7146-7152.

Diaz Calleja, R., Ribes Greus, A. & Gómez Ribelles, J., 1989. *Polymer Commun.*, Volume 30, p. 270.

Diaz Calleja, R., Ribes Greus, A. & Gómez Ribelles, J., 1989. *Polymer ,* Volume 30, p. 1433.

Díaz-Calleja, R., Domínguez-Espinosa, G. & Riande, E., 2007. *J. Non-Cryst. Solids* , Volume 353, p. 719.

Diaz-Calleja, R. & Riande, E., 1994. *J of NonCrystalline Solids ,* Volume 172-174, p. 1037.

Diaz-Calleja, R., Riande, E. & San Roman, J., 1992. *J. Polym Sci Part B: Polym Phys.* , Volume 30, p. 1239.

Díaz-Calleja, R. et al., 2000. *J. Polym. Sci.: Polym. Phys. ,* Volume 38, p. 2179.

Domínguez-Espinosa, G., Díaz-Calleja, R. & Riande, E., 2006. *Macromolecules ,* Volume 39, p. 5043.

Domínguez-Espinosa, G. et al., 2006. *Macromolecules* , Volume 39, p. 3071.

Dominguez-Espinosa, G. et al., 2008. *J. Chem. Phys.*, Volume 129, p. 104513.

Domínguez-Espinosa, G. et al., 2005. *J. Chem. Phys. ,* Volume 123, p. 114904.

Domínguez-Espinosa, G. et al., 2005. *Polymer ,* Volume 46, p. 8028.

Donth, E., 1996. *J. Polym. Sci. Part B Polym. Phys.*, Volume 34(17), p. 2881–2892.

Doolittle, A., 1951. *J. Appl. Phys.,* Volume 22(12), pp. 1471-1975.

Doolittle, A. K., 1952. *Appl. Phys.,* Volume 23(2), pp. 236-423.

Dudognon, E., Berne`s, A. & C., L., 2001. *Macromolecules ,* Volume 34, pp. 3988-3992.

Dudognon, E., Berne`s, A. & C., L., 2001. *Macromolecules ,* Volume 34, pp. 3988-3992.

Dudognon, E., Berne`s, A. & Lacabanne, C., 2002. *Macromolecules ,* Volume 35, pp. 5927-5931.

Dyre, J., 1988. *J. Appl. Phys.*, Volume 64(5), pp. 2456-2468.

Dyre, J., 1998. *J. Non-Crystal. Solids,* Volume 235-237, pp. 142-149.

Dyre, J. C., 1986. *J. Phys. C: Solid State Phys.* , Volume 19, p. 5655.

Dyre, J., Maass, P., Roling, B. & Sidebottom, D., 2009. *Rep. Prog. Phys.* , Volume 72, p. 46501.

Dyre, J. & Shrøder, T., 2000. *Rev. Mod. Phys.,* Volume 72(3), pp. 873-892.

Ediger, M. & Angell, C., 1996. *J. Phys. Chem,* Volume 100, pp. 13200-13212.

Ediger, M., Angell, C. & Nagel, S., 1996. *The Journal of Physical Chemistry,* Volume 100(31), pp. 13200-13212.

El-Begawy, S. E. M. & Huglin, M. B., 1991. *Eur. Polym. J.,* Volume 27, pp. 1023-1027.

Encinar, M. et al., 2008. *Polymer,* Volume 49 (26), pp. 5650-5658.

Ezquerra, T. et al., 1999. *Journal of Chemical Physics ,* 110(20), p. 10134.

Feldman, Y., Puzenko, A. & Ryabov, Y., 2002. *Chem. Phys.,* Volume 284, pp. 139-168.

Feldstein, M. M. et al., 2003. *Polymer,* Volume 44, pp. 1819-1834.

Feldstein, M. M., Shandryuk, G., Kuptsov, S. & Platé, N., 2000. *Polymer,* Volume 41(4), pp. 5327-5338.

Ferry, J., 1961. *Viscoelastic Properties of polymers, 2nd ed.*. New York: John Wiley&Sons.

Fioretto, D. et al., 1994. *J. Phys.: Condens. Matter,* Volume 6, pp. 5295-5302.

Floudas, G., 2004. *Progr. Polym. Sci,* Volume 29, p. 1143.

Floudas, G., Paluch, M., Grzybowski, A. & K.L., N., 2011. *Molecular Dynamics of Glass-Forming Systems. Effects of Pressure.* Berlin Heidelberg: Springer–Verlag .

Floudas, G. et al., 1995. *Macromolecules,* Volume 28, pp. 6799-6807.

Floudas, G. & Stepanek, P., 1998. *Macromolecules,* Volume 31, p. 6951.

Folttmann, H. & Quadir, A., 2008. *Drug Del. Tech,* 8(22-27).

Fox, T. & Flory, P., 1950. *J. Appl. Phys.,* Volume 21, pp. 581-91.

Fröhlich, H., 1958. *Theory of Dielectrics. Dielectric Constant and Dielectric Loss.*. s.l.:Oxford University Press.

Fujimori, H. & Oguni, M., 1995. *Solid State Commun.,* Volume 94, p. 157.

Fulcher, G., 1925. *J Am Ceram Soc.,* Volume 8, pp. 339-340.

Fuoss, R. & Kirkwood, J., 1941. *J Am Chem Soc,* Volume 63 , pp. 385-394.

Fuoss, R. & Kirkwood, J., 1941. *J Am Chem Soc,* Volume 63, pp. 385-394.

Gabbott, P., 2008. *Principles and Applications of Thermal Analysis.*. s.l.:Blackwell Publishing Ltd.

Gallardo, A. et al., 1999. *Macromolecules,* Volume 32, pp. 610-617.

Gargallo, L., Muñoz, M. I. & Radic´, D., 1986. *Polymer* , Volume 27, p. 1416.

Garwe, F. et al., 1994. *J. Phys.: Condens. Matter* , Volume 6, p. 6941.

Garwe, F. et al., 1996. *Macromolecules* , Volume 29, pp. 247-253.

Giebel, L., Meier, G., Fytas, G. & Fischer, E., 1992. *J. Polym. Sci., Part B: Polym. Phys.* , Volume 30, p. 1291.

Glarums, H., 1960. *Journal of Chemical Physics,* Volume 33, pp. 371-5.

Glatz-Reichenback, J., Sorriero, L. & Fitzgerald, J., 1994. *Macromolecules,* Volume 27, p. 1338.

Godard, M. & Saiter, J., 1998. *Journal Polymer Science:Polymer Physics* , Volume 36, p. 2865.

Godard, M. & Saiter, J., 1998. *Journal of non Crystalline Solids* , Volume 235-237, p. 635.

Goldstein, J. et al., 2003. *Scanning Electron Microscopy and X-Ray Microanalysis.* New York: Springer.

Gómez Ribelles, J. & Diaz Calleja, R., 1985. *J. Polymer Sci.* , Volume 23, p. 1297.

Gómez, C. et al., 2013. *Appl. Surf. Sci,* Volume 275, pp. 295-302.

Gomez, D., Alegria, A., Arbe, A. & Colmenero, J., 2001. *Macromolecules,* Volume 34, p. 503.

Gordon, M. & Taylor, J. S., 1952. *J. Appl. Chem.,* Volume 2, pp. 493-500.

Graessley, W., 1974. *Adv. Poymer Sci* , Volume 16, pp. 1-179.

Graessley, W., 1982. *Adv. Poymer Sci* , Volume 47, pp. 67-117.

Graham, N., 1990. *Controlled drug delivery systems. Chemical Industry,* pp. 482-486.

Grassi, M., Colombo, I. & Lapasin, R., 2000. *J. Control. Release,* Volume 68, pp. 97-113.

Grenet, J., Saiter, J. & Godard, M., 2002. *Journal of non Crystalline Solids* , Volume 307-310, p. 232.

Grigoraş, V. C. & Bărboui, V., 2008. *Rev. Roum. Chim.,* Volume 53, pp. 127-131.

Haaf, F., Sanner, A. & Straub, F., 1985. *Polym. J.,* Volume 17, pp. 143-152.

Hammami, H., Arous, M., Lagache, M. & Kallel, A., 2007. *J. All. Comp.* , Volume 430, p. 1.

Hart, E. & Waxman, B., 1983. *Encyclopedia of Chemical Technology.* New York: Interscience.

Havriliak, S. & Havriliak, S. J., 1997. *Dielectric and Mechanical Relaxation in Materials.* Munich: Hanser.

Havriliak, S. & Negami, S., 1966. *J. Polym. Sci. Part B Polym. Symp.,* Volume 14, pp. 99-117.

Havriliak, S. & Negami, S., 1966. *J. Polym. Sci. Part C: Pol. Symp.,* Volume 14(1), pp. 99-117.

Havriliak, S. & Negami, S., 1967. *Polymer,* Volume 8(4), pp. 161-210.

Havriliak, S. & Negami, S., 1997. *Dielectric and Mechanical Relaxation in Materials.* Munich: Hanser.

Heijboer, J., 1965. In: *In Physics of Non-Crystalline Solids; Prins, J. A., Ed.*. Amsterdam: North-Holland.

Heijboer, J., 1972. Leiden, The Netherlands: Ph.D. thesis, University of Leiden.

Hempel, E., Beiner, M., Huth, H. & Donth, E., 2002. *Thermochim. Acta* , Volume 391, p. 219.

Hempel, E., Huth, H. & Beiner, M., 2003. *Thermochim. Acta* , Volume 403, pp. 105-114.

Hiller, S. et al., 2004. *New Journal of Physics,* Volume 6, p. 10.

Hodge, I., 1983. *Macromolecules,* Volume 16(6), p. 898–902.

Hodge, I., Ngai, K. & Moynihan, C., 2005. *J. Non-Cryst. Solids,* Volume 351(2), pp. 104-115.

Huglin, M. B. & Rehab, M. M. A. M., 1987. *Polymer,* Volume 28(13), pp. 2200-2206.

Huglin, M. & Zakaria, M., 1986. *J. Appl. Polym. Sci.,* Volume 31, pp. 457-475.

Huo, P. & Cebe, P., 1992. *J. Polym. Sci. Part B Polym. Phys.,* Volume 30, pp. 239-250.

Ikeda, M. & Aniya, M., 2010. *Intermetallics,* Volume 18, pp. 1796-1799.

Ishida, Y., 1969. *J. Polym. Sci. A2,* Volume 7, p. 1835.

Ishida, Y. & Yamafuji, K., 1961. *Kolloid Z.,* Volume 177, p. 97.

Jablonski, A., Lang, A. & Vyazovkin, S., 2008. *Thermochim Acta,* Volume 474, pp. 78-80.

Janik, P. & Paluch, M., 2001. *Physical Review E.,* Volume 64, p. 042502.

Jobish, J., Charoen, N. & Praveen, P., 2012. *J. Non-Crystal Solids,* Volume 358, pp. 1113-1119.

Johari, G., 1976. *N.Y. Acad. Sci. ,* Volume 279, p. 117.

Johari, G. & Goldstein, M., 1971. *J. Chem. Phys.,* Volume 55(9), pp. 4245-4252.

Johari, G. & Pathmanathan, K., 1986. *J. Chem. Phys.,* Volume 85(11), pp. 6811-6812.

Johari, G. P. & Goldstein, M., 1970. *J. Chem. Phys.,* Volume 53, p. 2372.

Johari, G. P. & Goldstein, M., 1972. *J. Chem. Phys.,* Volume 56, p. 4411.

John Wiley & Sons, L., March 2011. *Properties and Behavior of Polymers, Two Volume Set.* s.l.:Wiley.

Jonscher, A., 1977. *Nature ,* Volume 267, p. 673.

Jonscher, A., 1992. *Universal relaxation law.* London: Chelsea Dielectric Press.

Ju, H., Ki, S. & Lee, Y., 2002. *J. Appl. Polym. Sci.,* Volume 83, pp. 1128-1139.

Kahle, S. et al., 1997. *Macromolecules,* Volume 30, p. 7214.

Kalakkunnath, S. et al., 2007. *Macromolecules,* Volume 40, pp. 2773-2781.

Kaoutit, H. E. et al., 2013. *Dyes and Pigments,* Volume 96, pp. 414-423.

Khursheed, A., 2011. *Scanning Electron Microscope Optics and Spectrometers.* London: World Scientific Publishing Co. Pte. Ltd..

Klein, R. J. et al., 2006. *J. Chem. Phys.,* Volume 124, p. 144903.

Kohlrausch, F., 1854. *Pogg Ann Phys Chem,* Volume 91, pp. 179-214.

Kovacs, A., 1963. *Adv. Polym. Sci.,* Volume 3, p. 394.

Kovacs, A., Aklonis, J., Hutchinson, J. & Ramos, A., 1979. *J. Pol. Sci.,* Volume 17(7), pp. 1097-1162.

Krause, C., Sangoro, J. & Kremer, F., 2010. *J. Phys. Chem. B,* Volume 114, p. 382.

Kremer, F. & Schönhals, A., 2003. *Broadband Dielectric Spectroscopy.* Berlin: Springer.

Ku, C. & Liepens, R., 1987. *Electrical Properties of Polymers. Chemical Principles..* Munich-Vienna-New York: Hanser Publishers.

Kuebler, S. et al., 1997. *Macromolecules,* Volume 30, p. 6597.

Kwei, T. K., 1984. *J. Polymer Sci.: Polymer Lett. Ed.,* Volume 22 (6), p. 307–313.

Kwei, T. K., Pearce, E. M., Pennacchia, J. R. & Charton, M., 1987. *Macromolecules,* Volume 20 (5), p. 1174–1176.

Laredo, E. & Grimau, M., 2003. *Macromolecules,* Volume 36, pp. 9840-9850.

Laredo, E. & Herandez, M. C., 1997. *J. Polym Sci.:Part B: Polym. Phys.* , Volume 35, p. 2879.

Lee, W. A. & Knight, G. J., 1966. *The Glass Transition of Polymers, Polymer Handbook.* New York: Wiley- Interscience Publishers.

Lee, Y.-H., Bur, A. J., Roth, S. C. & Start, P. R., 2005. *Macromolecules* , Volume 38, p. 3828.

Lemieux, E. & Prud'homme, R., 1989. *Polym. Bull.),* Volume 21, p. 621.

Lewis, I. & Edwards, H., 2001. *Handbook of Raman Spectroscopy.* New York: Marcel Dekker.

Lindsay, C. & Patterson, G., 1980. *J. Chem. Phys.,* Volume 73, p. 3348.

Lopérgolo, L., Lugao, A. & Catalani, L., n.d. *Polymer,* Volume 44, pp. 6217-6222.

Lovel, R., 1974. *J. Phys. C: Solid State Phys.,* Volume 7(23), pp. 4378-4384.

Lu, H. & Zhang, X. J. 3., 2006. *Macromol. Sci. Phys.* , Volume 45, p. 93.

Lu, H., Zhang, X. & Zhang, H., 2006. *J Appl Phys,* Volume 100(5), p. 054104.

Lunkenheimer, P., Schneider, U., Brand, R. & Loidl, A., 2000. *Contemp. Phys.,* Volume 41, pp. 15-36.

Macdonald, J., 1953. *Phys. Rev.* , Volume 92, p. 4.

Mark, J., 2007. *Physical Properties of Polymer Handbook.* s.l.:Springer.

Maxwell, J., 1893. *Electricity and Magnetism.* s.l.:Clarendon.

McCrum, N., Read, B. & Williams, W., 1991. *Anelastic and Dielectric Effects in Polymeric Solids.* New York: Dover Publications.

Meier, G., Kremer, F., Fytas, G. & Rizos, A., 1996. *J. Polym. Sci., Polym. Phys.* , Volume 34, p. 1391.

Menczel, J. & Bruce Prime, R., 2009. *Thermal Analysis of Polymers. Fundamentals and Applications.*. Hoboken, New Jersey: John Wiley & Sons.

Menissez C, S. B. D. L. V. G., 2005. *J. Non-Cryst. Solids* , Volume 351, p. 595.

Merino, E. et al., 2011. *European Polymer Journal,* Volume 47, pp. 1429-1446.

Michler, G., 2008. *Electron Microscopy of Polymers.* Berlin Heidelberg: Springer-Verlag.

Mijovic, J. & Fitz, B., 1998. *Novocontrol Applic Note Dielectrics* , Volume 29.

Miller, R. L., 1999. *Glass transition Temperatures of Polymers.* 4th Ed. ed. Hoboken: Polymer Handbook; Wiley-Interscience.

Morozov, V., 1984. *Methods for Solving Incorrectly Posed Problems;*. New York: Springer.

Mpoukouvalas, K., Floudas, G. & Williams, G., 2009. *Macromolecules,* Volume 42, pp. 4690-4700.

Mpoukouvalas, K., Floudas, G. & Williams, G., 2009. *Macromolecules* , Volume 42, p. 4690.

Murugaraj, R., 2007. *J. Mater. Sci.,* Volume 42, p. 10065.

Nakajima, T., 1972 . *Annual Report. Conf. Electric and Dielectric Phenomena.* Washington DC: National Academy of Science.

Namikawa, H., 1975. *J. Non-Cryst. Solids,* Volume 18, p. 783.

Neagu, E., Pissis, P., Apekis, L. & Gomez Ribelles, J. L., 1997. *J Phys D: Appl Phys,* Volume 30(11), p. 1551–60.

Ngai, K., 1979. *Comments Solid State Phys,* Volume 9, pp. 141-155.

Ngai, K., 1998. *J. Chem. Phys,* Volume 109, p. 6982.

Ngai, K., 1999. *J. Chem. Phys.,* Volume 110, p. 10576.

Ngai, K., 2003. *J. Phys. Condens. Matter,* Volume 15, pp. S1107-S1125.

Ngai, K., 2011. *Relaxation and diffusion in complex systems.* Berlin: Springer.

Ngai, K. & Capaccioli, S., 2004. *Physical Review E,* Volume 69, p. 031501.

Ngai, K. & Capaccioli, S., 2007. *Journal of Physics-Condensed Matter,* Volume 19(20), p. 205114.

Ngai, K. L., Gopalkrishnan, T. R. & Beiner, M., 2006. *Polymer* , Volume 47, p. 7222.

Ngai, K. L. & Paluch, M., 2004. *J. Chem. Phys.,* Volume 120, pp. 857-873.

Ngai, K. & Roland, C., 1993. *Macromolecules,* Volume 26, pp. 2688-2690.

Ngai, K. & Tsang, K., 1999. *Phys Rev E ,* 60(4511).

Ngai, K. & Tsang, K., 1999. *Phys Rev E,* Volume 60, p. 4511.

Nguyen, K. & West, J., 2002. *Biomaterials,* Volume 23, pp. 4307-4314.

Nicholson, J., 1994. *The chemistry of Polymers.* Cambridge: RSC Paperbacks.

Noda, N., 2005. *Polymer,* Volume 46, pp. 7201-7217.

Obrzut, J. & Page, K., 2009. *Phys. Rev. B* , Volume 80, p. 195211.

Odegard, G. & Bandyopadhyay, A., 2011. *Journal of Polymer Science Part B: Polymer Physics,* Volume 49(24), p. 1695-1716.

Odian, G., 2004. *Principles of Polymerization.* 4th ed. Hoboken: John Wiley & Sons, Inc..

Ortiz-Serna, P. et al., 2015. *J. Appl. Polym. Sci.,* Issue DOI:10.1002/APP.42007.

Ortiz-Serna, P. et al., 2010. *Macromolecules,* Volume 43, p. 5094–5102.

Ortiz-Serna, P. et al., 2011. *J. Non-Cryst. Solids,* Volume 357, p. 598–604.

Paluch, M. et al., 2005. *Journal of Chemical Physics,* Volume 122(23), pp. 234506-234506-6.

Papathanassiou, A., Sakellis, I. & Grammatikakis, 2007. *J. Appl. Phys. Lett.,* Volume 91, p. 122911.

Pascui, O., Beiner, M. & Reichert, D., 2003. *Macromolecules,* Volume 36, p. 3992.

Patil, P. et al., 2013. *Soft Matter,* Volume 9, pp. 3589-3599.

Patkpwski, A., Paluch, V. & Gapinski, J., 2003. *J. Non-Crystalline Solids,* Volume 330, pp. 259-263.

Peppas, N., 1987. *Hydrogels in medicine and pharmacy.* Florida: CRC Press.

Peppas, N., Bures, P., Leobandung, W. & Ichikawa, H., 2000. *Eur. J. Pharm. Biopharm.,* Volume 50, pp. 27-46.

Perrier, G. & Bergeret, A., 1997. *J. Polym Sci: Part B: Polym Phys.* , Volume 35, p. 1349.

Plazek, D., 1965. *J. Phys. Chem.* , Volume 69, p. 3480.

Plazek, D., 1996. *J. Rheol.* , Volume 40, p. 987.

Plazek, D. J. & Ngai, K., 1991. *Macromolecules* , Volume 24, p. 1222.

Plazek, D. & Ngain, K., 1996. The glass temperature. In: *Physical properties of polymers handbook.* Woodbury, N.Y.: AIP Press, p. 139.

Press, W. H., Teukolsky, S. A., Vetterling, W. T. & Flannerty, B. P., 1992. *In The Art of Scientific Computing, 2nd ed.*. New York: Cambridge University Press.

Qazvini, N. & Mohammadi, N., 2005. *Polymer,* Volume 46, pp. 9088-9096.

Qin, Q. & McKenna, B., 2006. *J. Non-Cryst. Solids,* Volume 352, pp. 2977-2985.

Reading, M. & Hourston, D. J., 2006. *Modulated-Temperature Differential Scanning Calorimetry. Theoretical and Practical Applications in Polymer Characterization.*. Dordrecht: Springer.

Redondo-Foj, B. et al., 2014. *Macromolecules,* Volume 47(15), p. 5334–5346.

Redondo-Foj, B. et al., 2013. *J. Phys. D: Appl. Phys.*, Volume 46, pp. 295304-295315.

Redondo-Foj, B. et al., 2015. *Polym. Int.,* Volume 64, pp. 284-292.

Reiner Zorn, A., 1999. *J. Polym. Sci. Part B: Polym. Phys.,* Volume 37, p. 1043.

Reppe, W., 1954. *Polyvinylpyrrolidon.* Weinheim: Verlag Chemie.

Riande, E. & Díaz-Calleja, R., 2004. *Electrical Properties of Polymers.* s.l.:Dekker, M..

Riande, E. et al., 2000. *Polymer Viscoelasticity: Stress and Strain in Practice.* New York: Marcel Dekker.

Riande, E. et al., 2000. *Polymers Viscoealsticity: Stress and Strain in Practice.* New York: Marcel Dekker.

Riande, E. & Saiz, E., 1992. *Dipole Moments and Birefringence of Polymers.* Englewood Cliffs, NJ : Prentice Hall.

Ribes-Creus, A., Gómez-Ribelles, J. & Díaz-Calleja, R., 1995. *Polymer ,* 26(12), p. 1849.

Roberts, G. & White, E., 1973. Relaxation processes in amorphous polymers. In: R. Haward, ed. *The Physics of Glassy Polymers.* London: Applied Science.

Roe, R., Rigby, D. & Furuya, H. T. H., 1992. *Computational Polymer Science ,* 2(1), p. 32.

Roland, C., 1994. *Macromolecules,* Volume 27, pp. 4242-4247.

Roland, C., Casalini, R. & Paluch, M., 2003. *Chemical Physics Letters ,* Volume 367, p. 259.

Roland, C., Santangelo, P. & Ngai, K., 1999. *J. Chem Phys,* Volume 111(12), pp. 5593-5598.

Rönnau, A. et al., 2000. *Br. J. Dermatol.,* Volume 143, pp. 1055-1058.

Rössler, E., Hess, K. U. & Novikov, V., 1998. *J. Non-Cryst.Solids,* Volume 223, pp. 207-222.

Rubi, M. & Pérez-Vicente, C., 1997. Berlin: Springer.

Ryabov, Y. & Nuriel, H., 2003. J. Polym. Sci. Part B Polym. Phys.. Volume 41(3), pp. 217-223.

Sabater i Serra, R. et al., 2009. *Journal of Polymer Science: Part B: Polymer Physics*, Volume 47, pp. 183-193.

Sanchis, M. et al., 2010. *Macromolecules,* Volume 43, p. 5723–5733.

Sanchis, M. et al., 2008. *J. Chem. Phys. ,* Volume 129, pp. 54903-15.

Sanchis, M. J. et al., 1999. *Macromolecules,* Volume 32, pp. 3457-3463.

Sanchis, M. J. et al., 2004. *Polymer,* Volume 45, pp. 1854-55.

Sanchis, M. J. et al., 2011. *J. Phys. Chem. B ,* Volume 115, p. 5730.

Sanchis, M. et al., 2011. *The Journal of Physical Chemistry ,* Volume 115, p. 5730.

Santangelo, P. & Roland, C., 1998. *Phys. Rev B,* Volume 58(21), pp. 14121-14123.

Sasabe, H. & Saito, S., 1968. *J. Polym. Sci. A2,* Volume 6, p. 1401.

Satti, G. & McLachlan, D. S., 2007. *J. Mater. Sci.,* Volume 42, p. 6477.

Schlessinger, M., 1995. *Infrared technology fundamentals.* New York: Marcel Dekker, Inc..

Schneider, H. A., 1989. *Polymer,* Volume 30(5), pp. 771-779.

Schönhals, A., 1997. In: *Dielectric Spectroscopy of Polymeric Materials. Fundamentals and Applications.* Washington: American Chemical Society.

Schröder, T. & Dyre, J., 2008. *Phys. Rev. Lett. ,* Volume 101, p. 025901.

Schröter, K. et al., 1998. *Macromolecules,* Volume 31, p. 8966.

Schröter, K. et al., 1998. *Macromolecules ,* Volume 31, p. 8966.

Schwarzl, F. & Struik, L., 1967. *Adv Mol Relax Process ,* Volume 1, p. 201.

Scott, T., Cook, W. & Forsythe, J., 2002. *Eur Polym J,* Volume 38, pp. 705-716.

Serghei, A., Tress, M., Sangoro, J. & Kremer, F., 2009. *Phys. Rev. B. ,* Volume 80, p. 184301.

Sillars, R., 1937. *Inst. Elect. Eng.,* Volume 80, p. 378.

Slark, A., 1999. *Polymer,* Volume 40, pp. 1935-1941.

Smaoui, H. et al., 2010. *J. Alloys and Compounds,* Volume 489, pp. 429-436.

Song, M., Hourston, D., Pollock, H. M. & Hammiche, A., 1999. *Polymer,* Volume 40, pp. 4763-4767.

Sperling, L., 2006. *Introduction to Physical Polymer Science.*. Hoboken: Wiley-Interscience.

Stephan, A., 2006. *European Polymer Journal,* Volume 42, pp. 21-42.

Stockmayer, W., 1967. *Pure Appl. Chem.,* Volume 15, p. 539.

TAInstruments, n.d. Thermal Analysis Review. Modulated DSC Theory. *TA Instruments. Thermal Analysis & Rheology,* Volume TA-211B.

Takeuchi, H. & Roe, R., 1991. *J. Chem. Phys. ,* Volume 94, p. 7446.

Tamman, G. & Hesse, W., 1926. *Z Anorg Allg Chem.,* Volume 156, pp. 245-247.

Tan, Y. Y. & Challa, G., 1976. *Polymer,* Volume 17, pp. 739-740.

Thomas, L., 2005. Modulated DSC® Paper #5 Measurement of Glass Transitions and Enthalpic Recovery. *TA Technical Paper (TP010).*.

Vallejos, S. et al., 2011. *Polym. Chem.,* Volume 2, pp. 1129-1138.

Vallejos, S. et al., 2012. *Sensors,* Volume 12, pp. 2969-2982.

Vallejos, S. et al., 2011. *Sensors & Actuators: B. Chemical,* Volume 157, pp. 686-690.

Vallejos, S. et al., 2012. *Journal of Hazardous Materials,* Volume 227-228, pp. 480-483.

Vandenbeele, P., 2013. *Practical Raman Spectroscopy-An Introduction.* Ghent: Wiley.

Viciosa, M., Rouzé, N., Dionísio, M. & Gomez-Ribelles, J., 2007. *European Polym Journal,* Volume 43, pp. 1516-1529.

Vogel, H., 1921. *Z Phys.,* Volume 22, pp. 645-646.

Volkenstein, M. V., 1963. *Configurational Statistics of Polymer Chains.*. New York: Interscience Publishers, Inc..

Wagner, K., 1914. *Arch. Electrotech.,* Volume 2, p. 371.

Weinmüller, C. et al., 2006. *J. Biomed. Mater. Res. A,* Volume 77, pp. 230-241.

Wichterle, O., 1971. *Encyclopedia of Polymer Science and Technology.* New York : Interscience.

Williams G., D. R. S. o. A. P. S. i. K. L. i. P. S., 1995. Madrid: edited by E. Riande CSIC .

Williams, G., 1964. *Trans. Faraday Soc.,* Volume 60, p. 1556.

Williams, G., 1966. *Trans. Faraday Soc. ,* Volume 6, p. 2091.

Williams, G., 1979. *Adv Polym Sci,* Volume 33, pp. 59-92.

Williams, G. & Watts, D., 1970. *Trans. Faraday Soc.,* Volume 66, p. 80.

Williams, G. & Watts, D. C., 1971. *Trans. Faraday Soc. ,* Volume 67, p. 2793.

Williams, G., Watts, D., Dev, S. & North, A. M., 1971. *Trans. Faraday Soc.,* Volume 67, p. 1323.

Wind, M., Graf, R., Heuer, A. & Spiess, H. W., 2003. *Phys. Rev. Lett.,* Volume 91, pp. 155702-I.

Wind, M., Graf, R., Renker, S. & W., S. H., 2005. *J. Chem. Phys,* Volume 122, p. 014906.

Wübbenhorst, M. & Van Turnhout, J., 2002. *J. Non-Crystal. Solids,* Volume 305, pp. 40-49.

Yamauchi, A., 2001. *Gels Handbook, Vol.1 The Fundamentals.* s.l.:Academic Press.

Yanez, F., Concheiro, A. & Alvarez-Lorenzo, C., 2008. *Eur. J. Pharm. Biopharm.,* Volume 69, pp. 1094-1110.

Zhang, S., Painter, P. C. & Runt, J., 2004. *Macromolecules,* Volume 37, p. 2636–42.

Zhao, J., McKenna, G., Willner, L. & Ritcher, J., 1997. *J.Chem. Phys.,* Volume 107, p. 3645.

Zorn, R., 1999. *J. Polym. Sci:Part B:Polym. Phys.,* Volume 37, p. 1043.

Zorn, R. et al., 1997. *J. Chem. Phys.,* Volume 107, p. 3645.

GLOSSARY

Notation	Description
A	Factor of the *ac* conductivity model
A_s	Area of the Sample
α_f	Thermal expansion coefficient of the free volume
α_p	Molecular polarizability
α_{process}	Main or segmental relaxation process
ac	Alternating current
a_{CC}	Shape parameter of the Cole/Cole model
α_{EP}	Electrode polarization process
a_T	Temperature dependence of the empirical shift factors
a_{HN}, b_{HN}	Symmetric and asymmetric broadening of the relaxation function for the Havriliak/Negami model
$\beta, \gamma, \delta \ldots$processes	Secondary relaxation processes
b_{CD}	Asymmetric broadening of the relaxation function for the Cole/Davidson model
β_{KWW}	Parameter that describes the non-exponential behavior of the decay function of Kohlrauch/Williams/Watts model
C_p	Heat capacity
d	The Bragg's spacing of the repeating domain unit
$D(t)$	Dielectric displacement
D_0	Strength parameter
dc	Direct current
ΔC_p	Heat capacity jump at the glass transition
ΔC_{pnor}	Normalized heat capacity jump at the glass transition
ΔE_{vib}	Energy difference between two vibrational energy levels
$\Delta\varepsilon = \varepsilon_s - \varepsilon_\infty$	Dielectric strength, dielectric intensity
ΔT	The broadening of the glass transition
ΔT_g	Difference between the T_g values calculated in the first (T_{g1}) and second (T_{g2}) heating ramps.
$\vec{E}$	Electric field
ε	Relative Permittivity of the Material $(\varepsilon = \varepsilon_a / \varepsilon_0)$
$\varepsilon^*(\omega)$; $\varepsilon'(\omega)$, $\varepsilon''(\omega)$	Complex dielectric function; Real and Imaginary part of the complex dielectric function
$\varepsilon^*_{dip}(\omega)$	Complex dielectric function of the dipolar contribution

$\varepsilon^*_{cond}(\omega)$	Complex dielectric function of the conductivity contribution
ε_0	Dielectric permittivity of the vacuum (ε_0=8.854·10^{-12} A·s·V^{-1}·m^{-1})
E_a	Activation energy
ε_a	Permittivity of the material
$E^*(\omega); E'(\omega), E''(\omega)$	Complex mechanical modulus; storage modulus, loss modulus
$\vec{E}_{loc}$	Local electric field
$\varepsilon''_{\max}$	Imaginary part of the complex dielectric function at the maximum of the peak.
ε_s	Static permittivity $\left(\varepsilon_s = \lim_{\omega\to 0}\varepsilon'(\omega)\right)$
ε_∞	Permittivity of the induced polarization $\left(\varepsilon_\infty = \lim_{\omega\to \infty}\varepsilon'(\omega)\right)$
$\Phi(t)$	Dielectric function
$\phi(t)$	Decaying function
f	Frequency of the external electric field
$F_{Onsager}$	Parameter of Onsanger-Fröhlich theory
Φ_g/B	Relative free volume
Φ_g	Relative free volume at T_g
f_{max}; T_{max}	Frequency and Temperature of the $\varepsilon''_{\max}$
$g = 1 + \langle \cos\theta_{ij} \rangle$	Correlation Factor; where θ_{ij} is the angle formed by the dipolar moment *i* with his neighbour *j*
η	Viscosity
k_B	Boltzmann constant
λ	Wavelength of the incident wave in the XRD technique
$L(\tau)$	Relaxation time distribution
L_D	Debye length
$M^*(\omega)$; $M'(\omega)$, $M''(\omega)$	Complex modulus function; Real and Imaginary part of the complex modulus function
M_n	Number average molecular weight
M_w	Weight average molecular weight
M_∞	$M_\infty = 1/\varepsilon_\infty$
m	Dynamic fragility index
m^*	Dynamic fragility index obtained from the Quin and McKenna model
m_{FK}	Shape parameter related to the width of the relaxation process for the

	Fuoss/Kirkwood model
$\vec{\mu}_{ind}$	Induced dipole moment
μ	Dipolar moment
N	Number of molecular dipoles that participates in the relaxation
$n = (1-\beta_{KWW})$	Coupling parameter
$\vec{P}$	Polarization vector
q	Scattering wave vector in the XRD technique
R	Ideal gas constant
s	Frequency exponent ($0 \leq s \leq 1$) of the *ac* conductivity model
$\sigma^*(\omega)$	Complex conductivity function
$\sigma'(\omega)$	Real Part of the complex conductivity function
$\sigma''(\omega)$	Real Part of the complex conductivity function
$\sigma_{dc} \equiv \sigma_0$	*dc* Conductivity $\sigma_{dc} = l \cdot A/R$
2θ	Scattering angle in the XRD technique
φ	Phase angle
$\tan\delta(\omega)$	$\tan\delta(\omega) = \varepsilon''(\omega)/\varepsilon'(\omega)$
τ	Characteristic or Relaxation time
τ_α	Characteristic time of α relaxation
τ*	Characteristic time of α relaxation obtained from Kohlrauch/Williams/Watts model
τ_β	Characteristic time of β Relaxation
τ_γ	Characteristic time of γ Relaxation
τ_σ	Characteristic time of Conductivity (σ) Relaxation
τ_0	Characteristic time of molecular vibrations
τ_{CC}	Characteristic relaxation time of the Cole/Cole Model
τ_{CD}	Characteristic relaxation time of the Cole/Davison Model
τ_{FK}	Characteristic relaxation time of the Fuoss/Kirkwood Model
τ_{HN}	Characteristic relaxation time of the Havriliak/Negami Model
τ_{KWW}	Characteristic relaxation time of Kohlrausch/Williams/Watts Model
τ_{EP}	Characteristic time of EP process
τ_∞	Pre-exponential Factors of the Arrhenius Equation
t_φ	Phase shift time
T_{on}, T_{end}	Onset and Endset Temperature of the Glass Transition (DSC) and Decomposition Process (TGA)
T_g	Glass transition temperature

T_g^{DRS}	Glass transition temperature obtained by DRS
T_{g1}; T_{g2}	T_g values calculated in the first (T_{g1}) and second (T_{g2}) heating ramps
T_m	Melting temperature
T_p	Temperature of the maximum rate of weight loss
T_v	Vogel temperature
ν	Wavenumber of a FTIR absorption band
ω	Angular frequency
ω_c	Critical angular frequency
ω_{max}	Angular Frequency at the maximum of the loss peak
$wt\%$	Weight percent
ξ	Viscosity (η) or Relaxation time (τ) of the α relaxation
$Z'(\omega)$	Real part of the complex impedance function
$Z''(\omega)$	Imaginary Part of the complex impedance function

LIST OF ACRONYMS

AIBN	α,α'- azo-bis-isobutyronitrile
ARR	Arrhenius
CC	Cole/Cole
CD	Cole/Davidson
CEOEMA	Poly(2-ethoxyethyl methacrylate) without crosslinker
DMA	Dynamic mechanical analysis
DMF	N,N´-dimethyl formamide
DRS	Dielectric relaxation spectroscopy
DSC	Differential scanning calorimetry
EGDMA	Ethylene glycol dimethacrylate
EOEMA	2-ethoxyethyl methacrylate
EP	Electrode polarization
Expt	Experimental
FK	Fuoss/Kirkwood
FTIR	Fourier transform infrared spectroscopy
GPC	Gel permeation chromatography
HN	Havriliak/Negami
HPLC	High permeation liquid cromatography
IR	Infrared
KWW	Kohlrausch/Williams/Watts
MWS	Maxwell-Wagner-Sillars
N_2	Molecular nitrogen
NMR	Nuclear magnetic resonance
PDBM23	Poly(2,3-dimethoxybenzyl methacrylate)
PDBM25	Poly(2,5-dimethoxybenzyl methacrylate
PDBM34	poly(3,4-dimethoxybenzyl methacrylate)
PEOEMA	Poly(2-ethoxyethyl methacrylate) with crosslinker
PnMAs	Poly-n- methacrylates
RF	Radio frequency
SEC	Size exclusion cromatography

SEM	Scanning electron microscopy
TEFLON	Poly(tetrafluoroethylene)
TGA	Thermogravimetry analysis
TMS	Tetramethylsilane
TSDC	Thermally Stimulated Depolarization Current Spectroscopy
UV	Ultraviolet
VFTH	Vogel Fulcher Tamman Hesse
WAXS	Wide-angle X-ray diffraction
XRD	X-ray Diffraction